UNIVERSITY OF CALIFORNIA, SAN DIEGO

Ecology of microbe/ basaltic glass interactions: Mechanisms and Diversity

A dissertation submitted in partial satisfaction of the
requirements for the degree Doctor of Philosophy

in

Marine Biology

by

Lisa A. Sudek

Committee in charge:

Professor Bradley M. Tebo, Chair
Professor Hubert Staudigel, Co-Chair
Professor Katherine A. Barbeau
Professor Douglas H. Bartlett
Professor Michael J. Sailor
Professor Alexis S. Templeton

2011

The Dissertation of Lisa A. Sudek is approved, and it is acceptable in quality and form for publication on microfilm and electronically:

_____

_____

_____

_____

_____

Co-Chair

_____

Chair

University of California San Diego

2011

This work is dedicated to my family:

Both, overseas and here, including the little lady who will join us soon. I wouldn't have accomplished this without your love and support.

Table of Contents

List of Figures

Chapter II

Chapter III

Chapter IV

Chapter V

Chapter VI

List of Tables

Chapter II

Chapter V

Chapter VI

Acknowledgements

This work would not have been possible without the help, love and support of many people I met on this journey. First and foremost I'd like to thank the three most important people, my two advisors Brad and Hubert and my advisor "by choice" Alexis. I can honestly say that the freedom that both Brad and Hubert gave me when it came to choosing the direction of my research to a large part fueled my excitement and passion for the work I was doing. Their financial support not only allowed me to entirely focus on my projects but enabled me to make the experience of joining them on cruises, something that really helped me identify with my study site and the scientific questions around it.

Brad graciously accepted my decision to remain his last San-Diego-based student for many years and supported me throughout the entire time by offering regular meetings. He somehow always had faith in me as a scientist and was still there to help whenever I needed his advice. Considering his growing responsibilities at OGI I wouldn't have blamed him if I often was the last person on his mind. I regret missing out on his lab meetings, which were always a source of fruitful discussions and on being an active part of his lab group.

Much like Brad, Hubert was a source of constant encouragement. His enthusiasm and willingness to often dedicate his full attention to my projects were priceless. I secretly consider him the main driving force behind my acceptance at SIO and I'm deeply thankful for all the time he spent with me, teaching me (or at least trying to) how to write.

Alexis not only took me surfing during my first year but also secretly taught me how to do be a successful and independent scientist. I blame her for my attitude to keep searching until I prove myself wrong. Just by example she made me want me to be the best scientist I can possibly be.

In addition I would like to thank my other committee members: Doug Bartlett, Kathy Barbeau and Mike Sailor for agreeing to serve on my committee and for their willingness to put so much thought into my work. Throughout the entire time at SIO Doug's and Kathy's doors were always open for me and Doug's kindness and enthusiasm is something I'd like to remember if I ever get to supervise my own students.

Thanks to Ron Burton I was able to keep my lab space after Brad's departure, which significantly contributed towards me finishing in a reasonable time.

Many more people, particularly in Hubbs Hall but also in other institutions played prominent roles in my grad student research and one way or the other contributed towards completion of this work:

Flip McCarthy became a real true lab mate and a friend over the years. Without his help large parts of Chapter V presented in this work would not have been accomplished. Thanks for being there for the past 3 years when everybody else left.

Many thanks to Alison Butler and her group at UCSB who provided an extensive

siderophore characterization of my model organism enabling and donated purified siderophores for me to work with.

Yongxuan Su and Ryan Anderson were to a critical part involved in the LC-ESI-MS, HPLC and MS work presented in Chapters IV, V and VI. They always provided an astonishing instrumental expertise.

I very much enjoyed working with Greg Wanger and Yuri Gorby at JCVI who collaborated with me on the electrochemical data presented in Chapters IV and V of this work. Over the years Greg also became a very good friend of mine. Thanks for always being willing to chat about the excitements and frustrations of geomicrobiological science as well as far more important things over lunch, a movie and/or a bottle of wine.

Many thanks to Francesca Malfatti and Farooq Azam for letting me use their AFM and benefit from their instrumental expertise. In order to obtain presented in Chapter VI of this dissertation Francesca was willing to dedicate endless hours at the AFM with both of us looking like we were on our way to a weekend ski trip.

Thanks to Dorothy Parker for collaborating me on the work presented in Chapter III. Her expertise on the biogeochemical implications of siderophores was what originially got me interested in this particular field and I’m thankful for everything she taught be during my time at SIO.

There are many more people that helped me to get through grad school in a relatively sane way:

Special thanks to Mark Hildebrand for always being there and for making me realize that, even if last minute, things will somehow work out. His presence in Hubbs Hall was one of the reasons that made it so much fun being at work.

Hsui Chin-Lin was my office mate for the past few years. We shared all of our ups and downs and co-parented our office fish, our constant source of entertainment ("I should get a scale and figure out how old he is!"). I admire her for her strength and her focus when it comes to simply continuing on even if you feel like hiding underneath a rock.

I would like to thank many more people whose help, support and friendship were driving forces in this journey. Former Tebo (and Hildebrand) lab members Rizlan, Hope, Greg, Brian, Brad, Luciano, Anna and Christine I all consider phenomenal scientists. Their attitude towards both science and life will always remind me that mine can certainly improve. Magali, even though not going through the same "joys" of grad school was a very close friend. Carolyn Sheehan, our former lab manager at SIO, made me feel welcome not only in the Tebo lab but more importantly in this country in general. Being able to spend time in her office chatting was a big part of staying motivated even if things at times did not work out.

Finally I'd like to thanks two people that are very important to me. Jake Perez and Arlene Jacobs. Jake saved me numerous times by helping me print posters (and dissertations!) the very last minute and provided keys to rooms that the (sometimes strange) SIO bureaucracy denied me access to. And yes, he practically also deserves a PhD for taking my paperwork up to OGSR for my final appointment while I had already moved north. I can't tell you how grateful I am for both, your help and your friendship.

Arlene not only assisted me when it came to planning field trips, conferences and eventually my defense but she generally always cared for me. Numerous hours of chats and yes, she also contributed significantly to me finally finishing. She is and will always be part of my "team" at SIO that helped me in the final stretch. I'll always remember her.

Funding agencies and administrative support made this work possible. The NSF Microbial Observatories and Biogeosciences programs (MCB-0348668 and OCE-0433692), NSF Ocean Sciences (OCE0526285), and the Agouron Institute supported my work thoughout the years. The SIO graduate department provided travel funding for meetings and covered my salary during my last quarter at SIO.

Last but not least I'd like to thank my family: My parents for always being proud of me and supporting my decision to move to the US which, based on the time difference alone, often made contact quite difficult. Their trust in me to always try my best made me reach for the stars in every aspect of my life. My mom's willingness to dedicate her whole life towards us as her family while staying a smart, strong, educated and most of all opinionated woman always showed me that it's most important who you are and not what

you are. She keeps telling me that she has no idea where my ambition towards science comes from. I always considered both of my parents tremendously ambitious and strong personalities and I'm deeply thankful for that heritage. Yes, and the stubbornness I also inherited from both of you! I may not be ready for all the punches society throws at you but once thing I learned growing-up is that I can do whatever I set my mind on.

Finally my biggest gratitude goes towards my husband Sebastian. There are not enough words to describe what he means to me. His presence and help is the only reason why I finished this work. I don't know how we managed to get through all this but we did and....we did great! I wouldn't want to imagine a life without him and I'm deeply grateful for him keeping up with my stubborn attitude towards everything work and life in general. The most important thing he taught me was patience and responding to emails in a diplomatic way. Thanks for protecting me from myself. I don't remember how often we said "this is the final stretch" but eventually you were right: "there's not only light at the end of the tunnel there's glistening sunshine".

***

The text of Chapter II, in full, is a reprint of the material as it appears in the Geomicrobiology Journal, 26: 8, 581-596. I was the primary investigator and author of this article. Alexis Templeton and my two advisors, Bradley Tebo and Hubert Staudigel were co-authors.

Chapter IV is currently being prepared for publication of the material. I am the primary investigator and author of this material. Greg Wanger, Yuri Gorby, Alexis Templeton, Hubert Staudigel and Bradley Tebo represent co-authors.

Vita

2004	Diploma (Geological Science), Freie Universitaet Berlin, Germany
1998-2004	Undergraduate Researcher, Max-Delbrueck-Center for Molecular Medicine, Berlin, Germany
2004	Fellowship from German Academic Exchange Service, visiting student, Scripps Institution of Oceanography, University of California San Diego
2004-2010	Graduate Student Researcher, University of California San Diego
2008	Teaching Assistant, Biology Department, University of California San Diego
2011	Ph.D., University of California San Diego

Publications

Sudek, L. A., G. Wanger, A. S. Templeton, H. Staudigel, Y. Gorby and B. M. Tebo (2010) Exploring the ecology of volcanic glass colonization by the marine deep-sea siderophore-producing bacterium *Pseudomonas stutzeri* VS-10 (in preparation)

Sudek, L. A., A. S. Templeton, B. M. Tebo and H. Staudigel (2009) Microbial Ecology of Fe (hydr)oxide Mats and Basaltic Rock from Vailulu'u Seamount, American Samoa. *Geomicrobiology Journal.* 26: 8, 581-596

Staudigel, H., S. R. Hart, A. Pile, B. E. Bailey, E. T. Baker, S. Brooke, D. P. Connelly, **L. Haucke**, C. R. German, I. Hudson, D. Jones, A. A. P. Koppers, J. Konter, R. Lee, T. W. Pietsch, B. M. Tebo, A. S. Templeton, R. Zierenberg and C. M. Young (2006) Vailulu'u Seamount, Samoa: Life and death on an active submarine volcano. *Proc Natl Acad Sci U S A.* 103: 6448–6453.

Bencheikh-Latmani, R., S. M, Williams, **L. Haucke**, C. S. Criddle, L. Wu, J. Zhou and B. M. Tebo (2005) Global Transcriptional Profiling of Shewanella oneidensis MR-1 during Cr(VI) and U (VI) Reduction. *Appl Environ Microbiol.* 71: 7453–7460.

Hammerschmidt, K., K. Kopp, **L. Haucke** (2003) Sm-Nd Dating on Minerals of a Silica Undersaturated, Ca-rich, Crustally Derived Gabbro of the Mid-German Crystalline Zone, drill hole Zullsdorf, Southern Brandenburg (Germany). *Z geol Wiss.* 31: 225-238.

Fields of Study

Major Field: Marine Biology (Geomicrobiology)

Marine Microbiology
Professor Bradley Tebo

Geosciences
Professor Hubert Staudigel

Aqueous and marine chemistry
Professor Kathy Barbeau

Surface texture analysis
Professor Farooq Azam

Electrochemistry
Professor Yuri Gorby

ABSTRACT OF THE DISSERTATION

Ecology of microbe/ basaltic glass interactions: Mechanisms and Diversity

by

Lisa A. Sudek

Doctor of Philosophy in Marine Biology

University of California, San Diego, 2011

Professor Bradley M. Tebo, Chair
Professor Hubert Staudigel, Co-Chair

Submarine basaltic glass constitutes a major part of the oceanic crust and contains a number of bio-essential nutrients including Fe and Mn. Substantial biological activity can be inferred from bio-alteration textures that dominate basaltic glass alteration. However, the role of basaltic glass in fueling diverse chemolithotrophic communities within deep-sea ecosystems remains enigmatic. Little is known about the key mechanisms and potential ecological advantages that drive basaltic glass colonization, the extent to which microbial activity may affect alteration rates and the biogeochemical cycling of elements in particular along the basalt/water interface. The nutrient and energy availability in basalt is considered to facilitate these processes.

Seamounts are substantial outcrops of the oceanic lithosphere and offer natural laboratories for the study the ecology of microbe/basaltic glass interactions. Studies of natural rock surfaces and hydrothermal metal-oxy-hydroxides from different hydrothermal settings at Vailulu'u Seamount (American Samoa), resulted in a detailed characterization of microbial communities and the isolation of a large number of metabolically diverse microbes. One of these strains, *Pseudomonas stutzeri* VS-10, was chosen as a model organism to study the processes of microbe/basaltic glass interactions. It was isolated from a rhyolite microbial trap and exhibits elevated growth under nutrient limited conditions in the presence of basalt. Key metabolic traits of VS-10 include heterotrophic Fe (II)-oxidation and siderophore production. I investigated this strain with respect to a number of metabolic processes, including the oxidative transformation of Fe and Mn, the production of metabolic byproducts (e.g. organic acids) and secondary metabolites (siderophores) along with their effects on the bio-alteration of the glass. Methods employed include Scanning Electron and Atomic Force Microscopy (SEM and AFM), Inductively Coupled Plasma Optical Emission Spectroscopy (ICP-OES), Reversed-phase High Performance Liquid Chromatography (HPLC), Liquid Chromatography Electrospray Ionization Mass Spectrometry (LC-ESI-MS) and microbial fuel cells (MFC). Fe availability and direct contact of the bacterium with the rock surface was shown to significantly facilitate growth of the strain suggesting basaltic glass as an important substratum in supporting metabolically diverse microbial communities in deep-sea ecosystems.

CHAPTER I: **Introduction**

“ The survival of the fittest is the ageless law of nature, but the fittest are rarely the strong. The fittest are those endowed with the qualifications for adaptation, the ability to accept the inevitable and conform the unavoidable, to harmonize with existing or changing conditions.”

Dave E. Smalley

While I have seen this quote used in a variety of contexts, most recently the global recession, I’d like to think Dave E. Smalley had a microbe’s approach to life in mind when he talked about survival of the fittest. Especially in habitats where microbial populations are subject to rapid environmental changes adaptation has always proven to ultimately be the best strategy to survive.

One such habitat are submarine hydrothermal vents. Here, the interactions between extensive hydrothermal activity in the Earth’s crust and the overlying oceanic and atmospheric lead to multiple physical and chemical gradients (Baross and Hoffman 1985). The discovery of deep-sea hydrothermal systems on the Galapagos ridge 30 years ago opened up the exploration of these entirely new ecosystems in which chemical metabolic energy replaces sunlight, the most used energy at the surface of the earth (Corliss et al. 1979). Bacteria and archaea utilizing such hydrothermally-derived energy

sources represent the primary producers in these habitats. Massive bacterial blooms triggered by the release of nutrients during volcanic eruptions, rapid colonization of new vents by invertebrates, and burial of extant vent communities by lava flows demonstrate the dynamic nature of hydrothermal systems (Shank 2010). Because the biology of vents is so intimately linked to the geological and chemical milieu, vent biological and ecological research demands an interdisciplinary approach including examinations of the geology, physical oceanography, marine chemistry, marine ecology and molecular biology (Van Dover 2000). Ever since the discovery of deep-sea hydrothermal systems in 1979 one of the major research question is how microorganisms survive under such harsh conditions. It is thought that the answer to this question may help us understand the principles of evolution and the origin of life. The biodiversity of hydrothermal ecosystems and the variety of microbiological metabolisms and strategies allowing diverse communities to exist has been of major interest. In this chapter I discuss seamounts as a habitat where microbes (biosphere) and oceanic crust (lithosphere) are intricately linked and introduce one bacterium as a model system to study these interactions.

1. Seamounts

Seamounts can be defined as active or extinct undersea volcanoes with heights exceeding ~100 m (Wessel et al. 2010). Their presence in the world's ocean, especially in the Pacific, has only become known in the last 50 years (Hess 1946; Menard and Dietz 1951; Menard and Ladd 1963). Most seamounts have a volcanic origin (Epp and Smoot 1989) so it is not surprising that some are associated with hydrothermal venting (Rogers

1994). As magmatically-active deep-sea habitats seamounts impact the ocean's biodiversity and chemical composition. Even older seamounts that exhibit reduced volcanism may still be conduits for fluid exchange between the rock mantle subsurface and the ocean (Wheat et al. 2004). Compared to other magmatically active deep-sea systems like mid-ocean riches in which approximately one-third of the heat is removed by convective circulation of seawater (Humphris et al. 1995) seamounts represent habitats with unique localized circulation patterns. This often results in the formation of strong geochemical gradients, which rapidly change depending on hydrothermal activity, composition of vent fluids and their interaction with the surrounding water masses. The global number of seamounts varies widely depending on their size definition and the methodology used to detect them. Multibeam bathymetric measurements and satellite altimetry are considered reliable detection methods (Wessel et al. 2010).

From the estimated 100,000 exceeding 1 km, only 30 to 50, 000 have been investigated at all (Roberts et al. 2006). Less than 200 have been studied in detail (Gjerde 2006). The geographic distance between seamounts and their topographic and hydrographic conditions are considered to result in faunal isolation (McClain 2007). Biologically, seamounts have long been characterized as unique and rugged ocean habitats hosting highly diverse and endemic faunas with high biomass endemism (Richer de Forges et al. 2000; Worm et al. 2003). While physical, biological and geological processes intrinsic to seamount systems can result in the isolation of populations, the limitations and variabilities of methodologies used have made it difficult to distinguish true local seamount endemicity (Shank 2010).

The main goal of todays seamount biological research is to increase our understanding of what factors are responsible for creating, structuring and maintaining biodiversity of life at seamounts through characterization and ecological process studies (Wessel et al. 2010).

The diversity and abundance of invertebrates at seamount systems is to a large part supported by the high biomass of microorganisms deriving energy and nutrition from hot, mineral-rich fluids (McCollom and Shock 1997). It has also been proposed that the alteration of oceanic crust, in particular the oxidation of reduced iron and sulfur present in volcanic rocks, provides the energy necessary for fuelling this seafloor biosphere (Bach and Edwards 2003; Edwards et al. 2005; Santelli et al. 2008).

2. Basaltic glass

The majority of the oceanic lithosphere is comprised of basalt, a volcanic rock enriched in bio-essential nutrients such as Fe(II) and Mn(II). The outer layers of submarine basaltic rocks typically consist of basaltic glass, formed through quenching of magma during eruption events. Volcanic glass therefore represents a significant part of the extrusive oceanic crust (Staudigel and Hart 1983; Straub and Schmincke 1998) and one of the most common materials available for microbial colonization in magmatically active deep-sea habitats. The glassy rims of submarine pillow basalts have been shown to host 10–10^4 times more biomass than adjacent seawater (Einen et al. 2008; Santelli et al. 2008). In addition thick microbial biofilms have been shown to cover natural basaltic glasses and are often associated with incipient ferromanganese crusts commonly found

on these surfaces (Templeton et al. 2009). Recent phylogenetic studies of submarine basaltic glass surfaces from various environmental settings reveal qualitative and quantitative differences between basaltic surfaces and the surrounding water (Mason et al. 2007; Santelli et al. 2008).

Our understanding of both the phylogenetic diversity of microbes associated with this material, their metabolic activities and the overall ecology of microbe/glass interactions in these biosphere ecosystems is still limited.

3. Ecology of microbe/surface interactions

Bacteria are known to preferentially live in matrix-enclosed communities (Costerton and Wilson 2004). In an aquatic ecosystems, free microorganisms represent only 0.1 to 1.0 % of total microorganisms, with the remainder attached to surfaces as biofilms (Brisou 1995; Madigan et al. 2000). In the past two decades several studies have shown that surface attachment is not random. Instead the proclivity of bacteria to adhere to surfaces and form biofilms is related to the selective advantage that surface association offers over a free-living, planktonic life-style. Proposed benefits from a surface-attached life-style are numerous. They include an elevated resistance to physical forces such as shear flow, enabling bacteria to remain within a favorable environmental niche (Jefferson 2004), an elevated concentration of nutrients, protection against predation through biofilm-specific chemical defense and the development of stable interactions, resulting in synergistic microconsortia (Flemming 2008). All of these features are likely to be more effective in a biofilm environment where diffusion is limited and pH and redox gradients

are more stable. While natural submarine basaltic glass surfaces have recently been shown to harbor extensive biofilms (Templeton et al. 2009), the mechanisms of biofilm development and the driving forces behind this natural phenomenon are largely unknown.

In particular it remains ambiguous if the colonization process is directed towards fulfilling specific ecological advantages such as nutrient acquisition and/or energy generation. In addition to its potential to provide a carbon source for microorganisms deep within the basaltic layer (D'Hondt et al. 2004), H_2 produced by basalt/water interaction is considered the primary energy source for some basalt-associated microbial communities (Stevens and McKinley 1995; Stevens and McKinley 2000). In addition basalt contains a number of nutrients (e.g. Fe and PO_4) and electron donors (Fe(II), Mn(II) and S^{2-}) or acceptors (Fe(III)) utilized by microbes (Bach and Edwards 2003; Bailey et al. 2009). Little is known about the microbial ecology of glass colonization, including the key mechanisms that drive the surface colonization in the first place, the effects of this interaction on the dissolution rates of the glass and the impact on the biogeochemical cycling of elements at the rock/water interface.

4. Basaltic glass alteration

Alteration of the oceanic crust refers to exchange of ions with the seawater. It leads to the transfer of bio-essential elements between the hydrosphere, lithosphere and biosphere and is both, biotically and abiotically mediated (Staudigel et al. 2008; Staudigel and Hart 1983). Key steps involved in the alteration process are hydration, dissolution, and secondary mineral formation (Banfield et al. 1999).

Abiotic alteration is mainly the result of hydration reactions with the surrounding seawater (Staudigel and Hart 1983), resulting in an isochemical removal of elements and leading to the formation of characteristic authigenic mineral phases. Nearly isomolar exchange of SiO_2, Al_2O_3, MnO, MgO, CaO, Na_2O, P_2O_5, Zn, Cu, Ni, Cr, Hf, Sc, Co and REE for H_2O and K_2O take place, while TiO_2 and FeO are passively accumulated, leading to the characteristic mineralization of palagonite (Staudigel and Hart 1983).

Evidence for bio-alteration of basalt is mainly based on the presence of morphologically distinct alteration textures in volcanic glasses. A variety of textures found in ancient and fresh submarine basalts have been attributed to microbial activity (Alt and Mata 2000; Fisk et al. 1998; Furnes et al. 1999; Furnes and Staudigel 1999; Furnes et al. 1996; Giovannoni et al. 1996; Staudigel et al. 1998; Thorseth et al. 1992; Thorseth et al. 1995; Thorseth et al. 2003; Torsvik et al. 1998). In addition to the abundance of such alteration textures many studies have also based the identification of both biotic and abiotic glass alteration on the mobility and release of elements during the alteration process (Daughney et al. 2004; Staudigel and Hart 1983). Mechanisms controlling the bio-alteration of basaltic glass resemble the ones previously proposed for mineral dissolution. They include the oxidative transformation of elements (Dong et al. 2003; Kostka et al. 1999; Roden et al. 2000) and the production of fermentation products (e.g. organic acids, Eick et al. 1996; Liermann et al. 2000a; Welch and Ullman 1993) or secondary metabolites (Barker et al. 1998; Hersman et al. 1995; Liermann et al. 2000a; Liermann et al. 2000).

5. *Pseudomonas stutzeri*

P. stutzeri has previously been found associated with oceanic crust (Ruby et al. 1981). It is a ubiquitous bacterium with a high degree of physiological and genetic adaptability (Lalucat et al. 2006). Strains belonging to this group are known to be able to grow under both aerobic and anaerobic conditions at a wide range of temperatures (4 - 45 °C) and with a variety of organic substrates. The high genetic and physiological diversity amongst strains have previously been suggested to be the result of an adaptation to various ecological niches (Lalucat et al. 2006). *P. stutzeri* strains can be abundantly found in both terrestrial and marine ecosystems (Ward and Cockcroft 1993). While several strains have been isolated from the marine environment (Bosch et al. 1999a; Bosch et al. 1999b; Kariminiaae-Hamedaani et al. 2004; Rossello´-Mora et al. 1991; Sikorski et al. 2002; Sorokin et al. 1999), only two strains were reported from the deep-sea environment (Ruby et al. 1981; Tamegai et al. 1997). These strains have been studied with regard to their ability of chemolithotrophic sulfur-oxidation (*P. stutzeri* NF13; Ruby et al. 1981) and their ecological role as denitrifyers (*P. stutzeri* MT-1; Tamegai et al. 1997). While strain MT-1 was isolated from mud, various materials including surface materials from mussels, clams and pieces of lava, pieces of glass slides and polycarbonate filters deposited in the vicinity of hydrothermal vents at the Galapagos rift lead to the isolation of strain NF13.

6. Research goals of this study

This investigation of the microbial colonization and potential alteration of basaltic glass attempts to evaluate the driving forces behind the colonization process and the

extent to which colonization is directed towards a specific benefit as described above. To study the significance of these processes in submarine basalt colonization a detailed characterization of the phenotypic and physiological characteristics of colonizing organisms is essential. While a number of studies have identified organisms associated with bio-alteration textures in volcanic rocks (Cockell et al. 2008; Herrera et al. 2008) they did not identified the metabolic processes that may promote the elevated dissolution of the rocks. Bailey et al. recently looked at the basalt-surface related growth of organisms with known metabolic characteristics but did not investigate the extent to which microbes may accelerate dissolution of the glass.

The objectives of this study were the phylogenetic investigation of natural basaltic glass surfaces from an active seamount system and a subsequent use of a strain shown to inhabit such surfaces as a model organisms to study microbe/glass interactions. Based on a metabolic characterization of the strain several features, including heterotrophic Fe(II)oxidation, siderophore biosynthesis and organic acid production, were investigated in particular with regard to their role in surface-related growth of the strain. In addition the effects of the microbial activity on basalt dissolution rates and surface texture were examined.

Initially the microbial community of a basaltic glass surface from Vailulu'u Seamount was investigated. **Chapter II of this dissertation offers insight into the overall community structure of microbial consortia associated with Fe (hydr)oxide mats and basaltic rock at Vailulu'u Seamount, American Samoa, using molecular**

and culture-based techniques. In addition to comparing the microbial diversity of the two substrata commonly associated with deep-sea hydrothermal systems to other geographical locations, Chapter II also provides evidence that metabolic versatility is an important trait in hydrothermally-influenced deep-sea ecosystems by presenting a number of isolated strains exhibiting variable metabolic capabilities.

Investigating one the mechanisms possibly facilitating microbe/glass interactions, **Chapter III makes an attempt to study the effect of siderophores on the bio-alteration of volcanic glasses based on the removal of Fe.** While ligand-promoted dissolution of Fe-bearing minerals has been the subject of numerous studies (Buss et al. 2007; Kraemer 2004; Liermann et al. 2000) their potential role in basalt dissolution, even though recently suggested (Homann et al. 2009), has never been shown. The study makes use of the siderophores desferrioxamine B (DFO-B) produced by several actinomyces (Albrecht-Gary and Crumbliss 1998) and pyoverdin (PVD), produced by a number of strains belonging to the groups of *P. aeruginosa* (Briskot et al. 1989; Cox and Adams 1985) and *P. putida* (Boukhalfa et al. 2006). The siderophore-promoted dissolution of volcanic rocks was determined based on Fe-complexation by DFO-B and PVD under aerobic and anaerobic condition. While one *P. aeruginosa* strain has been isolated from a deep-sea hydrothermal system (Wang et al. 2002), the relevance of siderophores in particular with regard to rock/microbe interactions in these ecosystems is questionable.

One of the strains isolated in Chapter II, *Pseudomonas stutzeri* VS-10, exhibited elevated elevated growth under nutrient-limited conditions in the presence of basalt. Its

metabolic characteristics including heterotrophic Fe(II)oxidation and siderophore production were investigates with particular emphasis on their role in basalt colonization in the remaining three chapters of this dissertation.

Chapter IV looks at the driving forces behind basaltic glass colonization by *P. stutzeri* VS-10 and the role of biofilm formation in elevated growth of the strain. An interdisciplinary approach using microscopic, chromatographic, molecular, culture-based and electrochemical techniques was chosen.

Chapter V documents a number of experiments investigating various metabolic features of *P. stutzeri* VS-10 potentially involved in the interaction with basaltic glass. I investigated mechanisms potentially involved in basalt-surface related growth of *P. stutzeri* VS-10. This includes VS-10 mutants derived through Tn5 transposon mutagenesis, the absorption characteristics of VS-10's siderophores with Fe and Mn and the production of low-molecular weight organic acids as determined by HPLC.

Chapter VI describes the textures and chemical transformation of basaltic glass during progressive colonization by *P. stutzeri* VS-10. This chapter is aimed towards the identification of morphological (surface-related) and chemical bio-alteration features on basaltic glass by atomic force microscopy (AFM) and inductively coupled plasma optical emission microscopy (ICP-OES).

In conclusion this work establishes *P. stutzeri* VS-10 as a valuable model organism to study the mechanisms behind microbe/basaltic glass interactions. Data presented here will hopefully contribute towards a better understanding of the ecology between metabolically diverse deep-sea bacteria and submarine basalts in magmatically active ecosystems.

References

Albrecht-Gary A. M. and Crumbliss A. L. 1998. Coordination chemistry of siderophores: thermodynamics and kinetics of iron chelation and release. Met Ions Biol Syst 35:239-327.

Alt J. C. and Mata P. 2000. On the role of microbes in the alteration of submarine basaltic glass: a TEM study. Earth and Planet. Sci. Letters 181:301-313.

Bach W. and Edwards K. J. 2003. Iron and sulfide oxidation within the basaltic ocean crust: implications for chemolithoautotrophic microbial biomass production. Geochim Cosmochim Acta 67:3871-3887.

Bailey B. E., Templeton A. S., Staudigel H. and Tebo B. 2009. Utilization of substrate components during basaltic glass colonization by Pseudomonas and Shewanella isolates. Geomicrobiology Journal 26:648-656.

Banfield J. F., Barker W. W., Welch S. A. and Taunton A. 1999. Biological impact on mineral dissolution: application of the lichen model to understanding mineral weathering in the rhizosphere. Proc Natl Acad Sci U S A 96:3404-3411.

Barker W. W., Welch S. A., Chu S. and Banfield J. F. 1998. Experimental observations of the effects of bacteria on aluminosilicate weathering. Amer Mineral 83:1551-1563.

Bosch R., Garcia-Valdes E. and Moore E. R. 1999a. Genetic characterization and evolutionary implications of a chromosomally encoded naphthalene-degradation upper pathway from Pseudomonas stutzeri AN10. Gene 236:149-157.

Bosch R., Moore E. R., Garcia-Valdes E. and Pieper D. H. 1999b. NahW, a novel, inducible salicylate hydroxylase involved in mineralization of naphthalene by Pseudomonas stutzeri AN10. J Bacteriol 181:2315-2322.

Boukhalfa H., Reilly S. D., Michalczyk R., Iyer S. and Neu M. P. 2006. Iron(III) coordination properties of a pyoverdin siderophore produced by Pseudomonas putida ATCC 33015. Inorg Chem 45:5607-5616.

Briskot G., Taraz K. and Budzikiewicz H. 1989. Pyoverdin-type siderophores from Pseudomonas aeruginosa. Liebigs Ann. Chem.:375-384.

Brisou J. F. 1995. J.F. Brisou, Biofilms: Methods for Enzymatic Release of Microorganisms. Boca Raton, Florida: CRC Press.

Buss H. L., Luettge A. and Brantley S. L. 2007. Etch pit formation on iron silicate surfaces during siderophore-promoted dissolution. Chem Geol 240:326-342.

Cockell C. S., Olsson-Francis K., Herrera A. and Meunier A. 2008. Alteration textures in terrestrial volcanic glass and the associated bacterial community. Geobiology 7:50-65.

Costerton W. J. and Wilson M. 2004. Introducing Biofilms. Biofilms 1:1-4.

Cox C. D. and Adams P. 1985. Siderophore activity of pyoverdin for Pseudomonas aeruginosa. Infect Immun 48:130-138.

D'Hondt S., Jorgensen B. B., Miller D. J., Batzke A., Blake R., Cragg B. A., Cypionka H., Dickens G. R., Ferdelman T., Hinrichs K. U., Holm N. G., Mitterer R., Spivack A., Wang G., Bekins B., Engelen B., Ford K., Gettemy G., Rutherford S. D., Sass H., Skilbeck C. G., Aiello I. W., Guerin G., House C. H., Inagaki F., Meister P., Naehr T., Niitsuma S., Parkes R. J., Schippers A., Smith D. C., Teske A., Wiegel J., Padilla C. N. and Acosta J. L. 2004. Distributions of microbial activities in deep subseafloor sediments. Science 306:2216-2221.

Daughney C. J., Rioux J. P., Fortin D. and Pichler T. 2004. Laboratory Investigation of the Role of Bacteria in the Weathering of Basalt Near Deep Sea Hydrothermal Vents. Geomicrobiology Journal 21:21-31.

Dong H., Kostka J. E. and Kim J. 2003. Microscopic Evidence For Microbial Dissolution Of Smectite. Clays and Clay Minerals 52:502-512.

Edwards K. J., Bach W. and McCollom T. M. 2005. Geomicrobiology in oceanography: microbe-mineral interactions at and below the seafloor. Trends Microbiol 13:449-456.

Eick M. J., Grossl P. R., Golden D. C., Sparks D. L. and Ming D. W. 1996. Dissolution kinetics of a lunar glass simulant at 25 degrees C: the effect of pH and organic acids. Geochim Cosmochim Acta 60:157-170.

Einen J., Thorseth I. H. and Ovreas L. 2008. Enumeration of Archaea and Bacteria in seafloor basalt using real-time quantitative PCR and fluorescence microscopy. FEMS Microbiol Lett 282:182-187.

Epp D. and Smoot N. C. 1989. Distribution of Seamounts in the North Atlantic. Nature 337:254-257.

Fisk M. R., Giovannoni S. J. and Thorseth I. H. 1998. Alteration of oceanic volcanic glass textural evidence of microbial activity. Science.

Flemming H.-C. 2008. Why microorganisms live in biofilms and the problem of biofouling. In: Marine and Industrial Bioufouling.

Furnes H., Muehlenbachs K., Tumyr O., Torsvik T. and Thorseth I. H. 1999. Depth of active bio-alteration in the ocean crust Costa Rica Rift (Hole 504B). Terra Nova 11:228-233.

Furnes H. and Staudigel H. 1999. Biological mediation in ocean crust alteration: how deep is the deep biosphere. Earth and Planet. Sci. Letters 166:97-103.

Furnes H., Thorseth I. H. and Tumyr O. 1996. Textural and chemical effects of bacterial activity on basaltic glass: an experimental approach. Chem Geol 119:139-160.

Giovannoni S. J., Fisk M. R., Mullins T. D. and Furnes H. 1996. Genetic evidence for endolithic microbial life colonizing basaltic glass/seawater interfaces. Proc. ODP Sci. Results 148:207-214.

Gjerde K. M. 2006. Ecosystems and biodiversity in deep waters and high seas. UNEP Regional Seas Report and Studies 178:1-60.

Herrera A., Cockell C. S., Self S., Blaxter M., Reitner J., Arp G., Droese W., Thorsteinsson T. and Tindle A. G. 2008. Bacterial Colonization and Weathering of Terrestrial Obsidian in Iceland. Geomicrobiology Journal 25:25-37.

Hersman L. E., Lloyed T. and Sposito G. 1995. Siderophore-promoted dissolution of hematite. Geochim Cosmochim Acta 59:3327-3330.

Hess H. H. 1946. Drowned ancient islands of the Pacific Basin. American Journal of Science 244:772-791.

Homann V. V., Sandy M., Tincu J. A., Templeton A. S., Tebo B. M. and Butler A. 2009. Loihichelins A-F, a Suite of Amphiphilic Siderophores Produced by the Marine Bacterium Halomonas LOB-5. J Nat Prod.

Humphris S. E., Zierenberg R., Mullineaux R. A. and Thomson R. E. 1995. Seafloor Hydrothermal Systems: Physical, Chemical, Biological, and Geological Interactions.: American Geophysical Union, Geophysical Monograph.

Jefferson K. K. 2004. What drives bacteria to produce a biofilm? FEMS Microbiol Lett 236:163-173.

Kariminiaae-Hamedaani H. R., Kanda K. and Kato F. 2004. Denitrification activity of the bacterium Pseudomonas sp. ASM-2-3 isolated from the Ariake Sea tideland. J Biosci Bioeng 97:39-44.

Kostka J. E., Haefele E., Viehweger R. and Stucki J. W. 1999. Respiration and Dissolution of Iron(III)-Containing Clay Minerals by Bacteria. Environ. Sci. Technol. 33:3127-3133.

Kraemer S. M. 2004. Iron oxide dissolution and solubility in the presence of siderophores. Aquatic Sciences- Research Across Bounderies 66:3-18.

Lalucat J., Bennasar A., Bosch R., Garcia-Valdes E. and Palleroni N. J. 2006. Biology of Pseudomonas stutzeri. Microbiol Mol Biol Rev 70:510-547.

Liermann L., Barnes A. S., Kalinowski B. E., Zhou X. and Brantley S. L. 2000a. Microenvironments of pH in biofilms grown on dissolving silicate surfaces. Chem Geol 171:1-16.

Liermann L. J., Kalinowski B. E., Brantley S. L. and Ferry J. G. 2000. Role of bacterial siderophores in dissolution of hornblende. Geochim Cosmochim Acta 64:587-602.

Madigan M. T., Martinko J. M. and Parker J. 2000. Brock Biology of Microorganisms. Prentice Hall, Upper Saddle River, New Jersey.

Mason O. U., Stingl U., Wilhelm L. J., Moeseneder M. M., Di Meo-Savoie C. A., Fisk M. R. and Giovannoni S. J. 2007. The phylogeny of endolithic microbes associated with marine basalts. Environ Microbiol 9:2539-2550.

McClain C. R. 2007. Guest Editorial: Seamounts: Identity crisis or split personality? Journal of Biogeography 34:2001-2008.

McCollom T. M. and Shock E. L. 1997. Geochemical constraints on chemolithoautotrophic metabolism by microorganisms in seafloor hydrothermal systems. Geochim Cosmochim Acta 61:4375-4391.

Menard H. W. and Dietz R. S. 1951. Submarine geology of the Gulf of Alaska. Geol. Soc. Amer. Bull. 62:1263-1285.

Menard H. W. and Ladd H. S. 1963. Oceanic islands, seamounts, guyots and atolls. In: The sea. Hill M. N., editors. 365-387.

Richer de Forges B., Koslow J. A. and Poore G. B. C. 2000. Diversity and endemism of the nethic seamount fauna in the southwest Pacific. Nature 405:944-947.

Roberts J. M., Wheeler A. J. and Freiwald A. 2006. Reefs of the deep: the biology and geology of cold-water coral ecosystems. Science 312:543-547.

Roden E. E., Urrutia M. M. and Mann C. J. 2000. Bacterial Reductive Dissolution of Crystalline Fe(III) Oxide in Continuous-Flow Column Reactors. Appl Environ Microbiol 66:1062-1065.

Rogers A. D. 1994. The biology of seamounts. In: Advances in marine biology. Blaxter J. H. S. and Southward A. J., editors. 305-350.

Rossello´-Mora R. E., Garcia-Valdes E., Lalucat J. and Ursing J. 1991. Genotypic and phenotypic diversity of Pseudomonas stutzeri. Sust. Appl. Microbiol. 14:150-157.

Ruby E. G., Wirsen C. O. and Jannasch H. W. 1981. Chemolithotrophic Sulfur-Oxidizing Bacteria from the Galapagos Rift Hydrothermal Vents. Appl Environ Microbiol 42:317-324.

Santelli C. M., Orcutt B. N., Banning E., Bach W., Moyer C. L., Sogin M. L., Staudigel H. and Edwards K. J. 2008. Abundance and diversity of microbial life in ocean crust. Nature 453:653-656.

Shank T. M. 2010. Seamounts: Deep-Ocean Laboratories of Faunal Connectivity, Evolution, and Endemism. Oceanography 23:108-122.

Sikorski J., Mohle M. and Wackernagel W. 2002. Identification of complex composition, strong strain diversity and directional selection in local Pseudomonas stutzeri populations from marine sediment and soils. Environ Microbiol 4:465-476.

Sorokin D. Y., Teske A., Robertson L. A. and Kuenen J. G. 1999. Anaerobic oxidation of thiosulfate to tetrathionate by obligately heterotrophic bacteria, belonging to the Pseudomonas stutzeri group. FEMS Microbiol Ecol 30:113-123.

Staudigel H., Furnes H., McLoughlin N., Banerjee N. R., Connell L. B. and Templeton A. S. 2008. 3.5 billion years of glass bioalteration: Volcanic rocks as a basis for microbial life? Earth-science Reviews (in press).

Staudigel H. and Hart S. R. 1983. Alteration of basaltic glass: Mechanisms and significance from the oceanic crust-seawater budget. Geochim. Cosmochim. Acta 47.

Staudigel H., Yayanos A., Chastain R., Davies G., Verdurmen E. A. T., Schiffman P., Bourcier R. and DeBaar H. 1998. Biologically mediated dissolution of volcanic glass in seawater. Earth and Planet. Sci. Letters 164:233-244.

Stevens T. O. and McKinley J. P. 1995. Lithoautotrophic Microbial Ecosystems in Deep Basalt Aquifers. Science 270:450-455.

Stevens T. O. and McKinley J. P. 2000. Abiotic controls on H2 production from basalt-water reactions and implications for aquifer biogeochemistry. Environ. Sci. Technol. 34:826-831.

Straub S. M. and Schmincke H.-U. 1998. Evaluation the tephra input into Pacific Ocean sediments: distribution in space and time. Geol Rundschau 87:462-476.

Tamegai H., Li L., Masui N. and Kato C. 1997. A denitrifying bacterium from the deep sea at 11,000-m depth. Extremophiles 1:207-211.

Templeton A. S., Knowles E. J., Eldridge D. L., Arey B. W., Dohnalkova A. C., Webb S. M., Bailey B. E., Tebo B. M. and Staudigel H. 2009. A seafloor microbial biome hosted within incipient ferromanganese crusts. Nature Geoscience 2:872-876.

Thorseth I. H., Furnes H. and Heldal M. 1992. The importance of microbiological activity in the alteration of natural basaltic glass. Geochim Cosmochim Acta 56:845-850.

Thorseth I. H., Furnes H. and Tumyr O. 1995. Textural and chemical effects of bacterial activity on basaltic glass: an experimental approach. Chem Geol 119:139-160.

Thorseth I. H., Pedersen R. B. and Christie D. 2003. Microbial alteration of 0-30-Ma seafloor and sub-seafloor basaltic glasses from the Australian Antarctic Discordance. Earth and Planet. Sci. Letters 215:237-247.

Torsvik T., Furnes H., Muehlenbachs K., Thorseth I. H. and Tumyr O. 1998. Evidence for microbial activity at the glass-alteration interface in oceanic basalts. Earth and Planet. Sci. Letters 162:165-176.

Van Dover C. L. V. 2000. The Ecology of Deep-Sea Hydrothermal Vents. New Jersey: Princeton University Press.

Wang C. L., Ozuna S. C., Clark D. S. and Keasling J. D. 2002. A deep-sea hydrothermal vent isolate, Pseudomonas aeruginosa CW961, requires thiosulfate for Cd2+ tolerance and precipitation. Biotechnology Letters 24:637-641.

Ward B. B. and Cockcroft A. R. 1993. Immunofluorescence detection of the denitrifying strain Pseudomonas stutzeri (ATCC 14405) in sea water and intertidal sediment environments. Microb. Ecol. 25:233-246.

Welch S. A. and Ullman W. J. 1993. The effect of organic acids on plagioklase dissolution rates and stoechiometry. Geochim Cosmochim Acta 63:2725-2736.

Wessel P., Sandwell D. T. and Kim S.-S. 2010. The Globald Seamount Census. Oecanography 23:24-33.

Wheat C. G., Mottl M. J., Fisher A. T., Kadko D., Davis E. E. and Baker E. T. 2004. Heat flow through a basaltic outcrop on a sedimented young ridge flank. Geochemistry Geophysics Geosystems 5.

Worm B., Lotze H. K. and Myers R. A. 2003. Predator diversity hotspots in the blue ocean. Proceedings of the National Academy of Sciences 100:9884-9888

CHAPTER II: **Microbial ecology of Fe (hydr)oxide mats and basaltic rock from Vailulu'u Seamount, American Samoa**

Abstract

Microbial community analysis of a deep-sea volcanic and hydrothermal system at Vailulu'u seamount yielded 89 new organisms and three detailed 16S-rRNA gene clone libraries (one rock and two microbial mats). Proteobacterial communities dominate in most environments, but important differences are found between microbial mats from distinctly different geochemical environments and for the rock surface. Many cultured organisms are metabolically and functionally diverse, displaying at least two of the tested functions: heterotrophy, Fe(II) and Mn(II) oxidation, and siderophore-production. Metabolic versatility of microorganisms is suggested as an important trait allowing diverse populations of bacteria to adapt to these environments.

Introduction

Tubeworms and chemosynthetic microbial communities associated with black smokers spewing 300 °C hot sulfide-rich fluids at mid ocean ridges were discovered

more than 30 years ago and have been amongst the most charismatic and widely known research topics in the biogeosciences. Over the last decade, much evidence has accumulated that suggests that life in these environments is not confined to high temperature fluids but can also be found in lower temperature seafloor volcanic and hydrothermal environments. Hydrothermal vents at temperatures less than 100°C produce characteristic Fe (hydr)oxide microbial mats (Longnecker and Reysenbach 2001; Moyer et al. 1995). Seafloor basalt surfaces adjacent to active ridges and seamounts have also been shown to be colonized by variably abundant microbial communities that may be as diverse as farm soils (Santelli et al. 2008). There is also much evidence for life inside the oceanic crust, from microbial community analyses in low temperature fluids recovered from drill holes (Cowen et al. 2003), and from trace fossils in volcanic glass in the oceanic crust, down to depths of 500 m (Furnes and Staudigel 1999; Staudigel et al. 2008). These findings support the idea that the oceanic crust may represent a large, subsurface biosphere that may be quite relevant in terms of total biomass, and where primary productivity may be based on chemolithotrophic metabolism related to globally relevant chemical fluxes between seawater and the oceanic crust. These environments also serve as possible candidates for the origin of life more than 3.5 Ba ago (Furnes et al. 2004; Shock 1996; Shock et al. 1998; Staudigel et al. 2004; Staudigel et al. 2008).

The tremendous potential impact of the deep-ocean biosphere on the chemical interaction between the lithosphere and hydrosphere motivates a broad interest in microbial communities and their function in chemically diverse environments. Most of what we know about lower temperature seafloor microbial communities comes from high

throughput molecular methods (qPCR, t-RFLP, EST, DGGE, TGGE, ARISA, ARDRA, Geochip, Davis and Moyer 2008; Lysnes et al. 2004; Sogin et al. 2006) but there also exist detailed 16S rRNA gene clone libraries from several seafloor locations (Hodges and Olson 2009; Longnecker and Reysenbach 2001; Moyer et al. 1995; Santelli et al. 2008). The isolation of organisms from marine hydrothermal environments and the analysis of their physiological properties, including a variety of sulfur metabolisms as well as Fe(II) and Mn(II) oxidation, has shed new light on the potential function of some members of these microbial communities in the environment. (Brinkhoff et al. 1999; Edwards et al. 2003; Emerson and Moyer 2002; Emerson et al. 2007; Kuever et al. 2002; Nakagawa et al. 2004; Nealson and Saffarini 1994; Sievert et al. 2008; Takai et al. 2004; Takai et al. 2005; Tebo et al. 2005; Templeton et al. 2005).

In this paper, we provide a comprehensive microbial community analysis of distinct hydrothermal environments at Vailulu'u Seamount (Samoa) in which 16S rRNA gene clone libraries are integrated with culturing approaches. The goal of this study is to better understand the microbial and metabolic diversity within seafloor volcanic hydrothermal settings and to begin to understand how the local environment influences the function and composition of microbial communities. We characterized one rock sample and two Fe (hydr)oxide mats from distinct hydrothermal environments with detailed clone libraries (419 clones/157 operational taxonomic units (OTU's)). We also isolated a total of 89 strains to explore a range of microbial functions (heterotrophy, Fe(II) and Mn(II) oxidation, and production of siderophores) under a variety of aerobic and microaerophilic conditions. Our work is broadly consistent with previous studies, but

also offers some new insights. We more than doubled the number of isolated organisms from such seafloor volcanic environments, and one quarter of these isolates appear to be capable of more than one function (heterotrophy, Fe(II) and Mn(II) oxidation or siderophore production). We suggest that this versatile metabolism represents an important adaptation to oligotrophic seafloor environments. Furthermore, we demonstrate distinct changes in the composition of the microbial communities between hydrothermal sites at Vailulu'u Seamount, further supporting the idea that microbial community composition will be strongly modulated by the geochemical structure and dynamics of local microenvironments.

Materials and Methods

1. Hydrothermal Setting and Sample Collection

Vailulu'u Seamount is located about 27 miles east of Ta'u Island, the eastern-most island of American Samoa (14.22°S/169.06°W, Figure 2.1). It rises 5000 m from the seafloor to its shallowest crater-rim depth of 593 m with a summit crater 2 km wide and 400 m below its summit. Vailulu'u is seismically, volcanically and hydrothermally active and considered the current location of the Samoan hotspot (Hart et al. 2000; Konter et al. 2004; Staudigel et al. 2006). Vailulu'u's most recent volcanic eruption in November 2004 (Sims et al. 2008) built Nafanua, a new 300 m volcanic cone inside the crater taller than breaches in the crater wall, but 100 m lower than its summit (Figure 2.1).

Intense hydrothermal venting at the crater floor, and the influx of seawater into the crater through its breaches offers pronounced hydrothermal gradients between the most intense hydrothermal input in the deepest parts of the crater and effectively clear open ocean waters at its main summit at 593 m water depth (Staudigel et al. 2006): Hydrothermal venting in the crater focuses on a small area in the moat to the north of Nafanua. This Northern Moat Hydrothermal Complex (NMHC, Figure 2.1) is characterized by fluid temperatures up to 81°C, low salinities and low pH (<2.7). The fluids incorporate rising droplets of liquid CO_2, and are likely to contain substantial amounts of sulfide, based on the precipitation of marcasite in the venting area. Some minor hydrothermal areas at shallower depths include in particular an area of diffuse venting at Nafanua (5.8°C; pH 7.5-8.4; at M4) producing prominent Fe (hydr)oxide mats.

Substantial gradients in crater water turbidity are caused by the interplay between the most prolific hydrothermal venting at the NMHC and the influx of ocean water in particular through the northwestern breach (Staudigel et al. 2006). Waters with the largest and most consistent hydrothermal contents are found in the deep, fully enclosed crater, decreasing slightly upward until the crater becomes breached, and rarely reaching the summit of Vailulu'u. Nafanua summit is located in an intermediate depth where turbid waters alternate with nearly clear seawater. The vertical zonation of hydrothermal contents in crater waters provides key boundary conditions for the microbial communities that are found in Fe (hydr)oxide mats and on volcanic rocks.

For the microbial community analysis we focused our sampling on two locations, the summit region of Nafanua and the deep crater moat to the east of Nafanua. At Nafanua summit we took a microbial mat sample: Nafanua summit mat (NSM) (14° 12.889S / 169° 03.568W; 707m) and a rock sample: Nafanua summit rock (NSR) (14°12.869S/169°03.613W; 752m). The turbidity in the Nafanua locations alternates between unaltered (nearly clear and oxygenated) seawater and hydrothermal plume waters with turbidities exceeding 0.3 NTU's (Nephelometer Turbidity Units; (Staudigel et al. 2006)). Much of the turbidity in this region is likely to come from sulfides vented at the NMHC. Mats accumulating at Nafanua are on average 2-4 cm thick but in depressions they may reach about 1m in thickness, all of which were likely formed since the original eruption of Nafanua. Their freshness is indicated by dark red colors yellowing towards the actual vent areas. The mat sample from the moat to the east of Nafanua (646-12-R5= Eastern Moat mat (EMM); 14° 12.875S / 169° 03.274W, Temp. 5.1 °C) was taken at 986 m water depth where waters are permanently highly turbid (0.4-1.4 NTU; (Staudigel et al. 2006)). At this depth, there is no direct access to oxygenated open ocean waters, and it is likely that mats from this section of the crater floor have accumulated over a longer time period than at Nafanua. For this reason it cannot be ruled out that they contain a range of sediment particles from the overlying water column and/or decaying organic matter from the "moat of death", a region of high metazoan mortality in the SE part of Vailulu'u crater.

For comparison, samples for the isolation of Fe- and Mn-oxidizing bacteria (FeOB and MnOB), as well as siderophore-producing strains, were also collected from

other locations: M1 (the area of the NW breach where seawater flows into the crater), M2 (the summit of Vailulu'u), M4 (Nafanua), M5 (the location of the crater floor below the main seawater entry into the crater), M45 (at the NMHC), M6+7 (two locations at the western rift of Vailulu'u, not shown in Figure 2.1) and an area east of Ta'u in ~1700 m water depth representing a non-hydrothermally influenced area (Not shown; Table 2.S1).

Our samples were collected in March/April and June/July 2005 using the Pisces V submersible operated from R/V *Ka'Imikai'O'Kanaloa* (operated by the Hawaii Undersea Research Laboratory). Rock samples were taken using the submersible manipulators and transported to the surface in a sealed "biobox" avoiding contamination from the upper water column during transport to the surface. Fe (hydr)oxide mats were collected with a rosette suction sampler in aseptic collection vessels. All samples were processed onboard using sterile techniques with sub-samples being frozen at -80 °C for subsequent DNA extraction or fixed in glutaraldehyde for SEM work.

2. Isolation of FeOB, MnOB and siderophore-producing strains

Small pieces of rock and sediment samples were transferred to filter-sterilized ambient seawater and shaken vigorously to release bacteria from the surface. The seawater was then used to inoculate liquid oligotrophic enrichment cultures and oligotrophic and organic-rich agarose plates specifically designed for detection and isolation of FeOB, MnOB or siderophore-producing bacteria. Depending on their particulate density, mat samples were either directly used to inoculate plates or were diluted 100-fold in filter-sterilized deep-seawater.

2.1 FeOB

Aerobic heterotrophic FeOB were cultured on organic-rich and oligotrophic plates and liquid media. Organic-rich plates ("F-plates") designed to enrich for heterotrophic FeOB were prepared from a defined medium[1] amended with 400 μM $FeSO_4$. F-plates were buffered at either pH 7.5 or pH 6. "xFe" plates, designed for isolation of potential oligotrophs, were based on an artificial seawater medium[2] amended with 100 μM $FeCl_2$ and 10 μM sodium acetate and were adjusted to pH 7.5. For isolation of heterotrophic and oligotrophic FeOB, orange colonies on F and xFe plates single colonies were picked and transferred 5 times. They were subsequently tested for the presence of Fe (hydr)oxides using the Prussian Blue assay (Dunbar and Heintz 1997).

Microaerophilic enrichment cultures as used for xFe plates contained the same artificial seawater medium amended with anaerobically prepared and filter-sterilized $FeCl_2$ to a final concentration of 50 μM. Cultures were bubbled with N_2 and amended with $NaHCO_3$ as the sole-carbon source for lithoautotrophic growth, and no organic carbon sources were added. Fe(II) additions (50 μM) were made every 3-4 days. Decreasing pH in the cultures was balanced through simultaneous addition of 50 μM anoxic $NaHCO_3$. Oxygen content in the headspace of the tubes was kept at ~1% by

---

[1] per L of ultrapure H_2O: 50 g NaCl, 0.94 g casamino acids, 0.625g proteose peptone #3, 0.125 g yeast extract, 0.375 g sodium citrate, 2.5 g $MgSO_4 \cdot 7H_2O$, 0.00625 g $Fe(NH_4)_2(SO_4)_2 \cdot 6H_2O$, 15 g agar, adjusted to pH~8.2 to balance addition of acidified $FeSO_4$ solution after autoclaving. After autoclaving at 121 °C for 30 min.: 1ml vitamin mix, 1 ml trace element mix (Pfennig and Lippert 1966), 1ml filter sterilized 400 mM $FeSO_4$

[2] per L of ultrapure H_2O: 27.5 g NaCl, 5.38 g MgCl, 0.72 g KCl, 0.2 g $NaHCO_3$, 1.4 g $CaCl_2$, 1 g NH_4Cl, 0.05 g K_2HPO_4, 15 g agar, pH 7.3, and 1ml trace element mix added after autoclaving at 121 °C for 30 min and cooling to ~50 °C.

regular additions of filter-sterilized air using a syringe and needle. Microaerophilic enrichments were transferred three times to fresh tubes containing the same medium incubating three months between transfers. Strains of oligotrophic FeOB from the enrichments were isolated in gradient tubes (Emerson and Moyer 1997; Kucera and Wolfe 1957). Briefly, cultures were set-up in screw-cap tubes containing an FeS plug as an electron source. The plug is overlaid with semisolid oligotrophic seawater medium buffered with bicarbonate and a headspace of air. Inoculation was done by pulling a pipet vertically through the semisolid medium (from bottom to top) and gradually expelling the inoculum. Taking into account that most oligotrophic FeOB are facultative and to accelerate the isolation process a sample taken in the area of the Fe-oxide band forming in the gradient tubes was transferred to F-plates where isolation of strains took place through multiple transfers under microaerophilic atmosphere (H_2:CO_2, BBL CampyPak).

2.2 MnOB

Three types of organic-rich plates (K, M, Lept) were used for the isolation of aerobic heterotrophic MnOB (Tebo et al. 2007), and "xMn" plates were used to select for Mn(II) -oxidizing oligotrophs (Templeton et al. 2005). These plates were based on the same seawater medium used for "xFe"-plates but amended with 100 μM $MnCl_2$ instead of $FeCl_2$. For isolation of heterotrophic MnOB dark brown colonies on the K, M, and Lept plates were tested for Mn oxides encrustation using the leucoberbelin blue (LBB) assay (Krumbein and Altmann 1973; Tebo et al. 2007). LBB-positive Mn(II) oxidizing colonies were transferred at least 5 times to obtain pure cultures and tested for continued Mn(II) oxidation capability.

2.3 Siderophore producers

Chrome-Azurol-S (CAS) plates for isolation of siderophore-producing strains were prepared as described previously (Schwyn and Neilands 1987), with glycerol provided as a carbon source. Inoculated plates were kept at 4 °C and re-plated/transferred until pure cultures were obtained. CAS plates were also used to randomly test about a third of the FeOB isolates for the production of siderophores. Siderophore-producing strains were identified based on the formation of characteristic halos around the colonies.

3. DNA Extraction

Total genomic DNA of environmental samples was extracted from rock and mat samples using the MO BIO PowerSoil DNA extraction Kit (MO BIO Laboratory Inc., Carlsbad CA). Due to the nature of the samples (high Fe content of the mats and generally low biomass) DNA extractions were challenging and a high concentration of isolated DNA was difficult to achieve. After the extraction DNA was eluted in ultrapure H_2O adjusted to pH 8 and concentrated using a speed-vac (Centrivap Concentrator; Labconco Corporation, Kansas City, MO). DNA from isolated strains of FeOB, MnOB and siderophore-producing bacteria was obtained by growing the strains in 5 ml of Luria-Bertani (LB) medium[3] at room temperature (~180 rpm) and extracting DNA from pelleted cells using the DNAeasy kit (Qiagen Inc., Valencia CA). Obligate oligotrophic strains of FeOB unable to grow on LB medium, were identified through colony PCR.

[3] Per L of ultrapure H_2O: 10 g Bacto Tryptone, 5 g Yeast Extract, 10 g NaCl, adjusted to pH 7.0

4. PCR, Clone library construction and sequencing

For 16S rRNA gene amplification of isolated strains, two universal eubacterial primers 27f and 1492r[4] (Lane 1991) were used. PCR products were purified using the QIAquick PCR Purification Kit (Qiagen Inc., Valencia CA). For environmental samples the same PCR primers and protocol were used but after purification PCR products were cloned into PCR2.1 vector using the TA cloning kit (pCR®2.1-TOPO®vector, Invitrogen, Carlsbad CA). Single clones were picked and grown in LB medium at 37°C overnight prior to extraction of the plasmid using a QIAprep spin Miniprep Kit (Qiagen Inc., Valencia CA). All clones were sequenced[5] using vector-specific primers M13f and M13r as well as one internal primer 1074r[6]. The sequencing reaction, performed on a capillary electrophoresis DNA sequencer (ABI PRSIM 3100 genetic analyzer), was carried out by Seqxcel Inc., San Diego.

---

[4] 27f (5'-AGA GTTT GAT CMT GGC TCA G-‘3)
1492r (5'-TAC GGY TAC CTT GTT ACG ACT T-’3)
PCR conditions: 95 °C = 3 min.; 35 x (95 °C = 30 sec., 50 °C = 30 sec., 72 °C = 1 min.); 72 °C = 7 min. Each 50 µl PCR reaction contained 1.5 µM of each primer, 1.25 units Taq DNA polymerase (Roche), 1x PCR buffer (Roche), a 200 µM concentration of each deoxynucleoside triphosphate (Invitrogen) and 0.2 mg/ml bovine serum albumin. PCR amplification was originally tried at a variety of annealing temperatures. However we were unable to amplify the product at temperatures higher than 50°C.

[5] Each sequencing reaction included 2 µl of BigDye Terminator v3.1 (Applied Biosystems), 5 pmols primer and 4-6 µl of PCR reaction (for isolates) or 3 µl of plasmid (for clones) in a total volume of 8 µl. The sequencing reaction consisted of: 96 °C = 10 sec. ; 28 x (96 °C= 10 sec., 50 °C= 5 sec., 60 °C= 4 min. After completion 40 µl of 75 % isopropanol were added to the reactions and incubated at room temperature for 15 minutes followed by a 30 minute centrifugation at 2,000 x g. The supernatant was removed and the samples were dried by inverted centrifugation for 1 minute at 700 x g prior to sequencing.

[6] M13f (5'-GTA AAA CGA CGG CCA G-3'), M13r (5’-CAG GAA ACA GCT ATG AC-3'), 1074r (5’-CAC GAG CTG ACG ACA GCC AT-’3)

5. Phylogenetic Analysis

Sequence reads were assembled and analyzed in Sequencher 4.6 (GeneCodes, Ann Arbor MI) resulting in near full-length 16S rRNA genes (~1300 bp). All sequences were checked for their orientation and their potential of being chimeric using OrientationChecker and Mallard (Ashelford et al. 2006). Clone sequences and numerous closely related strains identified via RDP sequence match (Cole et al. 2003) were aligned using Arb-silva (Pruesse et al. 2007) and then edited manually. Phylogenetic analysis was performed using the online tool RAxML (Stamatakis et al. 2008) based on maximum likelihood estimation (MLE). The MLE model was selected by hierarchial likelihood ratio tests (hLRTs) and Akaike information criterion (AIC) using Paup version 4.0 (Swofford 2002) and MrModeltest version 2.3 (Nylander 2004). Relative species richness in each sample was determined through rarefaction analysis. Distance matrices of all sequences were generated using DNAdist (Felsenstein 1993) and used to construct rarefaction curves in DOTUR (Schloss and Handelsman 2005) to determine sequence similarity of clones from the eastern moat and isolated strains. Evolutionary distances between orthologous sequences identified operational taxonomic units (OTUs) to predict the number of different microbial taxa in each sample (Chao 1984; Chao et al. 1993). OTUs were defined by assigning sequences with $\geq$ 97% similarity into one OTU. Duplicate isolate sequences were identified using the online tool ELIMDUPES[7]. To determine sequence similarity from other geographical locations all sequences were

[7] http://hcv.lanl.gov/content/sequence/ELIMDUPES/elimdupes.html

uploaded into myRDP, aligned and compared against the database using the RDP sequence match. The similarity score was used as a proxy for phylogenetic proximity.

6. Scanning Electron Microscopy (SEM)

To preserve internal structure and cell integrity natural mat samples were fixed on board ship for four hours in 2.5% glutaraldehyde, washed 3 times in 1x PBS buffer[8] and stored at 4 °C prior to observation by SEM. SEM analysis of the Fe (hydr)oxide structures produced by NSM enrichments and pure cultures occurred after they had been established for ~9 months and transferred three times. The cultures were fixed in 2.5% glutaraldehyde at 4 °C overnight. Samples were transferred to Whatman 47 mm 0.4 μm track etch membranes and gradually washed with 30 and 15 mM 2-[4-(2-sulfoethyl)piperazin-1-yl] dethanesulfonic acid (PIPES) to remove salts. Dehydration of samples was accomplished through washing with 10%, 25%, 50%, 75%, 90% and 100% ethanol for 5 minutes each. To prevent deformation and conserve surface morphology the samples were critical point dried for 10 minutes at 31.1°C and 1072 p.s.i.. Visualization of the samples was performed on a Philips XL30 field emission SEM (FESEM) at the Nano3 facility of the University of California, San Diego. The SEM was equipped with an Oxford Energy Dispersive X-ray (EDX) attachment and Inca Software; the same instrument was used to determine elemental composition of Fe (hydr)oxides.

---

[8] Per 800 ml of distilled water: 8 g NaCl, 0.2 g KCl, 1.44 g Na_2HPO_4 and 0.24 g KH_2PO_4, adjusted to pH 7.4, filled up to 1 L.

Genbank accession numbers

Sequences from this study have been deposited in Genbank under accession numbers: FJ497252-FJ497715, FJ662871-FJ662909 and GQ329843-GQ329847.

Results

Our investigations at Vailulu'u used an integrated approach focused on Fe (hydr)oxide mats and basaltic rock surfaces. We determined their microbial community composition, using phylogenetic characterization and isolation of FeOB, MnOB and siderophore-producing bacteria and microscopically characterized the Fe (hydr)oxide morphology inside the mats.

1. Molecular Phylogeny

To explore the phylogenetic diversity at Vailulu'u, we prepared clone libraries of 128 to 150 nearly full-length (~1300 bp) sequences of the 16S rRNA gene for two mat samples (NSM = 148 clones; EMM = 129 clones) and one rock sample (NSR = 142 clones). Our clone libraries suggest highly diverse microbial communities in all three samples. Rarefaction analysis comparing the bacterial richness within all samples reveals that the highest richness (Chao1 = 146) can be found on the NSR sample (Figure 2.2). This elevated richness estimate correlates with the one reported for basalts from the East Pacific Rise (440 OTUs) shown to be comparable to the one of terrestrial farm soil (Santelli et al. 2008). Chao1 estimations also indicate that bacterial richness is higher in the EMM (Chao1 = 117) than the NSM (Chao1 = 55). All three samples show a

substantially higher bacterial richness than background seawater samples taken from 1275 m depth at the Juan de Fuca Ridge (Huber et al. 2003) and from 2572 m depth at the East Pacific Rise (Santelli et al. 2008).

The NSM is dominated by ε-proteobacteria (67%; Figure 2.3A), with minor quantities of γ-(11%), α-(3%) and δ-proteobacteria (3%). In addition, we find Cytophaga-Flavobacteria-Bacteroides (CFB, 5%) and a minor abundance of Planctomyces (Figure 2.3A). The majority of clones from this mat are most closely related to uncultured strains from deep-sea hydrothermal environments. Fifty two percent (77 clones within 2 OTUs) of the clones were also found in an iron-containing mat at the Tangaroa Seamount, Kermadec Arc (Hodges and Olson 2009). The two most abundant OTUs in the NSM clone library (OTU_2 and OTU_6, Table 2.S2) were most similar to an uncultured γ-proteobacterial sponge symbiont found at the Great Barrier Reef (EU335079, OTU_6, similarity score (ss): 0.966) and the uncultured ε-proteobacterium clone (TF-16) from Tangaroa Seamount (FJ535281, OTU_2, ss: 0.991). Based on their phylogenetic relationship to cultured strains three-quarters of all of clones in this sample are closely related to sulfur-metabolizing bacteria (data not shown). Most of the close relatives (94.6%) are aerobic sulfur-oxidizers (Inagaki et al. 2003), while a few have been identified as sulfur-reducing strains. The remaining OTUs have very little resemblance to any specific metabolism.

The EMM is dominated by γ-proteobacteria (42%) and bacteria belonging to the CFB-group (38%) (Figure 2.3B). Other groups included ε- (8%), δ- (5%), α-

proteobacteria (4%). The two most abundant OTUs were most closely related to an uncultured γ-proteobacterium (DQ334375, OTU_2, ss: 0.999; Table 2.S2) and an uncultured Bacteroidetes bacterium (AM706607, OTU_5, ss: 0.994). Many clones from this library can be directly related to cultured organisms from a range of submarine environments. About 40% of the clones are genetically similar to cosmopolitan deep-sea strains found in hydrothermally active areas. 10% of sequences are most closely related to published strains from CH_4 and H_2S-rich environments (Sunamura et al. 2004). The other half of the clones can be correlated with bacteria from various non-hydrothermally influenced locations, including surface water. Overall 14% (18 clones within 11 OTUs) of the clones from this sample are phylogenetically most closely related to two uncultured strains (CM7 and CM10) amplified from an iron-manganese-rich hydrothermal mound at the Cleft Segment, Juan de Fuca Ridge (Davis et al. 2009, in press). Physiological are likely to be very diverse (Figure 2.4). Almost half of the clones also cluster with isolates of heterotrophic FeOB identified in this study (see below). Phylogenetic affiliation to cultured organisms showed that 16% of total clones can be related to cultured sulfur-metabolizing strains, about half of them appeared to be involved in sulfur reduction (Vogt et al. 2008), 30% in sulfur-oxidation (Inagaki et al. 2003), 20% in sulfite-oxidation (Ivanova et al. 2004) and 5% in sulfide-oxidation (Wirsen et al. 2002). Two of our clones are most closely related to methylotrophic bacteria (Chan and Anthony 2006).

Taxonomic groups recovered from the NSR are dominated by α- (17%) and γ-proteobacteria (44%) (Figure 2.3C). ε-proteobacteria make-up only 11% of the

sequences. Other phyla present include δ-proteobacteria (9%), CFB-group bacteria (6%) and β-proteobacteria (1%). Two clone sequences (VS_CL-318 and -407) match *Mariprofundus ferrooxydans* PV-1 within the ζ-proteobacteria. The two most abundant OTUs recovered from this sample (OTU_5 and OTU_11, Table 2.S2) are most closely related to an uncultured γ-proteobacterium pIR3BD09 amplified from carbonate-rich metalliferous sediment sample from the Rainbow vent field on the Mid-Atlantic Ridge (AY354134, OTU_5, ss: 0.993) and γ-proteobacterium EPR 3967-12-Bc73 (EU491877, OTU_11, ss: 0.992) recovered from the interior of slightly altered basalt samples collected at the East Pacific Rise (EPR) (Santelli et al. 2008). Sequences amplified from the rock sample are closely related to mostly uncultured strains found in a wide range of locations, 17% of which (24 clones, 14 OTUs) were also found on basalt samples from the EPR. Thirty nine percent of the clones show close phylogenetic similarity to sulfur-metabolizing strains. Similar to the mat from this location the majority (70%) appears to be linked to sulfur-oxidation (Inagaki et al. 2003). The remaining 30% are similar to sulfur-reducing bacteria (Purdy et al. 2003).

2. Isolation of FeOB, MnOB and Siderophore-producing strains

We isolated a total of eighty-seven FeOB, MnOB and siderophore-producing bacteria from a large number of locations, with sixty-three of them being non-identical based on their 16S sequence data (ElimDupes; Table 2.S1). The largest number of isolates from any particular location come from the NSM (22) and the NSR (7). Three isolates come from the EMM and the remaining isolates come from other locations at Vailulu'u and the submarine slopes of nearby Ta'u Island (Table 2.S1). 16S sequences

revealed that the majority of isolated strains belong to the class of γ-proteobacteria (85%) with *Pseudoalteromonas* being the most abundant genus (41% of all isolated strains). Other genera within the γ-proteobacteria include *Pseudomonas* (19%), *Halomonas* (7%), *Marinobacter* (5%), *Vibrio* (3%), *Shewanella* (2%) and *Idiomarina* (1%). Thirteen percent of all isolated strains cluster within the class of α-proteobacteria and 2% belong to the *Actinobacteria* (Figure 2.5).

Thirty-two out of eighty-nine strains show Fe(II) oxidation capability under heterotrophic conditions as determined by Prussian Blue test. The majority of them were isolated at pH 7.5, only three at pH 6. Seven strains of FeOB were isolated under oligotrophic conditions, four from microaerophilic enrichment cultures and three from xFe plates. The microaerophilic enrichments yielded the only obligate oligotrophs in our study. Twenty-one MnOB were isolated as determined by LBB test. Of those, eighteen strains were isolated on organic-rich enrichments (K, M, LEPT) while three strains were obtained through isolation on oligotrophic, carbon depleted "xMn" plates. We isolated a total of thirty-four siderophore-producers using CAS plates (Figure 2.5, Table 2.S1). Noticing a close phylogenetic similarity of several strains isolated on different media lead us to further test fifteen of our heterotrophic FeOB for the production of siderophores on CAS. Three strains isolated on "F"-plates at pH 7.5 (VS_57, 62 and 55) were tested positive for siderophore production.

Based on close phylogenetic relatedness within a maximum likelihood tree (Figure 2.4) we can divide our isolates into five groups of highly similar organisms:

-Group 1: three FeOB (VS-38, -50 and -60) and one siderophore-producing strain (VS-121).

-Group 2: six siderophore-producing strains (VS-103, -105, -106, -108, -117 and -119) and two FeOB (VS-39 and VS-44).

- Group 3: two FeOB (VS-74 and -77) and five siderophore-producing strains (VS-15, -23, -34, -114 and -116).

-Group 4: two FeOB (VS-75 and -79) and four siderophore-producing strains (VS-12, -30, -31 and -49).

- Group 5: three obligate oligotrophic FeOB (VS-124, -126 and -127).

We observed many cases of multiple isolations of identical organisms under diverse metabolic conditions (Table 2.1). As an example, oligotrophic MnOB VS-108 was identical to two heterotrophic MnOB (VS-1 and -3), one heterotrophic FeOB (VS-72) and CAS-active strain VS-122. VS-3, -108 and -72 were isolated from a scoop sample while VS-1 was isolated from basalt. They were all closely related to type strain *Pseudoalteromonas mariniglutinosa* KMM 3635 (ss: 0.990) isolated from the marine diatom *Chaetoceros lauderi* (Romanenko et al. 2003).

Understanding of the metabolic capabilities of our isolates is useful for further interpretation of environmental clone libraries. There is substantial overlap between our newly isolated FeOB, MnOB and siderophore-producing strains and clones obtained from the EMM (Figure 2.4). Specifically, based on a pairwise distance matrix, isolates

from Group 3 (4 members) were 99.8% similar to OTU_30 (2 clones). Fe-oxidizing isolates VS-57 and -63 were 99.8% and 99.9% similar to OTU_2 (19 clones) and 99.7% and 99.8% similar to clone M2p72. Siderophore-producing isolate VS-116 was 98% similar to clone M2p58. Group 4, consisting of 17 members matched OTU_19 (8 clones) by 100% (Figure 2.4). Correlations between the clone libraries and cultured organisms from the NSM or NSR are weak.

3. Fe (hydr)oxide mat structures

Some FeOB-microorganisms produce morphologically characteristic mineral products and organic structures that can be found in Fe (hydr)oxide mats studied in a variety of locations (Emerson and Moyer 2002; Hodges and Olson 2009). At Vailulu'u, we visualized the natural mat from Nafanua summit (Figure 2.6a+b), an enrichment culture of lithotrophic FeOB from Nafanua summit (644-X1) (Figure 2.6c+d), and an isolate (GQ329846 closely related to *Thioclava pacifica* TL-2, ss: 0.982*)* from an enrichment culture from sample 644-X1 (Figure 2.6e) using SEM. We also imaged an abiotic control (Figure 2.6f) as a contrast for our laboratory enrichments. Fe (hydr)oxide structures observed in all samples resemble those seen at other hydrothermal environments (Emerson and Moyer 2002; Hodges and Olson 2009; Rentz et al. 2007). Structures range from helical "stalks", tubular "sheaths" and "y-shaped", irregular filaments to amorphous particles and long filamentous minerals (Figure 2.6). While the natural mat and the enrichment culture appear to be a mixture of all of these structures with tubular "sheaths" being most abundant, the isolated culture appears to exclusively produce amorphous particles (Figure 2.6e). The abiotic control shows an abundance of

elongated and filamentous oxides and amorphous particles albeit in lower numbers (Figure 2.6f). EDX analysis identified all of those structures as Fe-oxides (data not shown). Even though most of the Fe-oxide structures observed in the natural samples resemble those produced by previously described lithotrophic FeOB and are therefore considered to be biogenic, in our case they cannot be ascribed to the activity of specific FeOB. Regular helical "stalks" resemble those produced by the β-proteobacterium *Gallionella ferruginea* (Emerson and Ghiorse 1993). However, presence of *Gallionella ferruginea* in the deep-sea environment has not been demonstrated (D. Emerson pers. comm.). Twisted stalks resembling those produced by *Gallionella* have more recently been shown to be also produced by *Mariprofundus ferrooxydans* PV-1, a representative of the new clade of ζ-proteobacteria (Emerson et al. 2007). Tubular "sheaths" shown to be very abundant in the natural mat (Figure 2.6a+b) have previously been attributed to the activity of the freshwater β-proteobacterium *Leptothrix ochracea* (Ehrlich 1996). "Y-shaped" irregular filaments have been abundantly found in mats from other locations (Emerson and Moyer 2002) but have yet to be uniquely attributed to the activity of FeOB. Few ζ-and no β-protoebacterium could be detected in the mat samples from Vailulu'u (Figure 2.3; Table 2.S2) indicating that those groups of bacteria might not be very abundant in this environment. However, overall the physical appearances of microbial mats and the products of cultures from these mats display substantial resemblance to microbial mats from other locations.

Discussion

1. Phylogeny

Characterizing the phylogeny of thriving microbial communities in deep-sea volcanic environments is critical in determining the dominant microbial groups and biogeochemical activities. Our data will help to constrain which clades are cosmopolitan and which ones appear to be specific to particular environmental conditions or niches, which is critical for then exploring the feedbacks between biological, chemical and physical processes in submarine volcanic systems.

In the past decade several molecular and culture-based techniques (e.g., t-RFLP, DGGE, small subunit (16S) rRNA gene clone libraries) have been used to characterize microbial communities in seafloor volcanic-hydrothermal environments including mid-ocean ridges (Edwards et al. 2003; Longnecker and Reysenbach 2001; Lysnes et al. 2004; Mason et al. 2007; Santelli et al. 2008; Sogin et al. 2006), seamounts (Emerson and Moyer 2002; Mason et al. 2007; Moyer et al. 1995; Santelli et al. 2008; Templeton et al. 2005) and arc settings (Hodges and Olson 2009) at a variety of seafloor depths. These studies focused on two main sample types, rock surfaces and hydrothermal Fe (hydr)oxide mats. To date, it appears that in low to mid-temperature seafloor volcanic and hydrothermal settings microbial communities are dominated by proteobacteria, independent of the type of material analyzed. Interestingly, proteobacterial phyla from these settings show some rather systematic distributions for different sample types. Fe (hydr)oxide mats appear to be less diverse and tend to be dominated by ε-proteobacteria

(Davis and Moyer 2008; Hodges and Olson 2009; Longnecker and Reysenbach 2001; Moyer et al. 1995). ζ-proteobacteria recently shown to be abundant in Lo'ihi mats (Rassa et al. 2009, submitted) are much rarer in Fe (hydr)oxide mats from Vailulu'u (this study). It is not clear whether this reflects a true difference in community structure or is due to artifacts from the method of sampling and/or choice of primers. Future comparisons on a more quantitative basis (e.g. q-PCR) may provide more insight. Basalt surfaces are more diverse and they appear to be commonly dominated by α- and γ-proteobacteria (Lysnes et al. 2004; Mason et al. 2007; Santelli et al. 2008). Our samples from Nafanua display the same type of phylogenetic dichotomy between sample types. α- and γ-proteobacteria dominate on the NSR, and ε-proteobacteria dominate on the NSM. Our second mat sample from the eastern moat, however, does not fit this distribution: While being dominated by γ-proteobacteria and CFB-group bacteria only 8% of the EMM clones fall into the class of ε-proteobacteria, offering evidence that Fe (hydr)oxide mats may not always be dominated by this class.

Despite their relative phylum and class level simplicity, seafloor volcano microbial communities display only minimal strain – level similarity between different locations. Currently available clone libraries for Fe (hydr)oxide mats and rocks generally show large numbers of strains that have been found in a variety of settings, but the strains found in a particular location tend to be distinct, with very little overlap between locations. We compare our mat data to mats from three other settings, the EPR (Longnecker and Reysenbach 2001), Lo'ihi Seamount (Moyer et al. 1995) and the Tangaroa Seamount (Hodges and Olson 2009). In mat communitites from the EPR and

Lo'ihi Seamount, even though they also show a great abundance of ε-proteobacteria, individual strains are not closely related to each other. In comparison two OTUs from the NSM were phylogenetically closest related to clones from a mat collected at the Tangaroa Seamount. Our rock sample from Nafanua (NSR) is best compared to clone libraries from rock surfaces from the EPR and Lo'ihi Seamount (Santelli et al. 2008). The largest similarity was found between strains in the NSR and the EPR whereby 17 % of the NSR strains overlap. This comparison shows that our data provide only very few strain-level similarities to those corresponding sample types from other settings. However, strain-level characterizations provide insight into the highly diverse communities inhabiting deep-sea hydrothermal samples as they display an adaptation to specific hydrothermal setting and its local conditions.

2. Microbial Function

Understanding microbial function in hydrothermal–volcanic deep-sea habitats is key to understanding the ecology of the deep-ocean crustal biosphere, its bio-geochemical fluxes and controls on primary productivity. Electron donors in volcanic/hydrothermal systems include in particular H_2, H_2S, S^0, Fe(II) and Mn(II), CH_4 as well as iron-sulfides. Electron acceptors include in particular dissolved O_2, NO_3^-, S^0, SO_4^{2-} or Fe(III) from oxidized volcanic Fe. At Vailulu'u Fe, Mn and sulfide are likely the most abundant and continuously available electron donors (Hart et al. 2000; Staudigel et al. 2006). Dissolved O_2 widely available at the summit of Nafanua, is likely to be absent or in minimal supply in the crater moat. In addition, one might consider that basalt-hosted systems contain a variety of nutrients and micronutrients in substantially higher

quantities than they are available in seawater which could also contribute to the growth of microbes in these systems, such as elevated levels of CO_2, P, or trace metals all needed for a range of prokaryotic cell functions.

One of our key goals is to explore the relationships between local geochemical environment and predominant microbial functions. First, we will explore the phylogenetic similarity of Vailulu'u clones to already characterized microbial organisms, and then we will evaluate their potential function on the basis of our culturing efforts. Each perspective offers valuable and complementary information.

Our clone libraries from two distinct geochemical environments (Nafanua and the eastern moat) show significant similarities to bacterial strains known for metabolisms that are consistent with the predicted energy sources for each environment. For example, in addition to a number of FeOB recovered from the Nafanua libraries, clones from this location are closely related to organisms that specialize in aerobic sulfur oxidation *(Sulfuvorum lithotrophicum* (T), 42BKT; AB091292; *Sulfurimonas autotrophica* (T), OK10; AB088431, Inagaki et al. 2003) as found in mats from Lo'ihi Seamount (Moyer et al. 1995; Rassa et al. 2009). This process offers high energy yields, and includes an electron donor that is quite common in hydrothermal systems. Sulfides enriched in hydrothermal plume water and dissolved O_2 from overlaying waters provide a substantial energy yield that could be responsible for the dominance of such organism in the mats at Nafanua. Metabolic functions of cultured strains similar to EMM clones appear to be much more diverse than NSR which suggests that there is no preferred energy source that

offers particularly high yields. However we are aware of the limitations of inferring metabolic function from phylogenetic position.

We find FeOB, MnOB and siderophore producers in all three samples characterized by clone libraries. This is clearly a reflection of the local chemical environments, but it does not provide any specificity for any of the three samples. Phylogenetic characterization of Fe- and Mn-oxidizing bacteria at Lo'ihi Seamount and the Juan de Fuca Ridge suggest that they are common within the α-, γ- and ζ-proteobacteria (Edwards et al. 2003; Emerson and Moyer 2002; Emerson et al. 2007; Templeton et al. 2005).

The abundance of siderophore producing bacteria in deep-sea environments has received little attention so far, but our results from Vailulu'u suggest that siderophore production appears to be quite common. Twenty-eight of our isolated strains produce siderophores, probably not too surprising given the abundance of Fe(III) in these environments. They may have two main functions, increasing Fe availability to cells and decreasing the amount of Fe(III) oxides which could encase the cells through metal complexation. Intriguingly, siderophore-producing fungi also appear to be common in the mats and rock surfaces at Vailulu'u.

3. Multifunctionality

Templeton et al. (2005) showed that many MnOB from Lo'ihi are actually heterotrophs, drawing attention to the fact that microbes in volcanic-hydrothermal

environments may display more than one metabolic function, and that microbial metal oxidation may not be directly linked to lithoautotrophic growth. The abundance of heterotrophic MnOB at Vailulu'u is consistent with the data from Lo'ihi, including the fact that many of the MnOB isolated from Vailulu'u are closely related to Lo'ihi strains.

About one quarter of the Vailulu'u isolates are identical to at least one Vailulu'u isolate obtained by a different isolation method. Furthermore, we tested fifteen heterotrophic FeOB for growth on CAS plates and found that three of them also produced siderophores. While we did not specifically aim our study at multifunctionality, these results do suggest that multiple metabolic functions are a common trait of microbial communities in seafloor volcanic systems. While we don't truly understand the benefits of Fe and Mn oxidation and siderophore production by heterotrophs in these systems, multifunctionality is likely to be an adaptation mechanism that helps microbes to succeed in oligotrophic environments or environments subject to fluctuating chemical conditions. Multiple functions may also help microbes to out-compete specialists simply by being able to draw energy or nutrients from multiple sources. Hence, we suggest that multifunctionality of bacteria may represent an important and probably common trait that helps microbes adapt to deep-sea hydrothermal environments, offering an opportunity for further investigation.

4. Fe (hydr)oxide structures

The abundance of Fe (hydr)oxide mats in a variety of hydrothermal settings has been shown before (Boyd and Scott 2001; Davis and Moyer 2008; Hodges and Olson

2009; Karl et al. 1989; Karl et al. 1988; Staudigel et al. 2006) . Fe-oxide structures within those mats range from filamentous and “y-shaped” oxides to regular helical “stalks”, tubular “sheaths” and amorphous minerals. SEM analysis of an Fe (hydr)oxide mat from Vailulu’u Seamount matches those findings indicating that a cosmopolitan morphological composition of these mats may exist.

Many of the morphologically distinct Fe-oxide structures are considered to have a biogenic origin (Hodges and Olson 2009). Low-oxygenated waters, hydrothermal emissions and basaltic rocks enriched in reduced metals are commonly associated with magmatically active deep-sea environments. They provide ideal conditions for lithotrophic FeOB to thrive offering an opportunity to compete with the otherwise rapid abiotic processes governing Fe(II) oxidation (Druschel et al. 2008; Rentz et al. 2007). Certain groups of organisms including the novel class of ζ-proteobacteria and some strains from with the α- and γ-proteobacteria have been shown to be involved in the formation of certain Fe-oxide structures found in the mats (Edwards et al. 2003; Emerson and Moyer 2002; Emerson et al. 2007). However, the majority of structures are still of unknown origin. While only few ζ-proteobacteria have been found in Vailulu’u mats, diverse groups of heterotrophic FeOB have been shown to be generally abundant and could be responsible for the formation of some of the characteristic oxides as suggested previously (Hodges and Olson 2009).

Conclusions

Isolation of 89 new organisms from Vailulu'u seamount (Samoa) and three detailed 16S rRNA gene clone libraries from two Fe (hydr)oxide mats and a rock sample offer new insights into phylogenetic diversity, metabolic versatility and environmental controls of diversity and function in volcanically-active submarine systems.

- The phylogeny of Fe (hydr)oxide mats and basaltic rocks from Nafanua is dominated by proteobacterial communities that are very similar at a class level to equivalent samples from other seafloor hydrothermal systems with a particularly high abundance of ε-proteobacteria (Hodges and Olson 2009; Longnecker and Reysenbach 2001; Moyer et al. 1995). However, a mat sample from the deeper crater is much more diverse and has a distinct microbial community suggesting a type volcanic ecological setting that has not been explored previously.

- Vailulu'u crater offers a natural laboratory to compare microbial communities in rather specific hydrothermal environments. Steady exposure to dense hydrothermal plumes correlates with microbial communities that have close phylogenetic similarity with bacteria involved in a variety of sulfur metabolisms or have been shown to gain energy through the oxidation of metals such as Fe(II)and Mn(II). At the interface between hydrothermal plume and open seawater, microbial communities are dominated by strains with similarities to known aerobic sulfur-oxidizing ε-Proteobacteria. These phylogenetic comparisons lead us to suggest the local microbial communities may have specifically

adapted to local environmental conditions.

- About one quarter of all microbial isolates from Vailulu'u display multiple metabolic functions, including heterotrophy, Fe(II) and/or Mn(II) oxidation and/or siderophore production. We suggest here that metabolic versatility is likely to be an important trait in oligotrophic habitats.

- Fe (hydr)oxide mat structures at Vailulu'u resemble those found in various other hydrothermal settings. Despite the fact that FeOB appear to be abundant at Vailulu'u it remains unclear which microbes are directly responsible for the formation of most of the Fe-oxide structures found in those mats.

Overall, this work shows that our understanding of microbial community structure and function in seafloor volcanic system is increasingly aided by phylogenetic comparisons across sites. To converge towards a much better understanding of the environmental controls, more detailed geochemical measurements of local environments will be required, as well as targeted culturing of community members directly involved in the cycling of Fe, Mn, CH_4, and sulfide under relatively low-temperature conditions. Such efforts are a critical and necessary step towards identifying, and understanding the activities of complex microbial communities in dynamic bio-geochemical systems.

Acknowledgements

The authors would like to thank the Captain and crew of the R/V Ka'imikai O' Kanaloa as well as the pilots and support staff for the HURL Pisces IV/V submersibles. Additional thanks to Daniel Rogers and Katrina Edwards for the protocol used for "F-plates", Rick Davis for his help with Dotur, Ryan Anderson at the Nano3 facility at UCSD for his assistance on the SEM and last but not least to Brad Bailey for his help in American Samoa and in the laboratory. The authors would also like to acknowledge the thoughtful comments of Dave Emerson and two anonymous reviewers. We would like to thank our funding sources for this work including the NSF Microbial Observatories and Biogeosciences programs (MCB-0348668 and OCE-0433692), NSF Ocean Sciences (OCE0526285), and the Agouron Institute. Any opinions, findings and conclusions or recommendations expressed in this material are those of the author(s) and do not necessarily reflect the views of these agencies.

***

The text of Chapter II, in full, is a reprint of the material as it appears in the Geomicrobiology Journal, 26: 8, 581-596. I was the primary investigator and author of this article. Alexis Templeton and my two advisors, Bradley Tebo and Hubert Staudigel were co-authors.

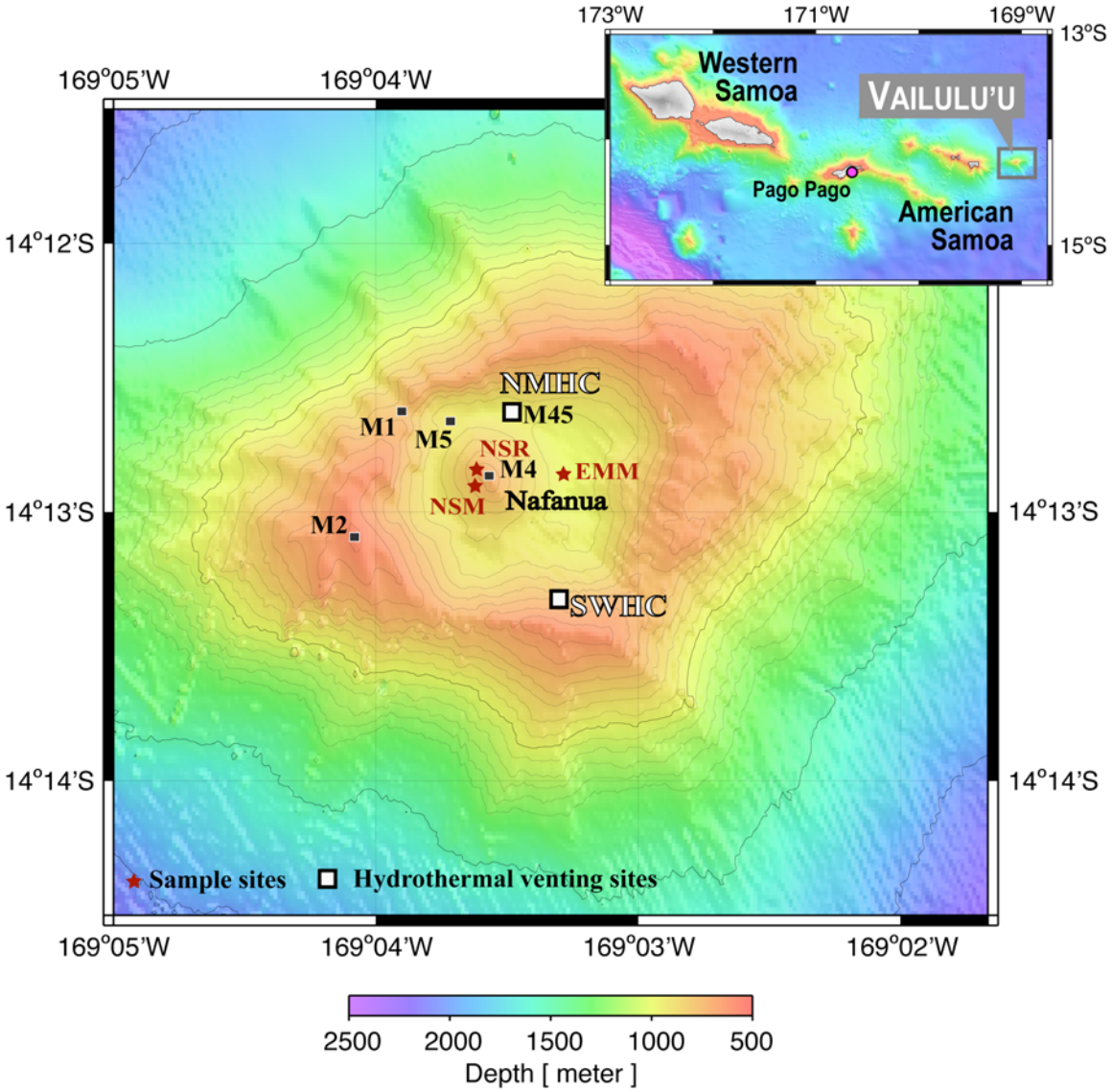

Figure 2.1: Bathymetric map of the summit region of Vailulu'u Seamount located to the East of Ta'u island the easternmost island of the Samoan archipelago (inset, modified from Staudigel et al., 2006). Clone library sample locations are indicated by red stars. Additional sample locations are indicated by Markers (M1, M2, M4, M45), the Northern Moat Hydrothermal Complex (NMHC) and the South Wall Hydrothermal Complex (SWHC). Note that sampling sites for Ta'u island and M 6 and M7 are outside the map. M1 marks the northwest breach in the crater, M2 the shallowest point of Vailulu'u and M4 is located at the summit of Nafanua that was formed during an eruption in November/December 2004. Nafanua is surrounded by a "moat" that represents the deepest portion of the crater and involves exposure to the densest hydrothermal plume waters.

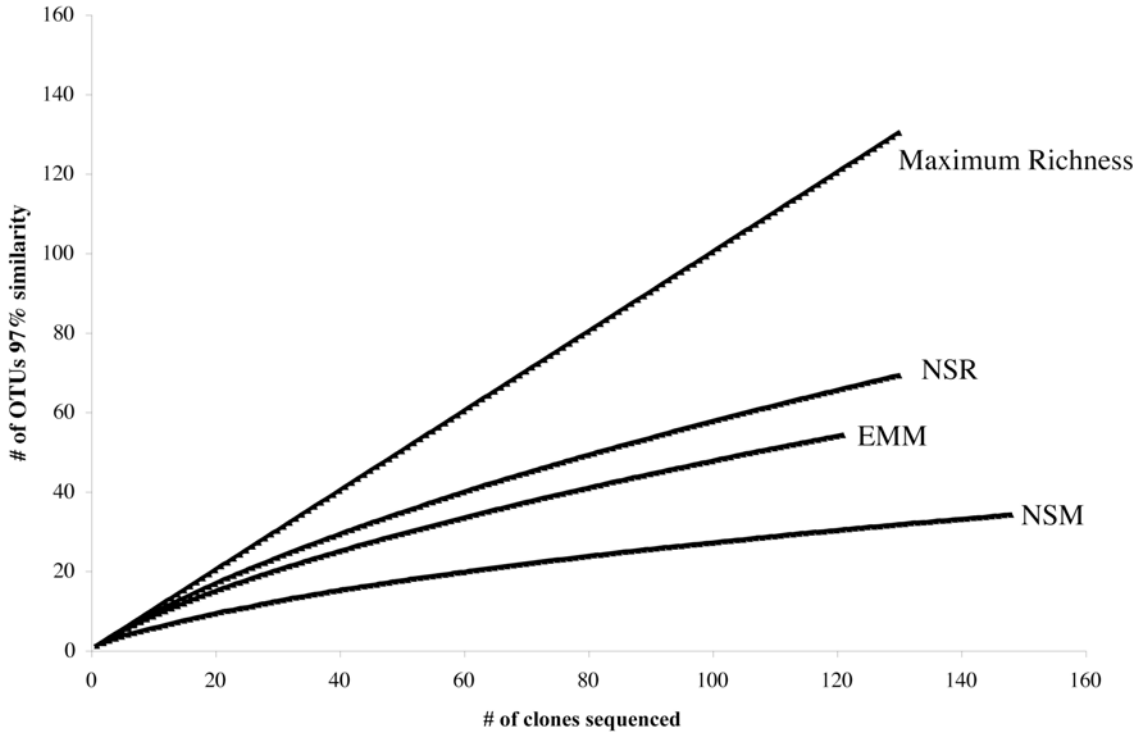

Figure 2.2: Rarefaction curves for clone libraries obtained from the Nafanua Summit Mat= NSM, the Nafanua Summit Rock= NSR and the Eastern Moat Mat = EMM. Species richness is shown to be highest in the NSR (Chao : 146), intermediate in the EMM (Chao1: 117) and lowest in the NSM (Chao :55) .

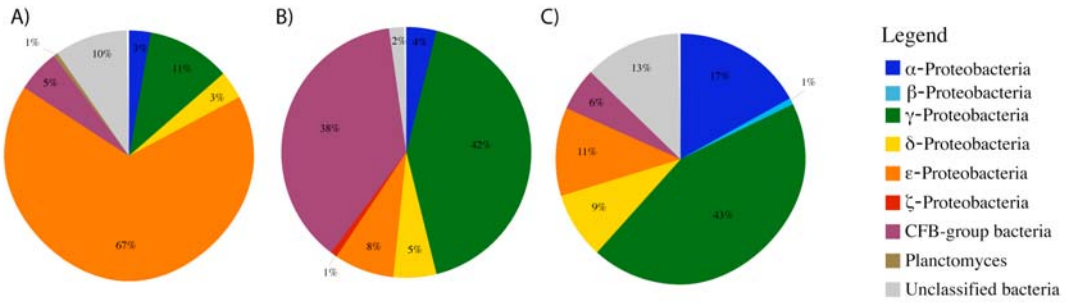

Figure 2.3: Phylogenetic composition of two mat samples and one rock sample from Vailulu'u seamount based on 16S rRNA gene data. A: Nafanua summit mat = NSM, 707 m: 148 clones total; B: Eastern Moat mat = EMM, 986 m: 129 clones total; C: Nafanua summit rock = NSR, 752 m: 142 clones total.

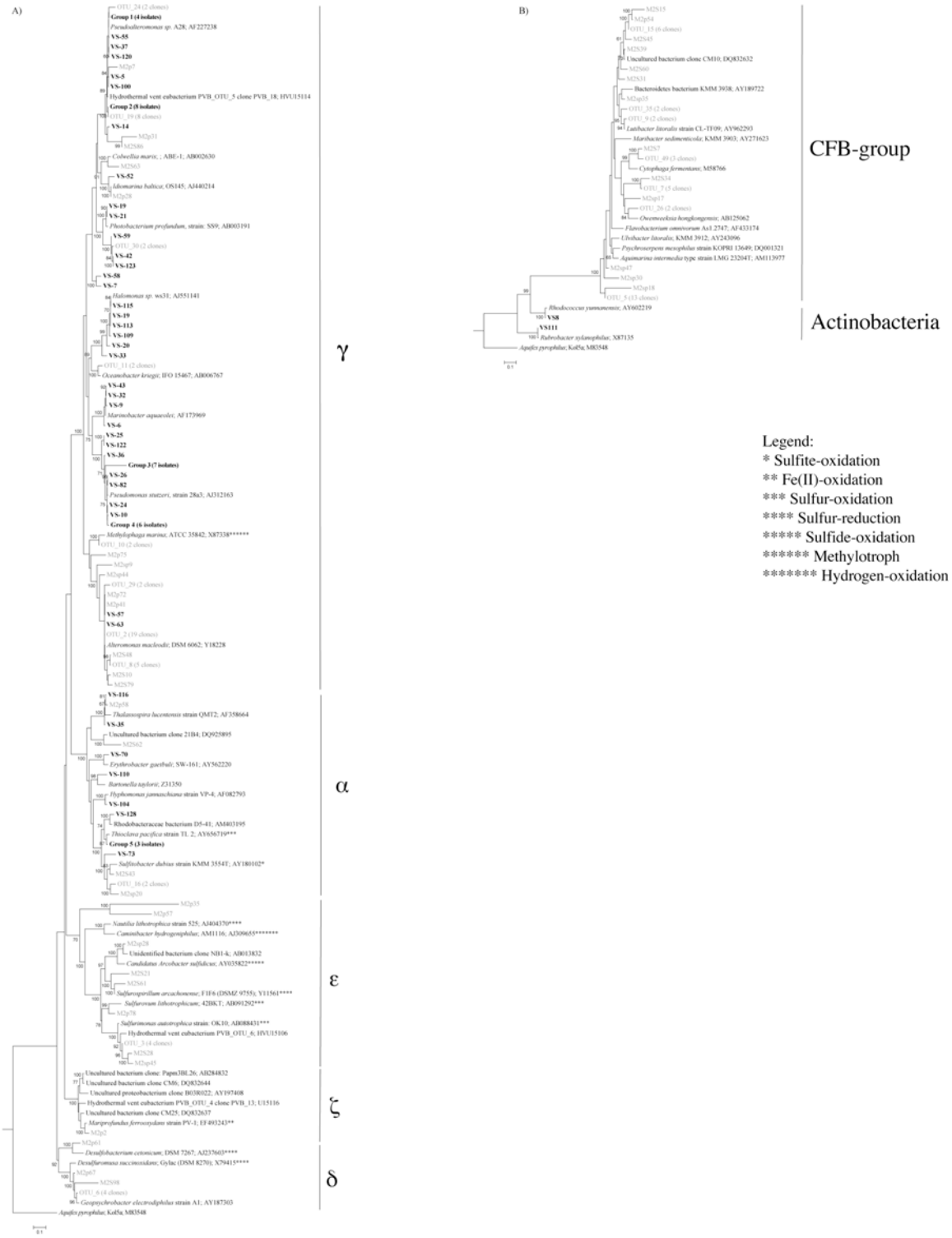

Figure 2.4: Phylogenetic affiliation of 16S rRNA genes retrieved from the EMM and Fe and MnOB as well as siderophore-producing strains isolated from a number of samples from various locations at Vailulu'u: A) Proteobacteria, B) CFB-group and Actinobacteria. Isolated strains are marked in bold. Clones from the EMM are marked in light grey while the most closely related type strains are marked in *italic*.

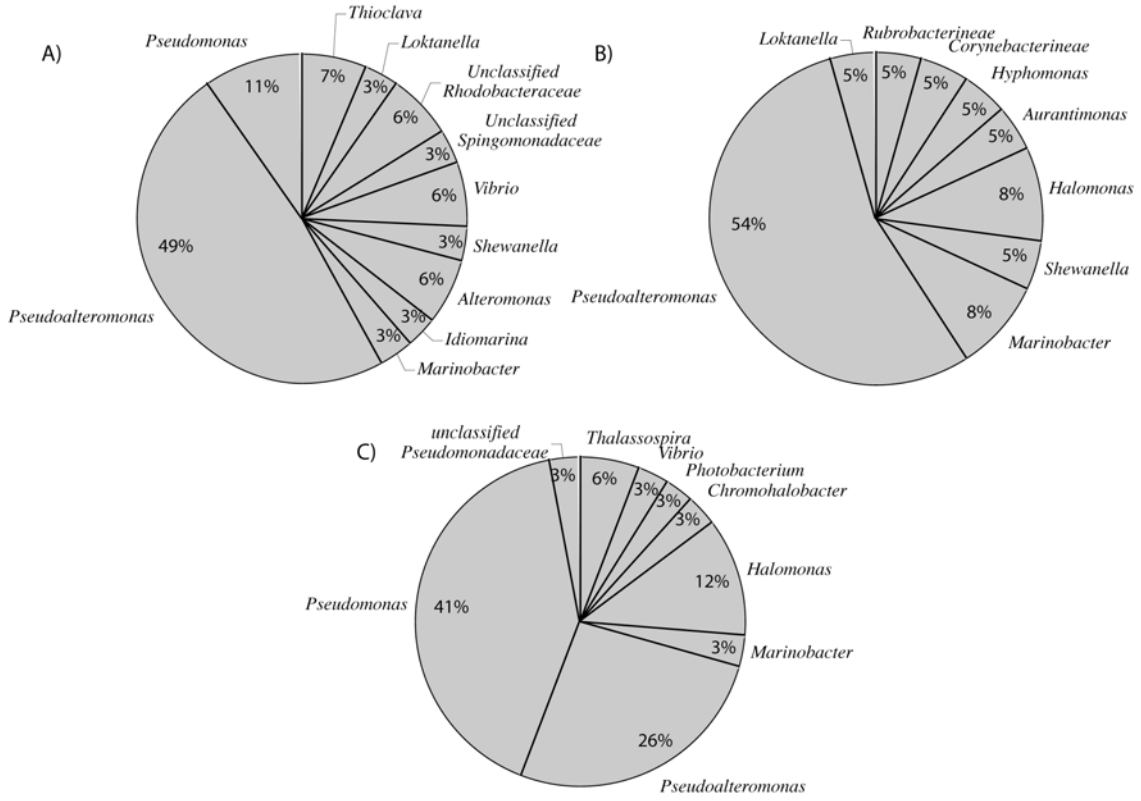

Figure 2.5: Phylogenetic distribution of cultured strains of A) Fe(II) oxidizing bacteria (32 total), B) Mn(II) oxidizing bacteria (21 total) and C) siderophore-producing strains (34 total).

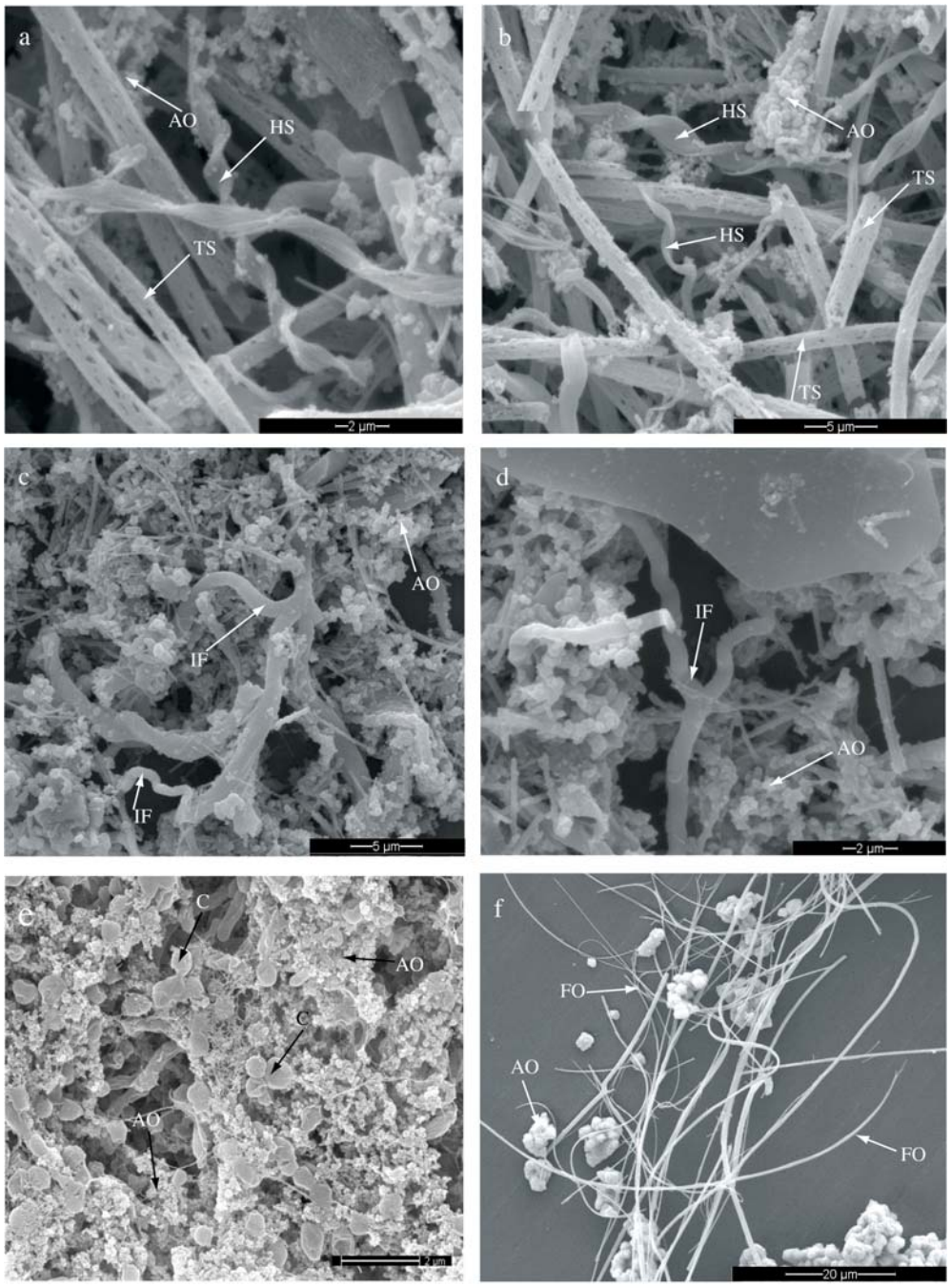

Figure 2.6: Scanning electron micrographs of Fe (hydr)oxides found in a natural mat sample from the summit of Nafanua (NSM: a+b); a microaerophilic enrichment culture of lithotrophic FeOB from the NSM (c+d); an isolated culture from those enrichments (e) and an abiotic control of the same experimental set-up (f). Letters indicate different Fe (hydr)oxide morphologies: AO = Amorphous oxides, HS = Helical "stalks", TS = Tubular "sheaths", IF = Irregular, y-shaped filaments, FO = filamentous oxides, C = Cells.

Table 2.1: List of identical isolated strains identified by ELIMDUPES analysis showing the identical strains, the metabolism they were isolated for, the sample type and their closest related type strain identified via SeqMatch including the similarity score. Listed are only identical strains isolated for a variety of metabolisms. Sample types include rocks "R", mats "M", sediment scoops "S" and exposed basalts with normal composition "NB".

Strain	**Identical strains**	**Metabolism**	**Sample types**	**Closest type strain**	**Similarity score**
VS-14	VS-78	Siderophore production, heterotrophic Fe	R	*Pseudoalteromonas issachenkonii* (T); KMM 3549	0.997
VS-120	VS-46	Siderophore production, heterotrophic Fe	M	*Pseudoalteromonas aliena* (T); KMM 3562	0.987
VS-12	VS-80, -83, -71	Siderophore production, heterotrophic+ oligotrophic Fe	R+M	*Pseudomonas stutzeri* (T); CCUG 11256	0.995
VS-108	VS-1, -3, -72, -122	Oligotrophic Mn, Heterotrophic Mn+Fe, Siderophore production	NB+S+R	*Pseudoalteromonas mariniglutinosa* KMM 3635	0.990
VS-121	VS-41, -4	Siderophore production, heterotrophic Fe+Mn	R+S	*Pseudoalteromonas aliena* (T); KMM 3562	0.989
VS-39	VS-118	Heterotrophic Fe, Siderophore production	R+S	*Pseudoalteromonas mariniglutinosa* KMM 3635	0.990
VS-55		Heterotrophic Fe, Siderophore production	M	*Alteromonas* sp. SSN-6	0.999
VS-57	VS-62	Heterotrophic Fe, Siderophore production	M	*Pseudoalteromonas* sp. S511-1	0.999
VS-119	VS-49, -53	Heterotrophic Fe, Siderophore production	R, M	*Pseudoalteromonas mariniglutinosa* (T)	0.990
VS-73	VS-101	Heterotrophic Fe+Mn	S, R	*Loktanella hongkongensis* (T)	0.989

Table 2.S1: Isolated strains of Fe(II)- and Mn(II)-oxidizing and siderophore-producing bacteria from Vailulu'u Seamounts. Samples used for isolation include Fe (hydr)oxide mats, basaltic rocks and volcanic sediment samples. Besides the strain ID the table provides information on the sample location, the closest related type strain, the medium (and pH) the strains were isolated on, the type of inoculum (S: Scoop, R: rock, M: mat, NB: normal basalt, Rhy: Rhyolite, Qz: Quarz), the indicated physiological function and the number of times a strain was isolated. Samples indicated with an "a", "b", "c", "d" and "e" represent bacteria belonging to five phylogenetically closely related groups: Group 1 ("a"), 2 ("b"). 3 ("c"), 4 ("d") and 5 ("e") (Figure 2.4).

Strain ID	Location	Closest BLAST	Accession #	Similarity score	Medium	Inoculum	Isolate type	# of isolat-ions
VS-4	M1	*Pseudoalteromonas aliena* (T); KMM 3562	AY387858	0.989	K	R, M	Heterotr. Mn	1
VS-5	M6	*Pseudoalteromonas aliena* (T); KMM 3562	AY387858	0.986	K	M	Mn	1
VS-6	M4	*Marinobacter flavimaris* (T); SW-145	AY517632	0.998	K	M	Heterotr. Mn	1
VS-7	M7	*Shewanella benthica* (T); ATCC 43992	X82131	0.989	K	R, M	Heterotr. Mn	1
VS-8	M4	*Rhodococcus fascians* (T); ATCC 12974T	X81930	0.995	M	R	Heterotr. Mn	1
VS-9	M4	*Marinobacter algicola* DG893 (T)	AY258110	0.992	K	R	Heterotr. Mn	1
VS-10	M2	*Pseudomonas stutzeri* (T); CCUG 11256	U26262	0.992	CAS	Exposure Rhy	Sid. prod.	1
VS-11	M6	*Pseudomonas stutzeri* (T); AW-1	AY017341	0.995	CAS	M	Sid. prod.	1
VS-12d	N of Ta'u	*Pseudomonas stutzeri* (T); CCUG 11256	U26262	0.995	xFe, F6, CAS	R, M	Oligotr. + heterotr. Fe, Sid. prod.	7
VS-13	Southern pit wall	*Pseudomonas plecoglossicida* (T); FPC951	AB009457	0.958	CAS	M	Sid. prod.	1
VS-14	N of Ta'u	*Pseudoalteromonas issachenkonii* (T); KMM 3549	AF316144	0.997	F7.5, CAS	R	Heterotr. Fe, Sid. prod.	2

(Table 2.S1: Isolated strains of Fe(II)- and Mn(II)-oxidizing and siderophore-producing bacteria from Vailulu'u Seamount, Continued)

Strain ID	Location	Closest BLAST	Accession #	Similarity score	Medium	Inoculum	Isolate type	# of isolat-ions
VS-15c	N of Ta'u	*Pseudomonas plecoglossicida* (T); FPC951	AB009457	0.997	CAS	R	Sid. prod.	1
VS-19	N of M4	*Halomonas meridiana* (T)	M93356	0.998	CAS	M	Sid. prod	1
VS-20	N of M4	*Halomonas sulfidaeris* (T); Esulfide1; ATCC BAA-803	AF212204	0.985	CAS	M	Sid. prod.	1
VS-21	M4	*Photobacterium frigidiphilum* (T); SL13	AY538749	0.999	CAS	M	Sid. prod.	1
VS-24	Eastern moat	*Pseudomonas stutzeri* (T); CCUG 11256	U26262	0.995	CAS	M	Sid. prod.	1
VS-25	M5	*Pseudomonas poae* (T); type strain: DSM 14936	AJ492829	0.999	CAS	R, Exposure NB	Sid. prod.	2
VS-30d	N of Ta'u	*Pseudomonas stutzeri* (T); CCUG 11256	U26262	0.998	CAS	R	Sid. prod.	1
VS-31d	N of Ta'u	*Pseudomonas stutzeri* (T); CCUG 11256	U26262	0.999	CAS	R	Sid. prod.	1
VS-32	M1	*Marinobacter algicola* DG893 (T)	AY258110	0.995	CAS	Exposure NB	Sid. prod.	1
VS-33	Between M4 and M1	*Chromohalobacter israelensis* (T); ATCC 43985 T	AJ295144	0.999	CAS	M	Sid. prod.	1
VS-35	M1	*Thalassospira lucentensis* (T); QMT2	AF358664	0.965	CAS	S	Sid. prod.	1
VS-36	Between M4 and M1	*Pseudomonas putida* (T); IFO 14164 (ATCC 12633)	D37923	0.998	CAS	M	Sid. prod.	1
VS-37	Near M6	*Pseudoalteromonas aliena* (T); KMM 3562	AY387858	0.990	F 7.5	R, M	Heterotr. Fe	1
VS-38a	M7	*Pseudoalteromonas aliena* (T); KMM 3562	AY387858	0.989	F7.5	R	Heterotr. Fe	1

(Table 2.S1: Isolated strains of Fe(II)- and Mn(II)-oxidizing and siderophore-producing bacteria from Vailulu'u Seamount, Continued)

Strain ID	Location	Closest BLAST	Accession #	Simil. score	Med-ium	Inocu lum	Isolate type	# of isolat-ions
VS-39b	M7	*Pseudoalteromonas mariniglutinosa* (T); KMM 3635	AJ507251	0.990	F7.5+ CAS	R	Heterotr .Fe, Sid. prod.	2
VS-41	Near M6	*Pseudoalteromonas aliena* (T); KMM 3562	AY387858	0.989	F7.5	R	Heterotr .Fe	1
VS-42	M45	*Vibrio alginolyticus* (T); ATCC 17749T	X74690	0.997	F 7.5	R	Heterotr . Fe	1
VS-43	M45	*Marinobacter algicola* DG893 (T)	AY258110	0.995	F 7.5	R	Heterotr .Fe	1
VS-44b	M4	*Pseudoalteromonas mariniglutinosa* (T); KMM 3635	AJ507251	0.990	F7.5	M	Heterotr . Fe	1
VS-50a	M4	*Pseudoalteromonas aliena* (T); KMM 3562	AY387858	0.989	F 7.5	M	Heterotr . Fe	1
VS-52	M4	*Idiomarina loihiensis* (T); L2-TR	AF288370	0.999	F 7.5	M	Heterotr . Fe	1
VS-55	Near M4	*Pseudoalteromonas aliena* (T); KMM 3562	AY387858	0.990	F7.5	M	Heterotr .Fe, Sid.prod .	1
VS-57	Near M4	*Alteromonas marina* (T); SW-47	AF529060	0.997	F 7.5+6	M	Heterotr .Fe	2
VS-58	M4	*Shewanella loihica* (T); PV-4; ATCC BAA-1088	DQ286387	0.998	F 7.5	M	Heterotr .Fe	1
VS-59	SWHC	*Vibrio natriegens* (T); ATCC 14048T	X74714	0.999	F 7.5	M	Heterotr . Fe	1
VS-60a	Near M4	*Pseudoalteromonas aliena* (T); KMM 3562	AY387858	0.989	F 6	M	Heterotr . Fe	1
VS-63	Near M4	*Alteromonas marina* (T); SW-47	AF529060	0.998	F 6	M	Heterotr .Fe	1

(Table 2.S1: Isolated strains of Fe(II)- and Mn(II)-oxidizing and siderophore-producing bacteria from Vailulu'u Seamount, Continued)

Strain ID	Location	Closest BLAST	Accession #	Simil. score	Medium	Inoculum	Isolate type	# of isolations
VS-70	M44, Ta'u	*Novosphingobium pentaromativorans* (T); US6-1	AF502400	0.967	X Fe	R	Oligotr. Fe	1
VS-71	N of Ta'u	*Pseudomonas stutzeri* (T); CCUG 11256	U26262	0.995	X Fe	R	Oligotr. Fe	1
VS-73	M4	*Loktanella hongkongensis* (T)	AY600300	0.989	F7.5,	S, R	Heterotr. Fe, Mn	2
VS-100	M2	*Pseudoalteromonas issachenkonii* (T); KMM 3549	AF316144	0.986		R	Heterotr. Mn	2
VS-103b	M7	*Pseudoalteromonas mariniglutinosa* (T); KMM 3635	AJ507251	0.990	K	Exposure NB	Heterotr. Mn	1
VS-104	M1	*Hyphomonas johnsonii* (T); MHS-2	AF082791	0.989	K	Exposure MB	Heterotr. Mn	1
VS-105b	M1	*Pseudoalteromonas mariniglutinosa* (T); KMM 3635	AJ507251	0.989	M	Exposure Qz	Heterotr. Mn	1
VS-106b	Eastern moat	*Pseudoalteromonas mariniglutinosa* (T); KMM 3635	AJ507251	0.989	F7.5	M	Heterotr. Mn	1
VS-108b	M4	*Pseudoalteromonas mariniglutinosa* (T); KMM 3635	AJ507251	0.990	xMn, K, F7.5, CAS	S, R, Exposure NB	Oligotr. Mn, Heterotr.Fe,Mn, Sid.prod	5
VS-109	M4	*Halomonas axialensis* (T); Althf1; ATCC BAA-802	AF212206	0.994	xMn	M+ Exposure MB	Oligotr. Mn	2
VS-110	M4	*Aurantimonas coralicida*, WP1	AY065627	0.999	M	M	Heterotr. Mn	1
VS-111	M45	*Rubrobacter xylanophilus*	X87135	0.993	LEPT	S	Heterotr. Mn	1
VS-113	M4	*Halomonas meridiana* (T)	M93356	0.997	CAS	M	Sid. prod.	1

(Table 2.S1: Isolated strains of Fe(II)- and Mn(II)-oxidizing and siderophore-producing bacteria from Vailulu'u Seamount, Continued)

Strain ID	Location	Closest BLAST	Accession #	Similarity score	Medium	Inoculum	Isolate type	# of isol-ations
VS-115	Near M4	*Halomonas meridiana* (T)	M93356	0.998	CAS	M	Sid. prod.	1
VS-116c	Southern pit wall	*Novispirillum itersonii* subsp. itersonii (T)	Z29620	0.914	CAS	M	Sid. prod.	1
VS-117b	M7	*Pseudoalteromonas mariniglutinosa* (T); KMM 3635	AJ507251	0.990	CAS	Exposure Rhy	Sid. prod.	1
VS-119b	Near M6	*Pseudoalteromonas mariniglutinosa* (T); KMM 3635	AJ507251	0.990	F7.5, CAS	R, M	Heterotrophic Fe, Sid. prod.	3
VS-120a	Between M4 and M1	*Pseudoalteromonas aliena* (T); KMM 3562	AY387858	0.987	F7.5, CAS	M	Heterotrophic Fe, Sid. Proc.	2
VS-121	Near M6	*Pseudoalteromonas aliena* (T); KMM 3562	AY387858	0.989	F7.5, M, CAS	R, M, S	Heterotrophic Fe+ Mn, Sid. prod.	3
VS-122	M7	*Pseudomonas poae* (T); type strain: DSM 14936	AJ492829	0.999	CAS	Exposure NB + Rhy	Sid. prod.	3
VS-123	M45	*Vibrio natriegens* (T); ATCC 14048T	X74714	0.998	CAS	R	Sid. prod.	1
VS-124e	M4	*Thioclava pacifica* (T); TL 2	AY656719	0.982	CAS	M	Oligotr. Fe	1
VS-126e	E edge of Nafanua	*Thioclava pacifica* (T); TL 2	AY656719	0.979	CAS	M	Oligotr. Fe	1
VS-1271127e	M4	*Thioclava pacifica* (T); TL 2	AY656719	0.982	CAS	R	Oligotr. Fe	1
VS-128	Eastern moat	*Haematobacter massiliensis* (T); Framboise	AF452106	0.954	CAS	M	Oligotr. Fe	1

Table 2.S2: Phylogenetic characterization of OTUs from all three clone libraries and their closest related strains identified through RDP Sequence as well as the number of clones in each OTU.

Clone library	**OTU**	**Closest related strain (similarity score in RDP)**	**# of clones**	**Accession #**
NSM	OTU_1	ε-proteobacteria uncultured bacterium; FS396_454_400bp_390B (1.000)	9	FJ497252
	OTU_2	ε-proteobacteria uncultured bacterium; TF-16; FJ535281 (0.991)	75	FJ497253
	OTU_4	δ-proteobacteria uncultured bacterium; S25_1669; EF575325 (0.923)	4	FJ497257
	OTU_5	CFB-group bacteria uncultured Bacteroidetes bacterium; CF16; AY274848 (0.975)	2	FJ497261
	OTU_6	γ-proteobacteria uncultured bacterium; DGGE gel band 27; EU335079 (0.966)	11	FJ497262
	OTU_7	Unclassified bacteria uncultured bacterium; 61-2R; EF470967 (0.968)	2	FJ497263
	OTU_8	ε-proteobacteria uncultured bacterium; Acs1S01; AB292900 (0.995)	5	FJ497265
	OTU_9	α-proteobacteria uncultured bacterium; Acs1S21; AB292913 (0.990)	2	FJ497266
	OTU_10	ε-proteobacteria uncultured epsilon proteobacterium; 233-Dilution83-G11; EU334610 (0.991)	4	FJ497267
	OTU_12	CFB-group bacteria uncultured bacterium; cvf67003; AY100557 (0.913)	2	FJ497279
	OTU_13	γ-proteobacteria uncultured bacterium; SSmNB04-25; AB175999 (0.995)	3	FJ497283
	OTU_14	γ-proteobacteria uncultured bacterium; Milano-WF2B-25; AY592913 (0.985)	4	FJ497283
	OTU_21	γ-proteobacteria uncultured bacterium; YS18Us77; AB329977 (0.895)	2	FJ497302
	OTU_22	ε-proteobacteria uncultured bacterium; YS18Us77; AB329977 (1.000)	2	FJ497307
EMM	OTU_2	γ-proteobacteria *Uncultured bacterium DGGE gel 1 band 1; DQ334375* (1.000)	19	FJ497497
	OTU_3	ε-proteobacteria, uncultured bacterium; YS18Us77; AB329977 (0.893)	3	FJ497498

(Table 2.S2: Phylogenetic characterization of OTUs from all three clone libraries and their closest related strains identified through RDP, Continued)

Clone library	OTU	Closest related strain (similarity score in RDP)	# of clones	Accession #
EMM	OTU_5	CFB-group bacteria uncultured Bacteroidetes bacterium; bacteroidetes_Raunefjorden 11; AM706607 (0.994)	13	FJ497500
	OTU_6	δ-proteobacteria uncultured delta proteobacterium; YS-UMF5_101; DQ901612 (0.989)	4	FJ497501
	OTU_7	CFB-group bacteria uncultured Bacteroides sp.; UMP-47B; AM268246 (0.893)	5	FJ497503
	OTU_8	γ-proteobacteria uncultured Alteromonadaceae bacterium; ESP450-K6I-59; DQ810660 (0.999)	5	FJ497504
	OTU_9	CFB-group bacteria uncultured Bacteroidetes bacterium; JBS_8n634; EU702827 (0.994)	2	
	OTU_10	γ-proteobacteria uncultured prokaryote; IB481; AM268859 (0.998)	2	FJ497510
	OTU_11	γ-proteobacteria uncultured marine microorganism; 4032AA_3; EU187875 (1.000)	2	FJ497511
	OTU_15	CFB-group bacteria uncultured Bacteroidetes bacterium; DGGE gel band FD 15; DQ385020 (0.974)	6	FJ497450
	OTU_16	α-proteobacteria uncultured alpha proteobacterium; DGGE band CBB009; DQ206721 (0.991)	2	FJ497399
	OTU_19	γ-proteobacteria uncultured alpha proteobacterium; DGGE band CBB009; DQ206721 (1.000)	8	FJ497408
	OTU_24	γ-proteobacteria Pseudoalteromonas sp. 35D6; EF033388 (1.000)	2	FJ497424
	OTU_26	CFB-group bacteria uncultured Bacteroidetes bacterium; 299; MERTZ_0CM_182; AF424352 (0.959)	2	FJ497425
	OTU_29	γ-proteobacteria Alteromonas sp. 06-028671; FJ177925 (1.000)	2	FJ497433
	OTU_30	γ-proteobacteria, uncultured bacterium; DGGE gel band 16; DQ831111 (1.000)	2	FJ497436
	OTU_35	CFB-group bacteria, uncultured bacterium; JBS_8n634; EU702988 (0.991)	2	FJ497451
	OTU_49	CFB-group bacteria uncultured bacterium; BHSS8; EU340058 (1.000)	3	FJ497484

(Table 2.S2: Phylogenetic characterization of OTUs from all three clone libraries and their closest related strains identified through RDP, Continued)

Clone library	OTU	Closest related strain (similarity score in RDP)	# of clones	Accession #
NSR	OTU_1	α-proteobacteria uncultured bacterium; EPR3967-O2-Bc58; EU491804 (0.990)	4	FJ497524
	OTU_2	δ-proteobacteria uncultured delta proteobacterium; U10.9_28_1; DQ453320 (0.991)	8	FJ497525
	OTU_3	CFB-group bacteria, uncultured bacterium; S1-456RC38; AY780629 (0.996)	2	FJ497526
	OTU_5	γ-proteobacteria uncultured bacterium; pIR3BD09; AY354134 (0.993)	12	FJ497529
	OTU_7	α-proteobacteria uncultured alpha proteobacterium; SP_C24; AY589481 (0.990)	2	FJ497531
	OTU_8	α-proteobacteria, uncultured bacterium; DY2-96; FJ624442 (0.982)	2	FJ497532
	OTU_9	γ-proteobacteria uncultured bacterium; pIR3BG10; AY354187 (0.992)	6	FJ497535
	OTU_10	ε-proteobacteria uncultured epsilon proteobacterium; OTU12; AY265983 (0.998)	4	FJ497536
	OTU_11	γ-proteobacteria uncultured bacterium; NY06dec-086; AB430194 (0.990)	10	FJ497537
	OTU_13	Unclassified bacteria uncultured bacterium; EPR3967-O2-Bc90; EU491836 (0.979)	2	FJ497540
	OTU_16	α-proteobacteria uncultured bacterium; 1C226995; EU799403 (0.957)	2	FJ497545
	OTU_19	γ-proteobacteria uncultured bacterium; PltcOP74; AB424949 (0.997)	6	FJ497551
	OTU_21	Unclassified bacteria uncultured gamma proteobacterium; SIMO-1131; AY710571 (0.980)	2	FJ497553
	OTU_26	α-proteobacteria uncultured alpha proteobacterium; G7-43; EU005353 (0.992)	2	FJ497563
	OTU_29	Unclassified bacteria uncultured bacterium; 261; MERTZ_0CM_6; AF424314 (0.998)	2	FJ497567
	OTU_33	Unclassified bacteria uncultured bacterium; PC-PA9-3; EF379735 (0.988)	2	FJ497573

(Table 2.S2: Phylogenetic characterization of OTUs from all three clone libraries and their closest related strains identified through RDP, Continued)

Clone library	OTU	Closest related strain (similarity score in RDP)	# of clones	Accession #
	OTU_38	ε-proteobacteria uncultured bacterium; FS396_454_1000bp_0652B; DQ909470 (0.988)	3	FJ497583
	OTU_39	γ-proteobacteria uncultured bacterium; EPR3965-I2-Bc73; EU491877 (0.972)	2	FJ497585
	OTU_40	Unclassified bacteria uncultured bacterium; EPR3967-O2-Bc90; EU491836 (0.989)	2	FJ497589
	OTU_41	ε-proteobacteria uncultured bacterium; Acs3P68; AB293072 (0.992)	2	FJ497591
	OTU_42	α-proteobacteria uncultured alpha proteobacterium; ESC3; EF061165 (0.993)	2	FJ497592
	OTU_45	γ-proteobacteria uncultured bacterium; YdcBP30; AB424981 (0.993)	4	FJ497598

References

Ashelford KE, Chuzhanova NA, Fry JC, Jones AJ, Weightman AJ. 2006. New screening software shows that most recent large 16S rRNA gene clone libraries contain chimeras. Appl Environ Microbiol 72:5734-5741.

Boyd T, Scott S. 2001. Microbial and hydrothermal aspects of ferric oxyhydroxides and ferrosic hydroxides: the example of Franklin Seamount, Western Woodlark Basin, Papua New Guinea. Geochem. Trans. 2:45-56.

Brinkhoff T, Sievert SM, Kuever J, Muyzer G. 1999. Distribution and diversity of sulfur-oxidizing Thiomicrospira spp. at a shallow-water hydrothermal vent in the Aegean Sea (Milos, Greece). Appl Environ Microbiol 65:3843-3849.

Chan HTC, Anthony C. 2006. Characterisation of a red form of methanol dehydrogenase from the marine methylotroph Methylophaga marina. FEMS Microbiol Ecol Lett 97:293-297.

Chao A. 1984. Non-parametric estimation of the number of classes in a population. Scand. J. Stat.:265-270.

Chao A, Ma MC, Yang MCK. 1993. Stopping Rules and Estimation for Recapture Debugging with Unequal Failure Rates. Biometrika 80:193-201.

Cole JR, Chai B, Marsh TL, Farris RJ, Wang Q, Kulam SA, Chandra S, McGarrell DM, Schmidt TM, Garrity GM, Tiedje JM. 2003. The Ribosomal Database Project (RDP-II): previewing a new autoaligner that allows regular updates and the new prokaryotic taxonomy. Nucleic Acids Research 31:442-443.

Cowen JP, Giovannoni SJ, Kenig F, Johnson HP, Butterfield D, Rappe MS, Hutnak M, Lam P. 2003. Fluids from aging ocean crust that support microbial life. Science 299:120-123.

Davis RE, Moyer CL. 2008. Extreme spatial and temporal variability of hydrothermal microbial mat communities along the Mariana Island Arc and southern Mariana back-arc system. Journal of Geophysical Research-Solid Earth 113.

Davis RE, Stakes DS, Wheat CG, Moyer CL. 2009. Microbial spatial variability within an iron-silica-manganese-rich hydrothermal mound off-axis at the Cleft Segment, Juan de Fuca Ridge. J. Geomicrobiol. In press.

Druschel GK, Emerson D, Sutka R, Suchecki P, Luther GW. 2008. Low-oxygen and chemical kinetic constraints on the geochemical niche of neutrophilic iron(II) oxidizing microorganisms. Geochim Cosmochim Acta 72:3358-3370.

Dunbar KR, Heintz RA. 1997. Chemistry of transition metal cyanide compounds: Modern perspectives. Progress in Inorganic Chemistry, Vol 45 45:283-391.

Edwards KJ, Rogers DR, Wirsen CO, McCollom TM. 2003. Isolation and characterization of novel psychrophilic, neutrophilic, Fe-oxidizing, chemolithoautotrophic alpha- and gamma-proteobacteria from the deep sea. Appl Environ Microbiol 69:2906-2913.

Ehrlich HL. 1996. In: Geomicrobiology, 3rd edn., editors. 12: 276-293.

Emerson D, Ghiorse WC. 1993. Ultrastructure and chemical composition of the sheath of Leptothrix discophora SP-6. J Bacteriol 175:7808-7818.

Emerson D, Moyer C. 1997. Isolation and characterization of novel iron-oxidizing bacteria that grow at circumneutral pH. Appl Environ Microbiol 63:4784-4792.

Emerson D, Moyer CL. 2002. Neutrophilic Fe-oxidizing bacteria are abundant at the Loihi Seamount hydrothermal vents and play a major role in Fe oxide deposition. Appl Environ Microbiol 68:3085-3093.

Emerson D, Rentz JA, Lilburn TG, Davis RE, Aldrich H, Chan C, Moyer CL. 2007. A novel lineage of proteobacteria involved in formation of marine fe-oxidizing microbial mat communities. PLoS ONE 2:e667.

Felsenstein J (1993). PHYLIP (Phylogeny Inference Package) version 3.5c. Distributed by the author., Department of Genetic, University of Washington, Seattle.

Furnes H, Banerjee NR, Muehlenbachs K, Staudigel H, de Wit M. 2004. Early life recorded in archean pillow lavas. Science 304:578-581.

Furnes H, Staudigel H. 1999. Biological mediation in ocean crust alteration: how deep is the deep biosphere? Earth and Planetary Science Letters 166:97-103.

Hart SR, Staudigel H, Koppers AA, Blusztajn J, Baker ET, Workman R, Jackson M, Hauri M, Kurz M, Sims K, Fornari D, Saal A, Lyons S. 2000. Vailulu'u Undersea Volanco: The New Samoa. G-Cubed:1-13.

Hodges TW, Olson JB. 2009. Molecular comparison of bacterial communities within iron-containing flocculent mats associated with submarine volcanoes along the Kermadec Arc. Appl Environ Microbiol 75:1650-1657.

Huber JA, Butterfield DA, Baross JA. 2003. Bacterial diversity in a subseafloor habitat following a deep-sea volcanic eruption. Fems Microbiology Ecology 43:393-409.

Inagaki F, Takai K, Hideki KI, Nealson KH, Horikishi K. 2003. Sulfurimonas autotrophica gen. nov., sp nov., a novel sulfur-oxidizing epsilon-proteobacterium isolated from hydrothermal sediments in the Mid-Okinawa Trough. International Journal of Systematic and Evolutionary Microbiology 53:1801-1805.

Ivanova EP, Gorshkova NM, Sawabe T, Zhukova NV, Hayashi K, Kurilenko VV, Alexeeva Y, Buljan V, Nicolau DV, Mikhailov VV, Christen R. 2004. Sulfitobacter delicatus sp nov and Sulfitobacter dubius sp nov., respectively from a starfish (Stellaster equestris) and sea grass (Zostera marina). International Journal of Systematic and Evolutionary Microbiology 54:475-480.

Karl DM, Brittain AM, Tilbrook BD. 1989. Hydrothermal and Microbial Processes at Loihi Seamount, a Mid-Plate Hot-Spot Volcano. Deep-Sea Research Part a-Oceanographic Research Papers 36:1655-1673.

Karl DM, Mcmurtry GM, Malahoff A, Garcia MO. 1988. Loihi-Seamount, Hawaii - a Mid-Plate Volcano with a Distinctive Hydrothermal System. Nature 335:532-535.

Konter JG, Staudigel H, Hart SR, Shearer PM. 2004. Seafloor seismic monitoring of an active submarine volcano: Local seismicity at Vailulu'u Seamount, Samoa. Geochemistry Geophysics Geosystems 5:-.

Krumbein WE, Altmann HJ. 1973. New Method for Detection and Enumeration of Manganese Oxidizing and Reducing Microorganisms. Helgolander Wissenschaftliche Meeresuntersuchungen 25:347-356.

Kucera S, Wolfe RS. 1957. A selective enrichment method for Gallionella ferruginea. J Bacteriol 74:344-349.

Kuever J, Sievert SM, Stevens H, Brinkhoff T, Muyzer G. 2002. Microorganisms of the oxidative and reductive part of the sulphur cycle at a shallow-water hydrothermal vent in the Aegean Sea (Milos, Greece). Cahiers de Biologie Marine 43:413-416.

Lane DJ. 1991. 16S/23S rRNA sequencing. In: Nucleic Acid Techniques in Bacterial Systematics. Stackebrandt E and Goodfellow M, editors. 115-148.

Longnecker K, Reysenbach A. 2001. Expansion of the geographic distribution of a novel lineage of epsilon-Proteobacteria to a hydrothermal vent site on the Southern East Pacific Rise. FEMS Microbiol Ecol 35:287-293.

Lysnes K, Thorseth IH, Steinsbu BO, Øvreås L, Torsvik T, Pedersen RB. 2004. Microbial community diversity in seafloor basalt from the Arctic spreading ridges. FEMS Microbiology Ecology 50:213-230.

Mason OU, Stingl U, Wilhelm LJ, Moeseneder MM, Di Meo-Savoie CA, Fisk MR, Giovannoni SJ. 2007. The phylogeny of endolithic microbes associated with marine basalts. Environ Microbiol 9:2539-2550.

Moyer CL, Dobbs FC, Karl DM. 1995. Phylogenetic diversity of the bacterial community from a microbial mat at an active, hydrothermal vent system, Loihi Seamount, Hawaii. Appl Environ Microbiol 61:1555-1562.

Nakagawa T, Nakagawa S, Inagaki F, Takai K, Horikoshi K. 2004. Phylogenetic diversity of sulfate-reducing prokaryotes in active deep-sea hydrothermal vent chimney structures. FEMS Microbiol Lett 232:145-152.

Nealson KH, Saffarini D. 1994. Iron and manganese in anaerobic respiration: environmental significance, physiology, and regulation. Annu Rev Microbiol 48:311-343.

Nylander JAA. 2004. MrModeltest v2. Program distributed by the author. Evolutionary Biology Centre, Uppsala University.

Pfennig N, Lippert KD. 1966. Uber Das Vitamin B12-Bedurfnis Phototropher Schwefelbakterien. Archiv Fur Mikrobiologie 55:245-256.

Pruesse E, Quast C, Knittel K, Fuchs B, Ludwig W, Peplies J, Gloeckner FO. 2007. SILVA: a comprehensive online resource for quality checked and aligned ribosomal RNA sequence data compatible qith ARB. Nuc. Acids Red. 35:7188-7196.

Purdy KJ, Nedwell DB, Embley TM. 2003. Analysis of the sulfate-reducing bacterial and methanogenic archaeal populations in contrasting Antarctic sediments. Appl Environ Microbiol 69:3181-3191.

Rassa AC, McAllister SA, Safran SA, Moyer CL. 2009. Zeta-Proteobacteria dominate the formation of microbial mats in low-temperature hydrothermal vents at Loihi Seamount, Hawaii. J.Geomicrobiol. In review.

Rentz JA, Kraiya C, Luther GW, 3rd, Emerson D. 2007. Control of ferrous iron oxidation within circumneutral microbial iron mats by cellular activity and autocatalysis. Environ Sci Technol 41:6084-6089.

Romanenko LA, Zhukova NV, Lysenko AM, Mikhailov VV, Stackebrandt E. 2003. Assignment of 'Alteromonas marinoglutinosa' NCIMB 1770 to Pseudoalteromonas mariniglutinosa sp. nov., nom. rev., comb. nov. Int J Syst Evol Microbiol 53:1105-1109.

Santelli CM, Orcutt BN, Banning E, Bach W, Moyer CL, Sogin ML, Staudigel H, Edwards KJ. 2008. Abundance and diversity of microbial life in ocean crust. Nature 453:653-656.

Schloss PD, Handelsman J. 2005. Introducing DOTUR, a computer program for defining operational taxonomic units and estimating species richness. Appl Environ Microbiol 71:1501-1506.

Schwyn B, Neilands JB. 1987. Universal chemical assay for the detection and determination of siderophores. Anal Biochem 160:47-56.

Shock EL. 1996. Hydrothermal systems as environments for the emergence of life. In: Evolution of Hydrothermal Ecosystems on Earth (and Mars?). editors. 40-60.

Shock EL, McCollom TM, Schulte MD. 1998. The Emergence of Metabolism from Within Hydrothermal Systems. In: Thermophiles: The Keys to Molecular Evolution and the Origin of Life? Wiegel J and Adams MWW, editors. 59-76.

Sievert SM, Huegler M, Taylor CD, Wirsen CO. 2008. Sulfur Oxidation at Deep-Sea Hydrothermal Vents. In: Microbial Sulfur Metabolism. Dahl C and Friedrich CG, editors. 238-258.

Sims KWW, Hart SR, Reagan MK, Blusztajn J, Staudigel H, Sohn RA, Layne GD, Ball LA. 2008. 238U-Th-230-Ra-226-Pb-210-Po-210, Th-232-Ra-228, and U-235-Pa-231 constraints on the ages and petrogenesis of Vailulu'u and Malumalu Lavas, Samoa. Geochemistry Geophysics Geosystems 9:-.

Sogin ML, Morrison HG, Huber JA, Mark Welch D, Huse SM, Neal PR, Arrieta JM, Herndl GJ. 2006. Microbial diversity in the deep sea and the underexplored "rare biosphere". Proc Natl Acad Sci U S A 103:12115-12120.

Stamatakis A, Hoover P, Rougemont J. 2008. A Rapid Bootstrap Algorithm for the RAxML Web-Servers. Systematic Biology 75:758-771.

Staudigel H, Furnes H, Kelley K, Plank T, Muehlenbachs K, Tebo B, Yayanos A. 2004. The Oceanic Crust as a Bioreactor. In: Deep Subsurface Biosphere at Mid-Ocean Ridges. Monograph A, editors. 235-341.

Staudigel H, Furnes H, McLoughlin N, Banerjee NR, Connell LB, Templeton AS. 2008. 3.5 billion years of glass bioalteration: Volcanic rocks as a basis for microbial life? Earth-science Reviews (in press).

Staudigel H, Hart SR, Pile A, Bailey BE, Baker ET, Brooke S, Connelly DP, Haucke L, German CR, Hudson I, Jones D, Koppers AA, Konter J, Lee R, Pietsch TW, Tebo BM, Templeton AS, Zierenberg R, Young CM. 2006. Vailulu'u Seamount, Samoa: Life and death on an active submarine volcano. Proc Natl Acad Sci U S A 103:6448-6453.

Sunamura M, Higashi Y, Miyako C, Ishibashi J, Maruyama A. 2004. Two bacteria phylotypes are predominant in the Suiyo seamount hydrothermal plume. Appl Environ Microbiol 70:1190-1198.

Swofford D. 2002. PAUP*. Phylogenetic Analysis Using Parsimony. Version 4. Sinauer Associates.

Takai K, Hirayama H, Nakagawa T, Suzuki Y, Nealson KH, Horikoshi K. 2004. Thiomicrospira thermophila sp. nov., a novel microaerobic, thermotolerant, sulfur-oxidizing chemolithomixotroph isolated from a deep-sea hydrothermal fumarole in the TOTO caldera, Mariana Arc, Western Pacific. Int J Syst Evol Microbiol 54:2325-2333.

Takai K, Moyer CL, Miyazaki M, Nogi Y, Hirayama H, Nealson KH, Horikoshi K. 2005. Marinobacter alkaliphilus sp. nov., a novel alkaliphilic bacterium isolated from subseafloor alkaline serpentine mud from Ocean Drilling Program Site 1200 at South Chamorro Seamount, Mariana Forearc. Extremophiles 9:17-27.

Tebo BM, Clement BG, Dick GJ. 2007. Biotransformations of manganese. In: Manual of Environmental Microbiology. Stetzenbach LD, editors. 1223-1238.

Tebo BM, Johnson HA, McCarthy JK, Templeton AS. 2005. Geomicrobiology of manganese(II) oxidation. Trends Microbiol 13:421-428.

Templeton AS, Staudigel H, Tebo BM. 2005. Diverse Mn(II)-oxidizing bacteria isolated from submarine basalts at Loihi Seamount. Geomicrobiology Journal 22:127-139.

Vogt C, Cyrus E, Herklotz I, Schlosser D, Bahr A, Herrmann S, Richnow HH, Fischer A. 2008. Evaluation of Toluene Degradation Pathways by Two-Dimensional Stable Isotope Fractionation. Environmental Science & Technology 42:7793-7800.

Wirsen CO, Sievert SM, Cavanaugh CM, Molyneaux SJ, Ahmad A, Taylor LT, DeLong EF, Taylor CD. 2002. Characterization of an autotrophic sulfide-oxidizing marine Arcobacter sp that produces filamentous sulfur. Applied and Environmental Microbiology 68:316-325.

CHAPTER III: **Siderophore-mediated weathering of the ocean's crust: Microbes and the role of free organic ligands**

Introduction

Fe is the fourth most abundant element in the Earth's crust (Crosa 1989). In spite of its high abundance the bioavailability of Fe, as one of the most essential elements for all life, is low. Fe availability in seawater is limited by its inorganic chemistry under generally oxic, slightly basic (pH ~8) conditions that dominate in the oceans (Street and Paytan 2005). The seawater chemistry of Fe is diverse and generally poorly understood. Fe occurs in multiple forms, particulate and dissolved, organic and inorganic (Street and Paytan 2005). It exists in two oxidation states Fe(II) and Fe(III). Fe(II), the more soluble but kinetically labile form of Fe can be transiently present in seawater as a consequence of photochemical redox reactions (in surface water) or biological redox reactions in reducing environments (Barbeau 2006). It has a solution chemistry very similar to other divalent anions such as Mn(II), Co(II), Ni(II), and Zn(II) which, in seawater are all weakly paired with Cl^- ions and are present mostly as free hydrate ions (Byrne 2002). Under aerobic conditions and near neutral pH Fe predominantly exists in its more thermodynamically stable oxidation state of Fe(III) which is highly reactive with respect to hydrolysis, adsorption and complex formation, and as a result is largely unavailable as dissolved, free Fe^{3+} (Street and Paytan 2005).

Central to understanding the behavior of Fe^{3+} in seawater is its ionic interactions with the major anions (F^-, Cl^-, SO_4^{2-}, OH^-, and CO_3^{2-}) and organic compounds (Millero 1998). In addition to ferric chlorides, fluorides, sulfates and $FeOH^{2+}$ above pH >6 it exists mostly as $Fe(OH)_2^+$ (aq) and aqueous and solid $Fe(OH)_3$ (Byrne 2002). Fe (hydr)oxides have solubility products ranging from 10^{-39} to 10^{-44}, which limits Fe(III) aqueous equilibrium concentration to ~10^{-17} M at near neutral pH. In addition ~99% of dissolved Fe(III) in seawater is bound to organic chelators (Gledhill and Van den Berg 1994; Rue and Bruland 1995). Complexation of Fe by organic ligands resulting in decreased concentrations of reactive Fe(III) and generally increased Fe solubility is thought to significantly affect the availability of this bio-essential element.

Most microorganisms require micromolar (10^{-6} M) concentrations of Fe to support growth (Hersman et al. 2001). There is considerable evidence that many of the Fe-binding ligands in seawater have been released by bacteria (Butler 1998; Gonye and Carpenter 1974; Martinez et al. 2000; Takahashi et al. 1987; Trick 1989). The ubiquitous presence of cytochromes and non-heme Fe in the respiratory chains of aerobic and facultative anaerobic bacteria provides a central role for Fe in the energy metabolism of microorganisms. Bacteria need Fe for a number of biological processes, including electron transport chains, and as a co-factor of enzymes in intermediary metabolism (Neilands 1981). Bacteria are known to acquire Fe(III) using high-affinity Fe(III)-chelating molecules (“siderophores”) that capture and solubilize otherwise unavaiable Fe species (e.g. oxide minerals, particle-bound, organic complexes(Granger and Price 1999; Neilands 1981; Soria-Dengg et al. 2001; Weaver et al. 2003). These low-molecular

weight biomolecules (~0.5-1.5 kDa) exhibit a high-affinity for Fe and help solubilize and sequester Fe(III) through chelation. Siderophore production and binding are part of a specialized biological machinery and considered a strategy to convert inaccessible Fe(III) to a form in which it becomes available to bacteria producing a certain siderophore and possibly not to others (Guan et al. 2001).

This machinery includes not only siderophore-producing proteins, but also membrane proteins that enable direct release of Fe at the cell surface or ingestion of siderophore-complexed Fe which is release inside the cell via reduction to Fe(II) or degradation of the siderophore itself (Street and Paytan 2005). In some strains these cell-membrane proteins are able to recognize and transport a number of structurally different siderophores which the bacterium then can benefit from.

Fluids released in hydrothermally active deep-sea systems contain high concentrations of reduced Fe acquired via dissolution during circulation of seawater through basaltic rocks at high temperatures and pressures equivalent to alteration of the volcanic rocks (Elderfield and Schultz 1996; Seyfried and Mottl 1995; Von Damm and Bischoff 1987; Von Damm et al. 1998). Most of these Fe species are rapidly oxidized and precipitated upon mixing with cold ambient bottom water resulting in large ferromanganese deposits (De Baar and De Jing 2001). Recent studies on natural basaltic glass surfaces have shown that microbes are often associated with these mineral deposits (Templeton et al. 2009). The possible impact of these communities on basalt alteration and the biochemical cycling of elements along the rock/water interface is discussed in

Chapter I of this work. The production of secondary metabolites such as siderophores is considered one potential mechanism by which microbes control the dissolution of metal oxides including ferromanganese deposits, resulting in elevated alteration rates of the rocks.

Based on the variability of ligands and the high number of ligand-complexed ions in seawater, the effect of structurally different siderophores on the dissolution of volcanic rocks is of particular interest. The work presented in this chapter addresses the effect of two siderophores, pyoverdin (PVD) and desferrioxamine B (DFO-B), on Fe acquisition from basalt and rhyolite powder under aerobic and anaerobic conditions, and then compares the results to an experiment containing a siderophore-producing deep-sea bacterium. Objectives of this study were to determine A) if siderophore-mediated dissolution of volcanic glasses does take place even under abiotic conditions, B) to compare Fe complexation rates of two commonly produced siderophores and C) to evaluate the role of oxygen in the alteration and subsequent complexation mechanism and compare it to the importance of siderophores in this process.

Materials and Methods

1. Isolation of siderophore producing strains

Seawater-based Chrome-Azurol-Sulfonate (CAS) plates (see Chapter IV) originally started by A. Templeton on a cruise to Loihi Seamount, Hawaii in 2003 (Figure

3.2), were used to isolate a number of siderophore-producing strains. Single colonies were picked from the original plates and transferred to new CAS plates until pure cultures were obtained. During this process the plates were kept at a temperature of 12 ºC. One of these siderophore-producing strains (548-03-X1) isolated from a natural basalt surface at Loihi Seamount was later used in one of the experiments.

1.1 DNA extraction

DNA from isolated strains of siderophore-producing bacteria was obtained by growing the strains in 5 ml of Luria-Bertani (LB) medium (per liter of ultra pure H_2O: 10 g Bacto Tryptone, 5 g Yeast Extract, 10 g NaCl, adjusted to pH 7.5) at 37 °C (~180 rpm) overnight and extracting DNA from pelleted cells using the DNAeasy kit (Qiagen Inc., Valencia CA).

1.2 PCR and sequencing

For the 16S rRNA gene amplification of isolates, two universal eubacterial primers: 27f and 1492r (Lane 1991) and one internal primer: 1074r (5'-CAC GAG CTG ACG ACA GCC AT-'3) were used. Samples were amplified using the following PCR conditions: 95 °C = 3 min.; 30 x (95 °C = 30 sec., 54 °C = 30 sec., 72 °C = 1 min.); 72 °C = 7 min. The PCR products were purified using the QIAquick PCR Purification Kit (Qiagen Inc., Valencia CA) and were subsequently sequenced on a capillary electrophoresis DNA sequencer (ABI PRSIM 3100 genetic analyzer), carried out by Seqxcel Inc., San Diego (http://www.seqxcel.com).

1.3 Phylogenetic identification

Sequence reads were assembled and analyzed in Sequencher 4.4 (GeneCodes, Ann Arbor, MI) resulting in near full-length (1200-1300 bp) 16S rRNA genes. All sequences were checked for their orientation and their potential of being chimeric using *OrientationChecker* and *Mallard* (Ashelford et al. 2006). Closely related sequences in Genbank were identified via BLAST (Altschul et al. 1997).

2. Volcanic rocks

Two different rock types were used for the experimental set-ups. Basalt was originally obtained from an active flow at Kilauea volcano (Pu'U'o'O). It was quenched and re-melted to obtain its glass-like texture. The Fe(II) content of this glass averages 10 wt%, the Fe(II)/Fe(III) ratio is 11 (Bailey et al. 2009). Rhyolite was collected from an obsidian dome in Long Valley (near Mono Lake) and was chosen as a volcanic rock containing ~ 10 times less Fe than the basalt with an otherwise similar chemical composition. Chemical analysis showed an average Fe(II) content of < 1% (0.91 %, data by B. Bailey). To normalize the rock surfaces in all experimental set-ups 20 g of the basalt and rhyolite were ground using a stainless steel rock grinder and then sieved to a grain size of approximately 63µm. 0.5 g rock powder was used in each experiment. A 0.5 g sample of each rock was analyzed by single point surface area measurement with krypton (BET technique, Porous Material Inc, Ithaca) to determine its exact surface area.

3. Siderophores

Two different types of siderophores were used. "Free" pyoverdine (PVD) was

obtained from culture medium of *Pseudomonas putida* strain MnB1 (gift from D. Parker). Desferrioxamine mesylate (DFAM), the commercially available salt of Desferrioxamine B (DFO-B), was obtained from Sigma (cat # D9533).

PVD

PVD consists of 2 hydroxamate and 1 catecholate groups as possible binding sites for metal ions (Figure 3.3). Spectra of the deferri-PVD are pH dependent whereas those of its metal complexes are unaffected by pH changes. At pH 5.0 and above PVD shows two absorption maxima at λ_{max} = 364 nm (ε= 16 000 mol^{-1} L) and at λ_{max} = 380 nm (ε= 16500 mol^{-1} L). Its Fe complexes show three peaks with absorption maxima at 403 nm (ε= 19 000 mol^{-1} L), a shoulder at 460 nm (ε=6500 mol^{-1} L) and one at 540 nm (e=3500 mol^{-1} L(Demanger et al. 1987).

DFO-B

DFO-B is a linear molecule containing three hydroxamate groups and a primary amine group at one end (Figure 3.4). The molecule therefore has four protonation constants (Hernlem et al. 1996). It forms very stable 1:1 complexes with Fe(III): logβ Fe(DFO-B)= 30.4 and less stable complexes with Fe(II): logβ Fe(DFO-B)= 10. For the Fe(III)–DFO-B complex the absorption maximum lies at ~430 nm with an extinction coefficient (ε) of ~2600 M^{-1}.

4. Experimental set-up

0.5 g of rock powder was added to glass tubes previously acid washed in 10%

HCl, rinsed 6 times with deionized H_2O and autoclaved at 121 °C for 30 minutes. Filter-sterilized siderophore solutions that were adjusted to pH 7.5 using 4-(2-hydroxyethyl)-1-piperazineethanesulfonic acid (HEPES) were added to the H_2O to obtain a final volume of 10 ml of reaction solution in each tube. In the negative controls not containing any siderophores the H_2O was adjusted to the same pH by addition of HEPES resulting in the same final volume. All solutions were checked under the microscope for their sterile status prior to use. The concentration of PVD and DFO-B in each tube was adjusted to 100 μM. Experiments were run at room temperature. For the anaerobic experiment PVD, DFO-B and deionized H_2O used in the experimental set-up were prepared in serum bottles, bubbled with N_2 for 1hr to minimize the O_2 content, and sealed. The bottles were visually checked for their sterility by light microscopy before they were subsequently transferred into the anaerobic chamber.

A preliminary washing step with PVD or DFO-B solutions adjusted to pH 7.5 was carried out on the rock powders to wash-off all potential surface Fe. After this washing step all samples were centrifuged for 20 minutes. The supernatant was removed and ligand-complexed Fe was measured spectrophotometrically. All Fe measured later in the actual experiment was assumed to be leached out of the rocks.

Three sets of experiments were set-up: “aerobic/abiotic”, “anaerobic/abiotic” and aerobic with addition of siderophore-producing isolate 548-03-X1 (from Loihi CAS plates) at an initial density of $OD_{600} = 0.05$ (“aerobic/biotic”). 10 ml of H_2O with and without addition of PVD or DFO-B was added to the washed rock powders to start the

incubations.

The following conditions were tested:

1) Basalt, PVD

2) Rhyolite, PVD

3) Basalt, DFO-B

4) Rhyolite, DFO-B

5) Basalt, Water (negative control)

6) Rhyolite, Water (negative control)

7) PVD, Water (negative control)

8) DFO-B, Water (negative control)

5. Iron-complexation measurements

The complexation of Fe was determined using a spectrophotometric method. Prior to each measurement samples were centrifuged to remove cells or particles. The spectra were measured between 300 and 600 nm. Fe-PVD was measured based on its maximum absorption at 460 nm with an extinction coefficient of ε= 6500 mol^{-1} L. Fe-DFO-B was measured based on its absorption maximum at 430 nm with an extinction coefficient of ε= 2600 mol^{-1} L. Free PVD had its main peak around 400 nm. Four different controls (water/rock, siderophore/water) were run. The rock/water experiments were set-up to ensure that no significant amount of Fe was derived from the rock/water reaction alone. At the end of the experiments all data were corrected for data from the negative controls and were normalized to the respective surface area of the rock to determine the actual

amount of Fe leached out by the siderophores.

Results

1. Isolation of siderophore-producing strains

Eight different strains of siderophore-producing bacteria were isolated from 2003 Loihi CAS plates (Figure 3.5). It took eight successive transfers to obtain pure cultures. 16S rRNA gene sequences of the eight isolates identified them as closely (98-99% identity) related to two *Pseudomonas stutzeri*, three other *Pseudomonas* species, as well as three *Pseudoalteromonae.* One of these isolates, 548-03-X1 was used in the biotic experiment. It was phylogenetically identified as *Pseudomonas stutzeri* DSM 5190T (AJ288151, NCBI score 100%) previously identified as a nitrate reducing bacterium (Petri and Imhoff 2000). Siderophores produced by strain 548-03-X1 were neither identified nor structurally characterized.

2. Role of siderophores in rock weathering

All experiments were performed over the period of 16 days. Particular interest was paid to the first few hours of the reaction since, at the given siderophore concentration of 100 μM, complete Fe complexation by PVD usually takes place within the first 4-6 hours.

Despite the fact that both rock powders were ground the same way for the same length of time, surface area measurements for both rock types result in quite different

results. The basalt has a specific surface area of 0.363766 m^2/g while the surface area of the rhyolite powder is ~ 4 times higher (1.279 m^2/g). The initial washing step resulted in very similar amounts of Fe being removed from the rock powder surfaces (data not shown).

Fe complexation over time was measured based on the increase in the absorption spectra of Fe-PVD and Fe-DFO-B over time as seen in Figure 3.6 (measured between 300 and 600 nm). The extinction coefficients of ε= 6500 mol^{-1} L for Fe(III)-PVD measured at 460 nm and ε= 2600 mol^{-1} L for Fe(III)-DFO-B measured at 430 nm were used to calculate the amounts of Fe complexed (Figure 3.7). All data were previously corrected for the two controls (rock/water and siderophore/water). As indicated by the increase in the A_{460} with time (Figure 3.6) absorbance at 460 nm is thought to reflect the change transfer band of Fe(III) with the hydroxamate of PVD, and thus is specific for ferri-PVD. For PVD the increase in the absorption at 460 nm (Fe(III)-PVD) is more apparent by correcting the data for the total PVD (complexed and non-complexed) with a maximum absorption around 400 nm. The A_{460}/A_{400} ratio of fully Fe-saturated PVD is 0.32 (Demanger et al. 1987). For basalt PVD in the anaerobic experiment this ratio is approached within 96 hours (A_{460}/A_{400} = 0.329). In the aerobic samples this ratio is reached after 192 hours (abiotic= 0.327; biotic = 0.357).

Based on spectrophotometric results little Fe is leached out in the rock/water controls without siderophores (Figure 3.8). In the rock/water controls the majority of Fe released from the rocks under anaerobic conditions is assumed to be in its reduced form

due to limited concentrations of oxygen inside the anaerobic chamber. As soon as the samples were taken out of the anaerobic chamber for spectrophotometric measurements a rapid oxidation is likely to have taken place. This reaction however does not change the total amount of Fe that was released and complexed.

The fastest and highest complexation of Fe takes place in the anaerobic/ abiotic experiments and the abiotic and the biotic experiments both carried out under aerobic conditions in the presence of PVD do not show any significant difference (Figure 3.7 A). In the presence of DFO-B the biotic experiment yields slightly higher amounts of Fe complexed (Figure 3.7 B). Detailed results for PVD prior to correction of data for the negative controls (rock/water, no PVD added) can be seen in Figure 3.8 and suggest that only minimal amounts of Fe are leached from the glasses in the control experiment.

3. Anaerobic ligand-induced oxidation of Fe

Compared to PVD, DFO is considered to be able to change the oxidation state of Fe without the presence of oxygen above pH 4. The interaction of Fe(II) and DFO-B, that occurs above pH 4, is accompanied by a continuous pH decrease and the parallel development of a characteristic charge-transfer band of the Fe(III)-tris(hydroxamate_ complex $[Fe(III)(HDFB)]^{+}$ at 430 nm (Farkas et al. 2001). Results from our anaerobic experiment are also indicative of a ligand-promoted oxidation of Fe(II). The UV-visible spectrum of the Fe-DFO-B complex shows a maximum absorption at 430 nm previously identified as the tris-chelated $[Fe(III)(HDFB)]^{+}$ ((Farkas et al. 2001). However, since we did not evaluate the anoxic status in our experiments (e.g. based on the addition of a

reducing agent) formation of this complex could also be related to the chemical oxidation of Fe by low amounts of oxygen within the experiments.

4. PVD vs. DFO-B

In general Fe complexation rates in the presence of DFO-B both under aerobic and anaerobic conditions is higher than with PVD (Figure 3.7 and 3.10). This indicates that DFO-B may represent a stronger complexing agent. Within ~100 hours the anaerobic complexation of Fe from basalt by DFO-B appears to be saturated. Significantly elevated Fe-DFO-B complexation rates under anaerobic conditions are likely the result of higher Fe(II) solubilities and ligand-promoted oxidation as described above.

5. Basalt vs. rhyolite

The amount of Fe released from each volcanic rock positively correlates with its natural Fe concentration as shown in Figure 3.11. However, the amount of Fe leached out from both rocks doesn't differ by a factor of 10 and therefore doesn't correlate completely with their natural Fe content. Fe release from rhyolite tends to start much slower in all experiments (Figure 3.7) but the trend in complexation shows the same pattern as in the basalt experiments.

Discussion and Conclusions

Experiments on the influence of siderophores on basalt and rhyolite dissolution indicated by the release and complexation of Fe show that purified siderophores are able

to leach Fe from volcanic rocks without any specific microbial activity. This demonstrates their potential to contribute to rock weathering.

The fastest and highest amount of Fe is released and complexed under anaerobic conditions. This is considered to be due to the greater solubility of Fe(II). Since it is assumed that little or no oxygen was present in this experiments and the rocks mainly contain Fe(II), it is assumed that oxygen plays a minor role in leaching the element from the rock powders.

The fact that similar amounts of Fe could be detected in the washing step of all experimental set-ups containing volcanic rocks might be related to the fact that the surface area of both rock types is so different. Even though rhyolite contains a lot less Fe its elevated surface area may have lead to similar amounts of Fe washed-off its surface.

In the presence of PVD the abiotic and the microbial experiments carried out under aerobic conditions show very similar results. This supports the assumption that siderophores, and not microbes, control a major part of the leaching of Fe from the rocks in our set-up. This is contrary to the results from abiotic and biotic dissolution experiments of hornblende, which previously showed an increased Fe release in the presence of a siderophore producing *Arthrobacter* strain (Brantley et al. 2001). Since the siderophore produced by the *Pseudomonas* stutzeri strain used in the biotic set-up was not identified, the interpretation of results from this set-up remains difficult. While the use of very fine fractions of volcanic rocks enables surface area determination and likely

higher reaction rates they complicate the determination of cell growth based on optical density measurements at 600 nm. Instead cell numbers should have been determined through serial dilutions on plates and subsequent counting of colony-forming units (CFUs). One likely reasons for the lack of biotically-mediated increased Fe release rates as reported by Brantley et al. lies in the use of deionized water as a medium in all of our experimental set-ups. Compared to artificial seawater it minimizes mineral precipitation (from the medium and from abiotic reactions with the rocks) and non-distinct complexation of elements. It does not however contain sufficient nutrient and energy sources to support microbial growth. Cell growth of *Pseudomonas* stutzeri DSM 5190T was not monitored but it is likely that cells accidentally either lysed upon addition to deionzied water or were at least inactive resulting in similar conditions as in the aerobic/abiotic experiment. Slightly elevated Fe complexation in the biotic over the abiotic (both aerobic) experiment in the presence of DFO-B (Figure 3.7 B) indicates the latter.

Overall the results support the assumptions that oxygen is not the main factor causing Fe release from volcanic rocks and presence of the siderophore-producing microbes in the experiment does not increase the release of Fe. In both aerobic experiments complexation of Fe from an abiotically formed Fe (hydr)oxide layer at the surface of the rock powder is likely. Such a constant removal of this layer could account for a considerably elevated release of Fe observed in all experimental set-ups containing siderophores. Elevated complexation of Fe by DFO-B under anaerobic conditions in contrast is potentially ascribable to a ligand-promoted oxidation of Fe(II) from basalt

resulting in generally elevated Fe complexation rates. Under the same conditions PVD is only able to complex whatever amount of either Fe(II), subsequently oxidized by the remaining oxygen in the system (solution), or Fe(III) is released from the rock.

In recent years the role of microbes in the dissolution of Fe-bearing minerals and rocks have been elucidated (Aouad et al. 2006; Daughney et al. 2004; Dong et al. 2003; Edwards et al. 2000; Frederickson et al. 1998; Herrera et al. 2008; Kolo et al. 2009; Liermann et al. 2000; Lovley and Phillips 1986; Uroz et al. 2009). Siderophores have been shown to be present at ca. 10-100 nm concentrations in most oxic enrivonments, including marine (Mucha et al. 1999) and fresh waters (Duckworth et al. 2009). Siderophore-producing bacteria have recently been shown to be abundant even in deep-sea environments (Homann et al. 2009; Kameyama et al. 1987; Sudek et al. 2009) where hydrothermal and biological alteration of volcanic rocks represents one of the major sources for Fe. Aside from rock/water interactions, the abundance of chemolithotrophic microbial communitities, including heterotrophic and autotrophic Fe(II) and Mn(II)-oxidizing bacteria, often associated with the rock surfaces, are assumed to contribute toward elevated rock alteration rates. The role of siderophores in the rock-surface-related lifestyle has so far received little attention. Our work emphasizes the role of siderophores in Fe acquisition from these rocks. We show that in batch culture these compounds have the potential to free Fe from the rocks to an even greater extend than oxygen. In addition to the direct oxidation and complexation of Fe from the rocks, elevated oxidation rates are thought to be the results of a siderophore-mediated removal of metal-oxide layers biotically and abiotically forming along the rock surface. Since siderophore production

has recently been shown to be a common trait in deep-sea environments (Sudek et al. 2009), siderophore-mediated elevated weathering rates of the volcanic glasses in these environments are likely to have a major impact on local and global ocean chemistry and the biochemical cycling of many bio-essential elements.

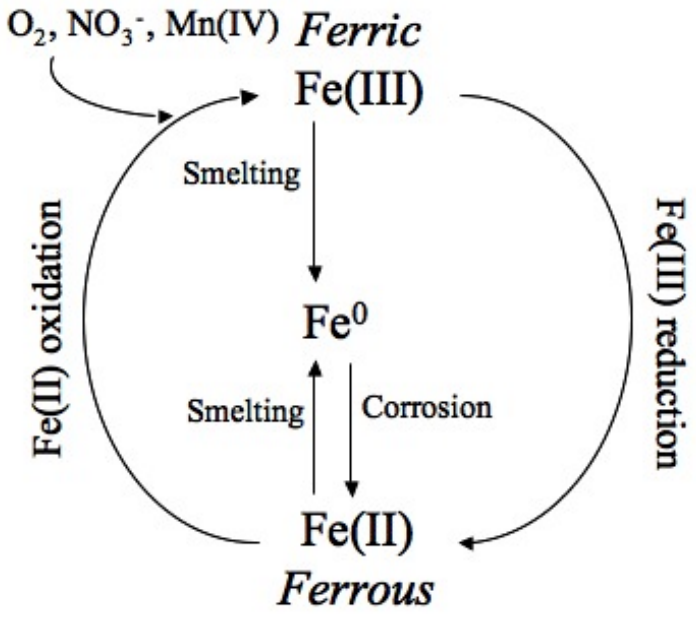

Figure 3.1: Basic redox cycles of Fe (Geomicrobiology-Fall 2005; Laura Crossey, University of New Mexico).

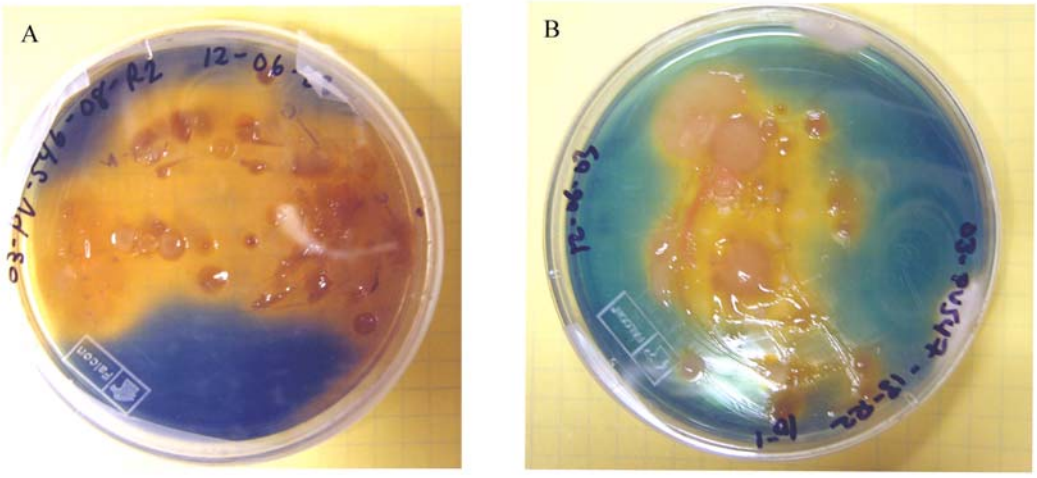

Figure 3.2: CAS plates from the 2003 cruise to Loihi Seamount, Hawaii (A. Templeton). Plates reveal a variety of morphologically and phenotypically distinct colonies, some of which could eventually be identified as siderophore-producing strains.

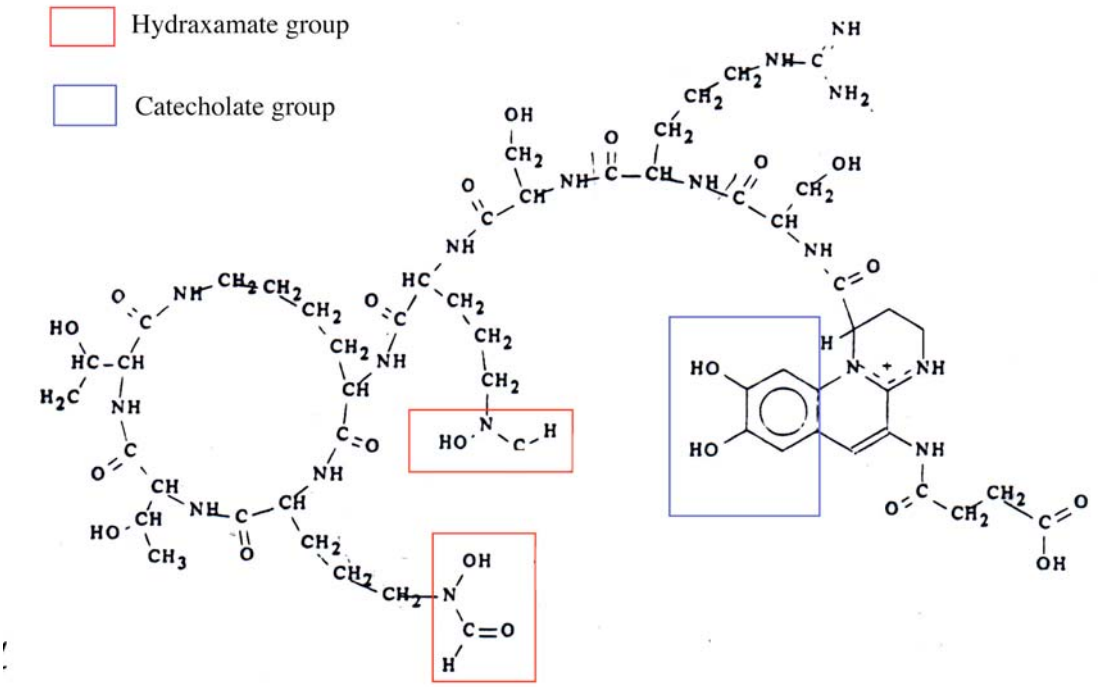

Figure 3.3: Structure of Pyoverdin. Two hydroxamate (in red) and one catechol (in blue) group represent the binding sites for Fe (modified from Demanger et al., 1987).

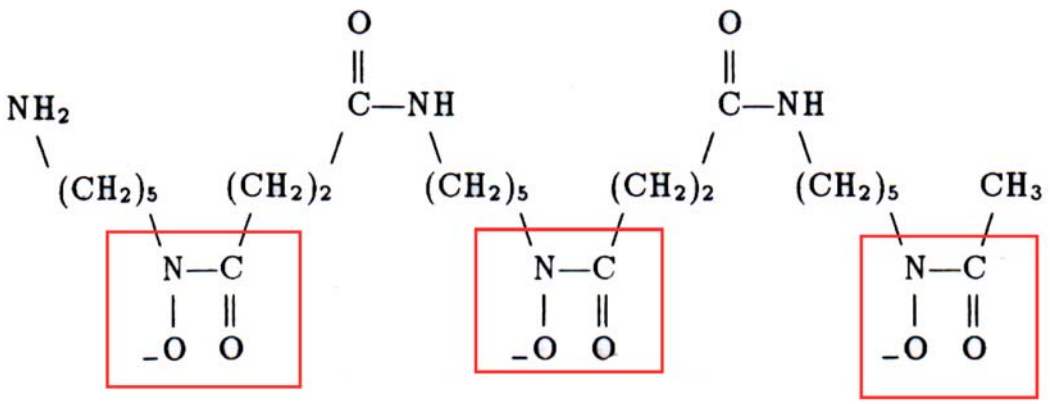

Figure 3.4: Structure of Desferrioxamine B (DFO-B). Three hydroxamate groups (red rectangles) are responsible for the binding of Fe (Hernlem et al. 1996).

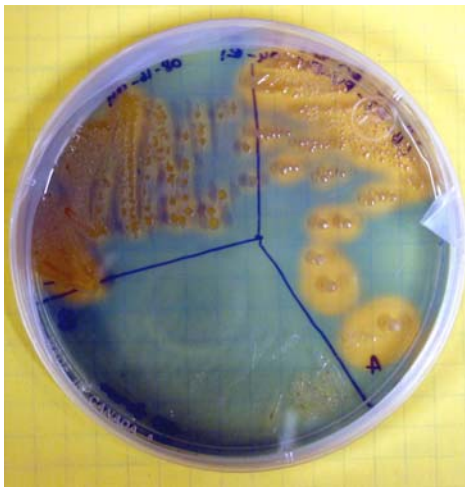

Figure 3.5: CAS plate after 1st transfer of colonies.

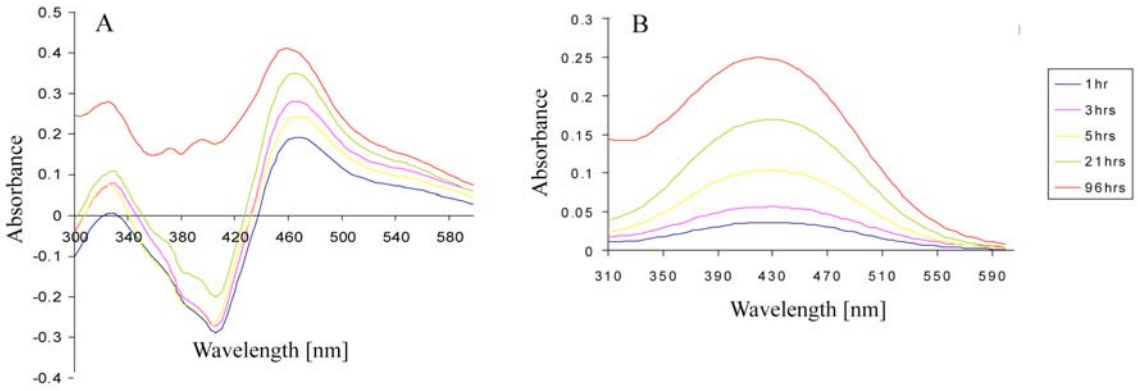

Figure 3.6: Spectrum for basalt PVD (A) and basalt DFO-B (B). A: measured between 300 and 600 nm. B: measured between 310 and 580 nm. The data have been corrected for PVD/water and DFO-B/water controls and show the change of the absorption at 460 nm (Fe(III)-PVD) and 430 nm (Fe(III)-DFO-B) over 96 hrs.

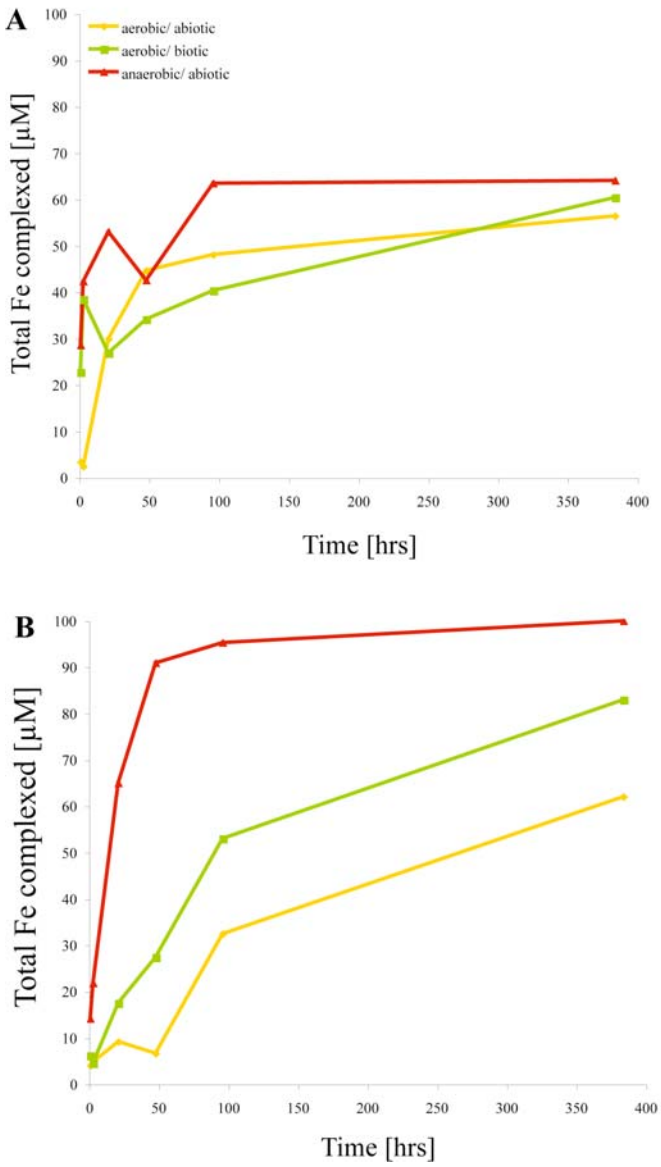

Figure 3.7: Complexation of Fe from basalt by PVD (A) and DFO-B (B) over 16 days. Y-axes show the total amount of Fe complexed [µM]. For the calculation of Fe-PVD and Fe-DFO-B extinction factors of ε=6500 mol^{-1} L and 2600 mol^{-1} L, respectively, were used.

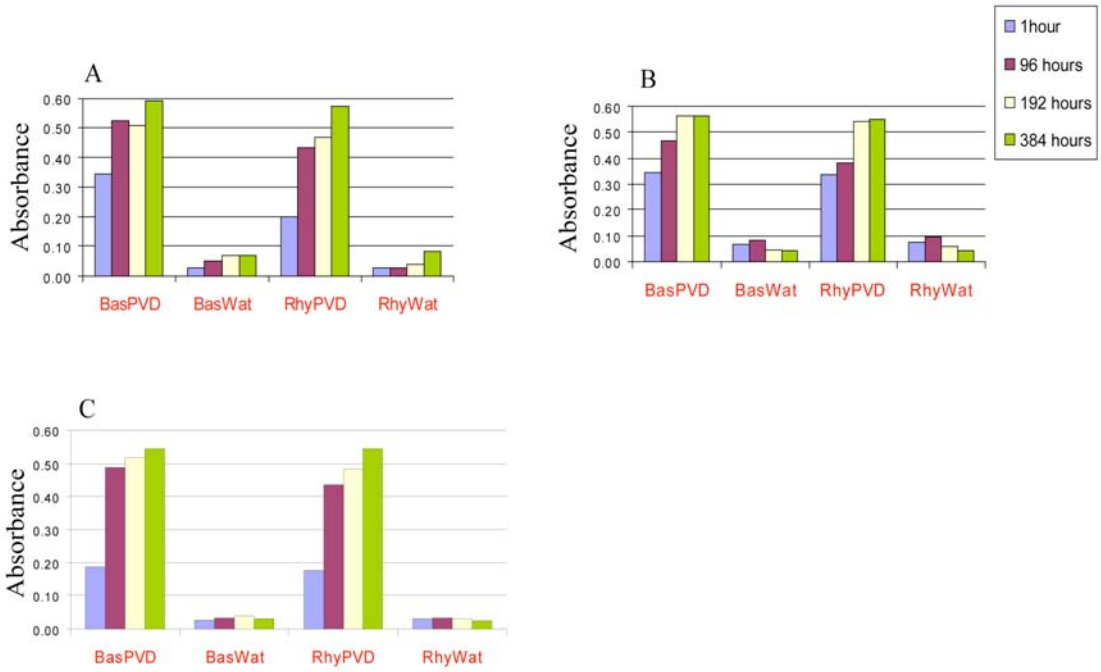

Figure 3.8: Fe-PVD complexation in all three experimental set-ups compared to the negative controls. A: Anaerobic/abiotic, B: Aerobic/biotic, C: Aerobic/abiotic. Increasing amounts of Fe are released from both volcanic rocks (Bas= basalt, Rhy= rhyolite) in the presence of PVD compared to a minimal release in the negative (rock/water: BasWat + RhyWat) controls without siderophores.

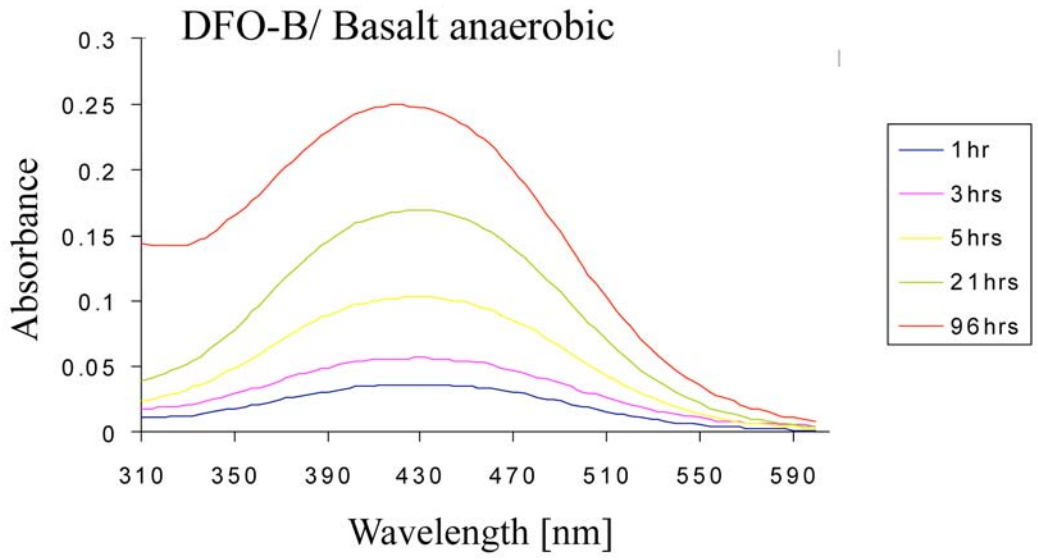

Figure 3.9: Basalt/DFO-B system under anaerobic conditions. Formation of a transfer band with maximum absorption at 430 nm representative of the triplicate $([Fe(III)(HDFB)]^{+}$ complex as previously shown by Farkas et al. (2001).

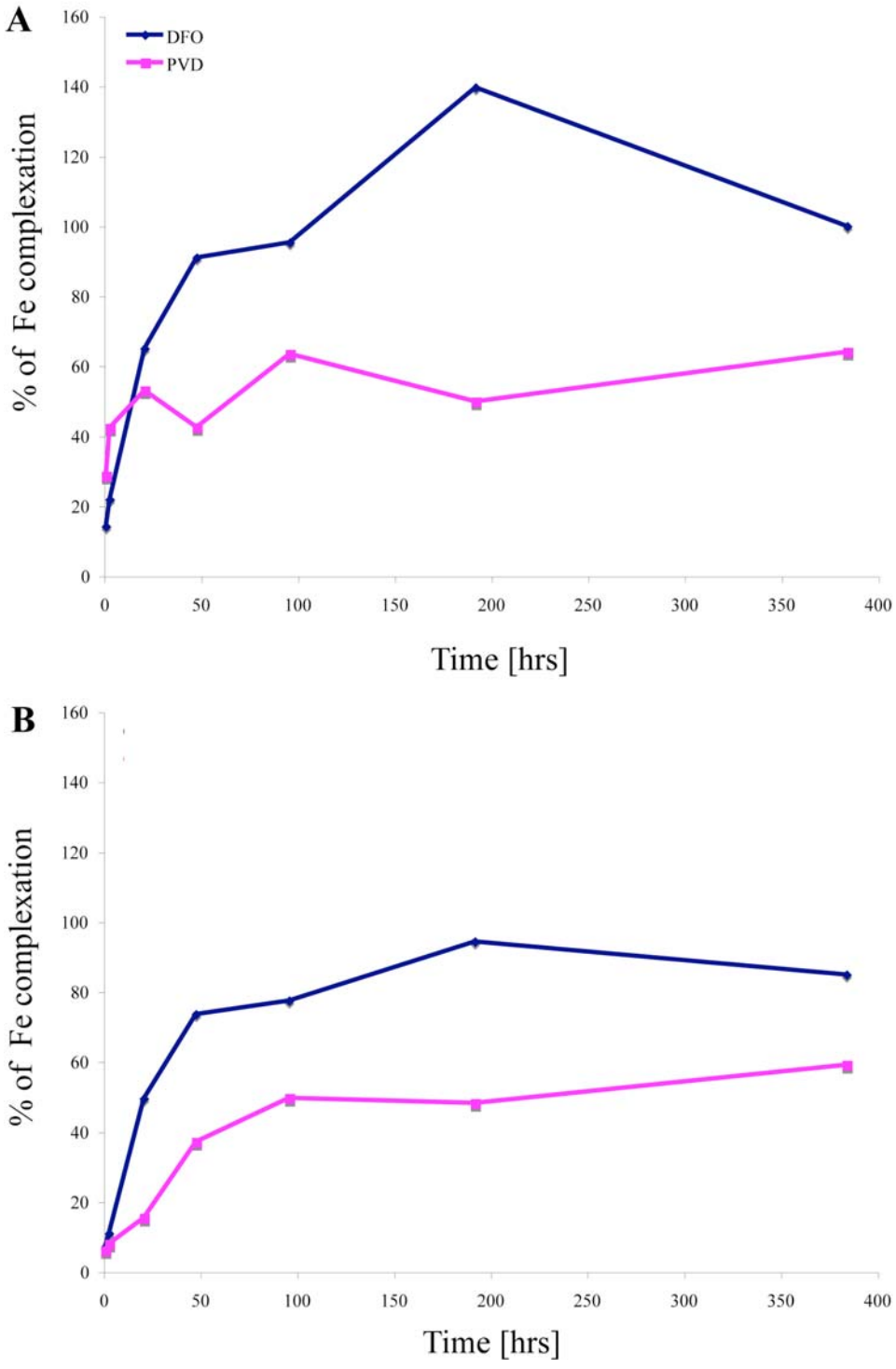

Figure 3.10: The complexation of Fe from basalt (A) and rhyolite (B) by PVD and DFO-B under anaerobic conditions. DFO-B appears to be a stronger complexing agent.

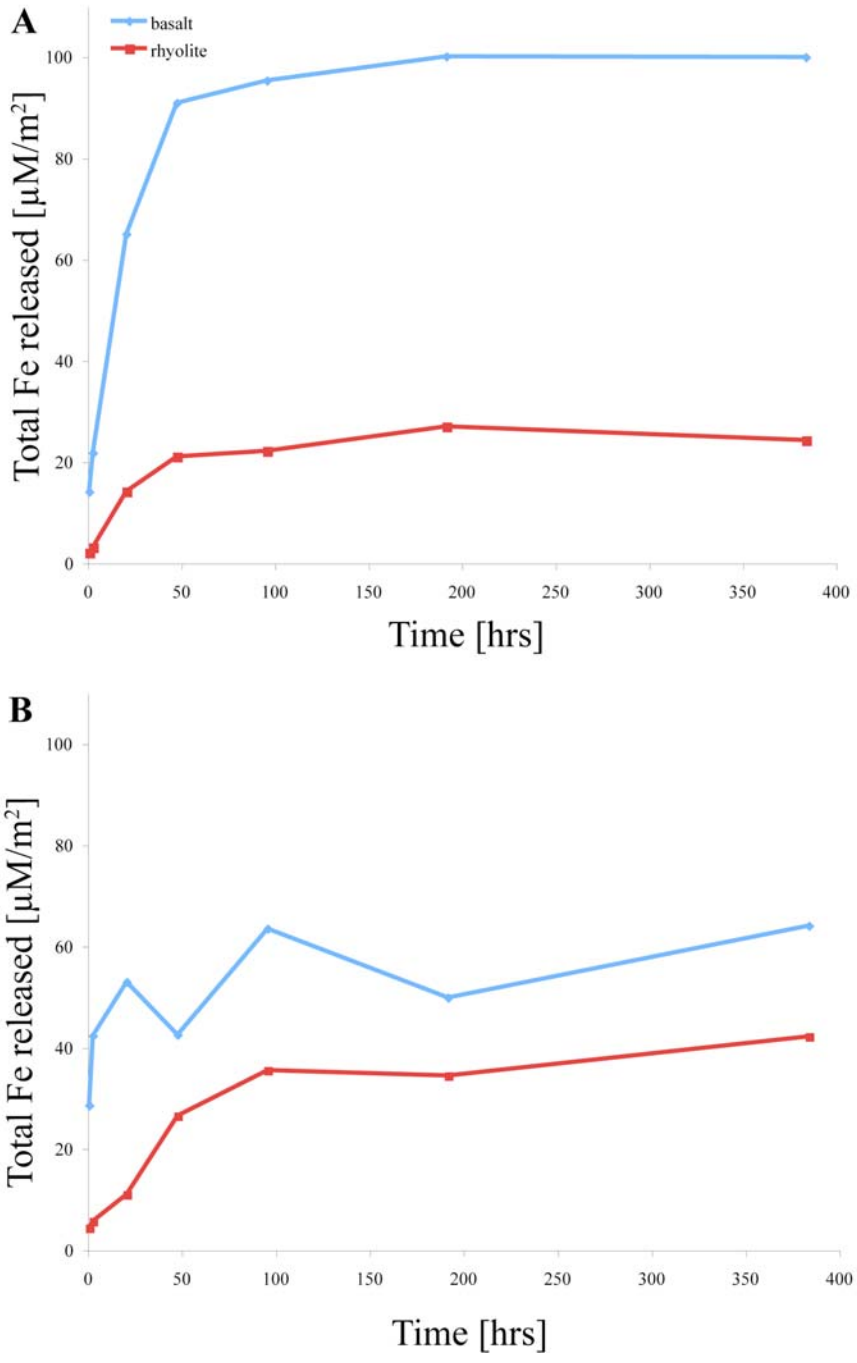

Figure 3.11: Amount of Fe released from basalt and rhyolite by A) DFO-B and B) PVD over 16 days normalized to the surface area of the rocks.

References

Altschul S. F., Madden T. L., Schaffer A. A., Zhang J., Zhang Z., Miller W. and Lipman D. J. 1997. Gapped BLAST and PSI-BLAST: a new generation of protein database search programs. Nucleic Acids Res 25:3389-3402.

Aouad G., Crovisier J. L., Geoffroy V. A., Meyer J. M. and Stille P. 2006. Microbially-mediated glass dissolution and sorption of metals by Pseudomonas aeruginosa cells and biofilm. J Hazard Mater 136:889-895.

Ashelford K. E., Chuzhanova N. A., Fry J. C., Jones A. J. and Weightman A. J. 2006. New screening software shows that most recent large 16S rRNA gene clone libraries contain chimeras. Appl Environ Microbiol 72:5734-5741.

Bailey B. E., Templeton A. S., Staudigel H. and Tebo B. 2009. Utilization of substrate components during basaltic glass colonization by Pseudomonas and Shewanella isolates. Geomicrobiology Journal 26:648-656.

Brantley S. L., Liermann L., Wu S. and Bau M. 2001. Uptake of trace metals and rare earth elements from hornblende by a soil bacterium. Geomicrobiology Journal 18:37-61.

Butler A. 1998. Acquisition and utilization of transition metal ions by marine organisms. Science 281:207-210.

Byrne R. H. 2002. Inorganic speciation of dissolved elements in seawater: the influence of pH on cencentration ratios. Geochem. Trans. 3:11-16.

Daughney C. J., Rioux J. P., Fortin D. and Pichler T. 2004. Laboratory Investigation of the Role of Bacteria in the Weathering of Basalt Near Deep Sea Hydrothermal Vents. Geomicrobiology Journal 21:21-31.

De Baar H. J. W. and De Jing J. T. M. 2001. Distributions, sources and sinks of iron in seawater. In: The biochemistry of iron in seawater. Turner D. R. and Hunter K. A., editors. 123-253.

Demanger P., Wendenbaum S., Bateman A., Dell A. and Abdallah M. A. 1987. Bacterial Siderophores: Structure and Physicochemical Properties of Pyoverdines And Related Compounds. In: Iron transport in microbes, plants and animals. Winkelmann G., Van der Helm D. and Neilands J. B., editors. 167-187.

Dong H., Kostka J. E. and Kim J. 2003. Microscopic Evidence For Microbial Dissolution Of Smectite. Clays and Clay Minerals 52:502-512.

Duckworth O. W., Holmström S. J. M., Peña J. and Sposito G. 2009. Biogeochemistry of iron oxidation in a circumneutral freshwater habitat. Chem Geol 260:149-158.

Edwards K. J., Bond P. L., Druschel G. K., McGuire M. M. and Hamers R., J. 2000. Geochemical and biological aspects of sulfide mineral dissolution: Lessons from Iron Mountain, California. Chem Geol 169:383-397.

Elderfield H. and Schultz A. 1996. Mid-ocean ridge hydrothermal fluxes and the chemical composition of the ocean. Ann. Rev. Earth Planet. Sct. 24:191-224.

Farkas E., Enyedy E. A., Zekany L. and Deak G. 2001. Interaction between iron(II) and hydroxamic acids: oxidation of iron(II) to iron(III) by desferrioxamine B under anaerobic conditions. J Inorg Biochem 83:107-114.

Frederickson J. K., Zachara J. M., Kennedy D. W., Dong H. L. and C. O. T. 1998. Biogenic iron mineralization accompanying the dissimilatory reduction of hydrous ferric oxide by a groundwater bacterium. Geochim Cosmochim Acta 62:3239-3257.

Gledhill M. and Van den Berg C. M. G. 1994. Determination of complexation of iron(III) with natural organic complexing ligands in seawater using cathodic stripping voltammetry. Mar. Chem. 47:41-54.

Gonye E. R. and Carpenter E. J. 1974. Production of iron-binding compounds by marine microorganisms. Limnol Oceanogr. 19:840-841.

Granger J. and Price N. M. 1999. The importance of siderophores in iron nutrition of heterotrophic marine bacteria. Limnol Oceanogr. 44:541-555.

Guan L. L., Kanoh K. and Kamino K. 2001. Effect of exogenous siderophores on iron uptake activity of marine bacteria under iron-limited conditions. Appl Environ Microbiol 67:1710-1717.

Hernlem B. J., Leland M. V. and Sayles G. D. 1996. Stability constants for complexes of the siderophore desferrioxamine B with selected heavy metal cations. Inorganica Chimica Acta 244:179-184.

Herrera A., Cockell C. S., Self S., Blaxter M., Reitner J., Arp G., Droese W., Thorsteinsson T. and Tindle A. G. 2008. Bacterial Colonization and Weathering of Terrestrial Obsidian in Iceland. Geomicrobiology Journal 25:25-37.

Hersman L. E., Forsythe J. H., Ticknor L. O. and Maurice P. A. 2001. Growth of Pseudomonas mendocina on Fe(III) (hydr)oxides. Appl Environ Microbiol 67:4448-4453.

Homann V. V., Sandy M., Tincu J. A., Templeton A. S., Tebo B. M. and Butler A. 2009. Loihichelins A-F, a Suite of Amphiphilic Siderophores Produced by the Marine Bacterium Halomonas LOB-5. J Nat Prod.

Kameyama T., Takahashi A., Kurasawa S., Ishizuka M., Okami Y., Takeuchi T. and Umezawa H. 1987. Bisucaberin, a new siderophore, sensitizing tumor cells to macrophage-mediated cytolysis. I. Taxonomy of the producing organism, isolation and biological properties. J Antibiot (Tokyo) 40:1664-1670.

Kolo K., Konhauser K., Krumbein W. E., Ingelgem Y. V., Hubin A. and Claeys P. 2009. Microbial dissolution of hematite and associated cellular fossilization by reduced iron phases: a study of ancient microbe-mineral surface interactions. Astrobiology 9:777-796.

Lane D. J. 1991. 16S/23S rRNA sequencing. In: Nucleic Acid Techniques in Bacterial Systematics. Stackebrandt E. and Goodfellow M., editors. 115-148.

Liermann L. J., Kalinowski B. E., Brantley S. L. and Ferry J. G. 2000. Role of bacterial siderophores in dissolution of hornblende. Geochim Cosmochim Acta 64:587-602.

Lovley D. R. and Phillips E. J. P. 1986. Organic matter mineralization with reduction of ferric iron in anaerobic sediments. Appl Environ Microbiol 51:683-689.

Martinez J. S., Zhang G. P., Holt P. D., Jung H. T., Carrano C. J., Haygood M. G. and Butler A. 2000. Self-assembling amphiphilic siderophores from marine bacteria. Science 287:1245-1247.

Millero F. J. 1998. Solubility of Fe(III) in seawater. Earth and Planet. Sci. Letters 154:323-329.

Mucha P., Rekowshi P., Kosakowska A. and al. e. 1999. Separation of siderophore by capillary electrophoresis. J Chromatogr A:183-189.

Neilands J. B. 1981. Iron absorption and transport in microorganisms. Annu Rev Nutr 1:27-46.

Petri R. and Imhoff J. F. 2000. The relationship of nitrate reducing bacteria on the basis of narH gene sequences and comparison of narH and 16S rDNA based phylogeny. Syst Appl Microbiol 23:47-57.

Rue E. L. and Bruland K. W. 1995. Complexation of iron(III) by natural organic ligands in the Central north Pacific as determined by a new competitive ligand equilibration/adsorptive cathodic stripping voltammetric method. Mar. Chem. 50:117-138.

Seyfried W. E. and Mottl M. J. 1995. Geological setting and chemistry of deep-sea

hydrothermal vents. In: The microbiology of deep-sea hydrothermal vents. Karl D. M.

Soria-Dengg S., Reissbrodt R. and Horstmann U. 2001. Siderophores in marine coastal waters and their relevance for iron uptake by phytoplankton: experiments with the diatom Phaeodactylum tricornutum. . Mar Eco. Prog Ser 22:73-82.

Street J. and Paytan A. 2005. Iron, phytoplankton growth, and the carbon cycle. In: Biogeochemical cycles of elements. A. S., Sigel H. and Sigel R. O., editors. 153-185.

Sudek L. A., Templeton A. S., Tebo B. and Staudigel H. 2009. Microbial Ecology of Fe (hydr)oxide mats and basaltic rock from Vailulu'u Seamount, American Samoa. Geomicrobiology Journal 26:581-596.

Takahashi A., Nakamura H., Kameyama T., Kurasawa S., Naganawa H., Okami Y., Takeuchi T., Umezawa H. and Iitaka Y. 1987. Bisucaberin, a new siderophore, sensitizing tumor cells to macrophage-mediated cytolysis. II. Physico-chemical properties and structure determination. J Antibiot (Tokyo) 40:1671-1676.

Templeton A. S., Knowles E. J., Eldridge D. L., Arey B. W., Dohnalkova A. C., Webb S. M., Bailey B. E., Tebo B. M. and Staudigel H. 2009. A seafloor microbial biome hosted within incipient ferromanganese crusts. Nature Geoscience 2:872-876.

Trick C. G. 1989. Hydroxamate-siderophore production and utilization by marine eubacteria. Current Microbiology 18:375-378.

Uroz S., Calvaruso C., Turpault M. P. and Frey-Klett P. 2009. Mineral weathering by bacteria: ecology, actors and mechanisms. Trends Microbiol 17:378-387.

Von Damm K. L. and Bischoff J. L. 1987. Chemistry of hydrothermal solutions from the southern Juan de Fuca Ridge. J. Geophys. Res. 92:11334-11346.

Von Damm K. L., Bray A. M., Bittermore L. G. and Oosting S. E. 1998. The geochemical relationship between vent fluids from the lucky strike vent field. Mid-Atlantic Ridge. Earth Planet. Eci. Lett 160:521-536.

Weaver R. S., Kirchbam D. L. and Hutchings D. A. 2003. Utilization of iron/organic ligand complexes by marine bacterioplankton. Aquatic Microb. Ecol. 31:227-239.

CHAPTER IV: **Exploring volcanic glass colonization by the deep-sea, heterotrophic Fe(II)oxidizing bacterium *Pseudomonas stutzeri* VS-10**

Abstract

There is evidence for microbial colonization of submarine volcanic rocks throughout most of Earth's history but the selective advantage driving this process is unclear. Our objective was to develop an environmentally relevant model system for studying the interactions between bacteria and submarine basalt surfaces. We used *Pseudomonas stutzeri* VS-10, a heterotrophic Fe(II)-oxidizing bacterium isolated from a volcanic rock surface at Vailulu'u Seamount. It showed elevated growth under nutrient-limited conditions in the presence of basaltic glass suggesting potential benefits of a surface association of the bacterium with the basalt. *P. stutzeri* VS-10 biofilm morphology on volcanic glass surfaces was examined using scanning electron microscopy. In addition an interdisciplinary approach of culture-based, chromatographic and nanolithographic techniques was used to determine the potential physiology behind the cell-glass interactions. Fe availability and direct attachment of cells to the glass surface were found to be pivotal factors in enhancing surface-related growth of this heterotrophic deep-sea bacterium. Fibrillar extracellular polymeric material (EPM), an

essential element of the biofilm structure, was shown to be conductive suggesting its involvement in electron transfer reactions.

We suggest that glass (aside from its role as a source of Fe) functions as a secondary energy source and/or sink based on VS-10's abilities to oxidize Fe(II) heterotrophically and to transfer electrons to/from solid surfaces. This mechanism may provide a key advantage in an environment with steep and dynamic geochemical gradients such as hydrothermally influenced seamount habitats. Furthermore, the resulting oxidative transformation of volcanic glass potentially affects the geochemical cycling of bio-essential nutrients.

Introduction

Bacteria have been shown to play a pivotal role in the geochemical cycling of elements and the overall ecological function of deep-sea aquatic systems (Deming and Baross 1993; Edwards et al. 2005). It has long been recognized that bacteria in natural aquatic populations have a marked tendency to interact with surfaces (Zobell 1943) and form matrix-enclosed communities (Costerton and Wilson 2004). The proclivity of bacteria to adhere to surfaces and form biofilms is related to the selective advantage that surface association offers over a free-living, planktonic life-style. Proposed benefits from a surface-attached life-style are: 1) resistance to physical forces such as shear flow, enabling bacteria to remain within a favorable environmental niche (Jefferson 2004); 2)

an elevated concentration of nutrients; 3) protection against predation through biofilm-specific chemical defense; and 4) the development of stable interactions and microenvironments, resulting in synergistic consortia (Flemming 2008). In deep-sea hydrothermal systems, where microbial communities are subject to strong and constantly changing physico-chemical gradients (Staudigel et al. 2006), the formation of biofilms is particularly advantageous.

Microbial colonization promotes mineral transformation, for example through the release of metabolic byproducts such as organic and inorganic acids and ligands (Barker and Banfield 1996; Edwards and Rutenberg 2001; Sheng et al. 2008; Templeton and Knowles 2009). Microorganisms modify rates of chemical and physical weathering of minerals, silicate rocks and volcanic glasses by directly or indirectly inducing hydration, dissolution, and secondary mineral formation (Banfield et al. 1999; Daughney et al. 2004). Colonization mechanisms have been classified into specific and non-specific interactions (Busscher and Weerkamp 1987). Non-specific colonization (e.g. facilitated through adhesin-receptors) represents a result of fortuitous physicochemical interactions (Fletcher 1996). In contrast, specific attachment is considered to evolve in situations where colonization promises an ecological advantage such as nutrient and/or energy acquisition (Bailey et al. 2009; Donlan 2002; Jefferson 2004).

The contribution of extracellular polymeric material (EPM) in biofilm formation, structure and function has been well studied (Allison et al. 1998; Danese et al. 2000; Watnick and Kolter 1999). The role of such substances in bioleaching of minerals has

been investigated (Kinzler et al. 2003; Sand and Gehrke 2006). Bacteria are able to adapt the composition and amount of their EPM according to the growth substrate (Rohwerder et al. 2003). EPM is widely observed in microbial biofilms in the amorphous form as well as in the form of filaments or bacterial appendages. More recently the role of such filaments in the electron transport chain of dissimilatory metal-reducing bacteria (DMRB) was demonstrated. Due to their conductivity and their "wire-like" appearance the term "nanowires" was introduced (El-Naggar et al. 2008; Gorby et al. 2006; Reguera et al. 2005). In case of DMRB the nanowires are considered to help bacteria overcome the poor solubility of terminal electron acceptors including Fe(III) and Mn(IV) minerals. Whether such filaments can be considered "wires" and are specifically formed for the transport of electrons is controversial. Other authors suggest they represent amorphous EPM structures that were altered during the dehydration process of samples (Dohnalkova et al. 2011). The abundance of such filaments in strains from variable environmental habitats and their role in metabolic processes remain for the most part unknown. Here we here investigate the role of EPM filaments in growth of an Fe(II)-oxidizing deep-sea strain on basaltic glass.

Basalt comprises major parts of the oceanic lithosphere and contains bio-essential elements including Fe, Mg, Ca, Mn and several other trace elements (Winkelmann 1997). Reduced elements such as Fe(II) and Mn(II) can serve as potential electron donors for chemolithotrophic communities (Bach and Edwards 2003; Christie et al. 2001). In addition, oxidized compounds (e.g. Fe(oxy)hydroxides) often found in association with

submarine basaltic glass surfaces represent potential electron acceptors which could be important in anaerobic microenvironments (Reguera et al. 2007).

Basaltic glass typically constitutes the outer layer of submarine volcanic rocks formed from lava rapidly quenched by seawater. Recent phylogenetic studies have shown that they harbor phylogenetically diverse microbial communities (Lysnes et al. 2004; Mason et al. 2007; Santelli et al. 2008; Sudek et al. 2009; Thorseth et al. 2001). Quantitative polymerase chain reaction (qPCR) measurements of the glass rim of young weathered basalts from the East Pacific Rise (EPR) have indicated total prokaryotic (bacterial and archaeal) cell densities between 3×10^6 to 1×10^9 cells per g of rock (Santelli et al. 2008). In contrast, the total microbial cell number of deep ocean waters (>1000 m) only ranges between 8×10^3 to 9×10^4 cells per ml of seawater (Santelli et al. 2008). Basalt surface-related microbial biofilms typically consist of cell clusters and mature biofilms of different morphological appearance (Templeton et al. 2009; Thorseth et al. 2001). These structures have been suggested to correlate with successive stages of colonization starting with incipient microbial colonization by single cells and prosthecate organisms (Einen et al. 2006) and developing into more mature microbial communities (Thorseth et al. 1995).

Bacterial metabolisms within such basalt surface-related communities have been shown to be versatile (Sudek et al. 2009; Templeton et al. 2005). Chemolithoautotrophic Fe(II)-oxidizing organisms are widely assumed to fix carbon that at least part of the basalt community relies upon (Santelli 2007). In addition, heterotrophic Fe(II)- and

Mn(II)oxidizing as well as siderophore-producing strains have been found in great abundance (Edwards et al. 2003; Sudek et al. 2009; Templeton et al. 2005). Many of these strains exhibit multiple metabolic functions (siderophore production and heterotrophic and oligotrophic Fe(II)-oxidation (Sudek et al. 2009). It is unclear to what degree basalt supports these communities and to what extent their metabolisms may affect basalt weathering rates and the biochemical cycling of Fe and Mn at biofilm/basalt interfaces.

Here, we present *Pseudomonas stutzeri* VS-10, one of the heterotrophic Fe(II)oxidizing bacteria isolated from submarine volcanic rock at Vailulu'u Seamount (Sudek et al. 2009). *P. stutzeri* can be found abundantly in both terrestrial and marine ecosystems (Lalucat et al. 2006). *P. stutzeri* VS-10 was used as a model organisms in an interdisciplinary approach to study the characteristics of microbe/glass interactions. This includes its biofilm morphology, electrochemical properties of structural elements (i.e. filamentous EPM) within surface-related biofilms and the importance of direct attachment of cells to the glass in growth of the strain. A physiological and metabolic characterization of the bacterium was used to evaluate the role of basaltic glass in facilitating growth of the strain. We offer insights into deep-sea biofilm formation by a ubiquitous marine bacterium and discuss the process of and potential benefits from microbial glass colonization.

Materials & Methods

1. Volcanic rocks and minerals

Rhyolitic glass used for the isolation of *Pseudomonas stutzeri* VS-10 was originally collected from an obsidian dome in Long Valley (near Mono Lake). Prior to its submarine deployment its surface area was increased by crushing it into a fraction between very fine sand and coarse silt (62.5-31.25 μm) using a stainless steel disc crusher. The rock was subsequently sieved to the appropriate grain size, washed with deionized water and filled into a nitex nylon sachet (mesh size: 31 μm) measuring ~ 1 cm x 0.5 cm (height x length). The sachet was loaded into a perforated polyvinyl chloride (PVC) pipe along with other rock samples and was autoclaved wrapped in tin foil at 121 °C for 30 minutes where it remained until sample deployment.

The basaltic glass used in all experimental setups was originally collected at Kilauea volcano (Pu'U-o'O) in 2002 and had been re-melted as described elsewhere (Bailey et al. 2009). Fe(II) content in the basalt averaged around 9-10 wt %. Rhyolitic glass and quartz minerals were used in other experimental setups to determine the growth characteristics of strain VS-10 on low Fe(II)-containing igneous rocks and silicate minerals. The same rhyolite previously used for the isolation of the strain was used. On average containing 0.9 wt % of Fe(II) it represents the felsic equivalent of basalt. Pure, transparent quartz crystals were chosen as a negative control in the form of a silica-rich but Fe depleted mineral highly abundant in the Earth's crust. Quartz crystals were

obtained from H&P minerals (Columbus Junction, Iowa) and did not contain any visible inclusions. For the growth experiment basalt, rhyolite and quartz were crushed to an approximate grain size of around 2-3 mm, washed several times in deionized water, washed twice in 0.1N HCl to remove potential surface Fe and sonicated in deionized water for 40 min. After a final rinse with deionized water the glasses were dried in sterile glass dishes covered with aseptic aluminum foil at 40 °C and then microwave sterilized in the glass dishes for 10 min.

2. Sample description and collection

P. stutzeri VS-10 was isolated from a rhyolitic rock surface exposed to low-temperature, non-hydrothermally influenced conditions (Marker 2: 14 13.103S / 169 04.106W; 582 m water depth) at Vailulu'u Seamount for three months. Samples were collected by the Pisces V submersible onboard the *R/V Ka'Imikai'O'Kanaloa* (operated by the Hawaii Undersea Research Lab, HURL) in July 2005. The PVC "charge" containing the rhyolite sample was deployed and retrieved in a sealable "bio-box". Deionized water placed inside the box for deployment was, upon sample collection, replaced by ambient seawater. The "biobox" was closed at depth preventing contamination of samples with surface waters upon retrieval.

Onboard the rock samples were further processed in a flow hood where part of the rock was transferred to tubes filled with 1 ml of filter sterilized deep-seawater collected at Vailulu'u. Bacteria were vigorously shaken off the rock and 100 µl of the resulting

cell/sea water suspension was spread onto Chrome-Azurol-Sulfonate plates (CAS, see below). The plates were subsequently stored at 4 C° in the dark until transport to Scripps Institution of Oceanography.

3. Growth media and conditions

3.1 Chrome-Azurol-Sulfonate (CAS) plates

A modified version of CAS plates previously described (Schwyn and Neilands 1987) was used for the isolation of siderophore-producing strains . Artificial seawater agar (49.4 g $MgSO_4$ x $7H_2O$, 5.85 g $CaCl_2$ x $2H_2O$, 70.2 g NaCl, 3 g KCl, 1 g NH_4Cl, 0.1 g glycerophosphate, 1.5 g glycerol, 15 g agar per L, 10 mM 4-(2-hydroxyethyl)-1-piperazineethanesulfonic acid, pH 7.4, 2 mM $NaHCO_3$) was amended with 30 ml of CAS dye (Schwyn and Neilands 1987). Plates were incubated at 4 °C and colonies were picked and successively transferred to new CAS plates until isolation of pure cultures was obtained.

3.2 Minimal glycerol medium

A defined glycerol-based artificial seawater medium was used in the majority of experiments. The medium contained per 1L of ultrapure H_2O: 100 mM $MgSO_4$, 20 mM $CaCl_2$, 600 mM NaCl, 20 mM KCl, 40 mM glycerol, 333 μM K_2HPO_4, 18.5 mM NH_4Cl and 50 mM HEPES (pH 7.4). To limit the potential contamination of the medium with Fe the medium was passed through a column containing Chelex-100 resin (analytical grade 100-200 mesh sodium form, Bio-Rad cat. # 142-2832) prepared based on a technique by

Price et al. (1989) and previously adjusted to pH 7.4. The Chelex was loaded in a previously acid washed (10 % HCl, Fisher cat. # A144-212) 1.5 x 15 cm glass column (Kontes class company flex column, cat. # 420400-1515) equipped with a 3-way nylon stopcock (Kontes cat. # 420 163-4503). The flow rate was adjusted to approximately one drop per second. The medium was subsequently filter sterilized through 0.22 μm Stericups (Millipore cat. #: SCGPU05RELC) and the pH was measured. To test for the role of basalt as a source for nutrients and energy no trace elements or vitamins were added.

3.3 F-medium

Organic-rich "F-plates", designed for the enrichment and isolation of heterotrophic Fe(II)-oxidizing bacteria, were prepared from a low-nutrient agar medium amended with 400 μM $FeSO_4$ as described previously (Sudek et al. 2009). The strain's potential to oxidize Fe(II) on F-plates was evaluated based on the formation of orange-colored colonies indicating the presence of Fe (hydr)oxides and confirmed by the Prussian Blue spot test described elsewhere (Kucera and Wolfe 1957).

3.4 Artificial seawater medium (X medium)

To test for the strain's ability to reduce soluble Fe(III) under anaerobic conditions *P. stutzeri* VS-10 was grown anaerobically in 5 ml of an oligotrophic artificial seawater medium amended with 20 mM Fe^{3+}citrate in the presence various electron donors. In 1L of pure water the medium contained: 0.5M NaCl, 30 mM $MgCl_2$, 14 mM KCl, 1 mM $CaCl_2$, 2 mM K_2HPO_4 and 2 mM $NaHCO_3$. The medium was brought to a boil. Five ml

were transferred to sterile hungate tubes. The tubes were sealed with a rubber stopper and bubbled with N_2:CO_2 (80:20) for 25 min. They were then autoclaved at 121 °C for 30 min. and allowed to cool before 5 μl of a filter-sterilized vitamin solution (Pfennig and Lippert 1966) was added. Additionally each tube was amended with anaerobically prepared solutions of Fe^{3+}citrate along with lactate, formate or glucose as carbon sources to final concentrations of 20 mM.

4. Growth experiments

Prior to the inoculation of all minimal medium cultures with *P. stutzeri* VS-10, the strain was grown at 37 C° overnight in Luria-Bertani (LB) medium (per L of ultrapure H_2O: 10 g Bacto Tryptone, 5 g Yeast Extract, 10 g NaCl, adjusted to pH 7.0). Cells were harvested by centrifugation at 8 000 rpm for 10 min. and washed three times in 5 ml of minimal glycerol medium. The optical density at 600 nm of the final resuspension of cells was measured to estimate cell numbers. 15 ml glass tubes, previously washed in 10 % HCl for 2 days, rinsed 6 times in deionized water and microwave-sterilized for 10 min., were used to determine growth of *P. stutzeri* VS-10 on minimal glycerol medium in the presence of basalt, rhyolite, quartz or soluble Fe. ~ 0.5 g of either volcanic rock grains or minerals was added to 5 ml of chelexed medium. For soluble Fe a filter-sterilized $FeCl_2$ solution was added to the medium to reach a final concentration of 100 μM. Due to the acidity of the $FeCl_2$ solution the pH inside these tubes had to be readjusted prior to inoculation with the culture. The pH in all tubes was tested and ranged around 7.5. Due to the aerobic and neutral nature of the setup all Fe in the experiment containing $FeCl_2$ is considered to have oxidized. No Fe(III) precipitation

was visible possibly due to the low Fe concentration. This setup therefore represents growth of the strain in the presence of Fe(hydr)oxides. Except for the abiotic (rock/water, mineral/water) controls each tube was subsequently inoculated with the washed cell suspension (see above) of *P. stutzeri* VS-10.

For the removal of biofilms from the interior of the glass tubes as well as from the rock and mineral grains prior to spectrophotometric cell density measurements at 600 nm the tubes were briefly vortexed and vigorously tapped onto a surface. Scanning electron micrographs (SEM) later showed the effectiveness of this method in removing bacterial cells from the surfaces. Due to the size and density of rock and mineral grains and their rapid settling after vortexing they are unlikely to have interfered with the measurements.

To determine anaerobic reduction of soluble Fe (III) by *P. stutzeri* VS-10, samples were continuously taken over 2 weeks. First soluble Fe(II) and, after reduction of the growth medium, total Fe was colorimetrically determined with ferrozine (Stookey 1970).

5. DNA extraction and phylogenetic identification

Total genomic DNA of *P. stutzeri* VS-10 was extracted using the CTAB extraction method (www.sou.edu/BIOLOGY/Faculty/Southworth/CTAB/htm). The two universal bacterial primers 27f (5'-AGA GTTT GAT CMT GGC TCA G-‘3) and 1492r (5'-TAC GGY TAC CTT GTT ACG ACT T-’3) (Lane 1991) were used to amplify the 16S gene. Each 50 µl PCR reaction contained 1.5 pmol of each primer, 1.25 units Taq

DNA polymerase (Roche), 1x PCR buffer (Roche), 1 nmol of each deoxynucleoside triphosphate (Invitrogen) and 10 μM of bovine serum albumin (BSA). After running the PCR at 95 °C = 3 min.; 30 x (95 °C = 30 sec., 54 °C = 30 sec., 72 °C = 1 min.) and 72 °C = 7 min., the PCR product was purified using the QIAquick PCR Purification Kit (Qiagen Inc., Valencia, CA). Sequencing was carried out by Seqxcel Inc., San Diego (http://www.seqxcel.com). Sequence reads were assembled and analyzed in Sequencher 4.8 (GeneCodes) resulting in a near full-length 16S rRNA gene (~1300 bp). The sequence was checked for its orientation and its potential of being chimeric using OrientationChecker and Mallard (Ashelford et al. 2006) before identifying the closest related strain via BLAST (Altschul et al. 1997).

6. Nucleotide sequence accession number

The 16S sequence of *P. stutzeri* VS-10 has been submitted to the GenBank database under accession number FJ662872.

7. Liquid chromatography electrospray ionization mass spectrometry (LC-ESI-MS)

LC-ESI-MS analysis was applied to detect siderophores in the media filtrates of strain VS-10 when grown under Fe-limited conditions on minimal glycerol medium in the presence of rhyolite. As described previously (see 4.), LB cultures of the strain were washed extensively to remove nutrients prior to inoculation of nutrient-limited media at OD_{600} of ~0.05. Cultures were incubated on a rotary shaker (~ 200 rpm) at room temperature for 4-6 days. The supernatant was subsequently filter-sterilized (0.22μm Millex GP sterile syringe filters, Millipore) and run on an LC-ESI-MS in the Department

of Chemistry and Biochemistry Mass Spectrometer Facility (University of California, San Diego). Between 10 and 20 µl of supernatant were loaded onto a Majic C-18 column (200a, 1mm x 50 mm) and absorption was measured at 250 nm. 2.5 % Acetonitrile (ACN) in H_2O with 0.08 % trifluoroacetic acid (TFA) (A) and 90 % ACN in H_2O with 0.08 % TFA (B) served as solvents in the following gradient protocol: Hold at 5 % B for 2 minutes, 5 to 90 % B in 20 minutes, hold at 90 % B for 6 minutes, 90 to 5 % B in 2 minutes, hold at 5 % B for 5 minutes. The flow rate was adjusted to 50 µl/min.

8. Diffusion chamber

The significance of direct attachment of cells to the basalt surface for growth of *P. stutzeri* VS-10 was investigated in diffusion chambers. Two dual compartment borosilicate chambers described elsewhere (Bretschger et al. 2007) were used.

The compartments were separated by a proton-exchange membrane (Nafion® 424, DuPont). Prior to inoculation with *P. stutzeri* VS-10 cells 5 g of sterile basalt was added to one of the compartments. The glass chambers were assembled, wrapped in aluminum foil and autoclaved at 121 ° C for 30 min. Upon cooling 50 ml of filter sterilized minimal glycerol medium was added to both compartments. Nutrient-limited washed cells (see 4.) of *P. stutzeri* VS-10 were added to an initial OD_{600} of ~0.05 to the compartment containing basalt grains in one setup and to the opposite side in the other setup. Cell growth was subsequently monitored based on optical density measurements at 600 nm. The abiotic status of the uninoculated compartment was continuously monitored based on optical density measurements and microscopic analysis. A constant flow of

filter-sterilized oxygen was applied to both sides of each chamber to assure sufficient oxygen concentrations for the growth of the strain and to support homogenization of the solution prior to optical density measurements. Biofilm formation on the inside walls of the glass chamber was minimized by vigorous shaking and careful tapping, resulting in the visible detachment and homogenization of biofilms from the glass walls. Using sterile pipets the solution was again homogenized prior to sampling.

9. Scanning Electron Microscopy (SEM)

SEM was utilized to investigate biofilm formation and morphology of *P. stutzeri* strain VS-10 on basaltic glass surfaces. To preserve the internal structure and cell integrity of all samples they were initially fixed in 2.5% glutaraldehyde (v/v) in 0.1 M sodium cacodylate buffer (pH 7, Fisher cat. # NC9842332) at 4 °C overnight. To remove salts the samples were then washed with 30 and 15 mM 2-[4-(2-sulfoethyl)piperazin-1-yl]dethanesulfonic acid (PIPES). The samples were then gradually dehydrated by washing with a graded series of 10, 25, 50, 75, 90 and finally 100% ethanol for 5 minutes each. To prevent deformation and collapse of the surface structure and to conserve surface morphology, the ethanol was replaced by liquid CO_2 via critical point drying at 31.1°C and 1072 p.s.i. for 10 minutes. After mounting the samples on SEM stubs they were sputter-coated with gold/palladium (80/20) in a coating unit at V = 2.5 KV and I = 20 mA for 60 sec. Visualization of the samples was performed on a Philips XL30 field emission SEM (FESEM) at the Nano3 facility of the University of California, San Diego.

10. Microbial Fuel Cell

Electrochemical properties of the *P. stutzeri* VS-10 biofilm under nutrient-limited conditions were investigated in microbial fuel cells (MFCs). Current production was observed using dual compartment MFCs of the type shown in Bretschger et al. (2007). MFCs were assembled using proton-exchange membranes (Nafion® 424, DuPont) and electrodes constructed from graphite felt (GF-S6-06, Electrolytica) bonded to platinum wire (0.3 mm, Alfa-Aesar). The cathode electrodes were electroplated with a platinum catalyst over the entire surface area to drive the oxygen reduction reaction. Rubber tubing was attached to each half-cell to prevent pressurization of the cells and enable inoculation and removal of samples. The fuel cells were wrapped in aluminum foil and autoclaved at 121 ° C for 30 min. Thirty ml of minimal medium was then added through 0.22 μm filters (Millipore) into each of the compartments. Prior to inoculation of the anode compartment *P. stutzeri* VS-10 was grown to exponential phase on LB medium and was inoculated at a final OD_{600} of ~0.05. In addition an uninoculated cell was run as a blank. Throughout the experiment samples were taken through sterilized disposable borosilicate glass Pasteur pipettes (Fisher cat # 13-678-20C) and the OD_{600} of the culture was spectrophotometrically determined. Initially, aerobic conditions inside the cell were established by supplying filter-sterilized oxygen (0.22 μm) to both compartments close to the electrodes. After 73 hrs conditions were changed from aerobic to microaerobic conditions by replacing the oxygen flow to the anode compartment with filter-sterilized (0.22 μm) nitrogen. While these conditions technically represent “microaerobic” conditions (because the MFC was incubated under aerobic conditions and is not air-tight)

they can be considered anaerobic due to heavy and constant bubbling with N_2 throughout the anode compartment but in particular near the electrode.

MFC voltage was measured every minute across a 100 Ω external resistor using a high-impedence digital multimeter (model 2700; Keithley Instruments). For the polarization the circuit was opened and the cell potential was allowed to build to a maximum (Open Circuit Potential, OCP). Once the OCP was reached, a potentiostat (Gamry Inc) was used to measure the polarization behavior of the MFC. During this process the external resistance is decreased from a maximum (infinite resistance) to a minimum (short circuit) and the corresponding current is measured. Current ('I') is calculated from these data using Ohm's law (I=V/R) and Power ('P') is calculated using P=I*V. The total surface area of the anode was 290 cm^2.

The fuel cell was also evaluated using cyclic voltammetry to determine the electrochemical activity of the abiotic components (e.g. electrodes) as well as the biotic components (e.g. bacteria). In this experiment the voltage of the electrode was swept at a scan rate of 25 mV/s from -500 mV to +500 mV vs. Ag/AgCl while measuring the current response. At the termination of the experiments the electrodes were harvested, fixed in 2.5% glutaraldehyde (v/v) in 0.1 M sodium cacodylate buffer (pH 7, Fisher cat. # NC9842332) at 4 °C overnight and visualized by SEM.

11. Nanolithography

Conductivity measurements of filamentous EPM within the *P. stutzeri* VS-10

biofilm were investigated using a nanolithographic technique. *P. stutzeri* VS-10 was grown under nutrient-limited conditions on 5 ml of minimal glycerol medium in the presence of rhyolite. After growth to an approximate optical density (OD_{600}) of 0.25 the supernatant was decanted. Next, 5 ml of fresh minimal glycerol medium was added to the rhyolite grains and bacterial cells were vigorously shaken off the rock surfaces. Since the cell suspension still appeared too dense, complicating the process of imaging single cells and EPM filaments, the cell suspension was decanted and another 5 ml of fresh medium was added to the rocks. Cells were shaken off as previously described and 250 μl of the final cell suspension was finally fixed in 2.5% glutaraldehyde at 4 °C overnight. A few μl of this suspension was then placed onto an oxidized silicon wafer chip upon which pre-patterned gold electrodes had been deposited. The samples were subsequently dehydrated in 10, 25, 50, 75 and 100 % (v/v) ethanol, critically-point dried and imaged on a Zeiss 1540 cross-beam (XB)-FESEM. The SEM was used to locate EPM filaments located between two of the gold electrodes. Using Ion-Assisted Vapor Deposition, platinum electrodes were drawn connecting the gold electrodes to the EPM filaments of *P. stutzeri* VS-10. Once the electrodes were drawn the samples were removed from the SEM and placed onto a voltage (Amtel 5156D) analyzer. Current-voltage (I-V) measurements were performed at room temperature. The voltage between the electrodes was swept (between +0.5 and -0.5V) and the corresponding current was measured.

Results

We isolated a new strain of *Pseudomonas stutzeri*, VS-10, a heterotrophic, siderophore-producing deep-sea bacterium and investigated it's ability to colonize basaltic glass. Biofilm characteristics were investigated based on the physiological characterization of the strain, a detailed microscopic description and a nanolithographic analysis of EPM filaments. In addition diffusion chamber experiments elucidated the importance of bacterial attachment in growth of the strain on basaltic glass.

1. Isolation of strain VS-10

P. stutzeri VS-10 was isolated as a siderophore-producing bacterium from rhyolitic rock exposed in situ at Vailulu'u Seamount from March through July 2005. It took 5 successive transfers on CAS plates until a pure culture was obtained. Sequencing of the 16S rRNA gene resulted in a nearly full-length (1345 bp) sequence for the strain. It was found to be 99.5 % identical to *Pseudomonas stutzeri* strain 13636M (Genbank accession number: EU741093), a marine isolate from the Caribbean coast, Costa Rica (Solano et al., unpublished).

2. Elevated growth on minimal medium in the presence of volcanic rocks and/or Fe

The growth characteristics of strain VS-10 on minimal glycerol medium (40 mM glycerol) were investigated based on optical density measurements at 600 nm. Growth

properties on this medium without any additions and in the presence of basalt, rhyolite, quartz or 100 μM Fe(II) were determined.

While the technique of shaking cells off the rock surfaces prior to the spectrophotometric determination of the optical density may appear inadequate, SEM analysis of rock grains demonstrated that most of the cells had been removed from the rock by the treatment (data not shown). To account for any interference from abiotically derived alteration products, all cultures were corrected for negative controls (rock/water, mineral/water) which represented less than 2 % of the measured OD of the cultures. The interference of biologically-derived secondary mineral deposits as well as small amounts of Fe (hydr)oxides inside the culture containing $FeCl_2$ with OD_{600} measurements was considered insignificant.

P.stutzeri VS-10 is growth-limited when grown on plain minimal glycerol medium. Amendments with either volcanic rocks, minerals or Fe(II) result in enhanced growth rates of the strain compared to glycerol alone (Figure 4.1). Since the medium was generally limited for trace elements this demonstrates that the abundance of Fe alone seem to support growth of the strain. While the presence of quartz (to the least extent), rhyolite and Fe(II) all increase growth rates, the strain exhibits the largest growth enhancement in the presence of basalt. In case of the cultures containing igneous rocks and minerals growth enhancement positively correlates with the Fe(II) content of the material. Growth in the presence of Fe(hydr)oxides (i.e. after the addition of Fe(II))

results in the second highest growth enhancement but still demonstrates significantly lower growth rates than in the presence of basalt.

3. Physiological characteristics of strain VS-10

P. stutzeri VS-10 was shown to grow heterotrophically on a minimal medium containing glycerol. Growth on organic-rich Fe(II)-containing F-plates results in the accumulation of Fe(III). The Fe oxides were clearly associated with orange colonies and not with the medium or with colonies of bacteria not able to oxidize Fe(II) (white in color). This was shown in form of positive (orange colonies) and negative (white colonies) Prussian-Blue spot tests (Figure 4.2).

When grown under Fe(II)- and nutrient-limited conditions on minimal glycerol medium in the presence of rhyolite, *P. stutzeri* VS-10 appears to produce two siderophores along with their degradation products as indicated by Liquid Chromatography Mass Spectometry (LC-MS) analysis (Figure 4.3 A). Both siderophores were identified as amonabactins (Telford and Raymond 1997; Thanyakoop 2009; Zawadzka et al. 2006). They represent two out of seven structurally different siderophores the strain is capable of producing when cells are Fe-limited without the addition of any amino acids (Thanyakoop 2009). When grown on minimal glycerol medium the two amonabactins were identified as amonabactin P750 (m/z 751) and P693 (m/z 694), two phenylalanine-containing types (Figure 4.4), along with some of their degradation products. Intriguingly, on minimal glycerol medium *P. stutzeri* VS-10 was

shown to only produce these amonabactins in the presence of rhyolite and not in the presence of basalt (Figure 4.3).

Anaerobic growth experiments on oligotrophic artificial seawater medium as well as minimal glycerol medium show that the strain is unable to grow strictly anaerobic using Fe(III) as an electron acceptor.

4. Role of *P. stutzeri* VS-10 biofilm in elevated growth on volcanic glass and its phenotypic appearance

P. stutzeri VS-10 was cultured in a diffusion chamber in which the cells were physically separated from basaltic glass. Under these conditions growth of the strain is minimal if not absent (Figure 4.5) indicating the importance of direct contact with the basaltic glass surface when grown under nutrient-limited conditions.

On basaltic glass surfaces *P. stutzeri* VS-10 produces extensive biofilms (Figure 4.6 A, B). Various biofilm morphologies, from monolayers of cells to more complex structures are observed. Biofilm distribution appears to be extensive and not limited to natural depressions (e.g. cracks) in the rock surface. Production of EPM in the form of filaments (with an approximate diameter of 10 nm) is a noticeable part of the VS-10 biofilm structure. These filaments are similar in appearance to pili, fimbriae or “strands of mucilage” produced by a wide range of marine bacteria (Dempsey 1981). The role of these extensions in VS-10 biofilms appears to be in facilitating both cell-to-cell and cell-to-glass interactions (Figure 4.6 C-E). They vary in number but appear to range between

1 or 2 to up to ~20 filaments per cell and are unevenly spread over the entire cell surface (Figure 4.6 C, E). The number of appendages on each cell appears to depend on biofilm thickness. Single cells seem to adhere to the glass surface via few (2-10) appendages (Figure 4.6 C, E). Cells within thicker parts of the biofilm exhibit more and longer extensions (Figure 4.6 D) or "sheet-like" structures (Figure 4.6 F). These "sheets" closely resemble the ones previously detected in other marine bacterial biofilms (Dempsey 1981). When grown on minimal glycerol medium in the presence of basalt the EPM appears to be mineral-encrusted (Figure 4.7 A) while it appears relatively clean in the presence of rhyolite (Figure 4.7 B). This encrustation with what likely represents secondary minerals (e.g. Fe (hydr)oxides and Mn(IV)oxides) seems to correlate with the Fe contents of the colonized material.

5. Electrochemical properties of biofilm

P. stutzeri VS-10's ability to transfer electrons to an electrode was investigated in microbial fuel cells (MFCs). Monitored for several days *P. stutzeri* VS-10 produces an electrochemical current under both aerobic and microaerobic conditions relative to a blank MFC operated under identical conditions (Figures 8 and 9). However a significant difference in maximum cell voltage was apparent under aerobic or anaerobic conditions.

In our first experimental setup the MFC was set to aerobic conditions prior to inoculation with a cell suspension of a nutrient-limited *P. stutzeri* VS-10 culture to allow for adequate growth of the bacterium. Under these conditions *P. stutzeri* VS-10 shows a slow increase in operational current density (V) for 73 hrs (Figure 4.8 A). Conditions

were then switched to microaerobic. After an initial period (~ 6 hrs) of slowly increasing voltage the current production grows stronger until the strain's maximum cell potential (~ 7 mV) is reached at around 50 hrs (Figure 4.8 B). Based on the 100 Ω resistor used in the experimental setup this represents a maximum operational current of ~ 70 μA. Normalized to the surface area of the anode felt (2.5 cm^2) this equals 280 mA/ m^2. SEM images of the anode felt fibers show heavy colonization by *P. stutzeri* VS-10 biofilms (Figure 4.10 A) including the presence of EMP filaments (Figure 4.10).

In a second experimental setup the MFC was adjusted to microaerobic conditions prior to the inoculation with the cell suspension. Figure 4.9 shows the increase in cell voltage over time. While the trend of the operational current density appears to be the same as in Figure 4.8 B, the maximum cell voltage in the second (microaerobically started) experiment is 15 times less (~ 0.22 mV) and is already reached after about 38 hrs of incubation. The cell densities (based on optical density measurements at 600 nm) decreased significantly over the 120 hrs of the experiment (data not shown). For this experiment the polarization curve (Figure 4.11) was obtained and the MFC was evaluated using cyclic voltammetry (Figure 4.12). Based on the polarization curve the maximum power density of the MFC inoculated with *P. stutzeri* VS-10 was 1.73 x 10^{-3} μW/cm^2 compared to an un-inoculated fuel cell (blank) which had a maximum power density of 3.07 x 10^{-6} mW/cm^2. The maximum current densities for the inoculated and un-inoculated MFCs were 1.12 x 10^{-2} μA/cm^2 and 5.90 x 10^{-5} μA/cm^2 respectively.

The cyclic voltammograms of the *P. stutzeri* VS-10 inoculated fuel cells show the presence of at least 2 redox-active components, one at ~ -120 mV the other at ~200 mV vs. an Ag/AgCl reference. These peaks may represent electron shuttles, cytochromes or other components of the external electron transport system of *P. stutzeri* VS-10. The peak at ~ -120 mV is in the same range as some phenazenes produced by *P. aeruginosa* (Rabaey et al. 2004).

6. Nanolithography

The conductivity of filamentous EPM produced by *P. stutzeri* VS-10 was evaluated. A *P. stutzeri* VS-10 culture, grown in the presence of rhyolite, was chosen for the analysis since the encrustation of EPM filaments when grown in the presence of basalt would interfere with the measurements. FESEM images of the silicon wafer chip showed cells along with copious EPM filaments (Figure 4.13). Nanofabricated electrodes patterned on top of single EPM filaments (Figure 4.14 A) were used to apply a voltage to a single EPM filament and its current response was subsequently measured. Results indicate that the filaments are conductive suggesting that they are capable of transferring electrons on the scale of at least one micron. Figure 4.14 B illustrates the current-voltage (I-V) response of a single filament. Measurements of the resistance at a variety of temperatures show a roughly linear decrease in resistance with increasing temperature (from 12 to 52 °C) with a generally non-linear curve.

Discussion

While heterotrophic Fe(II)-oxidizing bacteria are abundant on submarine basaltic glass surfaces, the role of the glass in supporting such communities and the benefits of glass colonization for the most part remains unknown. Although a utilization of the glass, or metal-oxides commonly associated with glass surfaces, as energy sources and sinks have previously been discussed, the potential mechanisms involved in these processes have not been described in detail.

Biofilm formation of marine *Pseudomonas stutzeri* VS-10 on basaltic glass was characterized using a combination of microscopic data and diffusion chamber experiments. To study the nature of microbe-glass interactions we investigated the strain's physiology, growth characteristics and conductivity of its biofilm.

When grown heterotrophically on glycerol the strain exhibits significantly enhanced growth in the presence of basalt compared to other substrata (Figure 4.1). We hypothesize that basalt supplies both sufficient Fe(II) and other potentially important trace nutrients such as Mn and PO_4 as well as a surface for colonization. This is supported by the strain's lack of siderophore production when grown in the presence of basalt and the need for cell-based contact for growth (Figure 4.5). Evidence for Fe-limitation in the presence of rhyolite (a low Fe(II)-containing rock) is the reduced growth and the production of siderophores.

Fe (hydr)oxides in the system seems to accelerate growth of the strain to a larger extent than the presence of rhyolite or quartz but not as drastic as basalt. Because the strain cannot grow either strictly anaerobically or microaerobically it is likely that growth after the addition of $FeCl_2$ is facilitated through Fe acquisition from the production of siderophores or some initial Fe(II) that existed in the system. The fact that Fe concentrations in this system are higher and the Fe is much easier accessible than from rhyolite or quartz is considered the main reason for elevated growth. Any Fe in the cultures containing quartz likely represents impurities of the mineral despite the absence of any visible inclusions.

Diffusion chamber experiments demonstrated the importance of direct attachment (e.g. biofilm formation) in growth of the strain (Figure 4.5) and that is consistent with the results of the growth experiments with basalt, rhyolite, quartz and Fe (hydr)oxide (Figure 4.1). Significantly elevated growth in the presence of basalt therefore may be due to the presence of additional bio-essential trace elements (i.e. Mn(II) and PO_4^{2-} present in basalt and minimal in rhyolite) but not in the experiment where only $FeCl_2$ was added. Growth could also be more efficient because siderophore production is not necessary.

While the ODs were all corrected for potential abiotically-derived dissolution products of rocks and minerals, a partial biotic dissolution of basalt, not taken into account, is likely. Therefore optical density measurements are not the most accurate technique to determine bacterial growth in this system (compared to protein assays or

measurements of dissolved organic carbon). However results repeatedly showed the described trends and were therefore considered to be valid.

The key physiological, metabolic, structural, electrochemical and nanolithographical characteristics of *P. stutzeri* VS-10 biofilms and their role in surface colonization and growth of the strain on natural submarine basaltic glass samples are discussed in the following sections.

1. Heterotrophic Fe(II)oxidation

While the actual quantity of dissolved organic carbon (DOC) in deep-sea water is still debated, the decomposition of particulate organic carbon is estimated to be about 2.2 mg C/m^2/day (Jannasch and Taylor 1984). This low DOC decomposition at depth generally results in elevated concentrations of free oxygen (on average 4 mg/liter or 130 μM; Jannasch 1994) compared to surface waters. Both conditions are likely to favor the establishment of diverse heterotrophic microbial communities.

The ability to oxidize Fe(II) when growing heterotrophically may suggest an additional energy benefit during or in the later stages of basalt (~10 wt% Fe(II)) colonization. *P. stutzeri* VS-10 may therefore be considered a mixotroph although this has not been proven. While in controlled laboratory experiments glycerol represents the more effective energy source compared to Fe(II), this does not reflect the natural conditions where dissolved organic carbon (DOC) concentrations (in hydrothermal and non-hydrothermal influenced deep-sea water) are generally lower (Lang et al. 2010).

Instead, these environments are commonly characterized by high advection rates and strong chemical gradients often leading to rapidly changing compositions of seawater including its carbon sources and concentration. Additionally, lower diffusion rates within biofilms (due to biofilm morphology) can result in limited amounts of solution-derived carbon at the bottom of the film. Heterotrophic bacteria may in this case become electron donor-limited. Cells at the bottom of the biofilm and in direct contact with the basalt surface may then benefit from the oxidation of Fe(II) for supplemental energy generation. The ability of *P. stutzeri* VS-10 to use a solid (i.e. basalt) surface as a terminal electron donor was recently supported by MFC data (Wanger, personal communication).

2. Fe(III)-reduction

P. stutzeri VS-10 appears to be unable to grow under strictly anaerobic or microaerobic conditions. However, its ability to use a solid surface as a terminal electron acceptor, particularly after a thick biofilm (estimated hundreds of nm thick based on AFM measurements, see Chapter VI) was allowed to establish, was shown in MFCs even under microaerobic to anaerobic conditions. This suggests that basalt may be used as an electron acceptor or an electron sink under natural conditions where deep-sea water contains enough oxygen for thick biofilms to form on basalt surfaces. Conditions presented in the first MFC experiment (Figure 4.8) are therefore likely closer to natural conditions where thick biofilms are allowed to form on the surface. Conditions may then become microaerobic either due to changes in environmental conditions (increased hydrothermal input) or, more likely, due to oxygen depletion through biofilm development (resulting in diffusion limitation). In either case cells within *P. stutzeri* VS-

10 biofilms in proximity to the basalt surface could benefit from the reduction of secondary mineral deposits (i.e. Fe (hydr)oxides, Mn(IV)-oxides) commonly associated with natural submarine basalt surfaces. Such metal oxide layers are hypothesized to form through either the weathering of basaltic glass or as a result of the precipitation of metal-rich hydrothermal emissions (Alt 1988; Fortin et al. 1998; Staudigel and Hart 1983).

3. Siderophore production

P. stutzeri VS-10 was recently shown to produce a set of fourteen structurally-related amonabactins constituting the largest suite of siderophores isolated from a single bacterium (Thanyakoop 2009). This structural diversity is considered to represent an environmental adaptation mechanism by altering the compound's surface adsorption characteristic.

The siderophores of *P. stutzeri* VS-10 are unlikely to play a prominent role in elevated growth of strain VS-10 on basalt. This is based on the fact that no siderophores are produced when the cells are nutrient-limited in the presence of basalt suggesting a sufficient enough Fe supply from the glass which eliminates the need for Fe(III)-chelating molecules. This Fe supply can result from both the biotic and abiotic weathering of rocks. Strain VS-10's production of siderophores in the presence of rhyolite positively correlates with the lower Fe contents of the rock. Therefore we propose that strain VS-10 produces siderophores strictly only when needed under Fe-limitation.

3. Biofilm structure and electrochemical properties

3.1 Role of EPM filaments

Extensive biofilm formation on basalt was microscopically observed in *P. stutzeri* VS-10 cultures. Several biofilm morphologies ranging from mono-layered cells to more complex, dome-like structures in combination with the expression of EPM were observed. The different morphologies could represent various stages of biofilm formation as described previously in other pseudomonads (Watnick and Kolter 2000). EPM, shown to facilitate cell-to-cell interaction and cell-to-surface adhesion is morphologically similar to extracellular appendages (type IV pili, fimbriae, mucilage) in other bacteria (Dempsey 1981). These appendages are involved in bacterial adhesion (Doig et al. 1988; Fletcher et al. 1993; Smyth et al. 1996) and twitching motility (Bradley 1980) but also likely play a role in biofilm formation, structure and stability (Reguera et al. 2007). In addition to the adhesive and motility function, this mucilage is considered to serve as protection against predation, as a possible carbon and energy source in times of nutrient depletion and as aid in nutrient uptake (Wilkinson 1958). In *P. stutzeri* strains type IV pili are additionally involved in binding of DNA affecting natural competence and transformation (Graupner et al. 2000). Surface attachment based on the interaction between extracellular DNA and type IV pili has recently been shown (Heijstra et al. 2009). Previous studies on the kinetics of biofilm formation suggest that appendages, especially force-generating organelles such as pili, are often used in the initial interaction with the surface (Watnick and Kolter 2000).

Under natural conditions both bacterial cells and basalt surfaces are negatively charged resulting in electrostatic repulsive interactions and van-der-Waals attractive interaction (Morisaki and Tabuchi 2009). Whether or not bacterial cells attach to the surface depends on which interaction dominates. Ohshima (1994) showed that due to polymers (such as EPM) on the bacterial surface, cells behave more like “soft colloidal particles”. Compared to regular smooth colloidal particles bacterial cells have a much lower surface electric potential reducing the energy barrier caused by electrical repulsion between the bacterial cell and the substratum surface (Morisaki and Tabuchi 2009). Once temporary contact with the surface is made the polymers (e.g. EPM, pili, fimbriae or mucilage) could be used in surface-related movement of single cells to find other cells and form microcolonies or to stabilize the biofilm structure and ensure more permanent attachment (Stoodley et al. 2002).

3.2 Electrochemical properties of biofilm in MFCs

Our results show that *P. stutzeri* is capable of growth in a microbial fuel cell with an electrode as the sole electron acceptor. This means that the bacterium can complete respiration by reducing a solid phase terminal electron acceptor coupled with the oxidation of glycerol. This result is well documented in other electrogenic bacterial species notably many metal reducing strains such as *Geobacter* sp and *Shewanella* sp. While *P. stutzeri* VS-10 can be characterized as an electrogenic bacterium the magnitude of the power and current produced is lower than that of *S. oneidensis* (Bretschger et al. 2007) particularly in the second MFC setup (started under anaerobic conditions). Compared to a maximum power density of 1.73×10^{-3} $\mu W/cm^2$ and the maximum current

density of 1.12 x 10^{-2} μA/cm^2 obtained from polarization curves of *P. stutzeri* VS-10, *S. oneidensis* reaches a maximum power density of 1.8 μW/cm^2 and a maximum current density of 4.58 μA/cm^2 (Bretschger et al. 2007), 1000 and 416 times higher than VS-10, respectively. It has to be considered, however, that *S. oneidensis*, even though preferring aerobic conditions, is much more capable of growing anaerobically then *P. stutzeri* VS-10. Also, Bretschger (2007) inoculated their MFCs at much higher initial cell densities. In addition, the growth conditions (medium, growth phase, wash etc.) of the cell suspension used for inoculation have to be considered. System parameters (e.g. buffer composition, ion exchange membrane selection) have also been shown to play a role (Bretschger et al. 2008). When inoculated to an OD_{600} comparable to the one in our MFCs, *S. oneidensis* displayed the same phenomenon of significantly lower current production (Wanger pers. comm.).

With regard to *P. stutzeri* VS-10's potential to oxidize Fe(II) when grown heterotrophically, Wanger et al. (in prep) recently showed that *P. stutzeri* VS-10 is also able to accept electrons from a solid phase, i.e. use an electrode (cathode) as an electron donor.

While *P. stutzeri* VS-10's potential to use solid surfaces as terminal electron acceptors and donors has been shown, two possible strategies for external electron transport in this strain will be discussed: A) the use of soluble mediators (electron shuttles) and B) electron transport through EPM.

A) Electron shuttles

Certain *Geobacter* and *Shewanella* sp. revealed the use of naturally occurring (Lovley et al. 1996) and/or biogenic soluble mediators as electron shuttles from cells to acceptors (Marsili et al. 2008; Newman and Kolter 2000; von Canstein, 2008). While the cyclic voltammograms of *P. stutzeri* VS-10 indicates the presence of at least two such mediators when cells are nutrient-limited inside a MFC, their structure remains unknown.

B) EPM filaments

More recently studies have shown that bacterial "nanowires" similar in appearance to pili, fimbriae and/or filamentous EPM produced by *P. stutzeri* VS-10 are involved in microbial electron transport of strains (El-Naggar et al. 2008; Gorby et al. 2006; Reguera et al. 2005). Studies all involve DMRB (*Geobacter sulfurreducense*, *Shewanella oneidensis* MR-1, *Synechocystis* PCC6803, *Pelotomaculum thermopropionicum*) making this the first report of a deep-sea bacterium in which the conductivity of such structures could be demonstrated. While the exact mechanism of external electron transport in *P. stutzeri* VS-10 remains unknown, nanolithography data show that EPM appendages produced by this strain are electrically conductive. In combination with results from diffusion chamber experiments, indicating the importance of attachment in growth of the strain, it appears likely that EPM filaments are involved in electron transfer. Compared to *Geobacter* or *Shewanella* sp the production of conductive EPM in *P. stutzeri* VS-10 can however not be linked to conditions of electron acceptor or donor limitation. This suggests that its EPM either represents just a structural element of the biofilm or it may be a mechanism for the cell to dispose of excess reducing power.

It remains unclear whether Fe(II)oxidation from basalt or secondary mineral (e.g. Fe(hydr)oxides, Mn(IV)-oxides) reduction represent mechanisms that support growth of *P. stutzeri* VS-10 on natural submarine basalt surfaces. Both mechanisms, however, are likely to contribute to elevated weathering of the rock. Either through accelerated ion-exchange (Fe(II)oxidation), removal of protective metal-oxide layers (Fe(III)/Mn(IV)-reduction) or simply through transfer of electrons to or from the rock leading to a weakening of the structural lattice of the rock.

Conclusion

An interdisciplinary approach was used to explore the basic mechanisms of basaltic glass colonization by a heterotrophic deep-sea bacterium, *Pseudomonas stutzeri* VS-10, isolated from a submarine volcanic rock. VS-10 exhibits elevated growth under nutrient-limited conditions in the presence of basalt. Fe availability within the substrate and the existence of surfaces available for colonization appear to play pivotal roles in supporting the strain's growth. In combination with a physiological characterization of strain VS-10, the role of EPM filaments in basalt surface-related growth within deep-sea environments was elucidated.

Growth experiments indicate that the concentration of Fe (and likely other bio-essential trace elements) present within the system and the type of material available for

colonization play a role in supporting growth of the strain under nutrient-limited conditions.

Direct attachment of cells (e.g. biofilm formation) to the basalt plays a significant role in supporting growth of *P. stutzeri* VS-10. Fe availability and the existence of a surface available for colonization appear to be crucial. While siderophores produced by strain VS-10 under Fe limitation do not appear to play a role in growth in the presence of basalt, they are likely to support growth in Fe-limited systems (in the presence of rhyolite, quartz or Fe(hydr)oxides).

Microscopic studies offer insight into the nature of the VS-10 biofilm on volcanic glasses emphasizing the role of filamentous “extracellular polymeric material” (EPM) in facilitating cell-to-cell and cell-to-surface interactions. Nanolithographic results reveal the conductivity of such EPM suggesting its involvement in electron transfer reactions.

The strain’s ability to oxidize Fe(II) when grown heterotrophically in combination with its potential to transfer or uptake electrons to/from solid surfaces (reduce and oxidize surfaces) suggest a function of the glass as a secondary energy source and/or sink during surface-related growth of strain VS-10.

P. stutzeri VS-10’s metabolic versatility and it’s potential to respire solid surfaces as both terminal electron acceptor and electron donor all represent advantages to thrive in

primarily oligotrophic submarine environments where the availability of nutrient and energy sources constantly change.

Overall our work contributes towards a better understanding of the complexity of microbe-rock interactions resulting in an advanced understanding of the potential role of submarine basaltic glass in supporting phylogenetically and metabolically diverse microbial communities within deep-sea ecosystems. Marine heterotrophic bacterium *P. stutzeri* VS-10, a ubiquitous member of such community has proven a useful model system to study these processes.

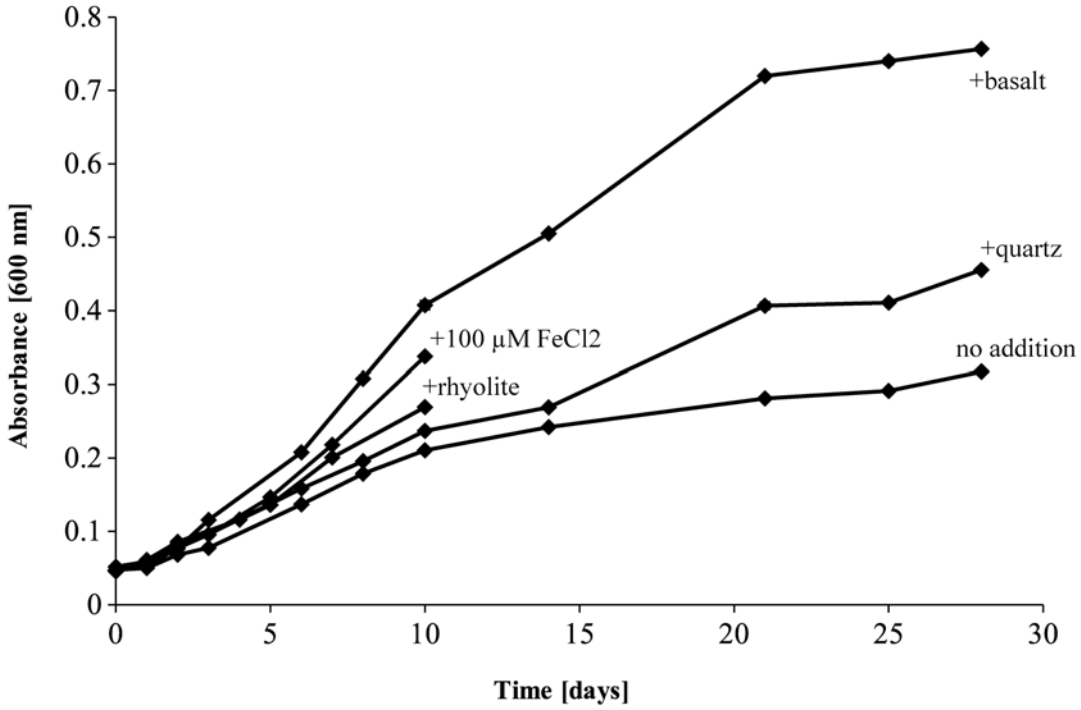

Figure 4.1: Growth of *P. stutzeri* VS-10 on chelexed minimal glycerol medium without additives or with the addition of either basalt, rhyolite, quartz or 100 µM $FeCl_2$. Growth was monitored based on optical density measurements at 600 nm. Data indicate that the strain is growth limited without any additions. While quartz, rhyolite and Fe(II) all enhance growth to various degrees, basalt has the most pronounced effect. Values are averaged from triplicate tubes. Standard errors are too small to graph.

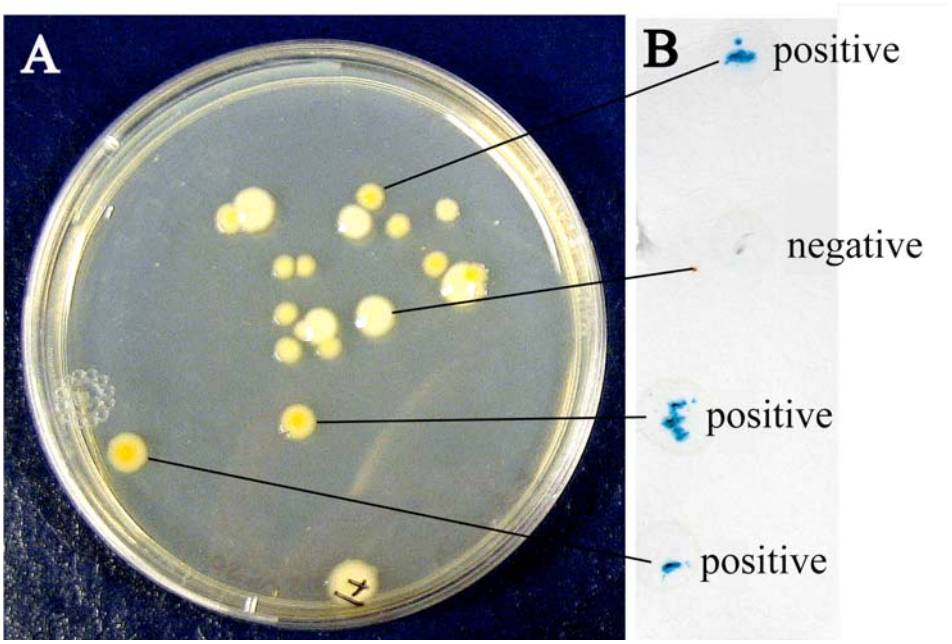

Figure 4.2: Photograph of deep-sea bacteria grown on organic-rich F-plates. The potential to oxidize Fe(II) while grown heterotrophically is indicated by an orange color of colonies on the plate (A) associated with positive Prussian-Blue tests (B) indicating the abundance of Fe(III) within the colonies. In comparison, colonies that remain white (A) result in negative Prussian-Blue tests (B).

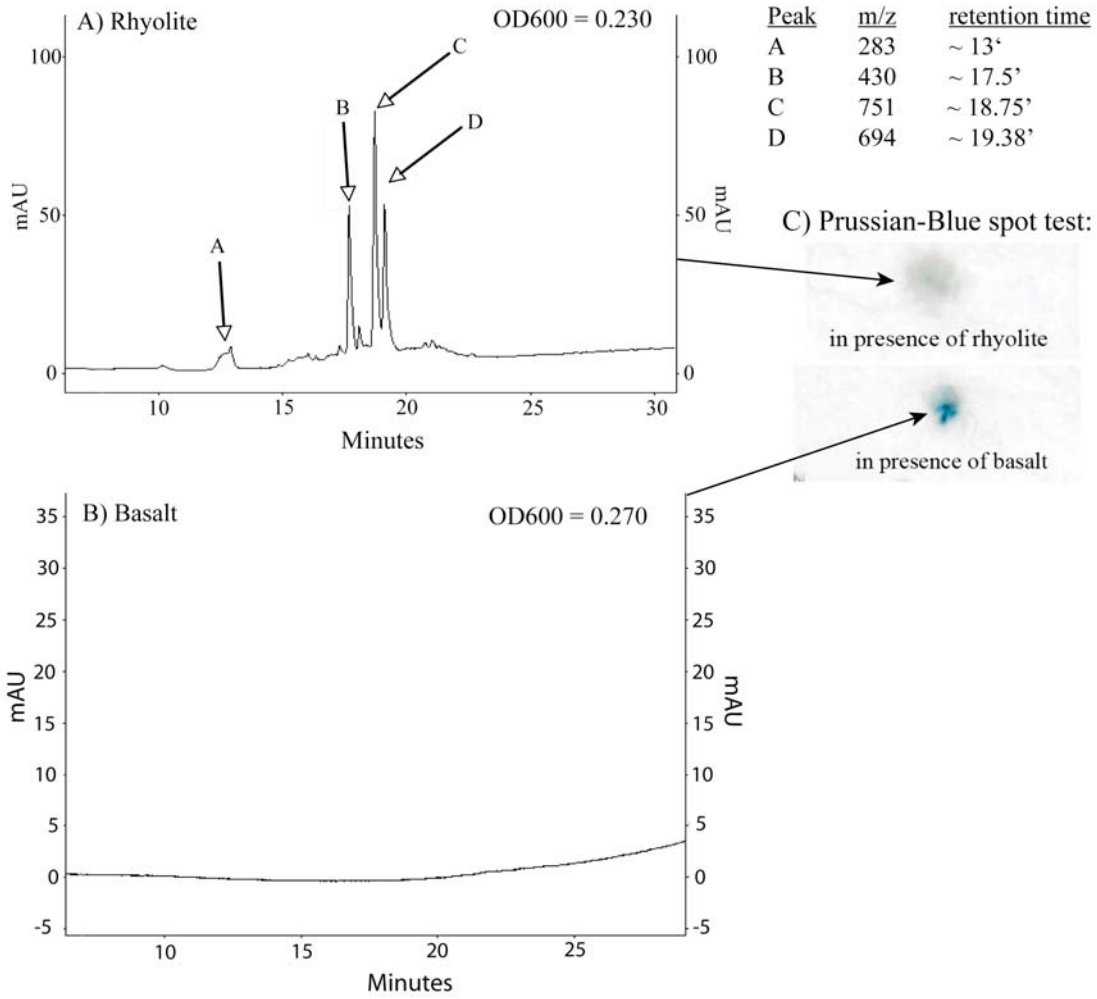

Figure 4.3: Liquid Chromatography Mass Spectrometry (LC-MS) results on the presence of siderophores in the supernatant of a *P. stutzeri* VS-10 grown on minimal glycerol medium: A) In the presence of rhyolite, B) in the presence of basalt. Fe limitation in the presence of rhyolite becomes apparent from the presence of amonabactin P750 (peak C) and P693 (peak D) in the supernatant. Peak A (m/z 283) and Peak B (m/z 430) presumably represent degradation products of the two amonabactins (Telford and Raymond 1997). The lack of siderophores in the culture containing basalt (B) is likely due to elevated content and availability of Fe(II) in the rock, and subsequently no Fe-deficiency. Fe sufficiency within this culture is also suggested by a positive Prussian-Blue test (C) in which the presence of Fe(III) is indicated by a blue color while Fe(III) is absent in the rhyolite culture as indicated by a lack of color (or alternatively it could not be detected in its complexed form).

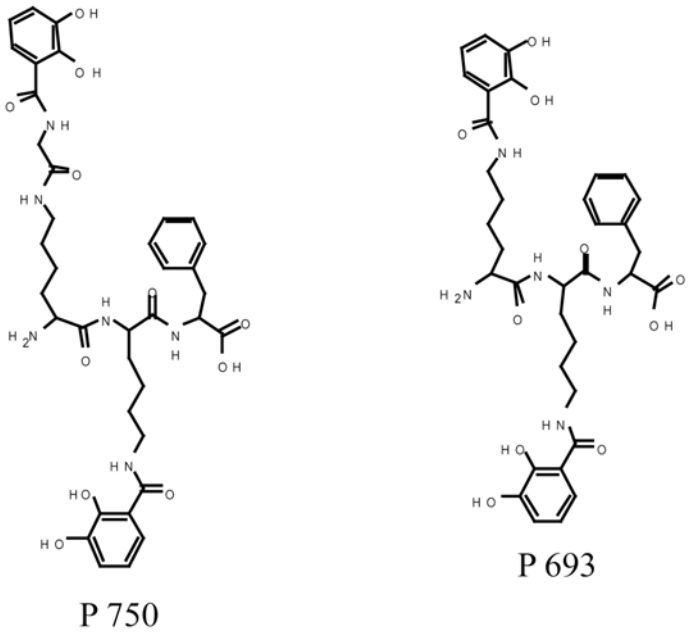

Figure 4.4: Structures of amonabactin P750 and P693, two phenylalanine-containing compounds produced by strains of *P. stutzeri* (Zawadzka et al. 2006).

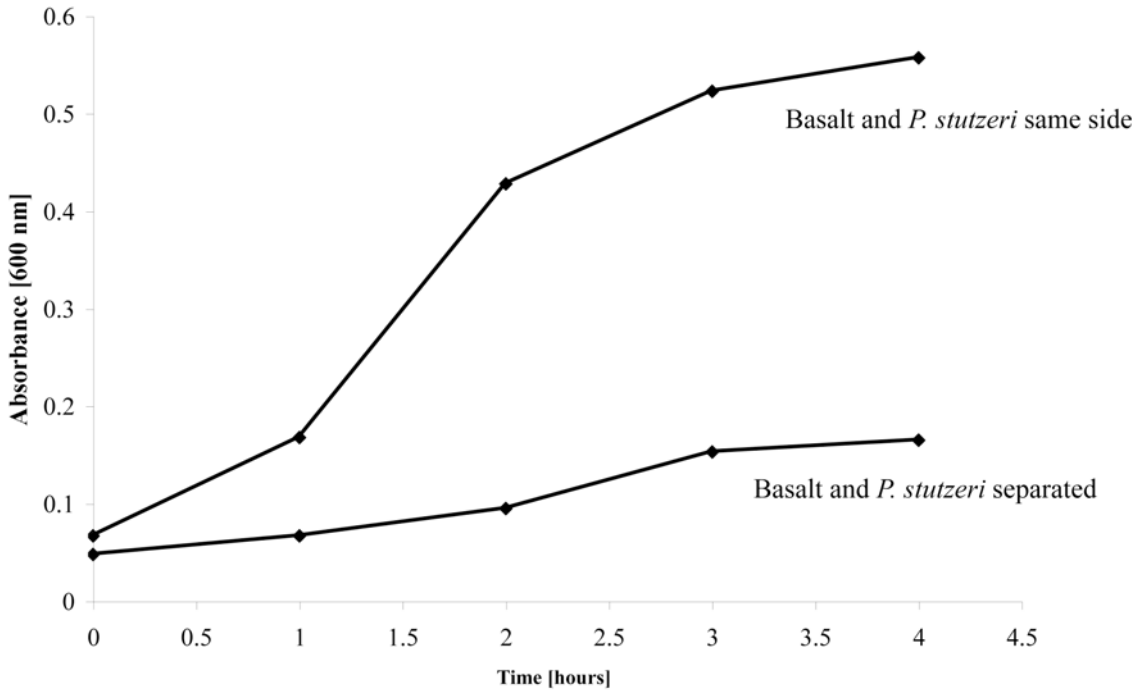

Figure 4.5: Diffusion chamber experiments demonstrating growth of *P. stutzeri* VS-10 on chelexed minimal glycerol medium with basalt being present in the culture. In one experiment basalt and the bacterium were incubated together (same side) in the other they were separated by a 0.2 μm membrane that allows the diffusion of ions throughout the medium (separated). Direct contact of cells to the glass surface results in enhanced growth.

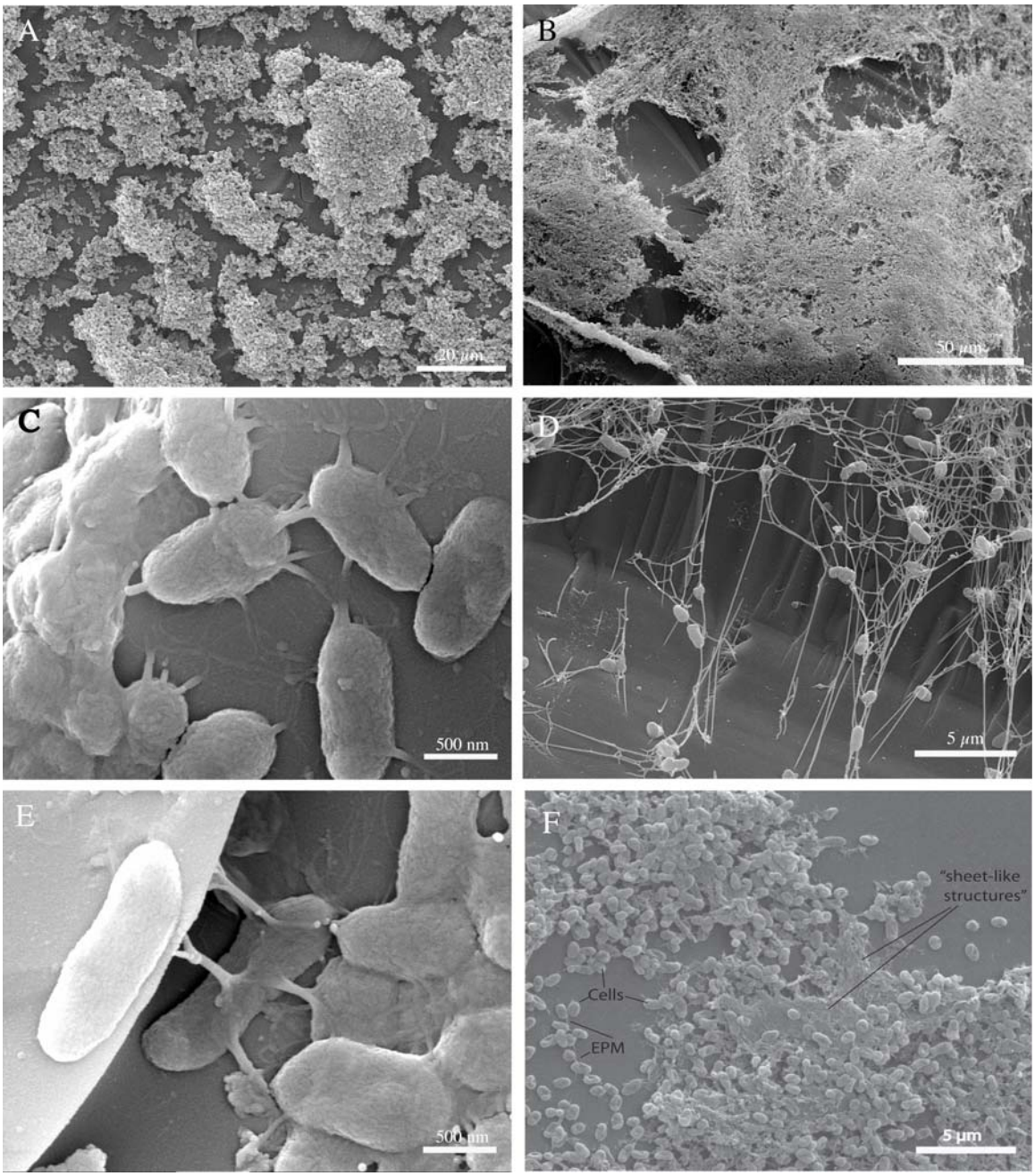

Figure 4.6: Scanning electron micrographs (SEMs) of *P. stutzeri* VS-10 cells on basaltic glass. Biofilm formation generally appears to be extensive and not limited to natural depressions (B, 18 days of incubation) and in part forms dome-like structures possibly artifacts of the dehydration process (Dohnalkova et al., 2011) (A, 22 days of incubation). Extracellular polymeric material (EPM) seems to be involved in cell-to-cell and cell-to substrate adherence (C-E, 4 days of incubation). More mature or thicker parts of the biofilm appear as "sheet-like" structures (F, 1 week of incubation). The order in which sheets and filaments evolve is unknown.

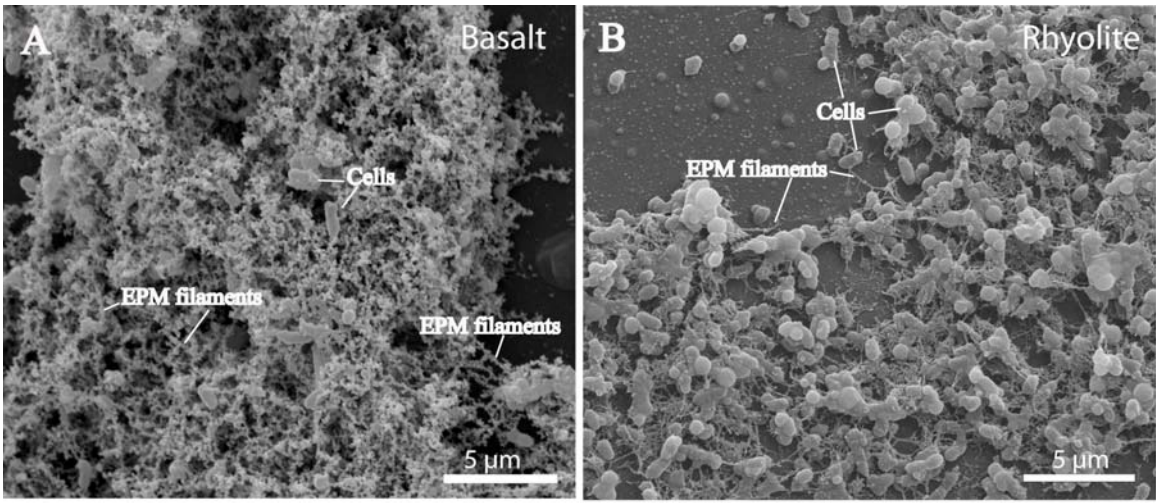

Figure 4.7: Scanning electron micrographs (SEM) showing biofilms of *P. stutzeri* VS-10 on basalt (A, 6 days of incubation) and rhyolite (B, 1 week of incubation). More significant encrustation of EPM filaments becomes apparent when grown in the presence of basalt. While not analyzed, the secondary minerals encrusting the filaments are likely metal oxides (i.e. Fe (hydr)oxides). Increased encrustation on basalt positively correlates with higher Fe contents of the rock.

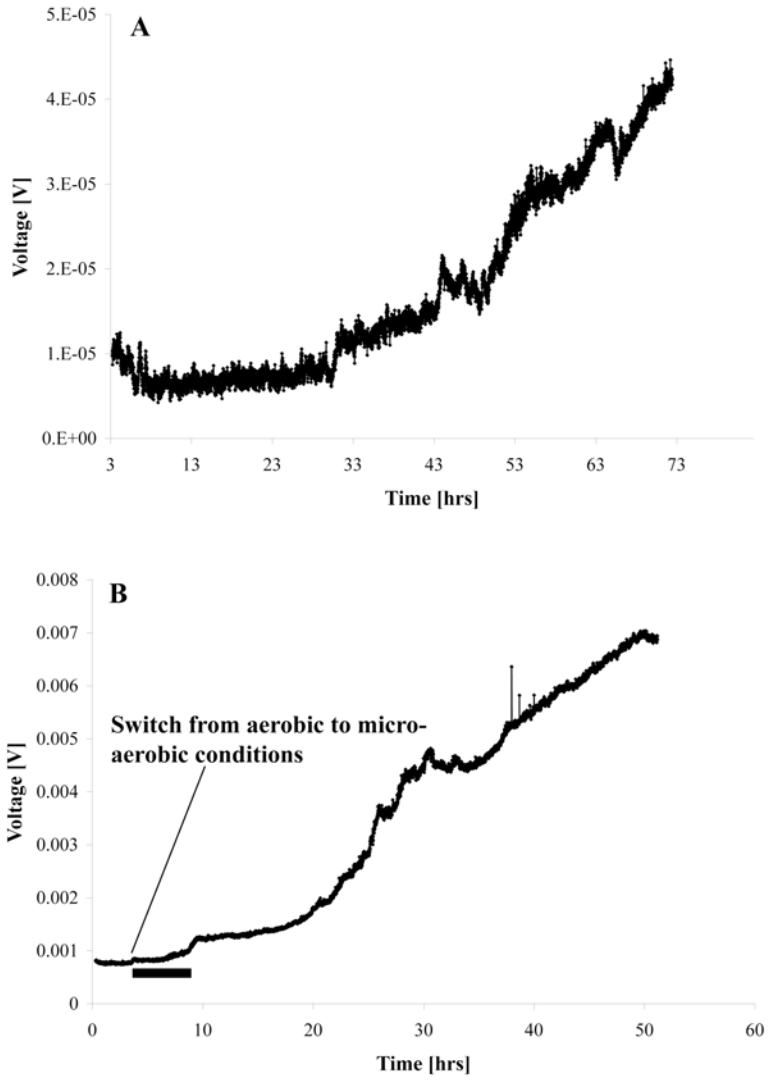

Figure 4.8: Power production by *P. stutzeri* VS-10 on minimal glycerol medium in a microbial fuel cell. Graphs show an increase of the voltage over time. A: Incubation under aerobic conditions indicates a slight increase. B: After switching to microaerobic conditions the voltage first continues to slowly increase during which time oxygen decreases (represented by the black bar in B). After 10 hrs voltage increases more significantly after oxygen depletion in the system. The maximum cell potential of *P. stutzeri* VS-10 is reached at ~ 50 hrs showing a voltage of ~ 7 mV. In combination with the surface area of the electrode this equals 280 μA/ m^2 of current produced by the strain. OD measurements showed decreasing cell numbers likely due to attachment of cells to the anode, the cation exchange membrane and the glass surface of the MFC.

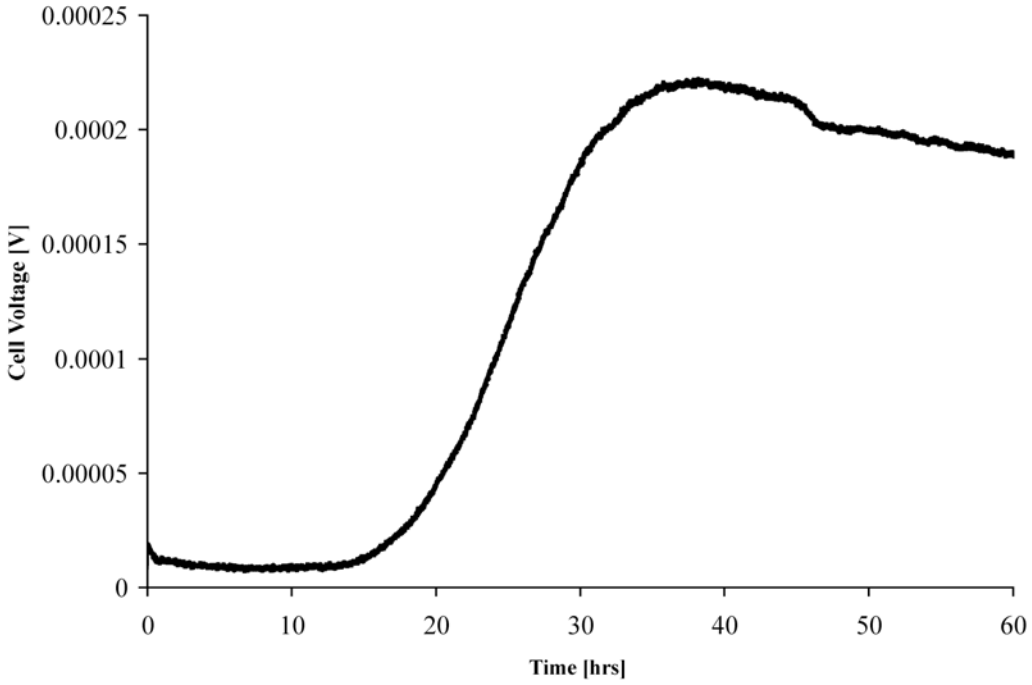

Figure 4.9: Microaerobic MFC run. After inoculation of the anode compartment with nutrient-limited cells of *P. stutzeri* VS-10 and an initial period of ~ 16 hrs an increase in cell voltage can be observed. A maximum cell potential of ~ 0.22 mV is reached after 38 hrs of incubation. OD measurements showed decreasing cell numbers likely due to attachment of cells to the anode, the cation exchange membrane and the glass surface of the MFC. A potential reason for the maximum cell voltage being ~ 15 times smaller than the one in Figure 4.8 could be overall higher cell numbers in the experiment shown in Figure 4.8. This experiment was started under aerobic conditions likely supporting cell growth to a larger extend than microaerobic conditions initially established in the experiment shown in Figure 4.9.

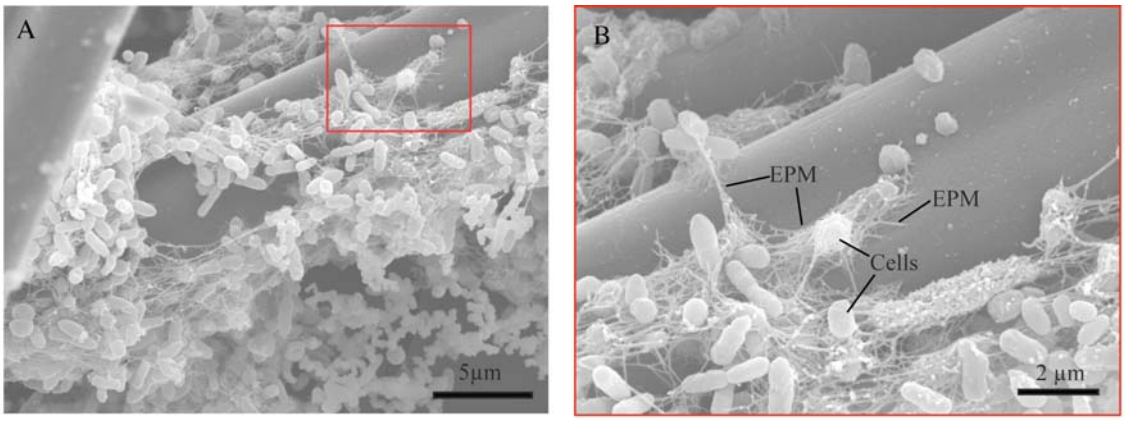

Figure 4.10: Scanning electron micrograph of the anode felt from the microbial fuel cell (Figure 4.8). Heavy colonization by a *P. stutzeri* VS-10 biofilm along the felt fibers can be observed (A) along with the occurrence of EPM filaments (B= close-up of red rectangle in A).

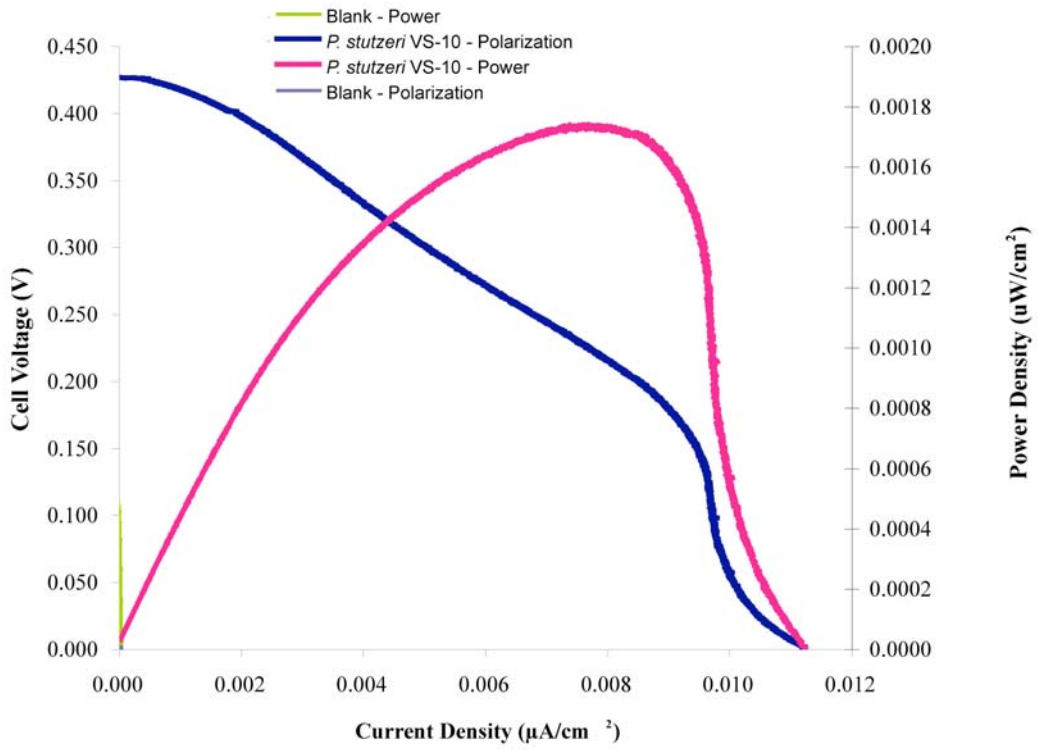

Figure 4.11: Polarization and power curves for the MFC inoculated with *P. stutzeri* VS-10 (see Figure 4.10). The maximum power density of the biotic MFC (pink line) is 1.73 x 10^{-3} µW/cm^2 compared to an un-inoculated fuel cell (blank) with a maximum power density of 3.07 x 10^{-6} mW/cm^2 (green line). The maximum current densities for the inoculated and un-inoculated MFCs were 1.12 x 10^{-2} µA/cm^2 (dark blue line) and 5.90 x 10^{-5} µA/cm^2 (light blue line).

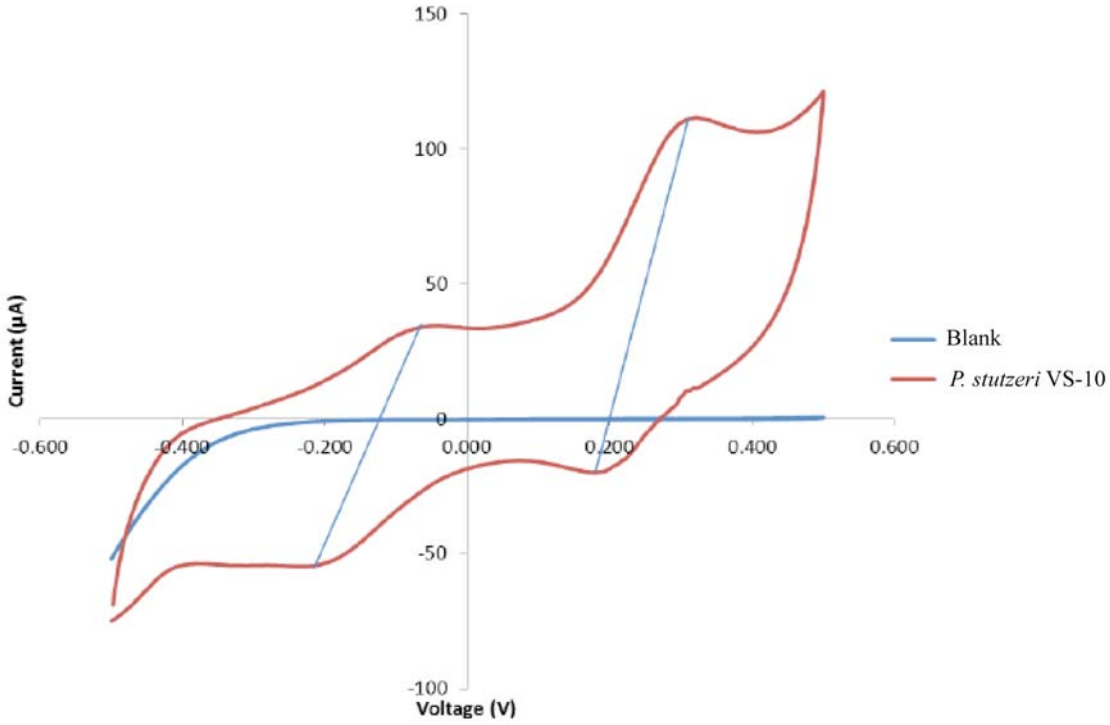

Figure 4.12: Cyclic voltammograms of the MFC inoculated with *P. stutzeri* VS-10 (see Figure 4.10). The presence of at least 2 redox-active components (in form of flat peaks) at ~ -120 mV and at ~200 mV becomes apparent. While none of them could be identified the peak at ~ -120 mV is in the same range as phenazenes produced by *P. aeruginosa*. The blue lines connect the peaks in the oxidation and the reduction sweep (in a reversible redox reaction).

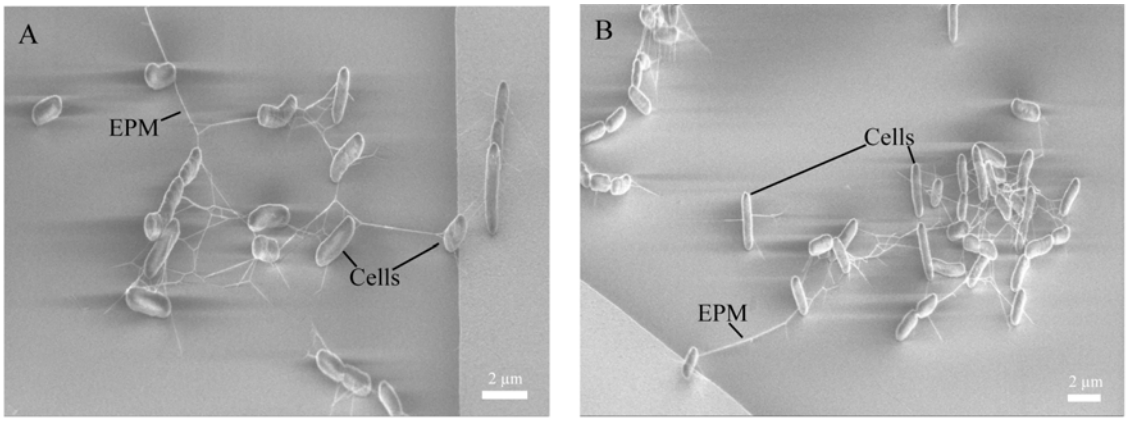

Figure 4.13: Scanning electron micrographs of *P. stutzeri* VS-10 cells on the silicon wafer chip prior to determination of EPM conductivity. Cells were fixed in 2.5% glutaraldehyde overnight, dehydrated in and ethanol series and then critical point dried. The cells are not coated leading to image aberrations. For sample preparation procedure see (El-Naggar et al., 2010)

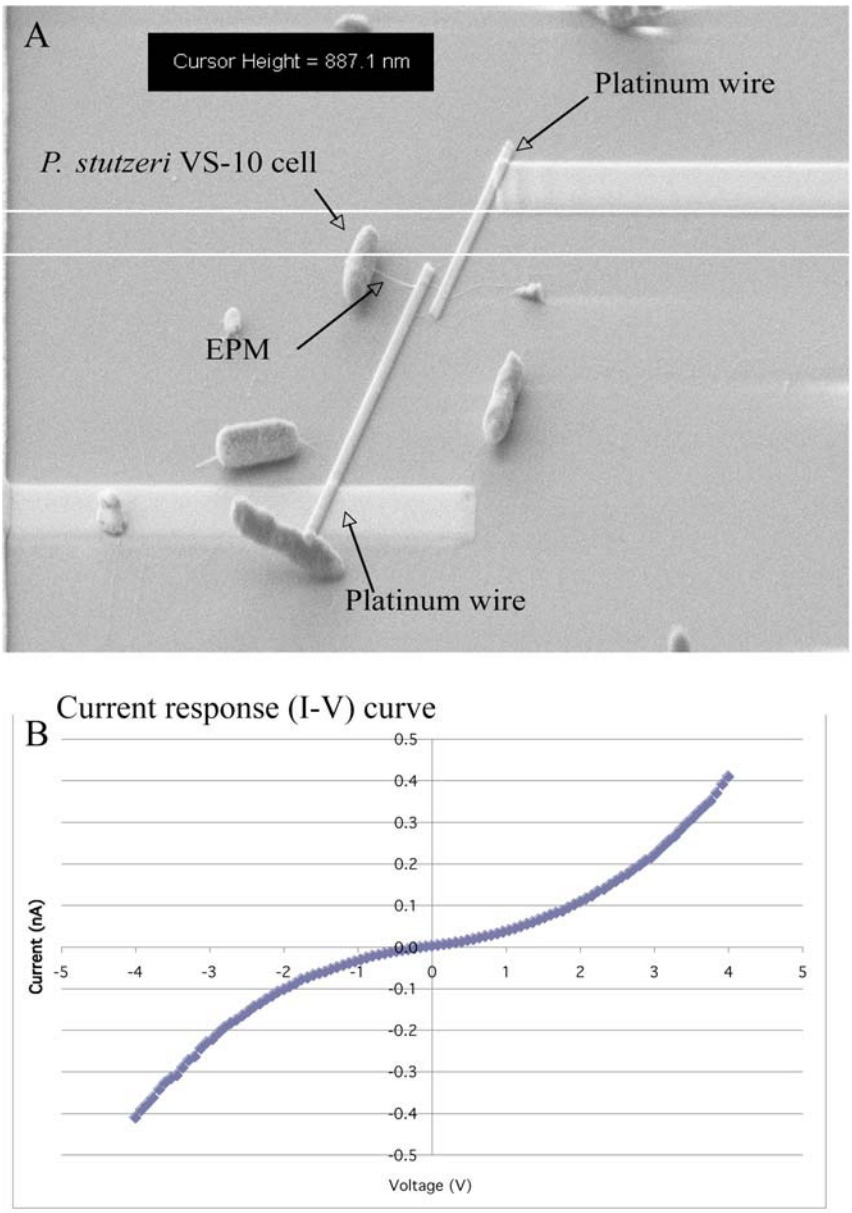

Figure 4.14: Results from nanolithographic experiments. A) Scanning electron micrograph (SEM) showing single cells of *P. stutzeri* VS-10 along with EPM filaments. Platinum wires were drawn to measure electron transfer along the length of filaments. B) Current response curve of one filament after a voltage was applied showing a non-linear response.

References

Allison D. G., Ruiz B., SanJose C., Jaspe A. and Gilbert P. 1998. Extracellular products as mediators of the formation and detachment of Pseudomonas fluorescens biofilms. FEMS Microbiol Lett 167:179-184.

Alt J. C. 1988. Hydrothermal oxide and notronite deposits on seamounts in the eastern Pacific. Mar. Geol. 81:227-239.

Altschul S. F., Madden T. L., Schaffer A. A., Zhang J., Zhang Z., Miller W. and Lipman D. J. 1997. Gapped BLAST and PSI-BLAST: a new generation of protein database search programs. Nucleic Acids Res 25:3389-3402.

Ashelford K. E., Chuzhanova N. A., Fry J. C., Jones A. J. and Weightman A. J. 2006. New screening software shows that most recent large 16S rRNA gene clone libraries contain chimeras. Appl Environ Microbiol 72:5734-5741.

Bach W. and Edwards K. J. 2003. Iron and sulfide oxidation within the basaltic ocean crust: implications for chemolithoautotrophic microbial biomass production. Geochim Cosmochim Acta 67:3871-3887.

Bailey B. E., Templeton A. S., Staudigel H. and Tebo B. 2009. Utilization of substrate components during basaltic glass colonization by Pseudomonas and Shewanella isolates. Geomicrobiology Journal 26:648-656.

Banfield J. F., Barker W. W., Welch S. A. and Taunton A. 1999. Biological impact on mineral dissolution: application of the lichen model to understanding mineral weathering in the rhizosphere. Proc Natl Acad Sci U S A 96:3404-3411.

Barker W. W. and Banfield J. F. 1996. Biologically versus inorganically mediated weathering reactions: relationship between minerals and extracellylar polymers in lithobiontic communities. Chem. Geol. 132:55-69.

Bradley D. E. 1980. A function of Pseudomonas aeruginosa PAO polar pili: twitching motility. Can J Microbiol 26:146-154.

Bretschger O., Cheung A. C. M., Mansfeld F. and Nealson K. H. 2008. Comparative Microbial Fuel Cell Evaluations of Shewanella spp. Electroanalysis 22:883-894.

Bretschger O., Obraztsova A., Sturm C. A., Chang I. S., Gorby Y. A., Reed S. B., Culley D. E., Reardon C. L., Barua S., Romine M. F., Zhou J., Beliaev A. S., Bouhenni R., Saffarini D., Mansfeld F., Kim B. H., Fredrickson J. K. and Nealson K. H. 2007. Current production and metal oxide reduction by Shewanella oneidensis MR-1 wild type and mutants. Appl Environ Microbiol 73:7003-7012.

Busscher H. J. and Weerkamp A. H. 1987. Specific and non-specific interactions in bacterial adhesion to solid substrata. FEMS Microbiol Ecol 46:165-173.

Christie D. M., Pedersen R. S. and Miller D. J. (2001). Proceedings of the Ocean Drilling Program, Initial Reports, Leg 187 [CD-ROM]. Ocean Drilling Program. College Station TX.

Costerton W. J. and Wilson M. 2004. Introducing Biofilms. Biofilms 1:1-4.

Danese P. N., Pratt L. A. and Kolter R. 2000. Exopolysaccharide production is required for development of Escherichia coli K-12 biofilm architecture. J Bacteriol 182:3593-3596.

Daughney C. J., Rioux J. P., Fortin D. and Pichler T. 2004. Laboratory Investigation of the Role of Bacteria in the Weathering of Basalt Near Deep Sea Hydrothermal Vents. Geomicrobiology Journal 21:21-31.

Deming J. W. and Baross J. A. 1993. The early diagenesis of organic matter: Bacterial activity.: Plenum Press; Topics in Geobiology, Vol. 11.

Dempsey M. J. 1981. Marine bacterial fouling: a scanning electron microscope study. Marine Biology 61:305-315.

Dohnalkova A. C., Marshall M. J., Arey B. W., Williams K. H., Buck E. C. and Fredrickson J. K. 2011. Imaging hydrated microbial extracellular polymers: comparative analysis by electron microscopy. Appl Environ Microbiol 77:1254-1262.

Doig P., Todd T., Sastry P. A., Lee K. K., Hodges R. S., Paranchych W. and Irvin R. T. 1988. Role of pili in adhesion of Pseudomonas aeruginosa to human respiratory epithelial cells. Infect Immun 56:1641-1646.

Donlan R. M. 2002. Biofilms: microbial life on surfaces. Emerg Infect Dis 8:881-890.

Edwards K. J., Bach W. and McCollom T. M. 2005. Geomicrobiology in oceanography: microbe-mineral interactions at and below the seafloor. Trends Microbiol 13:449-456.

Edwards K. J., Rogers D. R., Wirsen C. O. and McCollom T. M. 2003. Isolation and characterization of novel psychrophilic, neutrophilic, Fe-oxidizing, chemolithoautotrophic alpha- and gamma-proteobacteria from the deep sea. Appl Environ Microbiol 69:2906-2913.

Edwards K. J. and Rutenberg A. D. 2001. Microbial response to surface microtopography: the role of metabolism in localized mineral dissolution. Chem Geol 180:19-32.

Einen J., Kruber C., Øvreas L., Thorseth I. H. and Torsvik T. 2006. Microbial colonization and alteration of basaltic glass. Biogeosciences Discuss. 3:273-307.

El-Naggar M. Y., Gorby Y. A., Xia W. and Nealson K. H. 2008. The molecular density of states in bacterial nanowires. Biophys J 95:L10-12.

Flemming H.-C. 2008. Why microorganisms live in biofilms and the problem of biofouling. In: Marine and Industrial Bioufouling.

Fletcher E. L., Weissman B. A., Efron N., Fleiszig S. M., Curcio A. J. and Brennan N. A. 1993. The role of pili in the attachment of Pseudomonas aeruginosa to unworn hydrogel contact lenses. Curr Eye Res 12:1067-1071.

Fletcher M. 1996. Bacterial adhesion: Molecular and ecological diversity. New York: Wiley-Liss., Inc.

Fortin D., Ferris F. G. and Scott S. D. 1998. Formation of Fe-xilicate and Fe-oxides on bacterial surfaces in samples collected near hydrothermal vents on the Southern Explorer Ridge in the northeast Pacific Ocean. Am. Min. 83:1399-1408.

Gorby Y. A., Yanina S., McLean J. S., Rosso K. M., Moyles D., Dohnalkova A., Beveridge T. J., Chang I. S., Kim B. H., Kim K. S., Culley D. E., Reed S. B., Romine M. F., Saffarini D. A., Hill E. A., Shi L., Elias D. A., Kennedy D. W., Pinchuk G., Watanabe K., Ishii S., Logan B., Nealson K. H. and Fredrickson J. K. 2006. Electrically conductive bacterial nanowires produced by Shewanella oneidensis strain MR-1 and other microorganisms. Proc Natl Acad Sci U S A 103:11358-11363.

Graupner S., Frey V., Hashemi R., Lorenz M. G., Brandes G. and Wackernagel W. 2000. Type IV pilus genes pilA and pilC of Pseudomonas stutzeri are required for natural genetic transformation, and pilA can be replaced by corresponding genes from nontransformable species. J Bacteriol 182:2184-2190.

Heijstra B. D., Pichler F. B., Liang Q., Blaza R. G. and Turner S. J. 2009. Extracellular DNA and Type IV pili mediate surface attachment by Acidovorax temperans. Antonie Van Leeuwenhoek 95:343-349.

Jannasch H. W. 1994. The microbial turnover of carbon in the deep-sea environment. Global and Planetary Change 9:289-295.

Jannasch H. W. and Taylor C. D. 1984. Deep-sea microbiology. Annu Rev Microbiol 38:487-514.

Jefferson K. K. 2004. What drives bacteria to produce a biofilm? FEMS Microbiol Lett 236:163-173.

Kinzler K., Gehrke T., Telegdi J. and Sand W. 2003. Bioleaching-a result of interfacial processes caused by extracellular polymeric substances (EPS). Hydrometallurgy 71:83-88.

Kucera S. and Wolfe R. S. 1957. A selective enrichment method for Gallionella ferruginea. J Bacteriol 74:344-349.

Lalucat J., Bennasar A., Bosch R., Garcia-Valdes E. and Palleroni N. J. 2006. Biology of Pseudomonas stutzeri. Microbiol Mol Biol Rev 70:510-547.

Lane D. J. 1991. 16S/23S rRNA sequencing. In: Nucleic Acid Techniques in Bacterial Systematics. Stackebrandt E. and Goodfellow M., editors. 115-148.

Lang S. Q., Butterfield D. A., Schulte M., Kelley D. S. and Lilley M. D. 2010. Elevated concentrations of formate, acetate and dissolved organic carbon found at the Lost City hydrothermal field. Geochim Cosmochim Acta:941-952.

Lovley D. R., Coates J. D., Blunt-Harris E. L., Phillips E. J. P. and Woodward J. C. 1996. Humic substances as electron acceptors for microbial respiration. Nature 382:445-448.

Lysnes K., Thorseth I. H., Steinsbu B. O., Øvreås L., Torsvik T. and Pedersen R. B. 2004. Microbial community diversity in seafloor basalt from the Arctic spreading ridges. FEMS Microbiology Ecology 50:213-230.

Marsili E., Baron D. B., Shikhare I. D., Coursolle D., Gralnick J. A. and Bond D. R. 2008. Shewanella secretes flavins that mediate extracellular electron transfer. Proc Natl Acad Sci U S A 105:3968-3973.

Mason O. U., Stingl U., Wilhelm L. J., Moeseneder M. M., Di Meo-Savoie C. A., Fisk M. R. and Giovannoni S. J. 2007. The phylogeny of endolithic microbes associated with marine basalts. Environ Microbiol 9:2539-2550.

Morisaki H. and Tabuchi H. 2009. Bacterial attachment over a wide range of ionic strengths. Colloids Surf B Biointerfaces 74:51-55.

Newman D. K. and Kolter R. 2000. A role for excreted quinones in extracellular electron transfer. Nature 405:94-97.

Ohshima H. 1994. Electrophretic mobility of soft particles. Journal of Colloid and Interface Science 163:474-483.

Pfennig N. and Lippert K. D. 1966. Uber Das Vitamin B12-Bedurfnis Phototropher Schwefelbakterien. Archiv Fur Mikrobiologie 55:245-256.

Price N. M., Harrison G. I., Hering J. C., Hudson R. J., Palenik B. and Morel F. M. M. 1989. Preparation and chemistry of the artificial algal culture medium Aquil. Biol. Oceanogr. 6:443-461.

Rabaey K., Boon N., Siciliano S. D., Verhaege M. and Verstraete W. 2004. Biofuel cells select for microbial consortia that self-mediate electron transfer. Appl Environ Microbiol 70:5373-5382.

Reguera G., McCarthy K. D., Mehta T., Nicoll J. S., Tuominen M. T. and Lovley D. R. 2005. Extracellular electron transfer via microbial nanowires. Nature 435:1098-1101.

Reguera G., Pollina R. B., Nicoll J. S. and Lovley D. R. 2007. Possible nonconductive role of Geobacter sulfurreducens pilus nanowires in biofilm formation. J Bacteriol 189:2125-2127.

Rohwerder T., Gehrke T., Kinzler K. and Sand W. 2003. Bioleaching review part A: progress in bioleaching: fundamentals and mechanisms of bacterial metal sulfide oxidation. Appl Microbiol Biotechnol 63:239-248.

Sand W. and Gehrke T. 2006. Extracellular polymeric substances mediate bioleaching/biocorrosion via interfacial processes involving iron(III) ions and acidophilic bacteria. Res Microbiol 157:49-56.

Santelli C. M. (2007). Geomicrobiology of the Ocean Crust: the phylogenetic diversity, abundance, and distribution of microbial communities inhabiting basalt and implications for rock alteration processes, Massachusetts Institute of Technology
Woods Hole Oceanographic Institution.

Santelli C. M., Orcutt B. N., Banning E., Bach W., Moyer C. L., Sogin M. L., Staudigel H. and Edwards K. J. 2008. Abundance and diversity of microbial life in ocean crust. Nature 453:653-656.

Schwyn B. and Neilands J. B. 1987. Universal chemical assay for the detection and determination of siderophores. Anal Biochem 160:47-56.

Sheng X. F., Zhao F., He L. Y., Qiu G. and Chen L. 2008. Isolation and characterization of silicate mineral-solubilizing Bacillus globisporus Q12 from the surfaces of weathered feldspar. Can J Microbiol 54:1064-1068.

Smyth C. J., Marron M. B., Twohig J. M. and Smith S. G. 1996. Fimbrial adhesins: similarities and variations in structure and biogenesis. FEMS Immunol Med Microbiol 16:127-139.

Staudigel H., Furnes H., McLoughlin N., Banerjee N. R., Connell L. B. and Templeton A. S. 2008. 3.5 billion years of glass bioalteration: Volcanic rocks as a basis for microbial life? Earth-science Reviews (in press).

Staudigel H. and Hart S. R. 1983. Alteration of basaltic glass: Mechanisms and significance from the oceanic crust-seawater budget. Geochim. Cosmochim. Acta 47.

Staudigel H., Hart S. R., Pile A., Bailey B. E., Baker E. T., Brooke S., Connelly D. P., Haucke L., German C. R., Hudson I., Jones D., Koppers A. A., Konter J., Lee R., Pietsch T. W., Tebo B. M., Templeton A. S., Zierenberg R. and Young C. M. 2006. Vailulu'u Seamount, Samoa: Life and death on an active submarine volcano. Proc Natl Acad Sci U S A 103:6448-6453.

Staudigel H., Yayanos A., Chastain R., Davies G., Verdurmen E. A. T., Schiffman P., Bourcier R. and De Baar H. 1998. Biologically mediated dissolution of volcanic glass in seawater. Earth and Planet. Sci. Letters 164:233-244.

Stillings L. L., Drever J. I., Brantley S. L., Sun Y. and Oxburgh R. 1997. Rates of feldspar dissolution at pH 3-7 with 0-8 mM oxalic acid. Chem Geol 132:79-90.

Stoodley P., Sauer K., Davies D. G. and Costerton J. W. 2002. Biofilms as complex differentiated communities. Annu Rev Microbiol 56:187-209.

Stookey L. L. 1970. A new spectrometric reagent for iron. Anal. Checm. 42:779-781.

Sudek L. A., Templeton A. S., Tebo B. and Staudigel H. 2009. Microbial Ecology of Fe (hydr)oxide mats and basaltic rock from Vailulu'u Seamount, American Samoa. Geomicrobiology Journal 26:581-596.

Telford J. R. and Raymond K. N. 1997. Amonabactin: a family of novel siderophores from a pathogenic bacterium. JBIC, Journal of Biological Inorganic Chemistry 2:750-761.

Templeton A. and Knowles E. 2009. Microbial transformation of minerals and metals: recent advances in Geomicrobiology derived from synchrotron-based x-ray spectroscopy and x-ray microscopy. Annual Reviews in Earth and Planetary Sciences 37:367-391.

Templeton A. S., Knowles E. J., Eldridge D. L., Arey B. W., Dohnalkova A. C., Webb S. M., Bailey B. E., Tebo B. M. and Staudigel H. 2009. A seafloor microbial biome hosted within incipient ferromanganese crusts. Nature Geoscience 2:872-876.

Templeton A. S., Staudigel H. and Tebo B. M. 2005. Diverse Mn(II)-oxidizing bacteria isolated from submarine basalts at Loihi Seamount. Geomicrobiology Journal 22:127-139.

Thanyakoop C. (2009). Characterization and biosynthesis of siderophores from marine bacteria. Chemistry. Santa Barbara, University of California, Santa Barbara.

Thorseth I. H., Furnes H. and Tumyr O. 1995. Textural and chemical effects of bacterial activity on basaltic glass: an experimental approach. Chem Geol 119:139-160.

Thorseth I. H., Torsvik T., Torsvik V., Daae F. L. and Pedersen R. B. 2001. Diversity of life in ocean floor basalts. Earth and Planet. Sci. Letters 194:31-37.

Watnick P. and Kolter R. 2000. Biofilm, city of microbes. J Bacteriol 182:2675-2679.

Watnick P. I. and Kolter R. 1999. Steps in the development of a Vibrio cholerae El Tor biofilm. Mol Microbiol 34:586-595.

Wilkinson J. F. 1958. The extracellular polysaccharides of bacteria. Bact. Rev. 22:46-73.

Winkelmann G. 1997. Transition Metals in Microbial Metabolism. The Netherlands: Harwood Acad. Publ.

Zawadzka A. M., Vandecasteele F. P., Crawford R. L. and Paszczynski A. J. 2006. Identification of siderophores of Pseudomonas stutzeri. Can J Microbiol 52:1164-1176.

Zobell C. E. 1943. The Effect of Solid Surfaces upon Bacterial Activity. J Bacteriol 46:39-56.

CHAPTER V: **Towards an understanding of *Pseudomonas stutzeri* VS-10 interaction with basaltic glass**

1. Auxotrophic mutants of *P. stutzeri* VS-10 generated by Tn5 transposon mutagenesis: phenotypic, physiological and genetic characterization

Introduction

The marine siderophore producing bacterium *Pseudomonas stutzeri* VS-10, exhibiting elevated growth on minimal medium in the presence of basalt, was used as a model organism to explore the ecology behind microbe/glass interactions.

Pseudomonas stutzeri was first described by (Burri and Stutzer 1895). Its phenotypic characteristics were described by (Van Niel and Allen 1952). Phylogenetically it shares one branch with *Pseudomonas mendocina*, *P. alcaligenes*, *P. pseudoalcaligenes* and *P. balearica*, which also represents its closest relative

(Lalucat et al. 2006). From an environmental perspective *P. stutzeri* strains have mainly been of interest due to their ability to degrade a variety of environmental pollutants (crude oil, aromatic and aliphatic hydrocarbons (Criddle et al. 1990; Dijk et al. 2003; Hou et al. 2004). Over the past two decades *P. stutzeri* has also been studied in detail for its potential for denitrification (Carlson and Ingraham 1983; Ferguson 1994) and natural transformation (Lorenz and Sikorski 2000; Lorenz and Wackernagel 1994).

1. Environmental distribution

P. stutzeri can be found abundantly in both terrestrial and marine ecosystems (Ward and Cockcroft 1993). Marine isolates of *P. stutzeri* have been reported in sediment and wastewater from Barcelona, Spain (Bosch et al. 1999a; Bosch et al. 1999b; Rossello´-Mora et al. 1991), in sea sediment from Dangast, Germany (Sikorski et al. 2002), the Black Sea (Sorokin et al. 1999), the Ariake Sea tideland, Japan (Kariminiaae-Hamedaani et al. 2004) and more recently from the Caribbean coast, Costa Rica (Solano et al., unpublished). Only two strains were isolated from the deep-sea environment. One from marine sediment at 11,000-m depth in the Mariana Trench (strain MT-1; Tamegai et al. 1997) the other from a deep-sea hydrothermal vent in the Galapagos Rift (strain NF-13; Ruby et al. 1981). Recent molecular and culture-based studies on Fe (hydr)oxide mats and basaltic rocks have shown its presence in hydrothermally-influenced and low temperature environments at both Loihi and Vailulu'u Seamount (Sudek et al. 2009; Templeton et al. 2005).

2. Genetic properties

Knowledge of the genomic structure of a strain is essential to understand a species' characteristics (Lalucat et al. 2006) which might help to elucidate its abundance and role in various environments. The only *Pseudomonas stutzeri* genome publicly available is of strain A1501 (CGMCC 0351). This strain was isolated from rice roots in China and has been studied with respect to nitrogen-fixation (Yan et al. 2008). Its genome consists of one circular chromosome with a size of 4.6 Mb. *P. stutzeri* strains have been shown to exhibit high genetic diversity suggested as an adaptation mechanism to various environmental niches and rapidly changing environmental conditions. Genome analysis and molecular ecology studies have shown that horizontal gene transfer is a relevant force in bacteria for this kind of process (Lalucat et al. 2006). In addition to transduction and conjugation natural transformation is perhaps the most versatile mechanism of horizontal gene transfer. Transformability appears to be widespread among environmental *P. stutzeri* strains and has been studied extensively over the past two decades (Lalucat et al. 2006). One-third of the *P. stutzeri* members have been shown to be naturally transformable by both chromosomal and plasmid DNA (Carlson et al. 1983; Lorenz and Sikorski 2000; Sikorski et al. 2002). They can take-up foreign DNA as well as DNA from their own species which is considered the cause of the groups high degree of genetic, phenotypic, genotypic and physiological diversity and flexibility (Lalucat et al. 2006).

3. Physiological characteristics

P. stutzeri strains have been shown to grow at temperatures varying between 4 and 45 °C with an optimal growth temperature for most strains of approximately 35 °C. Its remarkable physiological and biochemical diversity and flexibility is reflected by its capacity to grow both aerobically and anaerobically on a wide range of organic substrates and terminal electron acceptors (Lalucat et al. 2006). Under conditions of Fe starvation a number of *P. stutzeri* strains (*P. stutzeri* ATCC 17588, RC7, JM 300, DSM 50238) have shown the ability to synthesize non-pigmented siderophores including nocardamine (Meyer and Abdallah 1980), desferriferrioxamines E (Essen et al. 2007) and catechol-like siderophores (Charkraborty et al. 1990) including amonabactins (Zawadzka et al. 2006). Its potential for mixotrophic Fe(II)oxidation has been shown under anaerobic conditions in the presence of nitrate (Muehe et al. 2009).

4. Transposon delivery vector pRL27

Larsen et al. (2002) showed that the pRL27 transposon delivery vector encoding a hyperactive Tn5 transposase is functional and can be used efficiently in the transformation of α-, β- and γ- Proteobacteria. Two *P. stutzeri* strain 567, a derivative of *P. stutzeri* WM88 (Metcalf and Wolfe 1998) and strain 1967, a derivative of WM567 were successfully mutagenized previously. There are two main advantages that are thought to make transformation with the pRL27 delivery vector so efficient:

1. The presence of a hyperactive Tn5 transposase gene under the control of the tetA (tetracycline-resistance) gene of plasmid RP4, functional in a wide variety of organisms.
2. The presence of an origin of replication facilitating subsequent cloning of the insertion site (Larsen et al. 2002).

Here we employ pRL27-based mutagenesis on *P. stutzeri* VS-10. The objectives of this study were the construction, isolation and characterization of insertion mutants of strain VS-10 deficient in growth on minimal medium and basalt.

Materials and Methods

1. Sample location

Pseudomonas stutzeri VS-10 isolation is described in detail in Chapter IV.

2. Volcanic rocks

A detailed description of basaltic glass and rhyolite used in the experiments is provided in Chapter IV.

3. Bacterial strains

Pseudomonas stutzeri strain VS-10 and mutants generated from this strain were used in all the experiments. For the quorum-sensing assay two other strains: 1. The

indicator organism *Chromobacterium violaceum* ATCC 12472 (donated by R. McLean, Texas State University- San Marcos, Texas) and 2. *Pseudomonas aeruginosa* PAO-1 (positive control, donated by D. Bartlett) were used. A detailed description of the modified assay originally described by McLean et al. (2004) is given in Chapter IV.

4. Growth media and conditions

4.1 Chrome Azurol-Sulfonate (CAS) plates

A detailed protocol for CAS plates used for the isolation of *Pseudomonas stutzeri* VS-10 and its mutants is provided in Chapter IV.

4.2 Luria Bertani (LB) medium

Prior to growth on minimal medium strains were grown to exponential phase in Luria-Bertani (LB) medium (as described in Chapter IV). This medium was also used to investigate any phenotypic abnormalities (color, general growth defects, motility) described in the physiological characterization of the mutants.

4.3 Minimal artificial seawater medium

The recipe for the minimal artificial seawater medium used in the growth experiments is given in Chapter IV. For mutant rescue experiments different amendments were made to the minimal medium: A) addition of ~5.2 μM purified amonabactin P750 (m/z 751); B) 4:1 dilution of medium with wild-type (WT) supernatant containing amonabactin P750 and P694: the WT was grown Fe-limited on minimal medium and

rhyolite for 5 days to OD 0.162. The supernatant was filtered (0.22 μm filter Millipore) and tested for the presence of siderophores by LC-MS (see Chapter IV); C) addition of 10 μM N-(3-Oxodecanoyl)-L-homoserine lactone; D) addition of various concentrations of L-proline (between 0.01 and 0.1 %); E) addition of various concentrations of Casamino Acids, CAA (between 0.01 and 1 %).

4.4 “EM” medium for gradient tubes

Gradient tubes were set-up as described in Chapter II and IV to test for the mutants oxidize Fe(II) when grown heterotrophically. Stationary phase LB and LB_{Kan} cultures of WT and mutants were used for inoculation. They were previously adjusted to approximately the same density (OD_{600} of ~1.24). 10 μl of each culture was used for inoculation.

4.5 F medium

F medium was used to prepare F plates at pH 7.5 as described in Chapter II. The plates were used as an additional test to investigate both WT and mutant ability to oxidize Fe(II) when grown on organics.

4.6 Succinate medium

Succinate medium was used to grow strains Fe-limited prior to detection of siderophores in the supernatant by Liquid Chromatography Electrospray Ionization Mass Spectrometry (LC-ESI-MS) as described in Chapter IV.

5. Random transposon mutagenesis

Transposon mutagenesis is defined by the relocation of specialized DNA elements, namely transposons and insertion elements, within or between chromosomes or extra chromosomal DNA. This process is mediated by either a transposase or an integrase. The substrate of transposition is DNA flanked by inverted repeats in its sequence that are recognized as the target for the transposase. The mobile stretch of DNA bordered by these inverted repeats is called the transposable element, the insertion sequence or the transposon (http://jbuchner.myweb.uga.edu/bcmb8019/body.html). The method we chose to transform strain VS-10 was developed and described by Larsen et al. in 2002. It makes use of a transposon delivery vector (pRL27) that encodes a hyperactive Tn5 transposase carrying a kanamycin resistance gene and an origin of replication to facilitate subsequent cloning of the resulting insertion site (Larsen et al. 2002).

5.1 Competent cells

Competent cells of strain VS-10 were prepared by growing the strain to mid-exponential phase (OD_{600}~ 0.8) on 10 ml of LB medium and collecting cells via centrifugation at 4 °C (2300 x g for 10 min.). After aspiration of the supernatant, the cell pellet was then resuspended in 10 ml of ice-cold microsome extract buffer (MEB: per L of ultra-pure H_2O: 240 mg HEPES, 203 mg $MgCl_2$ x H_2O adjust to pH 7.0, autoclave and refridgerate). After centrifugation at 4 °C (2300 x g for 10 min.) this process was repeated. After a final centrifugation step the cell suspension was resuspended in 500 µl of ice cold MEB and transferred into sterile 1.5 ml eppendorf tubes before centrifugation at 2300 x g for 5 min. at 4 °C. The supernatant was aspirated and the cell pellet was

resuspended in 100 µl MEB buffer (if continued right away) or SMEB (see MEB recipe, add 102.7 g sucrose before autoclaving; for storage at -80 °C).

5.2 Conjugation

150 ng of pRL27 plasmid DNA (Larsen et al., 2002) was mixed with 100 µl of cells and incubated on ice for 5 min. prior to electroporation. Electroporation was carried out on a Tune Gene pulser MXcell at 2.5 kv/cm, 200 Ω and 25 µF (in D. Bartlett's lab at SIO). Immediately following the discharge of the captacitor 900 µl of room temperature Super Optimal broth with Catabolite repression (SOC) medium (2% w/v Tryptone, 0.5 % (w/v) Yeast extract, 8.6 mM NaCl, 2.5 mM KCl, 20 mM $MgSO_4$ and 20 mM Glucose, filter sterilized, pH 7.0) was added to each cuvette. The cell suspension was transferred back to an eppendorf tube and incubated at 30 °C and ~ 200 rpm for 1 hr. After collecting cells via centrifugation the pellet was resuspended in 200 µl warm (~37 °C) SOC medium and ~75 µl were plated on LB plates containing 30 µg/ml Kanamycin. Plates were subsequently incubated at room temperature for 24 hrs.

5.3 Mutant screening

Single colonies appearing on LB_{Kan} plates the next day were picked and transferred to new rasterized LB_{Kan} plates subsequently used as archive plates. From there strains were tested on two media, F- and CAS- plates where the mutants were identified and selected based on their inability to grow.

6. Growth conditions on minimal medium

Prior to the analysis of growth under nutrient-limited conditions (on minimal medium in the presence of volcanic rocks or on succinate medium) WT and mutants of strain VS-10 were grown to exponential phase on LB or LB_{Kan} medium: A) 15 μg/ml for LB plates and B) 25 μg/ml in liquid culture were added to the mutant cultures to maintain the plasmids and prevent contamination by the WT. The WT was previously tested for its Kan sensitivity on LB_{Kan} plates of different concentrations. Its sensitivity lay somewhere between 3 and 6 μg/ml with no growth occurring at 6 μg/ml but visible growth on plates containing 3 μg/ml. LB cultures were washed in minimal medium as described previously (Chapter IV) prior to inoculation of the nutrient-deficient media (minimal and succinate). During incubations cultures were maintained between 21 and 25 °C.

7. Surface motility assay

Twitching motility of WT and mutants was investigated on LB low-agar plates (LB medium containing 0.25 % agar). After solidification of the agar for 24 hrs the plates were spot-inoculated with 1.5 μl of overnight LB and LB_{Kan} cultures of WT and mutants. After incubation at 30 °C for 16 hrs the colony sizes and morphologies were evaluated.

8. Liquid chromatography- Electrospray Ionization-Mass spectrometry (LC-MS)

The method is described in Chapter IV. LC-MS was used to investigate siderophore production in all the mutants both under low and high cell density conditions. ThermoFinnigan LCQdeca mass spectrometer with electrospray ionization source

(http://massspec.ucsd.edu/mmsf/instrumentation.html; UCSD, Mass spec facility, Department of Chemistry and Biochemistry) was used for the analysis.

8.1 Low cell density conditions

WT and mutants were grown on minimal medium and rhyolite. Washed LB cultures were inoculated at ODs of ~ 0.05 which in case of the mutants only raised to ~0.08 within six days. The WT culture had already reached these densities after ~ 1.5 days (see Chapter IV, Figure 5.1). At that point a sample was taken and filter sterilized (0.22 μM filter) and maintained at -20 °C until the mutant cultures were ready for analysis by LC-ESI- MS at the Department of Chemistry and Biochemistry Mass Spectrometer Facility (University of California, San Diego). 10 μl of WT and 40 μl of mutant supernatants were loaded.

8.2 High cell density conditions

Washed LB WT and mutant cultures were resuspended in succinate medium at an OD_{600} between 0.25 and 0.3. Starved for Fe for 4 days (25 °C, ~ 200 rpm) the cells were removed by centrifugation and the supernatant was filter sterilized (see above) prior to LC-ESI-MS analysis. 10 μl of WT supernatant and 20 μl of mutant supernatant were loaded.

8.3 Mutant rescue

As part of the mutant rescue experiments all strains were again grown on minimal medium and rhyolite to determine if siderophore production had been restored to WT-

levels. After 3 days of incubation at room temperature the OD of the cultures was determined and the supernatant was filter sterilized as described previously prior to the LC-MS analysis. 20 µl of both WT and mutant supernatants were loaded.

9. Scanning Electron Microscopy (SEM)

Sample preparation, instrument set-up and operating conditions are described in Chapter IV. The following samples derived from growth of WT and mutants on various media were analyzed by SEM:

9.1 LB medium

Strains (WT and mutants) were grown on LB and LB_{Kan} medium at 37 °C and ~ 200 rpm overnight. The next day sterile basalt grains added to the cultures and incubated overnight. Single grains were removed, fixed in 2.5% glutaraldehyde (v/v) in 0.1M sodium cacodylate buffer (pH 7.3) at 4 °C overnight and prepared as described in Chapter IV.

9.2 Succinate medium

After growth on LB and LB_{Kan} medium and washing steps as described in Chapter IV cells were resuspended in succinate medium containing sterile basalt grains at ODs between 0.20 and 0.30. After 4 days of incubation ODs in the cultures were measured, basalt grains were removed, fixed and prepared for SEM.

9.3 Minimal medium with amendments (mutant rescue)

After rescue of mutants by various amendments (see above under 4.3) the mutants were grown on minimal medium containing sterile basalt grains. Upon growth curve completion a few grains were removed for SEM analysis.

10. Fuel cells

Investigation of electrochemical properties of WT and mutants was performed in collaboration with G. Wanger and Y. Gorby at the J. Craig Venter Institute in San Diego. In addition to the WT two mutants (2A and 11G) were randomly chosen for the analysis. A typical fuel cell set-up is shown in Figure 5.1. Two experimental set-ups were run for WT and mutants:

A) Minimal medium as described in Chapter IV with the addition of 25 μg/ ml Kanamycin to the mutant and abiotic (blank) fuel cells

B) Minimal medium (+Kan) with the addition of 8.7 mM L-proline.

A detailed description for the microbial fuel cell set-up is given in Chapter IV with the exception of a few modifications:

1. Fuel cells were incubated at ODs between 0.1 and 0.2.
2. Current density production was correlated with growth of the strains monitored at 600 nm on a daily basis.

3. In addition to power curves measured under operating conditions (see Chapter IV), polarization curves were taken as follows:

For polarization measurements the fuel cells were set into open circuit mode and the cell potential was allowed to build to a maximum (~2 hrs). The fuel cell was then connected to a Gamry Reference 600 potentiostat and the current response within the system was measured. For polarization measurements the potentiostat varies the external resistance of the circuit from infinite resistance (open circuit) to short circuit (no resistance) and measures the voltage response at each resistances. At no resistance (indicated by the intersection of curves with the x-axis in the open circuit potential curves) the maximum amount of current is drawn. The potential curves consist of 3 regions: a) the activation polarization region: this represents the energy loss to the system due to the breaking of chemical bonds at the anode and cathode and is represented by the first flat part of the curve b) the ohmic polarization region: this represents the electrical loss to the system and is represented by the part of the curve that starts at the origin and ends at the proportional pinch-off voltage c) the concentration/diffusion polarization region: this represents mass transfer losses and is the results of diffusion restrictions within the system. The region is represented by the area close to the intersection with the x-axis.

11. DNA extraction

Mutants were grown to exponential phase on 5 ml of LB_{Kan} medium (37 °C, ~ 200 rpm) prior to extracting their DNA using the CTAB extraction method (www.sou.edu/BIOLOGY/Faculty/Southworth/CTAB.htm). Primers, PCR and sequencing conditions are described in Chapter IV.

12. Cloning and sequencing of transposon insertions

Mutants deficient in growth on CAS plates were grown on 5 ml of LB_{Kan} (30 µg/ml) medium at 30 °C overnight (~ 18 hrs). After cell collection via centrifugation DNA was extracted from the pellets using the CTAB method described in Chapter IV and the DNA was cleaned-up by an additional RNase treatment. Restriction digest (using BamH1), Ethanol precipitation, ligation and transformation back into One shot® PIR 1 competent *E. coli* cells (Invitrogen, Catalog no. C1010-10) followed manufacturer's recommendation. After incubation on LB_{Kan} (30 µg/ml) plates at 30 °C overnight colonies were picked and grown in 3 ml of LB_{Kan} (30 µg/ml) medium overnight and plasmids were extracted using the QIAprep Spin Miniprep Kit (Qiagen Inc., Valencia, CA). 3 µl of plasmid was added to the sequencing reaction containing primers 226f (CAGCAACACCTTCTTCACGA) and 227r (AACAAGCCAGGGATGTAACG) (tpnRL 13-2 and TpnRL17-1 from (Larsen et al. 2002) before running it on a capillary electrophoresis DNA sequencer (ABI PRSIM 3100 genetic analyzer) by Seqxcel Inc., San Diego. Sequences were analyzed using Sequencher (GeneCodes) and classified using the translated query vs. protein database (blastx) of the National Center for Biotechnology Information (NCBI).

13. Gene arrangement in *P. stutzeri* VS-10

The gene arrangement in strain VS-10, with regard to the region affected in three mutants, was analyzed by PCR. The following primers were used (locus tag = PST numbers are based on the genome of *P. stutzeri* A1501):

LS.pst3961.F1 (5'- TGA TAC ATC CGA TGC ACG CCG AAT ATG C -3') and **LS.pst3966.R1** (5'- TAA CGT TGA CCT GCA GAC AGA CAT TCA GC -3') to confirm the arrangement of PST_3961-3966 (~ 5.4 Kb product, see Figure 5.13).

LS.pst3968.F1 (5’- TCT TGC TGC GTT TCA TCC TGC AAT TGG -3') and **LS.pst3970.R1 (**5'- AAG GTT GTT CAG ACT GAC CAC GAA GAA GC -3') to confirm the arrangement of PST_3968- 3970 (~ 3.2 Kb product, Figure 5.13).

LS.pst3954.F1 (5'- TTA CCT CAC SGA RAT CAA CRT CAC CAG C -3') and **LS.pst3960.R1** (5'- TAG TGC GAC CAG CTC GGA TAA TTG TTC ACC -3') to confirm the arrangement of PST_3954-3960 (~ 4.4 Kb product, Figure 5.13).

PST_3974d.R1 (5'- TTG AAG TCR CAR TAC GGG CAY TTG C -3') to confirm the arrangement of PST_3970-3974 (~3.2 Kb product, Figure 5.13).

LS.pst3962.F1 (5'- ATT ATC CGC TCG GCT GAC TAC ACC ATG G -3') and **LS.pst3965.R1** (5'- AAG TCT TCC GCA AGA TCA CCG ATG TTC C -3') to confirm arrangement of PST_3962-3965 (Figure 5.13).

The following touchdown PCR protocol was used: 94 °C for 2 min. (denaturing); then 4 x (94 °C for 10 sec., 68 °C for 30 sec., 72 °C for 4 min.); then 4 x (94 °C for 10 sec., 63 down to 59 °C [decreasing by -1 °C] for 30 sec., 72 °C for 4 min.); then 22 x (94 °C for 10 sec., 58 °C for 30 sec., 72 °C for 4 min..

14. Quorum sensing (QS) assay

A modified plate assay developed by McLean et al., 2004 was used to investigate the production of homoserine-lactone antagonists in both WT and mutant 2A. A detailed description of the assay is given in Chapter IV. Additionally the assay was run with a lower layer containing 8.7 mM of L-proline.

Results

Energy gain through the oxidation of Fe(II) from basalt and/or nutrient acquisition from basalt facilitated through the production of siderophores were originally considered two potential processes controlling growth of strain VS-10 on basalt (for growth curves see Chapter IV, Figure 5.1). Thus mutant screens conducted after the Tn5 transformation of the strain were designed to select for strains deficient in any one of these processes. Mutants were streaked on F- and CAS plates. Mutants were subsequently picked based on their phenotypic profile (e.g. growth deficiency on plates, absence of orange color on F-plates or halo on CAS plates). In addition to the genetic identification of the insertion

site in each mutant a detailed phenotypic and physiological characterization was conducted to investigate further effects of the mutagenesis.

1. Random transposon mutagenesis

Out of 850 mutants screened for their potential to oxidize Fe(II) (on F-plates) and the ability to produce siderophores (on CAS plates) five mutants were generated: VIII21, XII5, 2A, 9G and 11G. They all were picked based on their deficiency to grow on CAS plates even though this does not indicate a deficiency in siderophore production. No mutant able to grow on CAS but lacking the distinct halo was obtained. Also, the mutagenesis did not result in the isolation of any mutants on F-plates.

2. Growth properties of mutants on minimal medium and basalt

Experiments investigating the growth of WT and mutants of strain VS-10 on minimal medium in the presence of basalt show that all mutants are growth-deficient under these conditions (Figure 5.2).

3. Phenotypic and physiological characterization of mutants

A phenotypic and physiological characterization of both WT and mutants was carried out to investigate the potential reason behind the mutants' lack of growth.

3.1 Growth characteristics on LB_{Kan} medium

Grown on liquid LB_{Kan} medium overnight three out of five mutants showed different phenotypic characteristics compared to the WT. While growth (based on density

and color) of mutants VIII21 and XII5 resembles the one of the WT, mutants 9G and 11G show a general growth deficiency indicated by significantly lowered ODs. Mutant 2A growing to approximately the same densities as the WT exhibits a dark brown color (Figure 5.3).

3.2 Motility on LB twitch plates

Colony morphology of all mutants and WT on a regular LB plate is similar (Figure 5.4 A). Motility investigated on LB twitch plates, appears to be elevated in all mutants compared to the WT strain (Figure 5.4 B)

3.3 Siderophore production

The production of amonabactins in the mutants prior to their rescue was investigated, under low and high cell density conditions.

3.3.1 Low cell density conditions

Both WT and mutants were grown to ODs of approximately 0.08. While LC-ESI-MS results showed the abundance of amonabactin P750 and P693 in the WT supernatant no signal could be detected in the mutant cultures.

3.3.2 High cell density conditions

After inoculation of succinate medium with washed WT and mutant cultures at ODs around 0.25 the cultures were starved for 4 days. At that point ODs in the cultures

still ranged between 0.20 and 0.28. LC-ESI-MS analysis of the supernatant showed the abundance of amonabactins P750 and P693 only in the WT cultures (Figure 5.5).

3.4 Fe(II)oxidation potential

As discussed in Chapter IV the WT of *P. stutzeri* VS-10 oxidizes Fe(II) when grown heterotrophically. Mutants were tested for this physiological feature both on organic-rich plates (F-plates) and in gradient tubes. Under both conditions the mutants seem to exhibit a potential for heterotrophic Fe(II)oxidation similar to the WT (Figure 5.6 and 7).

3.5 Biofilm formation on basaltic glass

When grown on LB medium and basaltic glass all mutants display biofilms resembling the one of the WT. This includes the presence of extracellular polymeric material (EMP) visible in the form of filamentous appendages facilitating both cell-to-cell and cell-to-substrate interactions (Figure 5.8).

To analyze the biofilm structure under nutrient-limited conditions high cell density LB and LB_{Kan} cultures of WT and mutants were washed as described before and resuspended in minimal medium containing sterile basalt at ODs between ~ 0.2 and 1. Cultures were incubated for 4 days prior to visualization of cells and biofilms on the basalt surface. Biofilm deficiency (Figure 5.9) and a lack of EMP production (Figure 5.10) is observed in all mutants compared to the WT. Instead cell distribution in the

mutant cultures is characterized by “patchy” mono-layers of cells that lack any structure (Figure 5.9).

3.6 Electrochemical properties

Power production by WT and mutants was investigated in microbial fuel cells (MFCs) containing minimal medium only. Each anode compartment was inoculated with washed cultures of either WT, mutant 2A or 11G at ODs of around 0.2. Within the first 2 days cell density dropped to an OD of around 0.1 and a biofilm formation on the inner walls of the fuel cell was visible in case of the WT. While current production in the WT cell is evident, no power is generated in any of the mutant cells (Figure 5.11). WT current densities are lower than the ones reported in Chapter IV which is likely due to the nutrient depletion of the culture used in this set-up (LB culture were used in Chapter IV). Scanning electron micrographs taken after 3 days of incubation show the abundance of cells on the anode surfaces albeit in low numbers on the mutant anodes. The WT instead exhibits biofilm-like structures including the presence of EMP (Figure 5.12).

4. Identification of mutated loci

Sequence results indicate that a total of 9 genes were affected by the Tn5 insertions (Table 5.1). Blastx (protein database using a translated nucleotide query) searches identified genes from *Pseudomonas stutzeri* A1501 (CGMCC 0351) as the most similar. This strain represents the only fully sequenced *P. stutzeri* up to this date. In four out of five mutants (except for mutant 11G) sequencing of the insertion sites indicate that the transposon insertion is located in-between two genes. In two mutants (2A and 9G)

these two genes are shown to be adjacent (based on the gene arrangement in strain A1501, Figure 5.13). Primers were designed for the entire gene region (from PST_3960 to PST_3970 see Table 5.1 and Figure 5.13). The length of the amplification from VS-10 is similar to A1501 suggesting that the gene arrangement of the two strains is identical within this region (data not shown). Large genomic gaps between other genes in *P. stutzeri* A1501 affected by the insertion indicate a difference in the gene arrangement between the two strains. For instance sequencing of mutant XII5 using the reverse primer resulted in the highest sequence similarity to homoserine-O-acyltransferase "metX" in strain A1501. Sequencing using the forward primer however results in a gene encoding a peptidase M23/M37 (PST_4081) located 128 kb bp downstream of "metX" (PST_3970).

While mutagenesis using the Tn5 delivery vector was previously shown to be random (Larsen et al., 2004) in our strain it is noticeable that in three out of five mutants the same gene region appears to be affected. This region includes two of the type IV pilus proteins ("pilU" and "pilT") known for being involved in twitching motility of strains. In addition to that sequencing of the insertion site in mutant VIII21 encoded a type IV prepilin-like protein "pilD", involved in pilin maturation. The number of genes encoding type IV pilus proteins, involved in motility of strains, correlates well with the altered motility of mutants on LB twitch plates (Figure 5.4B). Other genes appear to be involved in the biosynthesis and metabolism of various amino acids (Table 5.1: metabolic pathway) correlating with the growth deficiencies of the mutants and suggesting that they are amino acid auxotrophs.

5. Mutant rescue experiments

Several attempts were made to restore growth of the mutants which were all based on their physiological (lack of siderophore production) and genetic characteristic (disruption in autoinducer or amino acid biosynthesis). They included the addition of exogenous siderophores, autoinducers (homoserine lactone) or amino acids to the minimal medium cultures containing basalt.

5.1 Exogenous siderophores

Initially growth deficiency was thought to be due to the lack of siderophore production potentially involved in Fe acquisition from basalt. Both, supernatant containing exogenous siderophores produced by the WT (under Fe-limited conditions) as well as purified siderophores (amonabactin P750) were added to the cultures. The addition of WT supernatant (containing amonabactin P750 and P693) or ~ 5.2 μM purified Amonabactin P750 could not restore growth of the mutants (Figure 5.14 A and B).

5.2 Autoinducers

Based on the genetic results from mutant XII5 and previous results indicating the WT's ability to quorum sense (Chapter IV), the possibility of a growth deficiency of mutants based on the disruption in the autoinducer biosynthesis was investigated. The insertion site in mutant XII5 affected a gene encoding the homoserine-o-acyltransferase "metX" (in *P. stutzeri* A1501). "metX" is known for being involved in both cystein and methionine biosynthesis where it intermediates the transformation from homoserine to O-

acetylhomoserine to L-homocystein in *Pseudomonas syringae* (Andersen et al. 1998). L-homocystein is involved in biosynthesis of S-Adenosyl-L-methionine which is one out of two substrates for the biosynthesis of autoinducers such as homoserine lactones. Addition of 10 μM of N-(3-Oxodecanoyl)-L-homoserine lactone (HSL) to the mutant cultures however does not restore growth (Figure 5.14 C).

5.3 Amino acids

The analysis of genes affected by the mutagenesis indicated frequent disruption of genes involved in the biosynthesis of various amino acids. Therefore both gene-specific and general additions of amino acids were made to the minimal medium and growth of WT and mutants was monitored.

5.3.1 Gene-specific: L-Proline

Based on the disruption of “proC”, the pyrroline-5-carboxylate reductase in mutant 2A the minimal medium was amended with different concentrations of L-proline. Growth of mutant 2A on minimal medium was restored to WT levels (or better) under high (1% = 8.7 mM) concentrations of proline (Figure 5.15). No growth was detectable at proline concentrations below 1% (data not shown).

5.3.2 General: Casamino acids

Various concentrations of Casamino acids (CAA) which contains all amino acids required in growth of prokaryotes were added to the minimal medium. Growth of all

mutants on minimal medium could be restored to WT-levels through the addition of 0.5 % CAA (Figure 5.16).

5.4 Characterization of rescued mutants

Cultures of mutants grown in CAA-amended minimal medium show biofilm formation and EPM production similar to the wild type (Figure 5.17). Addition of 8.7 mM proline to the culture of mutant 2A has the same effect and also restores siderophore production, quorum-sensing and partly electrochemical properties of the biofilm in this mutant (Figure 5.18-19). Fuel cell experiments with WT and mutant 2A on minimal medium containing 8.7 mM of proline show that the current production in 2A, even though now present, is not fully restored. While the current densities of both strains measured under standard operating conditions (Figure 5.19 A) is similar, if not better in 2A, the open circuit potential represented in form of polarization curves is still higher in the WT fuel cell (WT ~ 425 mV, 2A ~357 mV, Figure 5.19 B). Results also show that despite the fact that the open circuit potential in the WT fuel cell is generally higher overall more current can be drawn from the mutant cell (represented by a higher current density, x-axis Figure 5.19 B).

Discussion and Conclusion

Over the course of this work we attempted to elucidate which physiological characteristic of the WT of *P. stutzeri* VS-10 may be responsible for elevated growth of

the strain in the presence of basaltic glass. Mutant screens were designed to select for strains deficient in either siderophore production or heterotrophic Fe(II)oxidation. Of 850 mutants screened none was deficient in Fe(II)oxidation. In addition to an insufficient number of mutants screened this could also indicate that the genes involved in Fe(II)oxidation are A) relatively small or B) less abundant. Both scenarios would result in a reduced chance that the transposon would hit in such a region.

A phenotypic and physiological characterization of five mutants exhibiting auxotrophic growth patterns on minimal medium provided insight into the potential cell-density dependence of various WT characteristics including siderophore production and electrochemical properties of the biofilm. A close association of biofilm formation, twitching motility, quorum-sensing and siderophore production has been suggested previously (Abbas et al. 2007; Aguilar et al. 2003; Harrison and Buckling 2009; Heydorn et al. 2002; Patriquin et al. 2008; Stintzi et al. 2006; Wang et al. 2007). For the most part it remains unknown exactly how these mechanisms are linked. While mutant rescue experiments in stain VS-10 support the assumption that all mutants are amino acid auxotrophs it must be considered that this alone would not explain their altered motility which also correlates well with the gene region affected in most mutants. It is noticeable that two regions affected in four out of five VS-10 mutants encode genes involved in twitching motility (type IV pilus proteins “pilD”, “pilU” and “pilT”). The fact that restoration of growth/biofilm formation also restored the mutants’ abilities to produce siderophores and to quorum-sense suggests that these mechanisms may all be linked in strain VS-10 and that siderophore production is cell density-dependent. The lack of

biofilm formation at high cell densities in all the mutants correlates well with noticeably lower cell numbers (mutants 9G and 11G) and different pigmentation (mutant 2A) of some mutants when grown in organic-rich (LB) medium. This is indicative that other parts of the bacterial metabolism (aside from auxotrophy) are likely to be affected by the mutagenesis.

Also, while morphologically the biofilm development of mutant 2A appeared to be fully restored to WT-levels upon the addition of proline, its electrochemical properties were still affected as suggested by a lower open circuit potential. The fact that eventually more current could be drawn from the mutant cell is likely due to a limitation inside the WT cell. In the WT polarization curve (Figure 5.19 B) this is indicated by a steep drop-off in area representing the mass transfer loss. A drop-off in this region generally suggests diffusion limitation (pers. comm. G. Wanger). Possible reasons for this could be the formation of a biofilm on the cation exchange membrane preventing free flow of cations within the system. It is unclear how the genes knocked out in mutant 2A (pyrroline-5-carboxylate-reductase, enzyme with TIM-barrel fold) are related to the strains' electrochemical properties. Instead, recent lithography measurements showed the conductivity of the WT EPM appendages (data not shown). Since EPM production simultaneously with biofilm formation was restored in 2A (upon addition of proline) it is likely that this is causing its electrochemical potential.

Overall the generation of mutants described here contributed towards a better understanding of several *P. stutzeri* VS-10 features and their potential role in basalt-

surface related growth of the strain. The main value of this work lies in the establishing of a robust mutagenesis system that in the future will facilitate additional studies with this intriguing strain.

2. Characterization of amonabactin-metal complexes in *P. stutzeri* VS-10

Introduction

Iron and manganese are the two most abundant redox-active metals in the Earth's crust. In the marine environment both metals form a wide variety of solid phases, with Fe (hydr)oxides and Mn (IV)oxides in particular functioning as effective sorbents of organics, metals, and oxyanions (Cornell and Schwermann 2003; Post 1999; Tebo et al. 2004). The concentration of particulate Mn is comparable to the one of total Fe in seawater (Boukhalfa et al. 2006; da Silva and Williams 2001; Landing and Bruland 1980; Yeats et al. 1992). Because of their abundance and redox activity, both metals are also utilized in the enzyme systems of animals, plants, and microbes (da Silva and Williams 2001).

Ferromanganese crusts are commonly associated with all geomorphological and tectonic environments in the ocean basin (Hein et al. 1997) and regularly occur on the surfaces of submarine volcanic rocks. Recent work on natural basalt surfaces at Loihi

Seamount has shown a high abundance of both metal-oxides in close association with microbial cells (Templeton et al. 2009). Other work has documented the cellular encrustation of endolithic cells by Mn-rich particles (Thorseth et al. 2003; Thorseth et al. 2001). The interaction of microbial metabolites, including siderophores with these metal-oxides is likely. *P. stutzeri* VS-10 was isolated from a submarine volcanic rock surface (details see Chapter IV). It produces a suite of structurally-related siderophores, the amonabactins (Thanyakoop 2009).

Here we study the formation of amonabactin-Fe/Mn complexes. A purple Fe-siderophore complex was discovered and analyzed in terms of its pH stability and spectrophotometric characteristics. In addition different complexes with Fe(II) and Mn(II) were investigated including the ligand-promoted oxidation of these metals under anaerobic conditions. Grown Fe-limited on minimal medium it was previously shown that *P. stutzeri* VS-10 produces the two amonabactins P750 and P693 (Chapter IV). The following work carried out on the supernatant of the strain therefore contains both siderophores. Since both molecules are likely interacting with Fe and Mn added to the solutions data presumably represent mixtures of complexes.

Materials and Methods

1. Fe-siderophore complex

For a general characterization of the Fe-siderophore complexes *P. stutzeri* VS-10 was grown on minimal medium and rhyolite for 4-6 days. The supernatant was filter-sterilized and adjusted to pH ~7 prior to the addition of 100 μM $FeCl_2$. After ~ 2 hrs the UV-visible (UV-Vis) spectrum for this solution was measured between 240 and 750 nm.

2. pH characteristics of the Fe-siderophore complexes

To determine the characteristics of Fe-siderophore complexes at different pH strain VS-10 was grown Fe-limited on minimal medium and rhyolite for 4-6 days. The supernatant was filter-sterilized and adjusted to pH ~3 with 1N trace element grade HCl (see Chapter VI for cat. #). $FeCl_2$ was added to the solution to a final concentration of 200 μM and the complexation was allowed to take place over 2 hrs before the color of the solution was reported and the UV-Visible spectrum was measured between 290 and 750 nm. The solution was subsequently titrated and adjusted to different pH between pH ~3-8.5 with KOH.

3. Aerobic complexes with Fe and Mn at pH 7

The complexation of both Fe(II +III) and Mn(II) were investigated at neutral pH. Either $FeCl_2$, $FeCl_3$ or $MnSO_4$ were added to the filter-sterile supernatant previously adjusted to pH 7 to final concentrations of 140 μM. Formation of the metal-siderophore

complexes (based on color generation) was allowed to happen before the UV-Vis spectra (between 230 and 740 nm) were recorded.

4. Ligand-promoted oxidation of Fe(II) and Mn(II)

Investigation of ligand-promoted oxidation and complexation of Fe(II) and Mn(II) was carried out under anaerobic conditions. The siderophore-containing supernatant was bubbled with N_2 for 1.5 hrs and transferred to the anaerobic chamber where it was inoculated with either anaerobic prepared $FeCl_2$ or $MnSO_4$ to final concentrations of 140 μM. After addition of the acidic Fe(II) solution (to keep it reduced and soluble during preparation) the pH of the Fe-siderophore solution was re-adjusted to pH 7 (with $NaHCO_3$) and shown to match the pH of the Mn solution. Prior to analysis of the UV-Vis spectrum the solution was transferred to a quartz cuvette inside the anaerobic chamber. It was then overlaid with mineral oil to prevent contamination with atmospheric oxygen upon removal from the chamber.

Results

1. Characteristic of metal-siderophore complexes

Addition of Fe(II) to the supernatant of strain VS-10 (at neutral pH) results in the formation of purple Fe-siderophore complexes (Figure 5.20 A). The UV-Vis spectrum shows 3 predominant peaks: at 290 nm, 330 nm and 550 nm (Figure 5.20 B).

2. pH characteristics of Fe-siderophore complexes

A first order investigation of the pH characteristics of the Fe-amonabactin complexes was conducted by titration. At pH < 3 the Fe^{3+}-containing supernatant shows no visible color. The spectrum indicates a λ_{max} of ~290 nm. Further titration to more alkalic conditions results in the development of a slightly blue-ish (pH 3.61-5), later purple (pH 6-7) color appears which (based on visual-optic interpretation) reaches its maximum intensity at pH 7. At pH 8 the complexes appear to be more pink before the solution eventually turns cloudy at pH 8.47 (Figure 5.21A). Spectrophotometric analysis indicates that the two peaks at 290 and 330 nm are likely less specific while the bump at ~550 nm appears to shift more significantly with the pH (correlating with the color of the solution). At pH ~3 the maximum peak at 290 nm is visible. Both other peaks are missing at such low pH. This peak therefore might represent the maximum absorption for the free amonabactins. At pH 4 and higher a maximum absorption at ~330 nm can be detected. Shifting to more alkalic conditions this peak continuously increases until it starts to level-out at pH 8.46 where the appearance of the solution changes from clear to cloudy. The apparently more significant bump at ~550 nm is shown to shift from ~560- 565 nm (at pH 4-5) to ~540 nm (at pH 6-7) and ~ 525-530 nm at pH 8. After that (pH>8) it disappears and appears to shift into a slight shoulder at ~ 495 nm (Figure 5.21B).

3. Aerobic complexes with Fe and Mn at pH 7

Based on the color intensity of the Fe-siderophore complexes and the pH stability curves further characterization including the complexation of both Fe(II and III) and Mn(II and IV) were conducted at pH 7. Formation of the distinct purple Fe-siderophore

complexes under aerobic conditions appears to be independent from the oxidation state of the metal. Addition of Fe(II) and Fe(III) (to a final conc. of 140 μM) under aerobic conditions both result in the formation of the purple complex (Figure 5.22A) with matching UV-Vis spectra (Figure 5.22B). Based on a general preference of siderophores to complex Fe(III) over Fe(II) this indicates that the purple color is likely indicative of Fe(III)-amonabactin complexes. Formation of the color is quick and appears within a few minutes, however peak intensities are shown to increase for 3 days of complex formation (Figure 5.22B).

Addition of Mn(II) (final conc. 140 μM) results in the formation of yellow complexes. Based on the appearance of color its formation is slower. It takes ~ 24 hrs for the first color changes to become apparent. The UV-Vis spectrum of the Mn-siderophore complexes shows two main peaks, one at 290 nm and one at 330 nm and a shoulder at 410 nm. Compared to the Fe-siderophore spectrum the peak at 290 nm appears to be more prominent for the Mn complexes. However, since it is always problematic to work at wavelengths in the higher 200s the shoulder at 410 nm (Figure 5.22B) appears to represent a more reliable feature for the Mn-siderophore complex as shown previously for Pyoverdin (PVD) where the maximum absorption at 410 nm represents the presence of a Mn(III)-PVD complex (Parker et al. 2004). Immediately after addition of Mn(II) to the siderophore solution this shoulder is present but it becomes more pronounced after complete formation of the Mn-ligand complex (Figure 5.22B).

4. Ligand-promoted oxidation of Fe(II) and Mn(II)

The potential for amonabactin-promoted oxidation of Fe(II) was tested under anaerobic conditions. Results show the formation of matching purple complexes under these conditions. While color development takes place rapidly under aerobic conditions it appears much slower under anaerobic conditions also apparent in the peak development of the spectra (Figure 5.23). After a day of incubation however colors (Figure 5.24A) and spectra (Figure 5.23) of the anaerobic Fe(II)-complex and the aerobic Fe(II) and Fe(III) complexes appear to match.

While addition of Mn(II) (final conc. 140 μM) to the siderophore-containing supernatant resulted in a yellow colored solution (Figure 5.22A and Figure 5.24C) indicating the formation of Mn-amonabactin complexes no such reaction took place under anaerobic conditions (Figure 5.24D). Removal of the solution from the anaerobic chamber and exposure to atmospheric oxygen resulted in the expected color change from clear to yellow within 24 hrs (data not shown).

Discussion and Conclusion

Prior to the structural analysis of the siderophores produced by *P. stutzeri* VS-10 the distinct purple color of the solution after Fe^{3+} addition was already indicative of amonabactin-like siderophores. Formation of such color in supernatants of *Aeromonas hydrophila*, another amonabactin-producing organism had been described before and was

related to the presence of a Fe^{3+}-amonabactin P693 complex (Bargouthi et al. 1989; Telford and Raymond 1998).

UV-Vis data acquired in our study also generally match with results on the coordination chemistry of the Fe^{3+} -amonabactin P693 complex at different pH (Telford and Raymond 1998). There it has been shown that the complex exhibits a red color at high pH (9-10) indicative of the $[Fe\ (Amo)_3]^{4-}$ complex. The UV-Vis spec shows the maximum absorption for this complex at ~ 492 nm. Lowering the pH then results in a protonation of the catecholate group(s) of the amonabactin resulting in the loss of one ligand which is replaced by H_2O (Telford and Raymond 1998). At pH between 6 and 9 the Fe^{3+} -amonabactin P693 was shown to exhibit a purple color with a maximum absorption at ~525 nm. This is thought to represent a $[H_2Fe_2\ (Amo)_3]^{4-}$ complex. At a pH below 6 the color of the complex turns to blue with a max. absorption at ~540 nm assigned as the 1:1 $[Fe\ (Amo)]^-$ complex (Telford and Raymond 1998). These color and UV-Vis spectra generally resemble the ones acquired here for the *P. stutzeri* VS-10 supernatant. Slight variations (~ nm in wavelength) are likely due to the presence of two amonabactins, P750 and P693. In addition to a color change from purple to red at pH >9 (in our case 8.46) the solution turns cloudy at high pH. This phenomenon not previously described by Telford and Raymond (1998) and could have something to do with the presence of two amonabactins or the degradation of certain complexes.

While the ferric-amonabactin complexes have extensively been studied for amonabactin P693 produced by *Aeromonas hydrophila* this is the first report showing the

existence of Mn-amonabactin complexes. Our results indicate that the supernatant containing amonabactin P750 and P693 are capable of forming different complexes with both transition metals.

1. Fe vs Mn complexes

Recent work has shown that microbial siderophores have an affinity for Mn(III) that is near (Duckworth and Sposito 2005), or can even exceed (Parker et al. 2004) that for Fe(III). This suggests that competition and/or exchange reaction between both metals and siderophores in the natural environment are likely to take place. Currently, Mn(III)-siderophore complexes are only known for the trihydroxamates, desferrioxamine B (DFOB; Duckworth and Sposito 2005; Faulkner et al. 1994) and desferrioxamine E (Faulkner et al. 1994), and for a mixed-moiety pyoverdin (PVD) siderophore (Parker et al. 2004). It is not known if catecholate siderophores stabilize $Mn(III)_{aq}$ although the PVD siderophore isolated by Parker et al. 2004 contains a catecholate moiety (Duckworth et al. 2009). In addition, data obtained through Extended X-ray absorption fine structure (EXAFS) analysis and X-ray absorption near edge structure (XANES) spectroscopy recently indicated that Enterobactin (a trixcatecholate) is unstable with Mn(III) (pers. comm.. O. Duckworth). On the other hand Protochelin represents the first triscatecholate siderophore that appears to form a Mn(III)-complex based on its UV spectrum (unpublished, pers. comm. O. Duckworth). The ability to form Mn(III) complexes therefore may depend on the structure of the catecholate siderophore. The complexation of Mn(II) by amonabactins represents the first data indicating the formation of Mn(III) complexes with a bis-catecholate siderophore. It therefore enhances our

knowledge on the variety of siderophores likely to participate in the sequestration of Fe and Mn in the marine environment.

2. Anaerobic ligand-promoted oxidation of Fe(II) and Mn(II)

The anaerobic oxidation of Fe(II) by the tris-hydroxamate siderophore desferrioxamine B (DFB) coupled to the reduction of a hydroxamate to an amide has been shown previously (Farkas et al. 2001; Kim et al. 2009; Kim et al. 2010). The ligand-promoted oxidation of Fe(II) under anaerobic conditions by a solution containing bis-catecholate siderophores has to our knowledge not been reported before. The amonabactins are hexaprotic acids with four catecholamide protons, one amine proton, and one carboxylic acid proton (Telford and Raymond 1998). The exact mechanisms of anaerobic amonabactin-promoted oxidation of Fe(II) by *P. stutzeri* VS-10 remain unknown. Based on our system it is most likely that Fe(II) was either oxidized by an unknown component in the medium and was coupled to e.g. the reduction of the siderophore or organic residue produced by the strain or that a pH-dependent oxidation took place. Another possibility is that the oxidation of Fe(II) was pH dependent. After the addition of the acidic Fe(II) solution to the anaerobic medium the pH of the solution was neutralized potentially triggering the oxidation process and subsequent formation of the purple Fe(III)-siderophore complex.

The complexation of Mn(II) previously converted to Mn(III) by air-oxidation has been reported before (Duckworth and Sposito 2005; Faulkner et al. 1994; Parker et al. 2007). Anaerobic auto-oxidation of Mn(II) in the presence of ligands is unknown.

Overall our results advance our knowledge on the role of bis-catecholate siderophores in the biogeochemical cycling and uptake of Fe and Mn in different oxidation states. While some of our data such as the anaerobic oxidation of Fe(II) by bis-catecholate siderophores may represent novel findings it has to be considered that contamination of anaerobic solutions with traces of atmospheric oxygen or pH-dependent oxidation could have interfered with the reaction. The fact that the complexation did not take place in the anaerobic solution containing Mn(II) may suggest however that oxygen concentration was low. Future experiments however should include the presence of a reducing agent such as Pyrogallol (benzene-1,2,3-triol) or Resazurin (7-Hydroxy-3*H*-phenoxazin-3-one 10-oxide) to visually check for the oxidative/reducing conditions within the system.

P. stutzeri VS-10's ability to perform variable physiological processes (heterotrophic Fe(II)oxidation, transfer of electrons to anode surface) and synthesize a high number of structurally diverse amonabactins (Thanyakoop 2009) all represent possible adaptation mechanisms for life in various environmental niches (Chapter IV). The ligand-promoted uptake of both Fe and Mn using the same siderophore may represent another benefit that assures the availability of both bio-essential nutrients in particular in hydrothermally-influenced deep-sea habitats where the concentration of both metal-oxides is high.

3. The potential role of organic acids produced by *P. stutzeri* VS-10 in basalt dissolution

Introduction

Bacterial energy metabolism is often based on fermentation and leads to the production of small organic acids like lactic, acetic, formic, citric, oxalic and uric acid. Due to reduced diffusion rates the accumulation of acids in biofilm environments is likely. The presence of such acids has been shown to increase dissolution rates of minerals, rocks and volcanic glasses (Chen and Brantley 1997; Eick et al. 1996; Neaman et al. 2005; Oelkers and Gislason 2001; Stillings et al. 1997; Welch and Ullman 1996) and play a fundamental role in the bioavailability of chemical elements that can be either beneficial or toxic to living organisms (Uroz et al. 2009). The identification of bacterial acids represents a powerful tool to study the ecology of certain microbe/substratum interactions.

Here we attempt the identification of low-molecular weight organic compounds produced by *P. stutzeri* VS-10 when grown nutrient-limited on glycerol to elucidate the potential role of such acids in basaltic glass dissolution.

Materials and Methods

1. Growth medium and conditions

P. stutzeri VS-10 was grown on minimal medium with and without the presence of basalt grains in the culture. ~ 5g of the basalt described in Chapter IV was used in each experiment. Cultures were set-up in sterile (acid washed and autoclaved at 121 °C, 30') 250 ml flat-bottom Erlenmeyer flasks at 21-25 °C and ~ 200 rpm. Two sets of the following experiments were set-up and run for 10 days:

A) Minimal medium with basalt
B) Minimal medium no basalt
C) *P. stutzeri* VS-10, minimal medium with basalt
D) *P. stutzeri* VS-10, minimal medium no basalt

One experimental set-up was used to determine growth of the strain and pH conditions of the growth supernatant during the course of the experiment, the other one to draw samples for reversed-phase HPLC analysis of organic acids present in the supernatant.

Prior to inoculation strain VS-10 was grown on LB medium and washed in minimal medium as described previously (Chapter IV). Aliquots of the homogenized cell suspension were taken daily to monitor growth of the strain at OD_{600} and determine the pH of the solution. Samples for the detection and characterization of potential organic

acids produced by the strain were taken on day 3 of the experiment. 2 ml samples were drawn, filter-sterilized (0.22 μm) and frozen at -20 °C. After 10 days solutions were analyzed by reversed phase HPLC. They were run against two standards containing a range of organic acids commonly produced by bacteria.

2. HPLC column and operating conditions

Instrument time and technical expertise was available at the UCSD mass spec facility (Department of Chemistry and Biochemistry). A silica-based Acclaim® Organic Acid column (4.0 x 150 mm format, particle size 5 μm, pore size 120 Å, surface area 300 m^2/g, Dionex cat. # 062903) was used for reversed phase HPLC analysis of organic acids produced by *P. stutzeri* VS-10. The column allows the separations of hydrophilic, aliphatic and aromatic organic acids at pH between 2 and 8, using UV detection. It can retain and separate C1 to C7 volatile aliphatic and aromatic acids using an aqueous low-pH mobile phase coupled with an acetonitrile gradient to elute the higher-molecular-weight organic acids. Acetonitrile (A) and 2.5 mM methanesulfonic acid (B) were used as the two solvents. The column was installed and flushed with acetonitrile and equilibrated based on the manufacturer's recommendations (http://www.dionex.com/en-us/webdocs/41786-Man-031996-031996-02-Acclaim-OA-Jul09.pdf). During the run the temperature averaged 30 °C. Flow rate was maintained at 1 ml/min., injection volume was 30 μl and absorbance was measured at 250 nm. The following protocol was used: hold B for 1 min., B to A/B (45/55) in 11 min., hold A/B (45/55) for 4 min.. Trifluoroacetic acid (TFA) was used as an ion-pairing agent.

3.HPLC acid standards

Two HPLC acid standards were prepared to attempt the identification of acids produced by strain VS-10. Based on the solvent used during HPLC analysis the following 10 mM standards were prepared in 2.5 mM methanesulfonic acid.

Standard I:

1. Formic acid
3. Propionic acid
4. N-Butyric acid
5. Isobutyric acid
6. Isovaleric acid
7. N-Valeric acid
8. N-Caproic acid

Standard II:

9. Benzoic acid
10. D-Gluconic acid
11. Citric acid
12. Glycolic acid
13. Pyruvic acid
14. Lactic acid

Standard I matched the one suggested in the HPLC column manual. Standard II contained acids that were picked based on their commercial availability and metabolic relevance.

Results

1. Growth curves and pH curves

P. stutzeri VS-10 was grown on minimal medium with and without basalt in the culture. Growth curves resemble the ones previously described (Chapter IV). As discussed in detail in Chapter IV, the strain exhibits elevated growth in the presence of basalt (Figure 5.25A). While pH values in both abiotic experiments stayed constant over the 14 days of the experiments, the pH dropped in both biotic set-ups. With basalt pH values drop slightly from pH ~7 to ~6.8 in two days. Without basalt a more significant decrease towards acidic conditions is observed after 3 days stabilizing at pH ~6.3 (Figure 5.25B). While the pH decrease of the solution is lower under no basalt conditions, cell densities negatively correlate with the pH measurements showing the overall highest growth yield in the biotic experimental set-up containing basalt (Figure 5.25A).

To identify the role of basalt in the elevated pH conditions at day 10 of the experiment sterile basalt grains were added to the biotic no basalt set-up. This addition resulted in a pH increase back to more alkaline conditions (pH ~6.9, Figure 5.25B).

2. HPLC analysis of organic acids

The presence of organic acids in the culture supernatant was analyzed by reversed-phase HPLC. Results from the run of both, biotic and abiotic set-ups indicate the presence of various peaks in both biotic cultures (Figure 5.26) but not in the abiotic supernatants. Peak heights and elution times differ between the two biotic samples indicating the presence of different components.

The first run was performed according to the conditions suggested in the HPLC column manual. The use of gradients acetonitrile and methanesulfonic acid as the two solvents results in clean peaks but prevented the identification of individual masses (Figure 5.26A).

A second run was conducted using gradients of acetonitrile and H_2O, resulting in an overall broadening of the standard peaks while sample peaks stay clean (Figure 5.26B). This run gives the mass charges for most peaks in either positive or negative ion mode.

None of the standard acids were identified. Masses were compared to the literature values of the most common carboxylic, dicarboxylic, tricarboxylic, sulfonic and mineral acids. The masses of some peaks found to be similar to known components (Table 5.2).

Discussion and Conclusion

The detection of organic acids in the growth supernatant of *P. stutzeri* VS-10 using reversed phase HPLC analysis resulted in inconclusive results. While the observed pH decrease indicates the production of acids none could be identified by HPLC. Due to the lack of identification of peaks it also remains purely hypothetical if they represent organic acids produced by strain VS-10. The lack of peak broadening during the acetonitrile/ H_2O run raises the concern that they indicate other low-molecular weight molecules which may or may not be responsible for the pH changes.

The negative correlation of cell numbers in the experiment containing no basalt, in which the pH drops more significantly (to pH ~6.3), may be due to an intolerance of strain VS-10 to such a low pH. The pH optimum for growth of the strain was not determined. Higher pH values in the biotic set-up containing basalt (pH ~6.8) are most likely due to the weathering of basalt which results in a buffering of the solution. Addition of basalt to the no-basalt set-up resulted in a pH increase supports this assumption. Possible reason behind this phenomenon could be the adsorption of acids to the glass surface as already reported for various clays and minerals (Davis 1982; Kubicki et al. 1997; Lindegren and Persson; Thomas and Kelley 2009; Tipping 1981). Ligand exchange (carboxyl and hydroxyl groups of the acids versus surface hydroxyl groups of the minerals) has been discussed as one possible binding mechanism (Balcke et al. 2002). Adsorption of acids produced by strain VS-10 onto the basaltic glass surface is likely to

simultaneously result in degradation of molecules which may be reflected in a disappearance of peaks and the occurrence of new ones as observed in our samples (Figure 5.26). While acid production in strain VS-10 is unlikely directed towards a specific benefit, the presence of such acids presumably enhances basalt dissolution rates as previously reported (Eick et al. 1996; Oelkers and Gislason 2001) leading to an overall change of local ocean water chemistry.

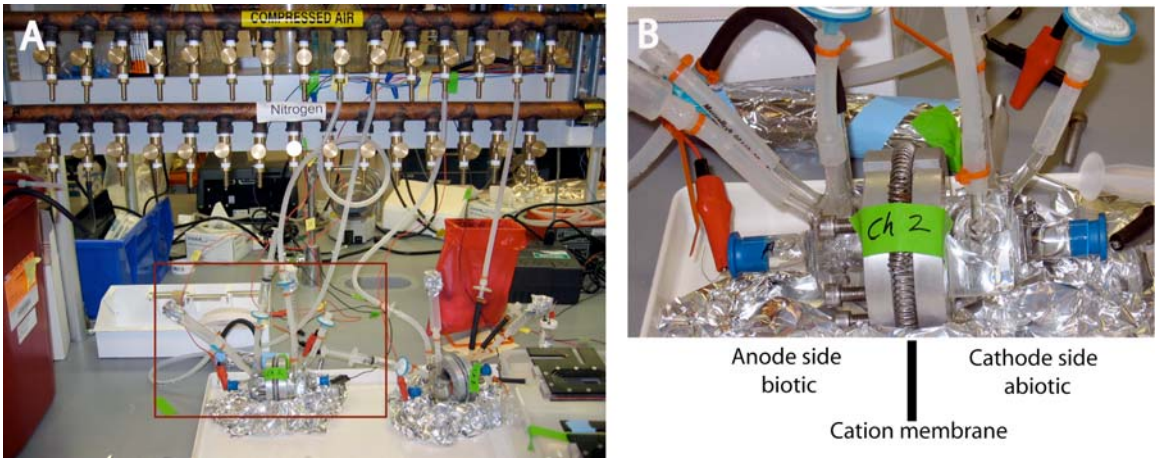

Figure 5.1: Typical set-up for a microbial fuel cell (MFC). Two glass half-cells separated by a cation exchange membrane were used. Total volume of minimal medium in the cell averaged 60 ml. The anode compartment was inoculated with WT or mutants of strain VS-10. B represents a close-up of the red rectangle area in A.

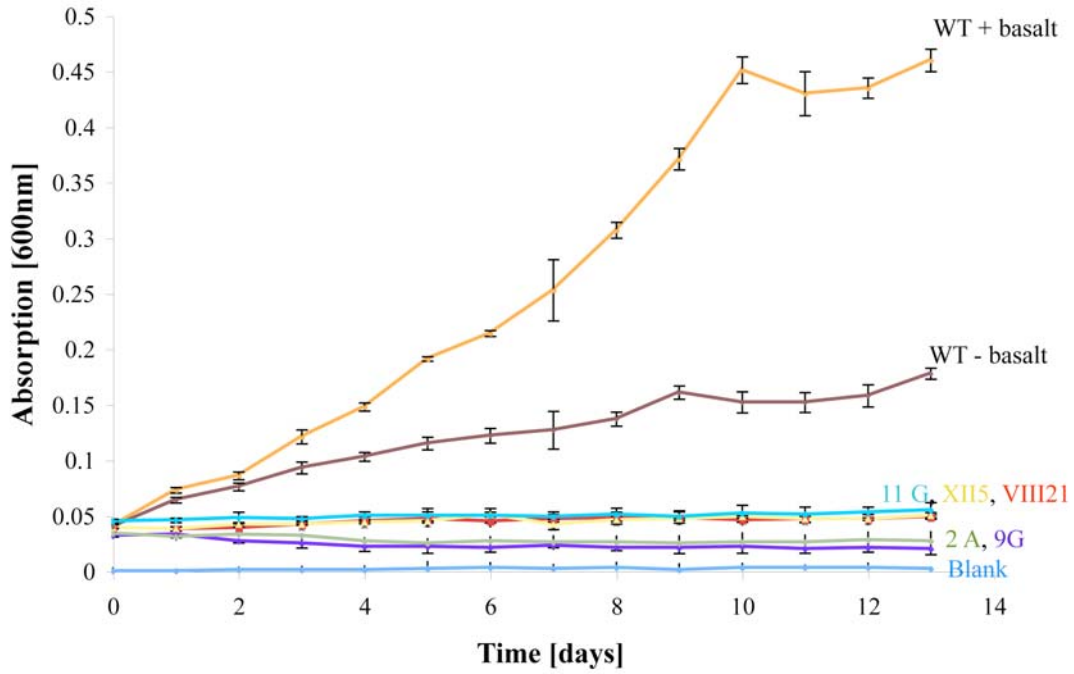

Figure 5.2: Growth curve of WT and mutants of strain VS-10 on minimal medium with (+) and without (-) basalt. All mutant cultures and the blank contained basalt. While growth of the WT is elevated in the presence of basalt mutant growth is not enhanced.

Figure 5.3: Growth of WT and mutants on LB and LB_{Kan} medium after 24 hrs at 37 °C. For technical reasons mutant 6B was excluded from further studies.

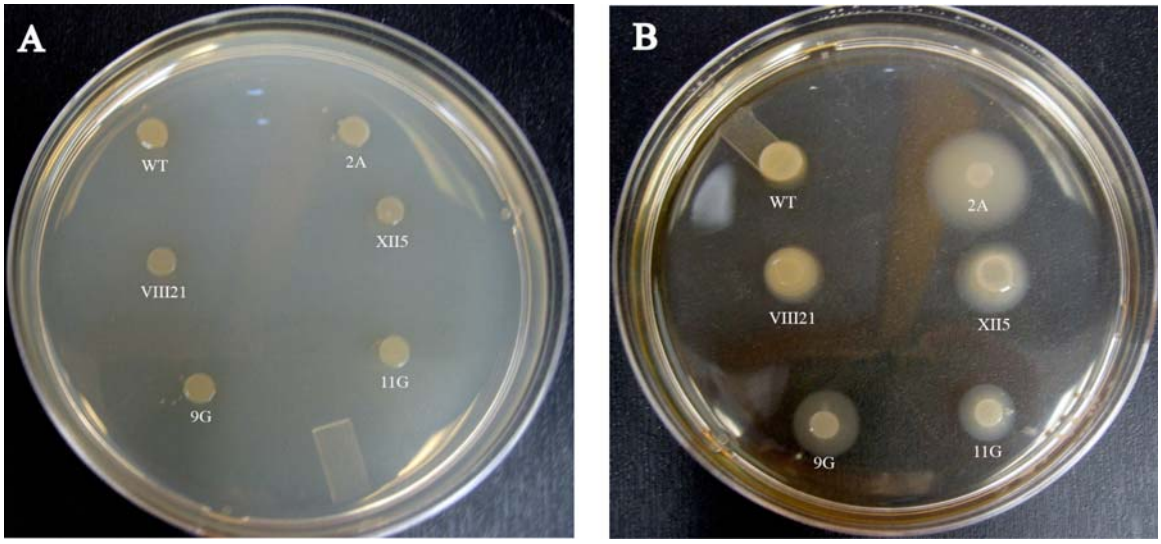

Figure 5.4: Growth of mutants and WT on a regular LB plate (A) and on a motility LB plate (B). Cultures on both plates were inoculated for 16 hrs at 30 °C. The twitch plate was prepared from full-strength LB broth containing 0.25 % agar and was spot inoculated with 1.5 µl of overnight LB cultures. Elevated twitching motility of mutants compared to the WT is visible.

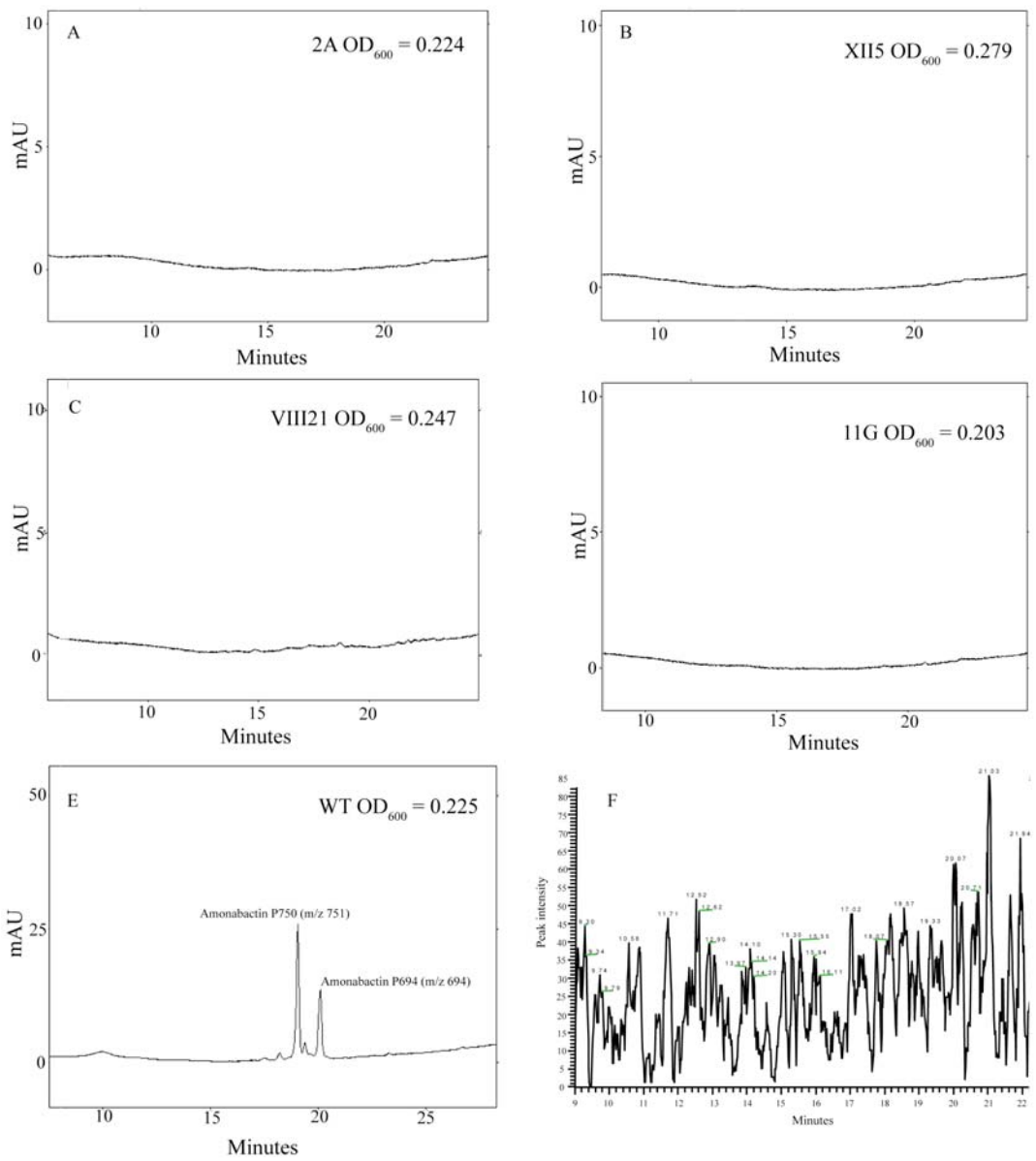

Figure 5.5: LC-ESI-MS results on the detection of siderophores in the supernatant of high cell densities WT and mutant cultures. Two amonabactins (P750: m/z 751 and P693: m/z 694) could be detected in the WT supernatant (E) while no siderophores were detectable in the mutant cultures (A-D). Specific screening in positive ion mode at mass charge (m/z) 751 (indicative for amonabactin P750) in the culture of mutant XII5 shows only background noise. 10 µl of WT and 40 µl of mutant cultures were loaded.

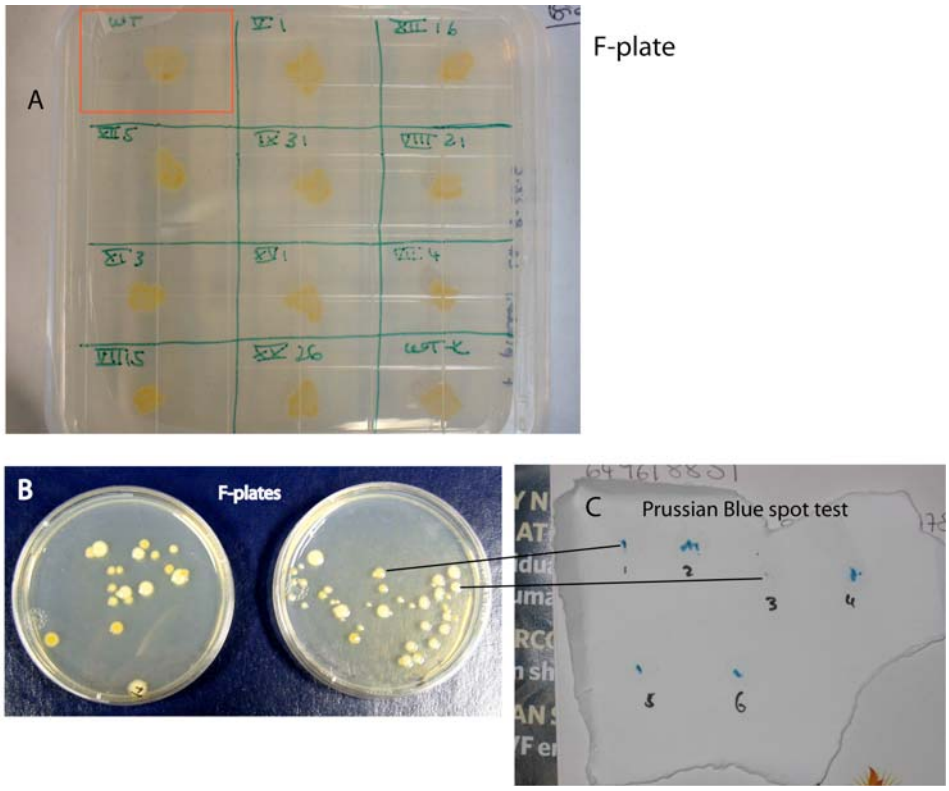

Figure 5.6: Growth of WT (red rectangle in A) and some mutants (including VIII21 and XII5) on organic-rich F-plates (A). Potential to accumulate Fe-oxides is indicated by orange color on the plate. B: F-plates inoculated with water containing microbial consortia from environmental samples at Vailulu'u Seamount. The abundance of both, orange and white colonies can be observed. The Prussian-Blue test (C) conducted on these colonies indicates the abundance of Fe-oxides only in orange colonies.

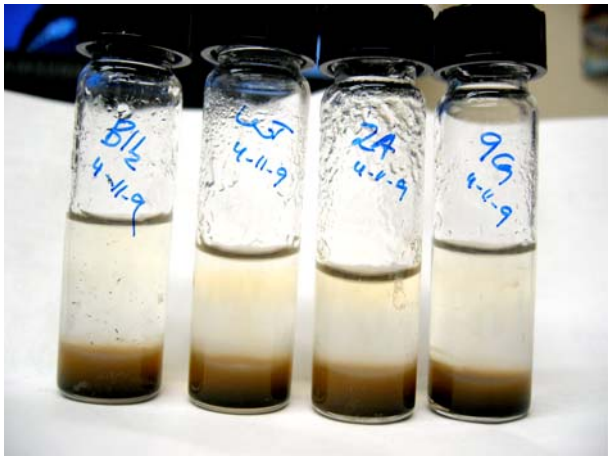

Figure 5.7: Gradient tubes inoculated with either WT or mutant cultures (2A and 9G). The ability to oxidize Fe(II) in both WT and mutants is indicated by a Fe-oxide band close to the agar/headspace interface. The band in the tube containing mutant 9G is very faint. This is likely due to a general growth deficiency of this strain.

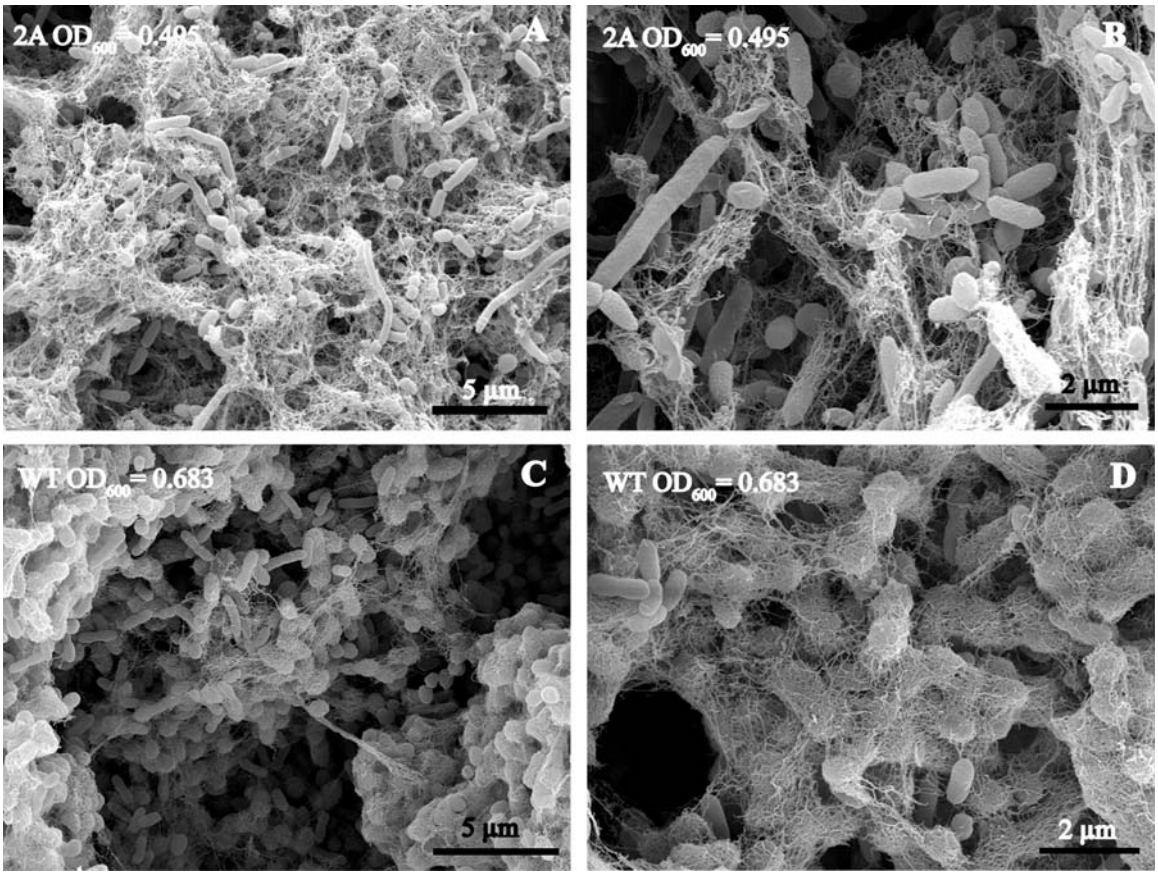

Figure 5.8: Scanning electron micrographs (SEMs) of mutant 2A and WT biofilms grown on LB medium with basalt. Production of extracellular polymeric material (EPM) is visible in both cultures.

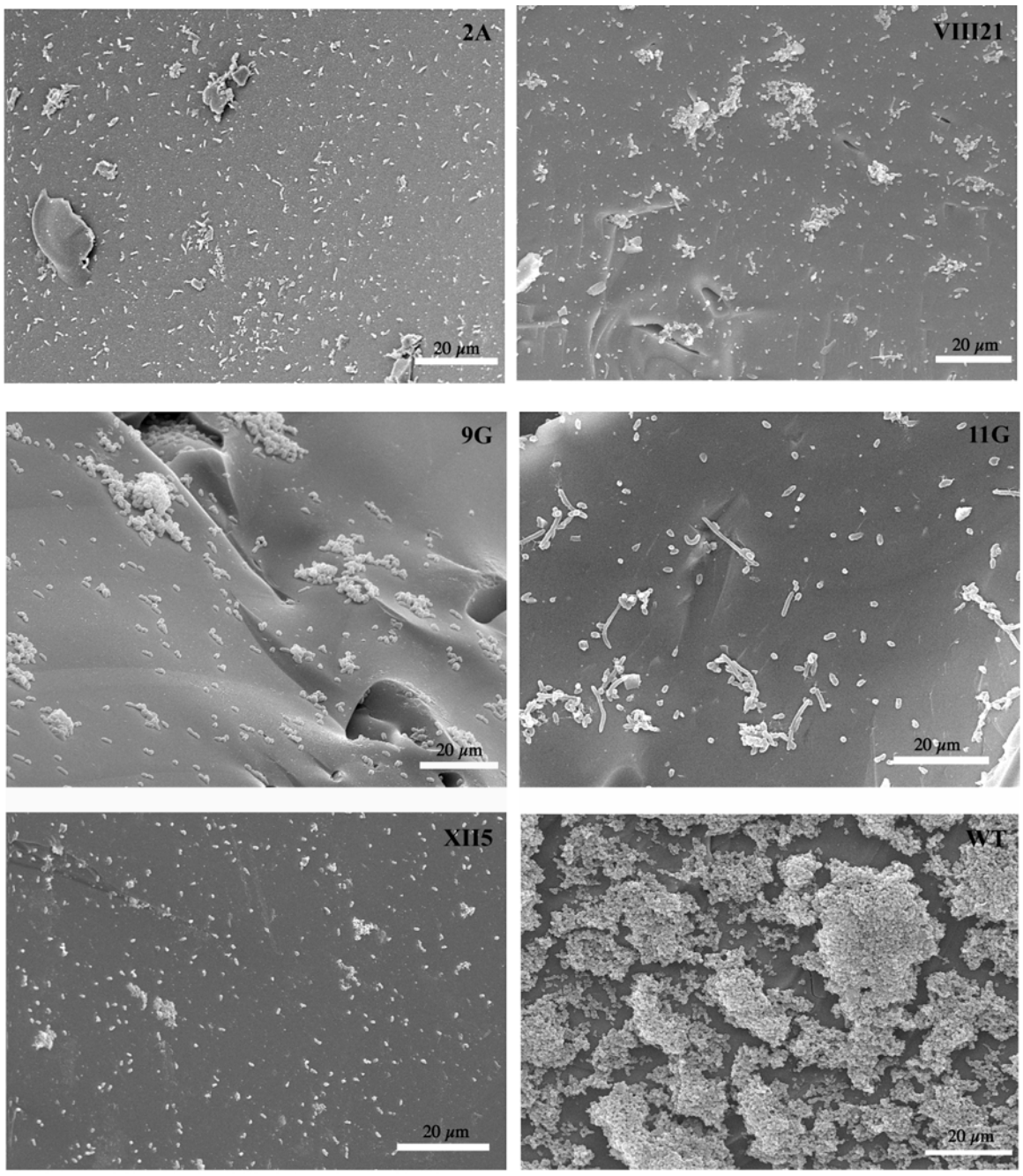

Figure 5.9: SEMs of WT and mutants grown on minimal medium and basalt for 4 days. Disruption of WT-level biofilm formation in all the mutants is visible. The dark background represents the (basaltic) glass surface.

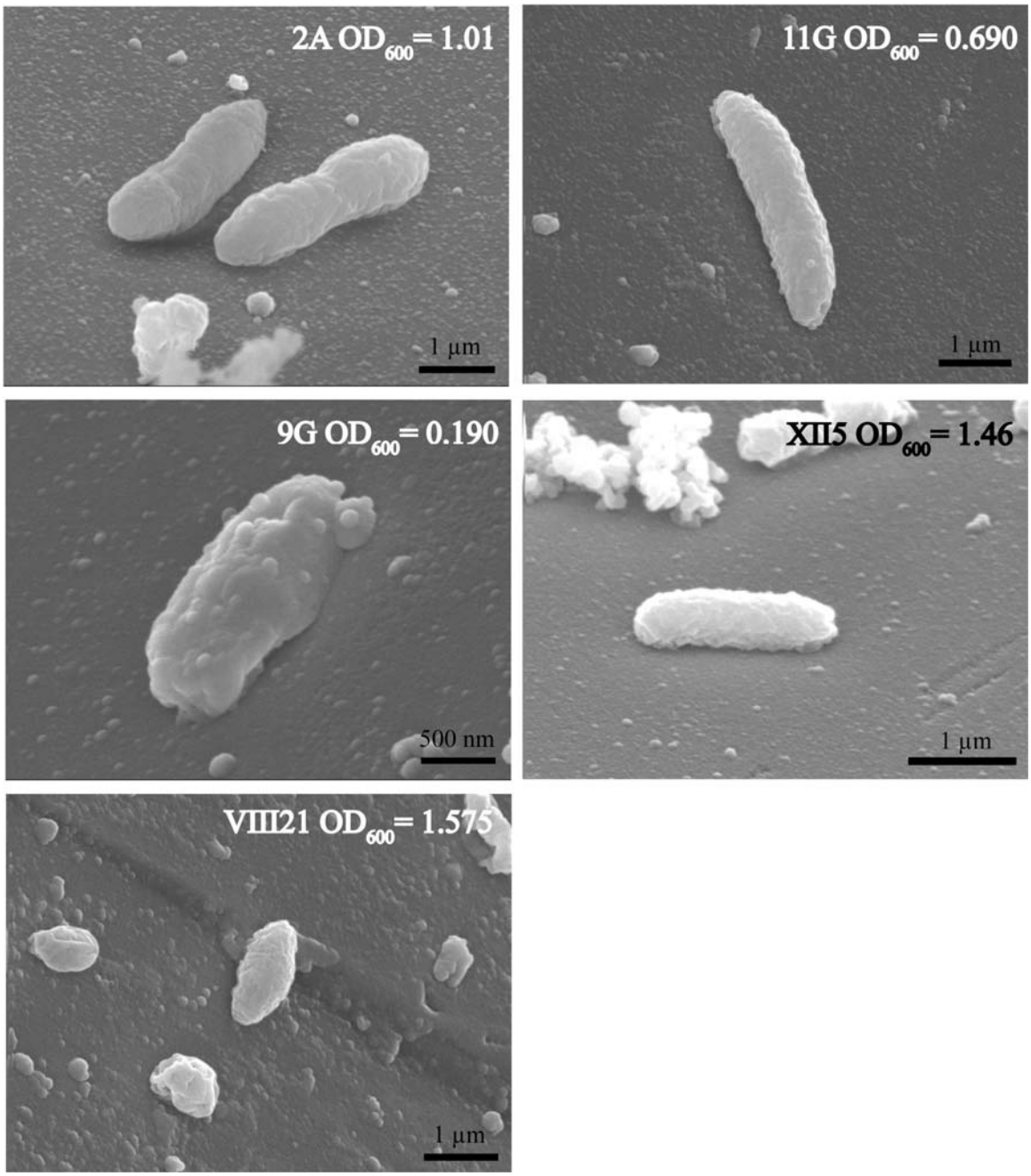

Figure 5.10: SEMs of mutants on basalt at high cell densities on minimal medium (close-ups of Figure 5.9). The lack of EPM production is visible. The dark background represents the (basaltic) glass surface.

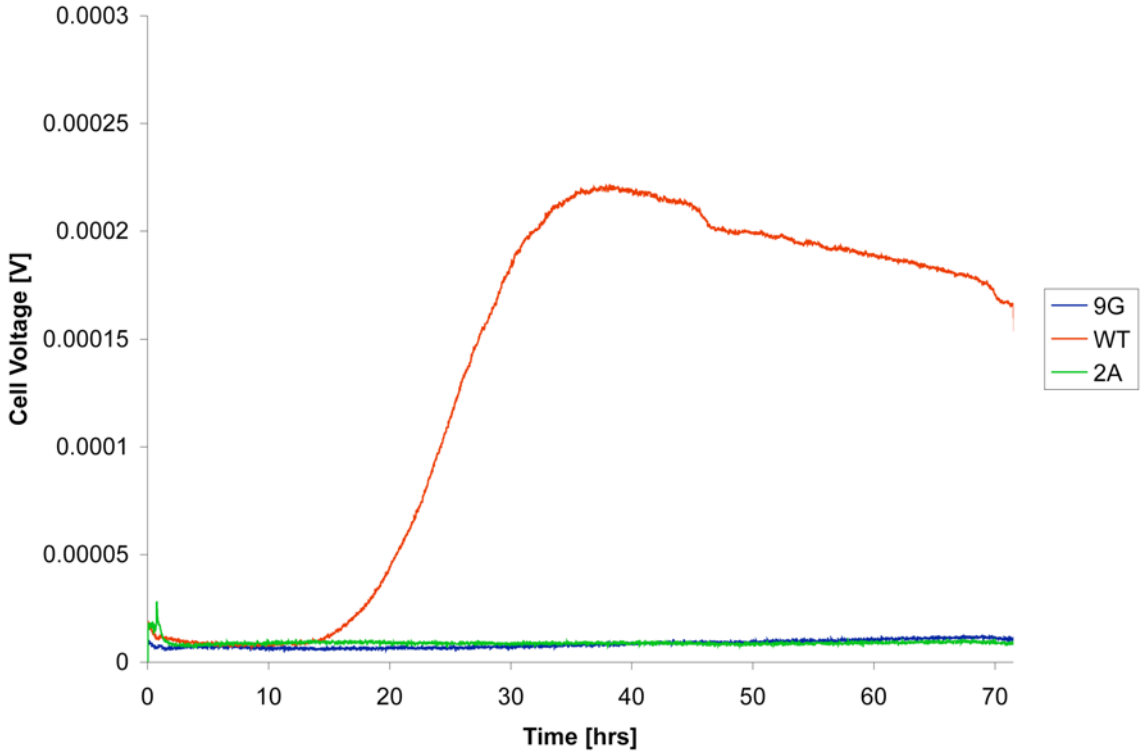

Figure 5.11: Power curves for WT and two mutants (2A and 9G) collected over a time period of ~ 70 hours. While increasing current densities can be observed in the WT fuel cell no power production is evident in the mutant cells.

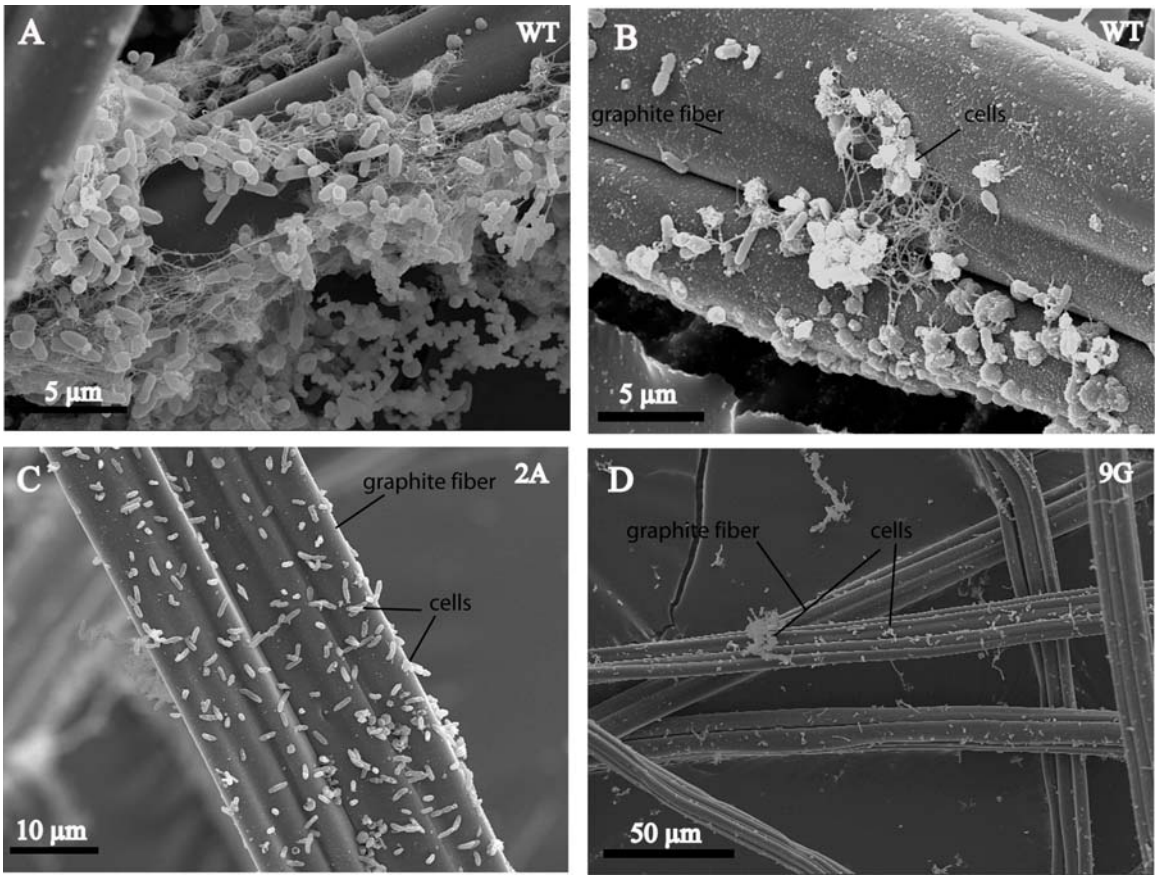

Figure 5.12: SEMs of anode graphite fibers from the fuel cell experiments (shown in Figure 5.8). Cells and graphite fiber have been indicated in the images. Biofilm formation (A) and attachment of cells via EPM (B) is visible on the WT anode. Cells of both mutants (2A and 9G) are present (C and D) albeit in low numbers.

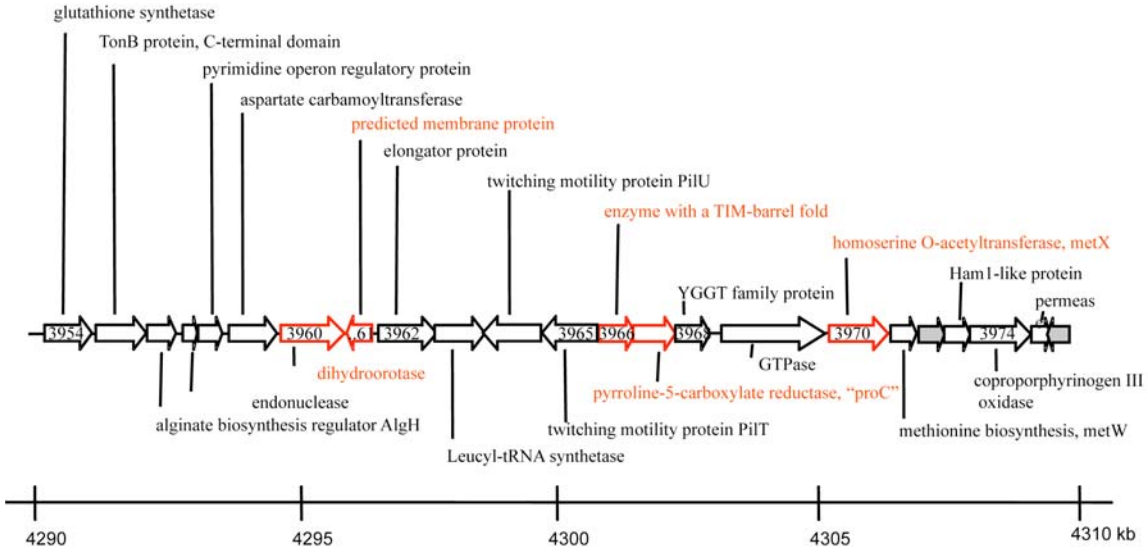

Figure 5.13: Genome region in *P. stutzeri* A1501. Genes hit in the transposon mutagenesis in red, hypotheticals in grey, all other genes in black. Numbers inside the arrows represent locus tags of the genes (PST_3954-3974).

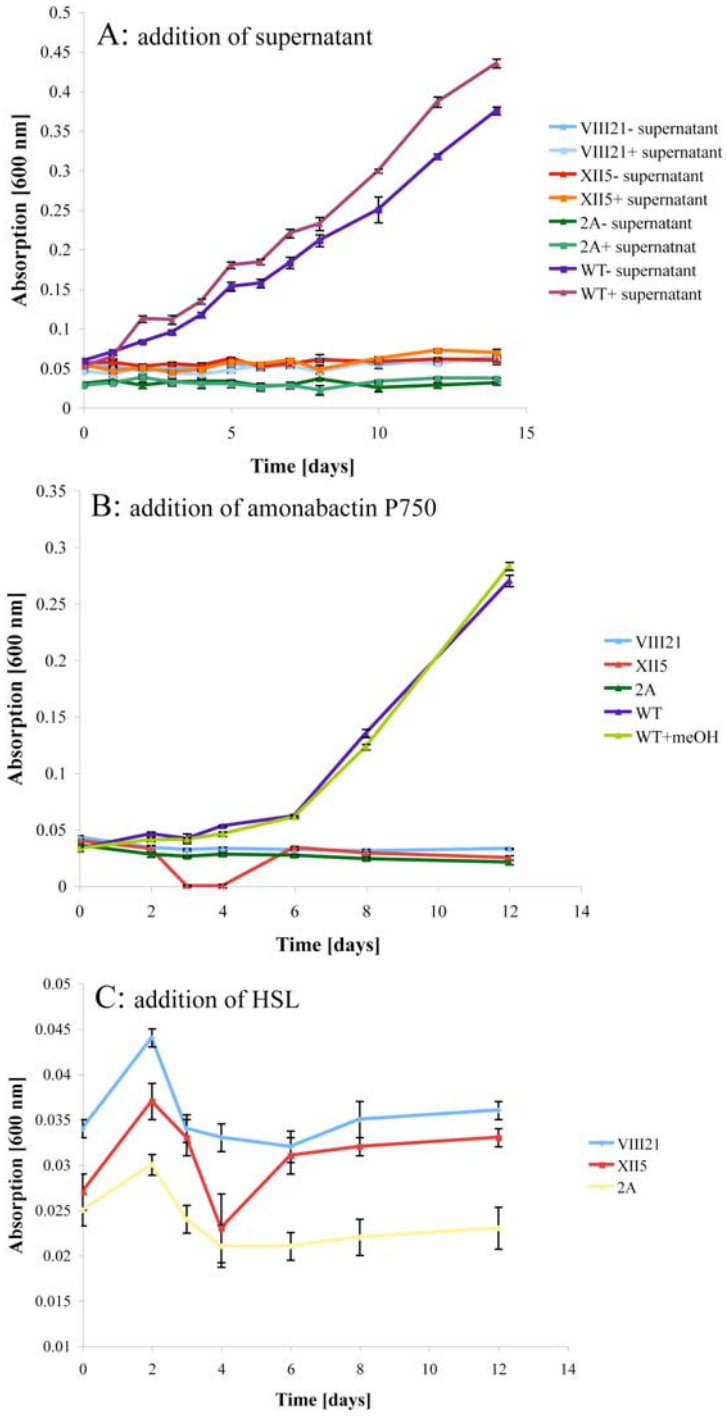

Figure 5.14: Mutant rescue experiments including amendments with exogenous siderophores and homoserine lactones. Additions did not restore growth of the mutants on minimal medium and basalt. A: Addition of min. medium supernatant containing amonabactin P750 and P693. B: Addition of ~ 5.2 µM purified amonabactin P750 (in Methanol= MeOH). "WT+MeOH" represents a culture in which only MeOH was added. It is shown not to effect growth of the strain. C: Addition of 10 µM N-(3-Oxodecanoyl)-L-homoserine lactone (HSL).

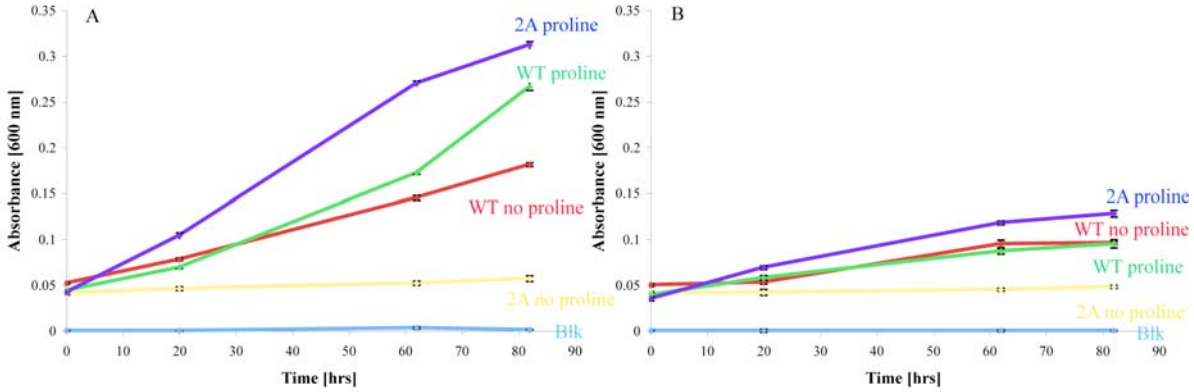

Figure 5.15: Growth curves for WT and mutant 2A on minimal medium with addition of 8.7 mM of L-proline. A) with and B) without basalt present in the culture. Growth of 2A was restored to WT-levels (or higher).

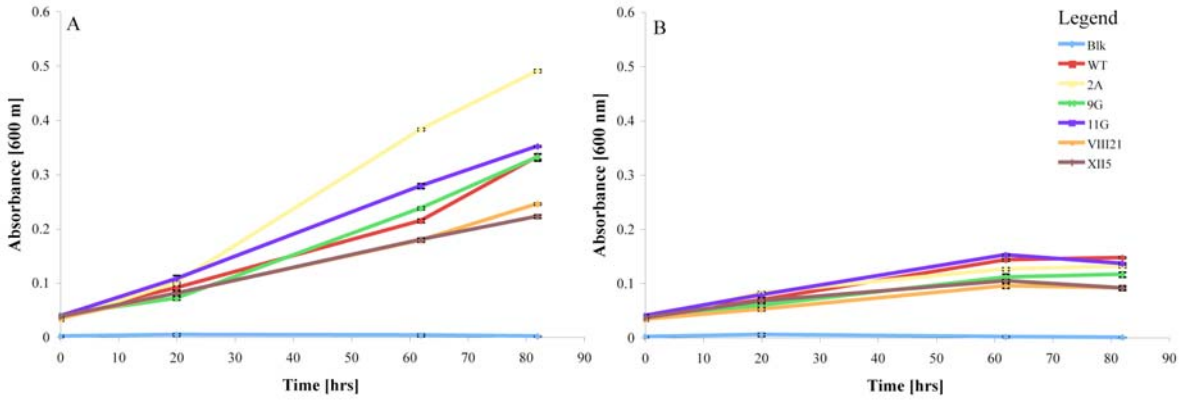

Figure 5.16: Growth curves for WT and mutants on minimal medium after the addition of 0.5 % of Casamino acids (CAA). A: with basalt, B: without basalt present in the culture.

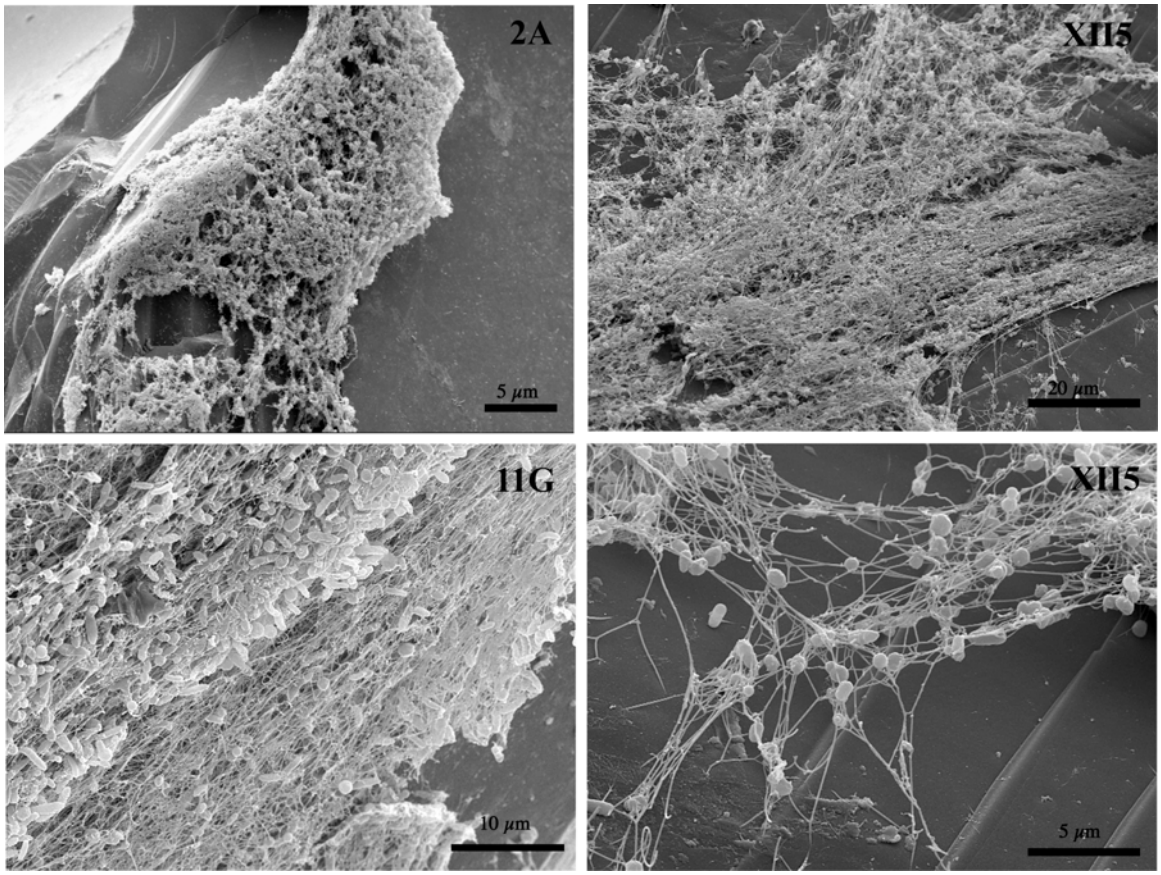

Figure 5.17: Scanning electron micrographs of mutants 2A, XII5 and 11G grown on minimal medium, basalt and 0.5 % of CAA for 3 days. Biofilm and EPM production was restored to WT-levels (for comparison of biofilms to WT see Chapter IV).

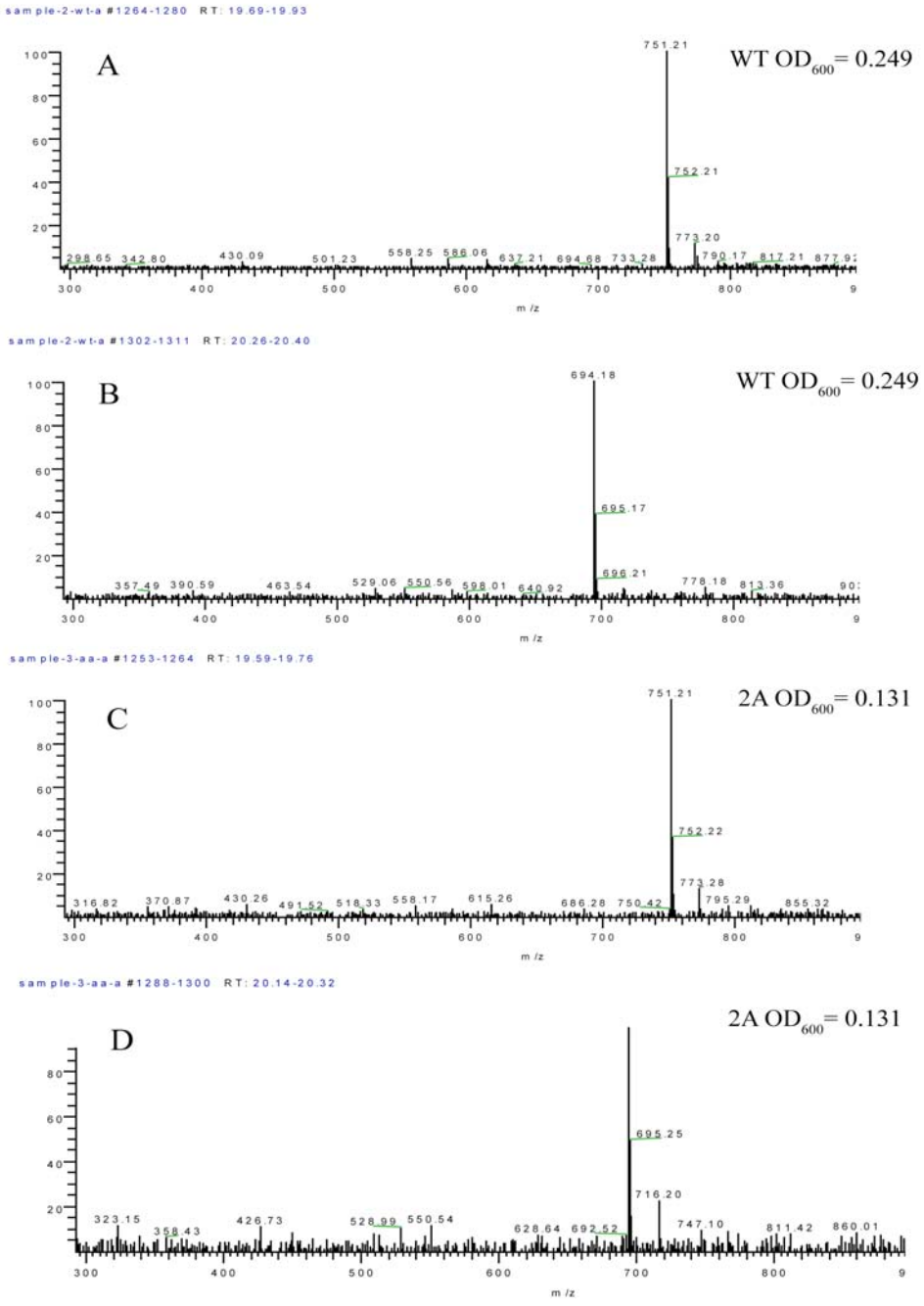

Figure 5.18: Presence of amonabactin P750 (m/z 751; A and C) and P693 (m/z 694; B and D) in the supernatant of WT and mutant 2A grown on minimal medium, rhyolite and 8.7 mM proline. 20 µl of samples were loaded.

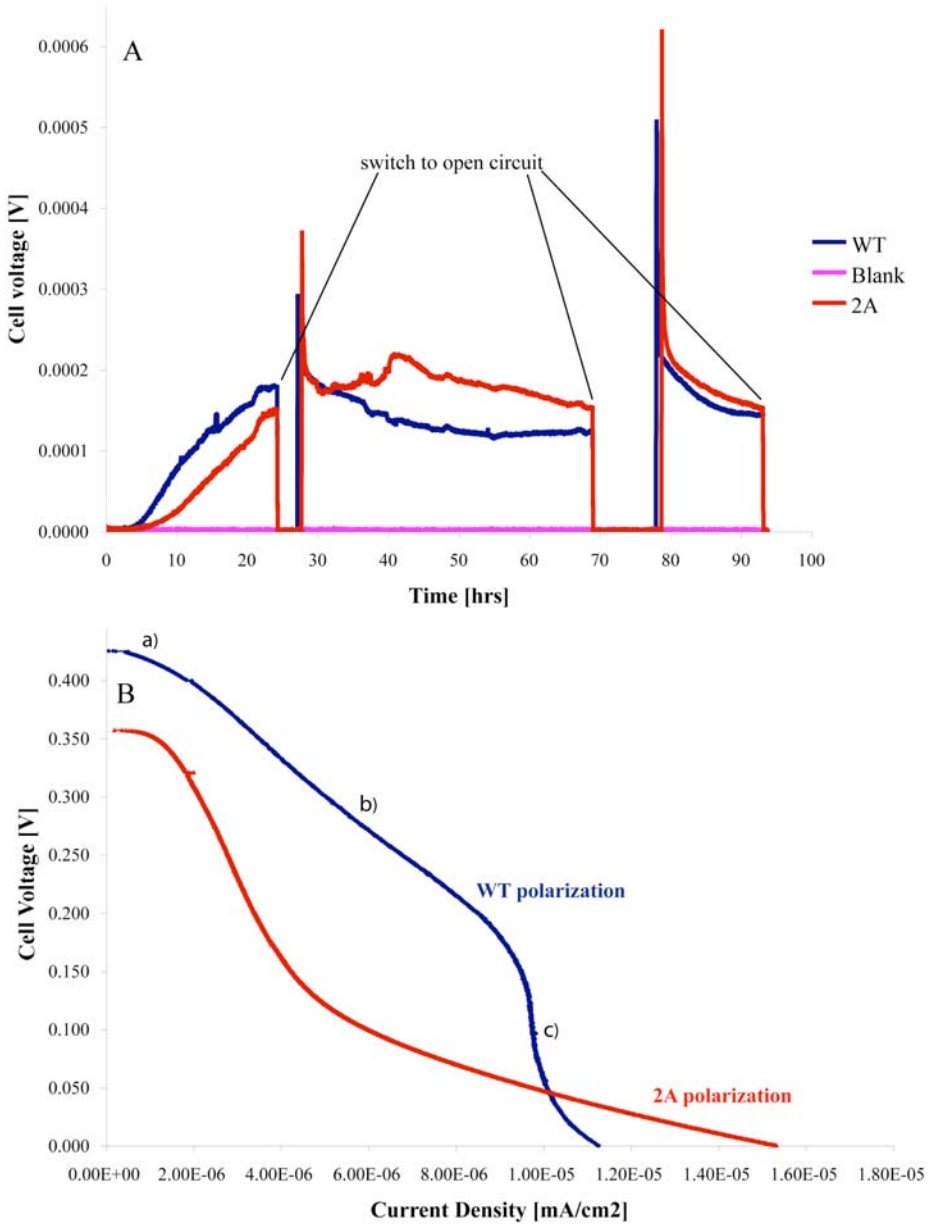

Figure 5.19: Power (A) and polarization (B) curves for WT and mutant 2A in minimal medium fuel cells containing 8.7 mM of L-proline. A: current production within the two fuel cells under standard operating conditions appears to be restored (if not higher) in the cell containing 2A. B) Polarization curves measuring power production in open circuit conditions: Cell terminal voltage is plotted against the current density. The regions of a) activation losses b) ohmic losses and c) mass transfer losses are marked. The open circuit potential in the WT cell is higher (~425 mV) than in the mutant cell (~357 mV) showing that the electrochemical properties in 2A were not fully restored to WT-levels.

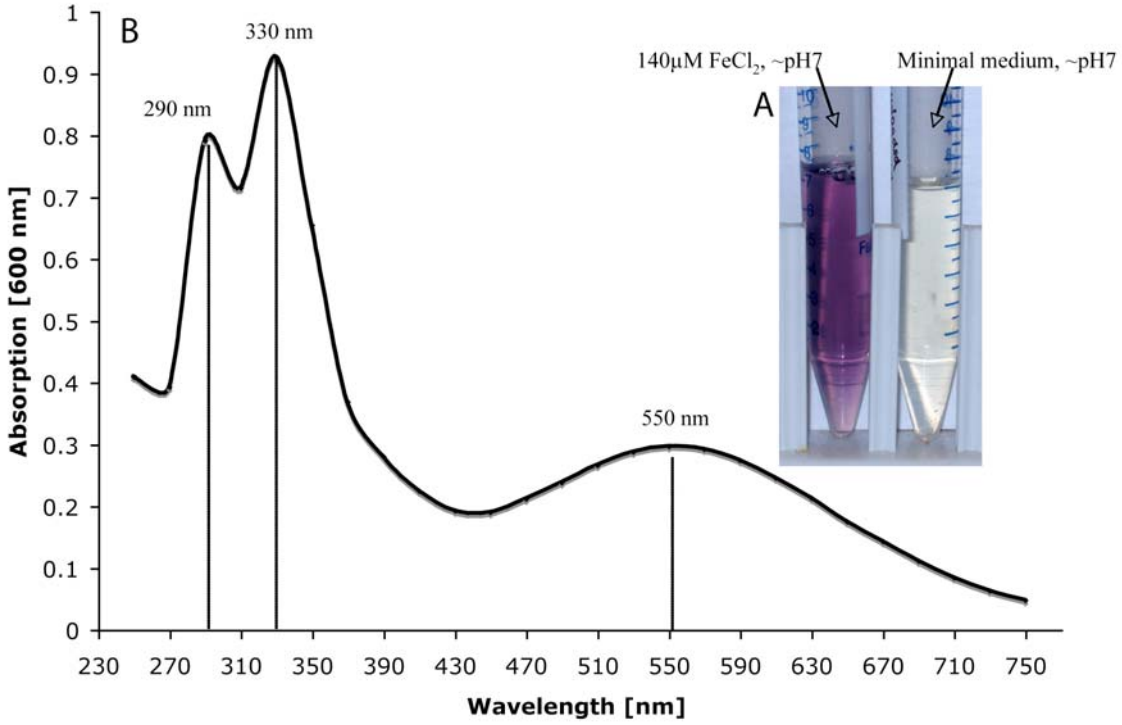

Figure 5.20: Color (A) and UV-visible spectrum (B) of the Fe-siderophore complexes. After filter-sterilization of the supernatant and adjustment to neutral pH (~7) the solution was clear (A: right tube). The addition of $FeCl_2$ to a final concentration of 140 µM changed its color to deep purple (A: left) indicating the formation of one of more Fe-ligand complexes. The spectrum shows three peaks. Two relatively sharp ones at 290 nm and 330 nm and one smaller and more round-shaped "bump" at 550 nm.

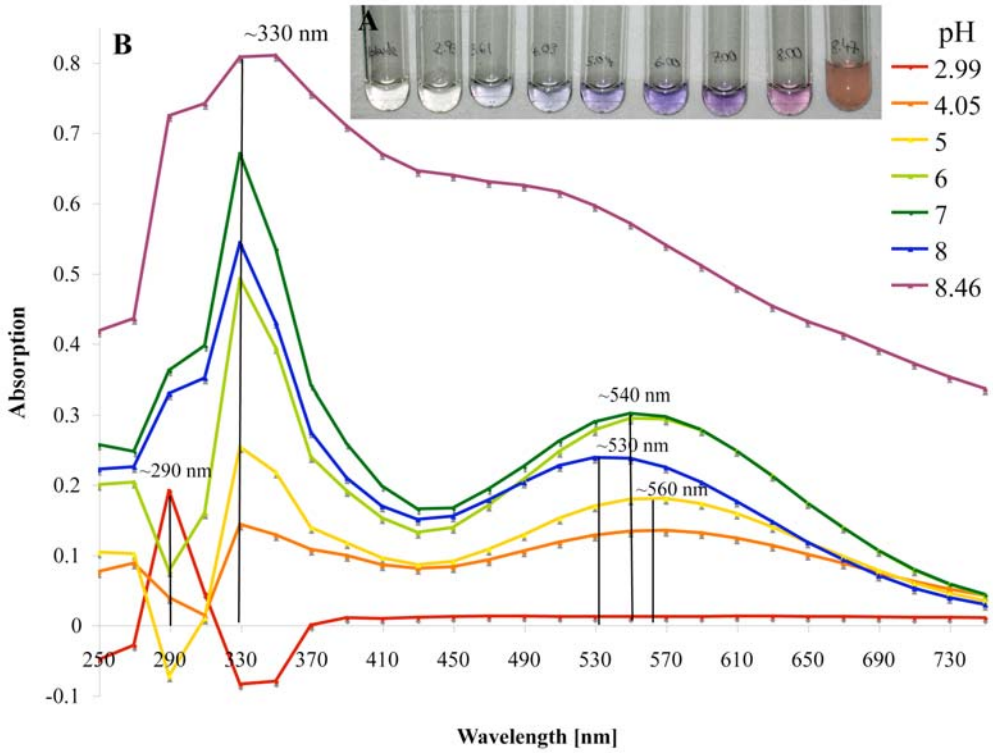

Figure 5.21: pH characteristics of Fe-siderophore complex(es). The supernatant, containing the two phenylalanine-amonabactins P750 and P693 was first adjusted to low pH (~3). $FeCl_2$ was added at this point (final conc. 200 μM) and the formation of Fe-siderophore complexes was allowed to form. A: Showing the color change within the solution between pH ~3 and ~8.5. B: The UV-Visible spectrum was measured against a blank between 250 and 750 nm. A peak shift from 290 nm to 330 and 550 nm with increasing pH is visible. While the intensity of the peak at 330 nm positively correlates with the alkalinity of the solution the bump at 550 nm appears to be more specific at different pH correlating well with the color changes of the solution.

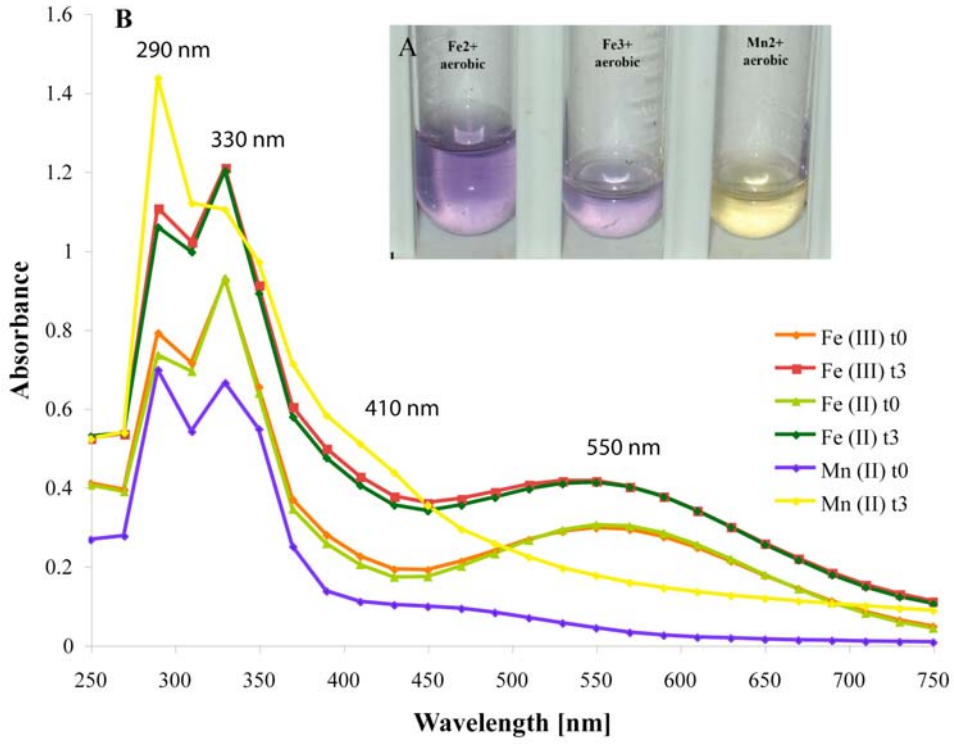

Figure 5.22: Formation of different siderophore complexes with Fe(II + III) and Mn(II). $FeCl_2$, $FeCl_3$ and $MnSO_4$ (final conc. 140 μM) were added to the supernatant of strain VS-10 pre-adjusted to pH 7. UV-Vis spectra were measured 2 hrs after addition and, to allow complete formation of the complexes after 3 days. Both Fe-complexes appear to match. UV-Vis spectra show increased peak sized at 290, 330 and most importantly 550 nm for Fe(II and III) and at 290, 330 and more importantly 410 nm for Mn(II).

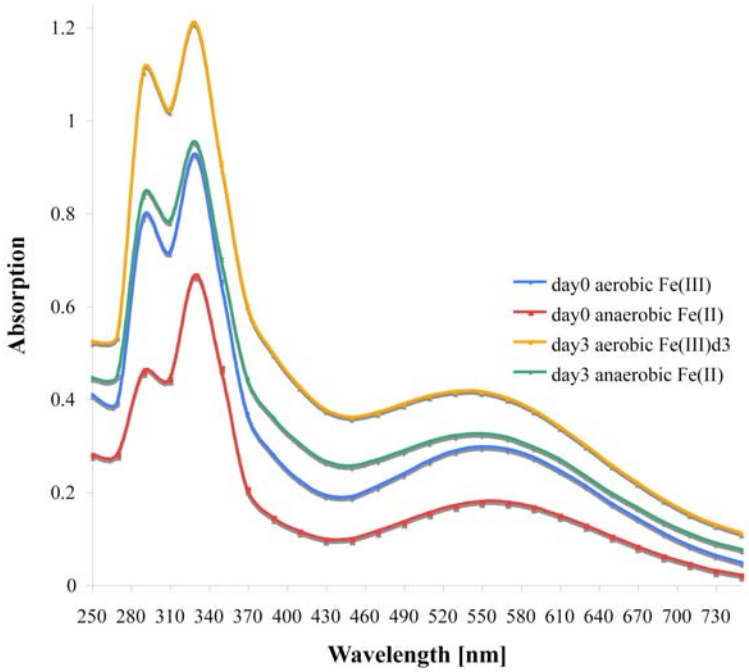

Figure 5.23: UV-Vis spectra of Fe(II) and Fe(III) complexes under aerobic and anaerobic conditions. Complexation indicated by peak development is slower under aerobic conditions.

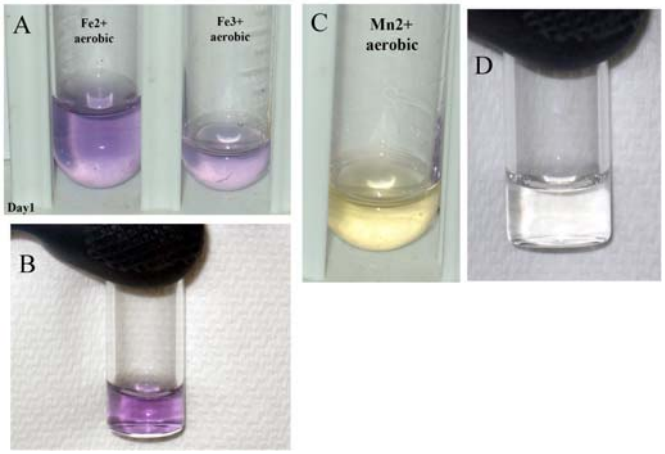

Figure 5.24: Color of the Fe(II) and Fe(III) and Mn(III)-siderophore complexes under aerobic (A: Fe and C: Mn) and anaerobic (B: Fe and D: Mn) conditions. The formation of the purple Fe(III)-siderophore complex does take place under anaerobic conditions indicating a ligand-promoted oxidation of the metal. For Mn, with which complexation is generally slower no such complex formation appears to take place under anaerobic conditions (D).

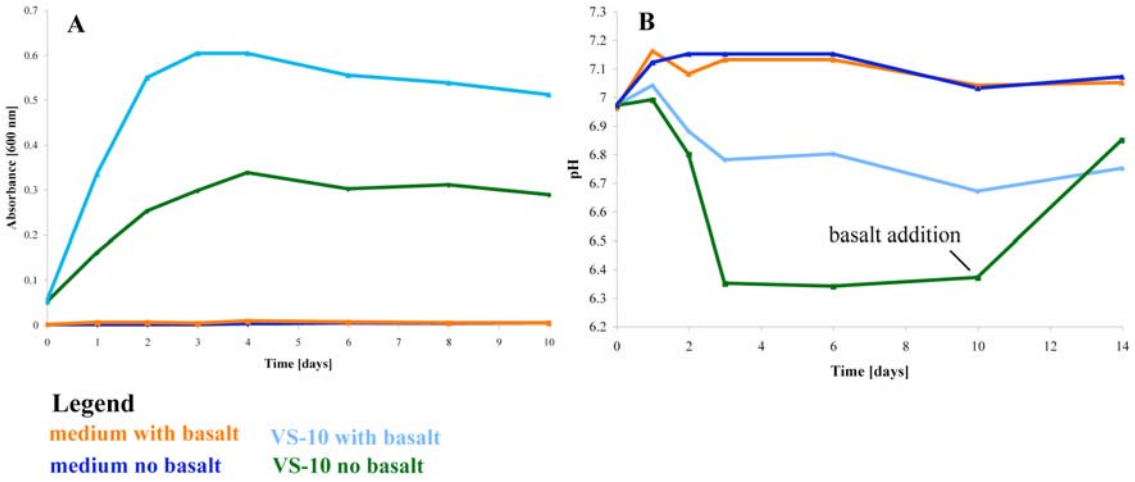

Figure 5.25: Growth curves (A) and pH (B) of *P. stutzeri* VS-10 cultures on minimal medium with and without basalt. The most significant pH decrease is obtained in the biotic experiment without basalt negatively correlating with growth of the strain. Addition of basalt at day 10 resulted in a pH increase (B).

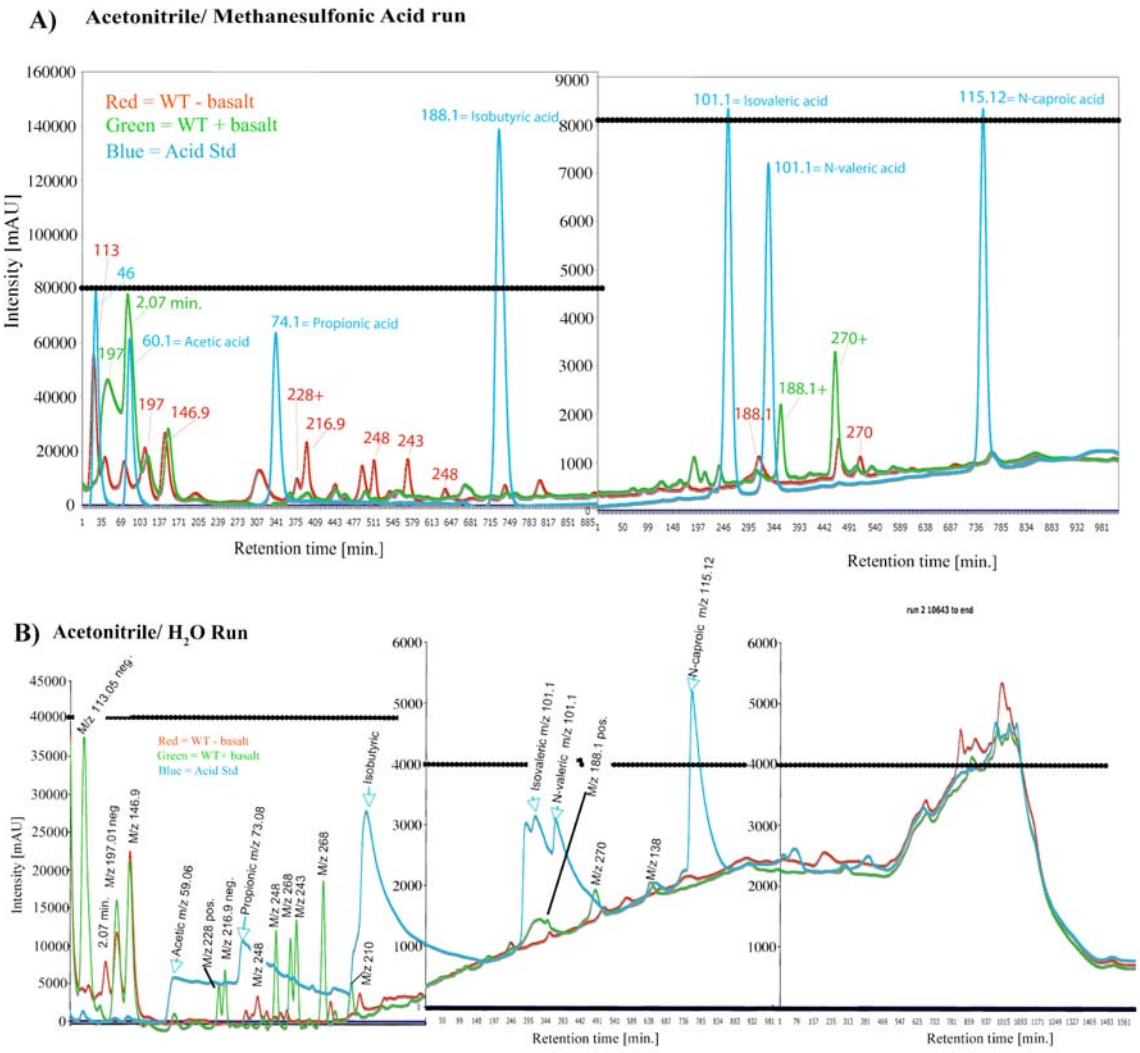

Figure 5.26: Detection of organic acids in *P. stutzeri* VS-10 supernatants determined by reversed-phase HPLC. Masses of peaks are indicated by numbers. Colors of the numbers correlate with the samples: red = VS-10, minimal medium + basalt, green = VS-10 minimal medium – basalt and blue = organic acid standard I. Peak intensities of 80 000 mAU (A) and 40 000 mAU (B) is indicated by black lines.. Three different solvents: Acetonitrile, methanesulfonic acid and H_2O were used. An initial peak with a molecular mass of 113 (in negative ion mode) represents TFA (CF_3COOH, molecular weight: 114.03).

Table 5.1: Genes affected by the Tn5 insertion in each mutant: Locus tags, percentile sequence identity to the listed genes, the closest related organism, the proposed function of the gene and the metabolic pathway are listed. Forward (226f) and reverse (227r) primer gave two different genes indicating that the insertion site in four out of five mutants was located in-between two genes. Sequence results from the forward primer are marked in red, from the reverse primer in blue.

Mutant	Locus Tag	Gene	% identity	Organism	Function	Metabolic Pathway
2A	PST_3967	Pyrroline-5-carboxylate reductase "proC"	82	*Pseudomonas stutzeri* A1501	Oxidizes pyrroline-5-carboxylate to L-proline	Proline biosynthesis
	PST_3966	Predicted enzyme with a TIM-barrel fold	78	*Pseudomonas stutzeri* A1501	Unknown	Unknown
XII5	PST_3970	Homoserine O-Acyltransferase	90	*Pseudomonas stutzeri* A1501	Acylation of L-homoserine to O-acetyl-L-homoserine	Amino acid metabolism
	PST_4081	Peptidase M23/M37	90	*Pseudomonas stutzeri* A1501	Endopeptidase	Unknown
9G	PST_3960	Dihydroorotase "pyrC"	86	*Pseudomonas stutzeri* A1501	Hydrolyzes (S)-dihydroorotate to N-carbamoyl-L-aspartate	Pyrimidine biosynthesis
	PST_3961	Predicted membrane protein	89	*Pseudomonas stutzeri* A1501	Unknown	Unknown
VIII21	PST_1047	Histidinol-phosphate aminotransferase	82	*Pseudomonas stutzeri* A1501	Transaminase	Phenylalanine and tyrosine biosynthesis
	PST_1057	Type 4 prepilin-like protein leader peptide-processing enzyme "pilD"	84	*Pseudomonas stutzeri* A1501	Cleaves type-4 fimbrial leader sequence off and methylates the N-terminal (generally Phe) residue	Pilin maturation
11G	PST_3852	Pyruvate dehydrogenase subunit E1 "aceE"	98	*Pseudomonas stutzeri* A1501	Acyl transfer	Energy metabolism, Amino acid metabolism

Table 5.2: Possible acids and compounds representing HPLC peaks.

Mass [g/mol]	Mass in Figure 5.3	Name/Formula
146.2	147	Adipic acid
243	243	$CH_3(CH_2)_{13}$-COOH
248.5	248	Stearic acid
268	248	$CH_2(CH_2)_3$ CH=COOH
188.1	188	Azelaic acid
270	270	$CH_3(CH_2)_{15}$-COOH

References

Abbas A., Adams C., Scully N., Glennon J. and O'Gara F. 2007. A role for TonB1 in biofilm formation and quorum sensing in Pseudomonas aeruginosa. FEMS Microbiol Lett 274:269-278.

Aguilar C., Friscina A., Devescovi G., Kojic M. and Venturi V. 2003. Identification of quorum-sensing-regulated genes of Burkholderia cepacia. J Bacteriol 185:6456-6462.

Andersen G. L., Beattie G. A. and Lindow S. E. 1998. Molecular characterization and sequence of a methionine biosynthetic locus from Pseudomonas syringae. J Bacteriol 180:4497-4507.

Balcke G. U., Kulikova N. A., Hesse S., Kopinke F.-D., Perminova I. V. and Frimmel F. H. 2002. Adsorption of Humic Substances onto Kaolin Clay Related to Their Structural Features. Soil Science Society of America Journal 66:1805-1812.

Bargouthi S., Young R., Olson M. O. J., Arceneaux J. E. L., Clem L. W. and Byers B. R. 1989. Amonabactin, a novel tryptophan- or phenylalanine-containing phenolate siderophore in Aeromonas hydrophila. J Bacteriol 171:1811-1816.

Bosch R., Garcia-Valdes E. and Moore E. R. 1999a. Genetic characterization and evolutionary implications of a chromosomally encoded naphthalene-degradation upper pathway from Pseudomonas stutzeri AN10. Gene 236:149-157.

Bosch R., Moore E. R., Garcia-Valdes E. and Pieper D. H. 1999b. NahW, a novel, inducible salicylate hydroxylase involved in mineralization of naphthalene by Pseudomonas stutzeri AN10. J Bacteriol 181:2315-2322.

Boukhalfa H., Reilly S. D., Michalczyk R., Iyer S. and Neu M. P. 2006. Iron(III) coordination properties of a pyoverdin siderophore produced by Pseudomonas putida ATCC 33015. Inorg Chem 45:5607-5616.

Burri R. and Stutzer A. 1895. Ueber Nitrat zerstoerende Bakterien und den durch dieselben bedingten Stickstoffverlust. Zentbl. Bakteriol. Parasitenkd., Abt II 1:257-265, 350-364, 392-398, 422-432.

Carlson C. A. and Ingraham J. L. 1983. Comparison of denitrification by Pseudomonas stutzeri, Pseudomonas aeruginosa, and Paracoccus denitrificans. Appl Environ Microbiol 45:1247-1253.

Carlson C. A., Pierson L. S., Rosen J. J. and Ingraham J. L. 1983. Pseudomonas stutzeri and related species undergo natural transformation. J Bacteriol 153:93-99.

Charkraborty R. N., Patel H. N. and Desai S. B. 1990. Isolation and partial characterization of catechol-type siderophore from Pseudomonas stutzeri RC7. Curr. Microbiol. 20:283-286.

Chen Y. and Brantley S. L. 1997. Temperature- and pH-depdence of albite dissolution rate at acidic pH. Chem Geol 135:275-292.

Cornell R. M. and Schwermann U. 2003. The Iron Oxides: Structure, Properties, Reactions, Occurences, and Uses. Weinheim, Germany: Wiley-VCH.

Criddle C. S., DeWitt J. T., Grbic-Galic D. and McCarty P. L. 1990. Transformation of carbon tetrachloride by Pseudomonas sp. strain KC under denitrification conditions. Appl Environ Microbiol 56:3240-3246.

da Silva J. J. R. and Williams R. J. P. 2001. The biological chemistry of the elements: the inorganic chemistry of life. Oxford: Oxford University Press.

Davis J. A. 1982. Adsorption of natural dissolved organic matter at the oxide/water interface. Geochim Cosmochim Acta 46:2381-2393.

Dijk J. A., Stams A. J., Schraa G., Ballerstedt H., de Bont J. A. and Gerritse J. 2003. Anaerobic oxidation of 2-chloroethanol under denitrifying conditions by Pseudomonas stutzeri strain JJ. Appl Microbiol Biotechnol 63:68-74.

Duckworth O. W., Bargar J. R. and Sposito G. 2009. Coupled biogeochemical cycling of iron and manganese as mediated by microbial siderophores. Biometals 22:605-613.

Duckworth O. W. and Sposito G. 2005. Siderophore-manganese(III) interactions. I. Air-oxidation of manganese(ll) promoted by desferrioxamine B. Environ Sci Technol 39:6037-6044.

Eick M. J., Grossl P. R., Golden D. C., Sparks D. L. and Ming D. W. 1996. Dissolution kinetics of a lunar glass simulant at 25 degrees C: the effect of pH and organic acids. Geochim Cosmochim Acta 60:157-170.

Essen S. A., Johnsson A., Bylund D., Pedersen K. and Lundstrom U. S. 2007. Siderophore production by Pseudomonas stutzeri under aerobic and anaerobic conditions. Appl Environ Microbiol 73:5857-5864.

Farkas E., Enyedy E. A., Zekany L. and Deak G. 2001. Interaction between iron(II) and hydroxamic acids: oxidation of iron(II) to iron(III) by desferrioxamine B under anaerobic conditions. J Inorg Biochem 83:107-114.

Faulkner K. M., D. S. R. and Fridovich I. 1994. Characterization of Mn(III) complexes of linear and cyclic desferrioxamine as mimics of superoxide dismutase acticity. Arch Biochem Biophys 310:341-346.

Ferguson S. R. 1994. Denitrification and its control. Antonie Leeuwenhock 66.

Harrison F. and Buckling A. 2009. Siderophore production and biofilm formation as linked social traits. Isme J 3:632-634.

Hein J. R., Koschinsky A., Halbach P., Manheim F. T., Bau M., Kang J.-K. and Lubick N. 1997. Iron and manganese oxide mineralization in the Pacific. Geological Society of London 119:123-138.

Heydorn A., Ersboll B., Kato J., Hentzer M., Parsek M. R., Tolker-Nielsen T., Givskov M. and Molin S. 2002. Statistical analysis of Pseudomonas aeruginosa biofilm development: impact of mutations in genes involved in twitching motility, cell-to-cell signaling, and stationary-phase sigma factor expression. Appl Environ Microbiol 68:2008-2017.

Hou Y. F., Kong Y., Yang J. R., Xin W. and Yu H. W. 2004. Study on immobilization of petroleum biodesulfurization catalust Pseudomonas stutzeri UP-1. Acta Petrol. Sin. 20:75-80.

Kariminiaae-Hamedaani H. R., Kanda K. and Kato F. 2004. Denitrification activity of the bacterium Pseudomonas sp. ASM-2-3 isolated from the Ariake Sea tideland. J Biosci Bioeng 97:39-44.

Kim D., Duckworth O. W. and Strathmann T. J. 2009. Hydroxamate siderophore-promoted reactions between iron(II) and nitroaromatic groundwater contaminants. Geochim Cosmochim Acta 73:1297-1311.

Kim D., Duckworth O. W. and Strathmann T. J. 2010. Reactions of aqueous iron-DFOB (desferrioxamine B) complexes with flavin mononucleotide in the absence of strong iron(II) chelators. Geochim Cosmochim Acta in press.

Kubicki J. D., Ithoh M. J., Schroeter L. M. and Apitz S. E. 1997. Bonding Mechanisms of Salicylic Acid Adsorbed onto Illite Clay: An ATF-FTIR and Molecular Orbital Study. Environ. Sci. Technol. 31:1151-1156.

Lalucat J., Bennasar A., Bosch R., Garcia-Valdes E. and Palleroni N. J. 2006. Biology of Pseudomonas stutzeri. Microbiol Mol Biol Rev 70:510-547.

Landing W. M. and Bruland K. W. 1980. Manganese in the North Pacific. Earth and Planet. Sci. Letters 49:45-56.

Larsen R. A., Wilson M. M., Guss A. M. and Metcalf W. W. 2002. Genetic analysis of pigment biosynthesis in Xanthobacter autotrophicus Py2 using a new, highly efficient transposon mutagenesis system that is functional in a wide variety of bacteria. Arch Microbiol 178:193-201.

Lindegren M. and Persson P. Competitive adsorption involving phosphate and benzenecarboxylic acids on goethite--effects of molecular structures. J Colloid Interface Sci 343:263-270.

Lorenz M. G. and Sikorski J. 2000. The potential for intraspecific horizontal gene exchange by natural genetic transformation: sexual isolation among genomovars of Pseudomonas stutzeri. Microbiology 146113081-3090.

Lorenz M. G. and Wackernagel W. 1994. Bacterial gene transfer by natural genetic transformation in the environment. Microbiol. Rec. 58:563-602.

McLean R. J., Pierson L. S., 3rd and Fuqua C. 2004. A simple screening protocol for the identification of quorum signal antagonists. J Microbiol Methods 58:351-360.

Metcalf W. W. and Wolfe R. S. 1998. Molecular genetic analysis of phosphite and hypophosphite oxidation by Pseudomonas stutzeri WM88. J Bacteriol 180:5547-5558.

Meyer J. M. and Abdallah M. A. 1980. The Siderochromes of Non-fluorescent Pseudomonads : Production
of Nocardamine by Pseudomonas stutzeri. Journal of General Microbiology 118:125-129.

Muehe E. M., Gerhardt S., Schink B. and Kappler A. 2009. Ecophysiology and the energetic benefit of mixotrophic Fe(II) oxidation by various strains of nitrate-reducing bacteria. FEMS Microbiol Ecol.

Neaman A., Chorover J. and Brantley S. L. 2005. Implications of the evolution of organic acid moieties for basalt weathering over geological time. American Journal of Science 305:147-185.

Oelkers E. H. and Gislason S. R. 2001. The mechanism, rates and consequence of basaltic glass dissolution: I. An experimental study of the dissolution rates of basaltic glass as a function of aqueous Al, Si and oxalic acid concentration at 25°C and pH = 3 and 11. Geochim Cosmochim Acta 65:3671-3681.

Parker D. L., Morita T., Mozfarzadeh M. L., R. V., McCarthy J. K. and Tebo B. M. 2007. Interrelationships of MnO2 precipitation, siderophore-Mn-(III) complex formation, siderophore degradation, and iron limitation in Mn-(II)-oxidizing bacterial cultures. Geochim Cosmochim Acta 71:5672-5683.

Parker D. L., Sposito G. and Tebo B. M. 2004. Manganese(III) binding to a pyoverdine siderophore produced by a manganese (II)-oxidizing bacterium. Geochim. Cosmochim. Acta 68:4809-4820.

Parker D. L., Sposito G. and Tebo B. M. 2004. Manganese(III) binding to a pyoverdine siderophore produced by a manganese(II)-oxidizing bacterium. Geochim Cosmochim Acta 68:4809-4820.

Patriquin G. M., Banin E., Gilmour C., Tuchman R., Greenberg E. P. and Poole K. 2008. Influence of quorum sensing and iron on twitching motility and biofilm formation in Pseudomonas aeruginosa. J Bacteriol 190:662-671.

Post J. E. 1999. Manganese oxide minerals: crystal structures and economic and environmental significance/. Proc Natl Acad Sci U S A 96:3447-3454.

Rossello´-Mora R. E., Garcia-Valdes E., Lalucat J. and Ursing J. 1991. Genotypic and phenotypic diversity of Pseudomonas stutzeri. Sust. Appl. Microbiol. 14:150-157.

Ruby E. G., Wirsen C. O. and Jannasch H. W. 1981. Chemolithotrophic Sulfur-Oxidizing Bacteria from the Galapagos Rift Hydrothermal Vents. Appl Environ Microbiol 42:317-324.

Sikorski J., Mohle M. and Wackernagel W. 2002. Identification of complex composition, strong strain diversity and directional selection in local Pseudomonas stutzeri populations from marine sediment and soils. Environ Microbiol 4:465-476.

Sikorski J., Teschner N. and Wackernagel W. 2002. Highly different levels of natural transformation are associated with genomic subgroups within a local population of Pseudomonas stutzeri from soil. Appl Environ Microbiol 865-873.

Sorokin D. Y., Teske A., Robertson L. A. and Kuenen J. G. 1999. Anaerobic oxidation of thiosulfate to tetrathionate by obligately heterotrophic bacteria, belonging to the Pseudomonas stutzeri group. FEMS Microbiol Ecol 30:113-123.

Stillings L. L., Drever J. I., Brantley S. L., Sun Y. and Oxburgh R. 1997. Rates of feldspar dissolution at pH 3-7 with 0-8 mM oxalic acid. Chem Geol 132:79-90.

Stintzi A., Evans K., Meyer J. M. and Poole K. 2006. Quorum-sensing and siderophore biosynthesis in Pseudomonas aeruginosa: lasRIlasI mutants exhibit reduced pyoverdine biosynthesis. FEMS Microbiol Ecol 166:341-345.

Sudek L. A., Templeton A. S., Tebo B. and Staudigel H. 2009. Microbial Ecology of Fe (hydr)oxide mats and basaltic rock from Vailulu'u Seamount, American Samoa. Geomicrobiology Journal 26:581-596.

Tamegai H., Li L., Masui N. and Kato C. 1997. A denitrifying bacterium from the deep sea at 11,000-m depth. Extremophiles 1:207-211.

Tebo B. M., Bargar J. R. and Celement B. G. 2004. Biogenic manganese oxides: properties and mechanisms of formation. Annu Rev Earth Planet Sci 32:287-328.

Telford J. R. and Raymond K. N. 1998. Coordination chemistry of the amonabactins, bis(catecholate) siderophores from Aeromonas hydrophila. Inorg Chem 37:4578-4583.

Templeton A. S., Knowles E. J., Eldridge D. L., Arey B. W., Dohnalkova A. C., Webb S. M., Bailey B. E., Tebo B. M. and Staudigel H. 2009. A seafloor microbial biome hosted within incipient ferromanganese crusts. Nature Geoscience 2:872-876.

Templeton A. S., Staudigel H. and Tebo B. M. 2005. Diverse Mn(II)-oxidizing bacteria isolated from submarine basalts at Loihi Seamount. Geomicrobiology Journal 22:127-139.

Thanyakoop C. (2009). Characterization and biosynthesis of siderophores from marine bacteria. Chemistry. Santa Barbara, University of California, Santa Barbara.

Thomas J. E. and Kelley M. J. 2009. The adsorption of salicylic acid onto gamma-alumina and kaolinite from solution in hexane studied using diffuse reflectance infrared Fourier transform spectroscopy (DRIFT). J Colloid Interface Sci 338:389-394.

Thorseth I. H., Pedersen R. B. and Christie D. 2003. Microbial alteration of 0-30-Ma seafloor and sub-seafloor basaltic glasses from the Australian Antarctic Discordance. Earth and Planet. Sci. Letters 215:237-247.

Thorseth I. H., Torsvik T., Torsvik V., Daae F. L. and Pedersen R. B. 2001. Diversity of life in ocean floor basalts. Earth and Planet. Sci. Letters 194:31-37.

Tipping E. 1981. The adsorption of aquatic humic substances by iron oxides. Geochim Cosmochim Acta 45:191-199.

Uroz S., Calvaruso C., Turpault M. P. and Frey-Klett P. 2009. Mineral weathering by bacteria: ecology, actors and mechanisms. Trends Microbiol 17:378-387.

Van Niel C. B. and Allen M. B. 1952. A note on Pseudomonas stutzeri. J. Bacteriol. 64.

Wang Q., Liu Q., Ma Y., Rui H. and Zhang Y. 2007. LuxO controls extracellular protease, haemolytic activities and siderophore production in fish pathogen Vibrio alginolyticus. J Appl Microbiol 103:1525-1534.

Ward B. B. and Cockcroft A. R. 1993. Immunofluorescence detection of the denitrifying strain Pseudomonas stutzeri (ATCC 14405) in sea water and intertidal sediment environments. Microb. Ecol. 25:233-246.

Welch S. A. and Ullman W. J. 1996. Feldspar dissolution in acidic and organic solutions: compositional and pH dependence of dissolution rate. Geochim Cosmochim Acta 60:2939-2948.

Yan Y., Yang J., Dou Y., Chen M., Ping S., Peng J., Lu W., Zhang W., Yao Z., Li H., Liu W. T., He S., Geng L., Zhang X., Yang F., Yu H., Zhan Y., Li D., Lin Z., Wang Y., Elmerich C., Lin M. and Jin Q. 2008. Nitrogen fixation island and rhizosphere competence traits in the genome of root-associated Pseudomonas stutzeri A1501. Proc Natl Acad Sci U S A 105:7564-7569.

Yeats P. A., Dalzeil J. A. and Moran S. B. 1992. A comparison of dissolved and particulate Mn and Al distributions in the Western North Atlantic. Oceanol Acta 15:609-619.

Zawadzka A. M., Vandecasteele F. P., Crawford R. L. and Paszczynski A. J. 2006. Identification of siderophores of Pseudomonas stutzeri. Can J Microbiol 52:1164-1176.

CHAPTER VI: **Growth of *Pseudomonas stutzeri* VS-10 on basaltic glass and its effect on rock surface texture and chemistry**

Introduction

It is widely accepted that the subsurface environment mineralogy, microbial ecology and water chemistry form an intimately linked biogeochemical system (Bennett et al. 2001). Microorganisms are known to preferentially live in matrix-enclosed communities or "biofilms" (Costerton and Wilson 2004). As a result, free microorganisms represent only 0.1 to 1.0 % of total microorganisms in an aquatic ecosystem, with the remainder being attached to surfaces (Brisou 1995; Madigan et al. 2000). Bacteria are known to modify the rates and mechanisms of chemical and physical weathering of minerals and silicate rocks, including basaltic glasses, by directly or indirectly inducing mineral disaggregation, hydration, dissolution, and secondary mineral formation (Banfield et al. 1999). Therefore an increased interest in the detection of features indicative of microbial alteration exists. While it's often ambiguous if microbially accelerated weathering is simply a consequence of microbial metabolic processes, or if it is directed towards filling a specific evolutionary niche, several advantages including nutrition and protection have been discussed (Cockell et al. 2008). Microbial dissolution of silicates in particular has been demonstrated as being driven by

trace nutrient requirements of microbes available in the colonized material (Bennett et al. 1998; Bennett et al. 2001; Rogers et al. 1998; Taunton et al. 2000b; Taunton et al. 1998).

1. Alteration of volcanic glass

Volcanic glass represents a significant part of the extrusive oceanic crust (Staudigel and Hart 1983; Straub and Schmincke 1998). It is chemically unstable in the presence of water (Staudigel et al. 2008), so low temperature dissolution has a major effect on the re-distribution and large-scale geochemical cycling of both major and trace elements in the aquatic environment. Ion-exchange reactions during volcanic glass dissolution leads to the formation of characteristic mineral assemblages such palagonite and zeolites. Smectite and carbonates also act as a sink for a significant portion of elements liberated during glass alteration (Staudigel and Hart 1983).

2. Alteration textures and mechanisms

Over the past few decades a variety of distinct alteration textures indicative of both biotic and abiotic origin have been studied and documented in volcanic glasses from a large number of terrestrial and aquatic settings (Furnes et al. 2007; Staudigel et al. 2008). While both types of textures are oftentimes found along edges or natural defects (e.g. cracks) of the glass their characteristic morphologies have been studied extensively and formation mechanisms have been proposed (Staudigel et al. 2008). Aside from the abundance of such alteration textures many studies have also based the detection and identification of both biotic and abiotic glass alteration on the mobility and release of elements during the alteration process (Daughney et al. 2004; Staudigel and Hart 1983).

A) Abiotic alteration

Abiotic glass alteration has been studied for decades (Furnes 1975; Staudigel and Hart 1983; Thorseth et al. 1995). Textures associated with this type of alteration have recently been characterized by a smoothing of sharp edges and an overall reduction of the fresh glass surface (Staudigel et al. 2008). Abiotic alteration is known to be mainly the result of hydration reactions with the surrounding seawater (Bonatti 1965) resulting in an isochemical removal of elements and leading to the formation of characteristic authigenic mineral phases. Nearly isomolar exchange of SiO_2, Al_2O_3, MnO, MgO, CaO, Na_2O, P_2O_5, Zn, Cu, Ni, Cr, Hf, Sc, Co and REE for H_2O and K_2O take place, while TiO_2 and FeO are passively accumulated, leading to the characteristic mineralization of palagonite (Staudigel and Hart 1983). The composition of the solution in contact with the glass has been shown to largely determine the rate of dissolution.

B) Biotic alteration

Over the past decades a variety of alteration features found in ancient and fresh submarine basaltic glass have been attributed to microbial activity (Alt and Mata 2000; Fisk et al. 1998; Furnes et al. 1999; Furnes and Staudigel 1999; Furnes et al. 1996; Giovannoni et al. 1996; Staudigel et al. 1998; Thorseth et al. 1992; Thorseth et al. 1995; Thorseth et al. 2003; Torsvik et al. 1998). Two types of bioalteration textures have been described: a) granular alteration and b) tubular alteration. Granular alteration is characterized by clusters of micron-sized irregular voids and is typically found on glass surfaces and along cracks. Tubular alteration is characterized by tunnel-like structures that are on the order of one to a few microns in diameter and up to hundreds of microns

in length (Staudigel et al. 2008). Size and shape of granular alteration features include mostly irregular patches (pits and spherules of varying sizes: 0.3- 10 μm) often located along natural glass fractures, while tubular alteration is represented by tubes or vermicular channels (1-10 μm wide and up to 100 μm long) extending into the glass near alteration fronts (Alt and Mata 2000; Cockell et al. 2008; Staudigel et al. 2008). Aside from the morphologically distinct alteration textures much evidence for biotic glass alteration is based on the abundance of molecular and chemical signatures in the glass (Giovannoni et al. 1996; Torsvik et al. 1998).

Recent molecular studies on basaltic glass from various submarine settings have shown that basalt surfaces harbor diverse microbes (Mason et al. 2007; Santelli et al. 2008; Sudek et al. 2009) far exceeding the level of background seawater. Based on recent cultivation studies microbial communities on these surfaces exhibit a variety of metabolic characteristics including heterotrophic Fe(II) and Mn (II)-oxidation as well as the production of secondary metabolites such as siderophores (Daughney et al. 2004; Edwards et al. 2003; Sudek et al. 2009; Templeton et al. 2005) indicating an energetic and nutritional advantage of life on volcanic rocks. Little is known about the direct interaction of these organisms with basalt surfaces, but bio-alteration of silicate minerals has been studied extensively. Microbes influence mineral formation and dissolution in two ways: 1) passive catalysis of mineral formation by the cells directly (biologically induced mineralization, “BIM”) and 2) active alteration of microenvironmental geochemistry and mineral dissolution (microbially induced corrosion “MIC”, Douglas 2005).

Extracellular polymeric substances (EPS), considered the primary matrix of biofilms (accounting for 50-90 % of the total organic carbon, Flemming et al. 2000) are known to modify the substrate surface properties by modifying surface charge, wettability and surface free energy resulting in both enhanced corrosion (Fletcher and Marshall 1982) or corrosion inhibition (Chongdar et al. 2005; Schneider 1997). Mineral and rock weathering can also be promoted inadvertently from the microbial release of metabolic byproducts, such as inorganic and organic acids (fermentation products: e.g. lactate, formate; Krebs cycle compounds: citrate, succinate, α-ketoglutarate, oxalacetate, pyruvate) as well as ligands (Barker et al. 1998; Hersman et al. 1995; Liermann et al. 2000). These components have been shown to etch the silica substrates, sometimes leaving behind features such as etch pits, which can potentially reflect the morphology of the etching microorganism (Brehm et al. 2005). Because biological growth exhibits spatial heterogeneity, these features are often concentrated in natural depressions of mineral grains, joints between crystal lattices, or where the lattices have many defects (Wacey 2009).

3. Techniques to determine and visualize glass alteration

Several microscopic and analytical methods have so far been used to study the feedbacks between microbial activity and the dissolution, redox transformation and biomineralization processes minerals, glasses and rocks. Surface-related microscopic methods to examine bio-signatures include preservation of cells and observation of alteration features adjacent to biofilms (Barker et al. 1998; Bennett et al. 1996; Rogers et al. 1998), removal of organic matter prior to imaging (Buss et al. 2007) and physical

removal of cells during imaging and after short-time incubations (Grantham et al. 1997; Maurice and Forsythe 1997). Due to difficulties in identifying surface texture alterations and associating them with biological activity a combination of both microscopic and analytical techniques has so far shown the most promising results regarding the identification of bio-alteration signatures.

Atomic force microscopy (AFM) has been widely used to visualize surfaces of biologically-colonized minerals (Davis and Luettge 2005; Forsythe and Maurice 1998; Mangold et al. 2008a; Mangold et al. 2008). The method does offer extremely high spatial resolution and surface sensitivity that other methods often lack and therefore represents a powerful tool for the identification of microbial footprints on solid surfaces. It is often combined with fluorescent or confocal microscopy to complement the AFM's weakness in identifying certain biomolecules including DNA, RNA, proteins, polysaccharides or lipids.

Our study focuses on the effect of biofilm formation by marine *Pseudomonas stutzeri* VS-10 on the alteration of basaltic glass. Originally isolated from a volcanic rock surface the strain exhibits increased growth in the presence of basalt when grown nutrient-limited (see Chapter IV). A physiological characterization revealed its capability to perform various metabolic processes including heterotrophic Fe(II)oxidation, siderophore production and the production of low-molecular weight organic acids (Chapter VI). This chapter is intended to determine the effects of basaltic glass-related growth of this strain on the textural and chemical transformation rates of the glass.

Materials and Methods

The investigation of surface-related alteration textures on polished basalt surfaces, and a chemical analysis of elements release into solution over the time course of 46 days, was used to determine the biological component of basalt alteration. Both experiments were set-up in batch experiments. The effect of a biofilm on the surface texture of the glass was investigated by Atomic Force Microscopy (AFM). The chemical exchange during basalt dissolution was determined by measuring the release of elements from the glass into solution by Inductively Coupled Plasma Optical Emission Spectrometry (ICP-OES).

1. Volcanic glass

Basaltic glass used in both experiments was originally collected at Kilauea volcano (Pu'U-o'O). Liquid lava was harvested from an active flow and was quenched in a water bucket before re-melting to obtain glass-like texture. Thick sections 1-2 mm thick and ~ 0.4 cm diameter were polished to a grain size of 0.25 μm. The glass did not contain any minerals but dark brown schlieren within the material were apparent both under the microscope and when held against a light source. This could point towards either inhomogenous composition of the material or simply be an effect of the cooling process after re-melting.

For the chemical dissolution experiment the original re-melted basalt was crushed to a grain size of around 3 mm, first by using a stainless steel disc crusher and then by sieving the basalt until the correct grain size was obtained. The basalt grains were washed several times in deionized water, washed twice in 0.1N HCl to remove surface Fe and sonicated in deionized water for 40 min. After a final rinse with deionized water the basalt was microwave-sterilized for 10 min. (2 x 5 min. to prevent overheating) and was dried in sterile (autoclaved) tin foil in a drying oven at 40 °C. 5 g of glass grains were used in each flask of the chemical dissolution experiment.

2. Growth medium

50 ml of low-nutrient, artificial-seawater-based "minimal" medium (see Chapter IV) amended with ammonium, phosphate and glycerol was used in all set-ups. All cultures were set-up as batch experiments in 250 ml flat-bottom glass Erlenmeyer flasks (Fisher cat. #: FB-501-250) that were previously acid washed in 10 % trace-element grade hydrochloric acid (37 %; Sigma cat. # 84415) for 2 days, rinsed 6 times with deionized water and autoclaved at 121 °C for 30 min.

3. Microbial strain

Pseudomonas stutzeri VS-10 isolated as a siderophore-producing bacterium from a volcanic rock surface at Vailulu'u Seamount in 2005 was used in both experimental set-ups. It was grown on Luria-Bertani (LB) medium (see Chapter IV) at 37 °C (~180 rpm) overnight and was subsequently washed with "minimal" medium 3 times. The bacterial pellet was resuspended in 5 ml of "minimal" medium and the culture's optical density

was spectrophotometrically determined. The biotic experiment was started by adding a portion of the resuspended pellet to 50 ml of "minimal" medium to achieve an initial optical density (OD_{600nm}) of 0.3, and the absorbance was periodically monitored on a spectrophotometer to ensure growth of the organism. When grown nutrient-limited on minimal medium in the presence of rhyolite, a low-Fe containing volcanic rock, P. stutzeri VS-10 was shown to produce two bis-catecholate siderophores, Amonabactin P750 and P693 (see Chapter IV). Identification and purification of amonabactins was performed by C. Thanyacoop in A. Butler's lab at UCSB as described elsewhere (Thanyakoop 2009). Amonabactin P750 was subsequently added to one of the abiotic set-ups in the chemical dissolution experiment.

4. Experimental set-up

4.1 Effect of biofilm on rock surface texture

Basaltic glass thick sections were incubated in 50 ml of minimal medium on a benchtop shaker at ~ 50 rpm. The agitated incubation was chosen to mimic seawater movements and to provide enough oxygen for strain VS-10 to grow. Basalt surfaces were imaged prior and after exposure to both medium and culture. Surface textures after exposure to *P. stutzeri* VS-10 cultures was investigated by a) chemical removal of organic material from the surface prior to imaging and b) displacement of organics by the AFM tip. The following experiments were set-up:

A) Biotic

50 ml of minimal medium, bacterial culture started at $OD_{600\ nm}$ of 0.3, two basalt slides: one for visualization of the basalt topography after biofilm removal, one for visualization of the biofilm and topographic features after cell displacement.

B) Abiotic

50 ml of minimal medium, one basalt slide: for determination of textural changes caused by the medium alone.

C) Non-incubated, “fresh” basalt

Used as reference to investigate natural textural features of the basalt as well as polishing marks and any potential alteration textures caused by the removal of organic matter from the slides.

4.2 Elemental release into the medium over time

Flasks containing basalt grains were incubated without agitation for 46 days. The non-agitated set-up was chosen to minimize dissolution of basalt and subsequent release of elements based on the physical interaction of basalt grains. Cultures were mixed once a day to provide sufficient oxygen for growth of the bacterium. Samples were taken on day 0, 10, 23, 35 and 46. The supernatant in the flasks was swirled up to the point where it looked homogenized after which the basalt grains quickly settled to the bottom of the flasks. In a laminar flow hood 2 ml samples were transferred to sterile round-bottom

polypropylene snap-cap tubes (Fisher cat. # 14-959-11B) for subsequent chemical digestion. The following experiments were set-up:

A) Biotic (medium, basalt and *Pseudomonas stutzeri* VS-10 started at OD_{600nm} of 0.3.

B) Abiotic (medium and basalt only)

C) Abiotic containing amonabactin P750 (medium, basalt, ~ 150 μM amonabactin P750).

5. Atomic force microscopy (AFM)

AFM imaging was performed with the help of Francesca Malfatti in the Azam laboratory with an MFP-3D (Asylum Research, Santa Barbara, USA) mounted on an inverted epifluorescence microscope (Olympus IX 51).

5.1 Cleaning treatment

All slides were removed from the flasks after 35 days. One of the slides exposed to the culture was instantly fixed in 2.5 % filter-sterilized glutaraldehyde at 4 °C overnight to preserve the biofilm structure. The other biotic slide, the abiotic and the "fresh" slides were cleaned according to a procedure previously shown not to effect either surface texture or chemistry of minerals (Buss et al. 2003): After an initial ultrasonication in 2 % (v/v) sodium dodecyl sulfate (SDS) for 45 min., the slides were again sonicated in DDI water for 10 min. and rinsed with DDI water before air-drying. To remove any loose particles, condensation, fingerprints, and other contaminants prior to AFM imaging the cleaned slides were rinsed in sterile 50 ml falcon tube (Becton Dickinson, Fisher cat. #: 14-432-24) filled with HPLC-grade water (Fisher, cat. # PI-

51140) by vigorously shaking the tubes for a few minutes prior to drying them in sterile petri dishes in a dry oven at ~ 40 °C. Inside the petri dishes the slides were kept at an angle by placing one side of the slide on the rim of a halfway-closed dish to prevent drying marks caused by water drops.

5.2 Sample preparation

An EM copper grid (Electron Microscopy Science, USA; 801-01-cu, item is discontinued) was mounted on the bottom of each basalt thick section and the XY stage as well as the slide was marked to allow repeated imaging of the same area (personal communication F. Malfatti).

5.3 Operating conditions

The strategy we adopted was to localize an area, image it in AC (dynamic mode) and then switch to DC (contact mode) to displace the cells on one of the biotic basalt slides, allowing us to image the basalt surface underneath the biofilm. Images were acquired in AC mode in air with a silicon nitride cantilever AC160TS (Olympus, Japan; k = 42 N m^{-1}; tetrahedral shape) and in Contact mode in air with a silicon nitride cantilever TR400PB (Olympus, Japan; k =0.02 N m^{-1}; pyramidal shape). Scan rates were 0.8 to 2 Hz. Image resolution was 256 x 256 or 512 x 512. We recorded trace and retrace of height, amplitude, phase, and *Z (Z*= height) sensor channels. Topography images were processed with Planfit and Flatten functions (Igor Pro 6.03A MFP3D 070111+830). The AFM image acquisition details are given in the figure captions.

6. Magnetic measurements of "authigenic" mineral phase

The formation of an authigenic mineral phase was repeatedly detected in biotic (containing *P. stutzeri* VS-10) and abiotic lab cultures of minimal medium when incubated under agitated conditions in the presence of basalt. Mineral formation was usually apparent after roughly 2 weeks. The bulk chemical composition of the material was determined by energy-dispersive X-ray spectroscopy analysis (EDS).
Al, Fe, Ti and Mn present in both basalt and the mineral phase but not the minimal medium were later chosen to indicate basalt dissolution analyzed by ICP-OES.

Additionally a series of magnetic and spectroscopic data were obtained from the mineral in collaboration with T. Berquó at the University of Minnesota (Institute for Rock Magnetism, group of S. K. Banerjee). Measurements are based on the fact that the spontaneous magnetization of ferromagnetic minerals can be influenced by the application of very low magnetic fields caused by the existence of small regions within minerals called "magnetic domains" that greatly vary with grain size. Domains are small (1-100's microns), but much larger than atomic distances. A rock carries a natural remanent magnetization (NRM) that is the vector sum of all the different possible components of magnetization acquired over its history. Single domain (SD), pseudo-single domain (PSD), and multi domain (MD) grains may all contribute to this signal (www.irm.umn.edu/hg2m/hg2m_d/hg2m_d.html). Subdivided into grain sizes the magnetic behavior of a material helps to investigate its mineral composition including the presence of ferromagnetic minerals such as magnetite, hematite and goethite. These iron minerals have typical transitions and/or magnetic behavior at low temperature which is

used to identify their existence in a material (Cengiz Cinku et al. 2009; Hargraves and Banerjee 1973).

6.1 Remanent magnetization curves (to investigate the presence of magnetite, hematite or goethite)

i. Thermoremanent magnetization (TRM: Magnetization acquired during cooling from a temperature above the Curie Temperature in an external field): A thermoremanent magnetization curve was obtained by field cooling the sample from room temperature in an applied field of 2.5 T to the lowest temperature (10 K), and then variation of remanent magnetization was measured with increasing temperature up to 300 K (TRM curve).

ii. Induced remanent magentization (IRM: Magnetization acquired instantaneously in an external field): This curve was obtained by cooling the sample to the lowest temperature without any applied field, then at 10 K a 2.5 T field was applied. The resultant remanent magnetization was measured with increasing temperature up to 300 K. IRM acquisition is a useful technique to distinguish between magnetite and hematite.

iii. Room temperature saturation isothermal remanent magentization (RTSIRM): obtained by applying a 2.5 T magnetic field at room temperature, the field was turned off and the remanent magnetization was measured during the cooling and re-warming process.

6.2 AC susceptibility curves

AC susceptibility curves were measured on a LakeShore Cryotronics AC Susceptometer in the temperature range 2-300 K. These data suggest mineral content and grain size. The method allows mineral identification through low-temperature crystallographic transitions, and identification and quantification of superparamagnetic populations through both frequency- and temperature-dependence of low-field susceptibility (www.irm.umn.edu/equipment/lakeshore/index.htm).

6.3 Hysteresis loops

Hysteresis loops were obtained using maximum applied fields up to 5 T at temperatures of 2, 10 and 18 K. The hysteresis loops are magnetization loops obtained with induced magnetization. Parameters that can be observed are the saturation magnetization (Ms - magnetization at the highest field), remanent magnetization (Mr - when the field is zero) and coercive force (Bc - when the magnetization is zero). These parameters can give a clue about minerals content and grain size of a material.

6.4 Mössbauer spectra

Mössbauer spectra (to investigate the composition of Fe-containing minerals) were measured on a Ranger Scientific Mössbauer Spectrometer (conventional constant-acceleration spectrometer) at room temperature in transmission geometry with a ^{57}Co/Rh source, using α- Fe at room temperature to calibrate isomer shifts and velocity scale. The Mössbauer spectrometer uses a radioactive ^{57}Co source to generate gamma rays that are absorbed by ^{57}Fe in a sample. The nature of absorption by ^{57}Fe is a function of the

valence state and type of bonding in a Fe-mineral's lattice, and so the Mössbauer effect can be diagnostic of magnetic Fe sulfides and oxides (www.irm.umn.edu/equipment/lakeshore/index.htm).

7. Chemical digestion

All samples were chemically digested prior to ICP analysis. This assures complete detection of elements otherwise trapped as metal oxides or in bacterial cells. A three-step wet digestion method using sequential addition of trace-element-grade acids was followed by an evaporation to dryness to ensure proper resuspension of samples in 1 % HNO_3.

7.1 Wet digestion

All of the steps from the first sampling to the removal of supernatant after centrifugation, transfer of sample solutions to new tubes and resuspension of bacterial and mineral pellets in acid were performed inside a laminar flow hood to prevent contamination with air-born particles. The method resulted in three fractions (solutions) for each sample (Figure 6.1). Blanks for all acids and the water were taken at each time to ensure that they were stored in polypropylene tubes the same length of time that the respective samples did (e.g. three water samples: a) after HCl wash step, b) after HF wash step and c) fresh prior to evaporation). This ensured documentation of all elements leached from the polypropylene.

1) Centrifuged fraction:

After homogenization of experimental solutions through swirling and a short period of time where all the basalt grains quickly settled to the bottom of the flasks 2 ml samples were transferred to sterile polypropylene tubes, and centrifuged at 8000 rpm for 10 min. The supernatant was removed by carefully pipetting it into a new, sterile set of polypropylene tubes, which was kept at 4 °C until the other fractions were ready.

2) HCl fraction:

After removing the supernatant (from the centrifuged fraction) the remaining pellet, which included both authigenic minerals/metal oxides and cells (only in the biotic set-up) was resuspended in 0.5 ml of trace-element-grade HCl (37 %; Sigma cat. # 84415) and incubated at room temperature over night. The samples were subsequently centrifuged at 8000 rpm for 10 min. and the supernatant was removed and transferred to new polypropylene tubes. The pellets were washed in 0.5 ml of HPLC-grade water (Fisher, cat. # PI-51140) and centrifuged again at 8000 rpm for 10 min. The water was removed with a pipet and was added to the HCl fraction so that total volume of this fraction was 1 ml. The samples were also stored at 4 °C until completion of the 3rd fraction.

3) HF fraction:

The pellet left over from the HCl step was resuspended in 0.5 ml of trace-element-grade HF (99%; Sigma cat. #: 47559) to destroy the difficult-to-digest

silicates. The samples were incubated at room temperature over night and transferred to fresh polypropylene tubes. The old tube was quickly washed with 0.5 ml of HPLC-grade water and the solution was added to the HF fraction.

7.2 Evaporation

Samples were evaporated to dryness in teflon digestion vials (15 ml screw-cap; Savillex, Minnetonka, MN). The vials, previously washed in 10 % HCl (reagent grade) for 2 days, were washed and rinsed in deionized water 6 times prior to transfer of sample from polypropylene tubes to the vials.

Open-vessel evaporation was performed in a small flow-hood designed for the evaporation of acid fumes at temperatures between 80 and 100 °C. Evolving volatile reaction products such as SiF_4 from the following reactions

$4HF + SiO_2$ (Pu'U-o'O glass content averages 52 wt %) $\rightarrow SiF_4 + 2H_2O$

$SiF_4 + 2HF \rightarrow H_2SiF_6$

were removed by a filter-containing fan creating a constant flow of air through the chamber into a fume hood.

8. Inductively Couple Plasma Optical Emission Spectrometry (ICP-OES)

8.1 Sample preparation

After evaporation to dryness, the residue was taken up in 4 ml of TE-grade HNO_3 (Fisher cat #: A509SK-212) diluted to 1% and each sample was filtered through a 0.2 μm filter prior to measurement.

Measurements were performed on an Inductively Couple Plasma Optical Emission Spectrometer (PerkinElmer 3700 with AS90 Autosampler, capable of axial or radial emission measurements) at the Scripps Institution of Oceanography.

Standard solutions were prepared from a calibration standard (Claritas PPT Instrument Calibration std 2 ICP, Fisher cat. #: CL-CAL-2) at the following concentrations: 5 μM, 50 μM, 100 μM, 500 μM, 1 mM, 5 mM, 25 mM

8.2 Operating conditions

Each element of interest was measured at various wavelengths. The following wavelengths were determined based on previous methods (other protocols) and the accuracy of calibration curves (0.99-1.00):

A) Aluminum (Al): 396.153 nm
394.401 nm

B) Iron (Fe):	238.204 nm
	234.349 nm
	239.562 nm
	259.939 nm
	273.955 nm
C) Titanium (Ti):	334.940 nm
	336.121 nm
	337.279 nm
	334.903 nm
	368.519 nm
D) Manganese (Mn):	257.610 nm
	260.568 nm
	294.920 nm

Results

Pseudomonas stutzeri VS-10, isolated from a volcanic rock surface at Vailulu'u Seamount had demonstrated enhanced growth with basalt in the medium (Chapter IV). Strain VS-10 was used as a model organism to study the textural and chemical transformation of basaltic glass during progressive colonization.

1. Effect of biofilm on rock surface texture

The textural nature of water/microbe and glass interactions was examined microscopically based on the physical appearance and abundance of alteration textures on polished basaltic glass surfaces. Imaging of polished basalt glass surfaces after exposure to a seawater-based minimal medium and a culture of the marine siderophore-producing bacterium *P. stutzeri* VS-10 for 35 days resulted in the identification of few alteration textures visible on exposed surfaces relative to the unexposed ones. Analysis of the glass surface texture by AFM was conducted inside a relatively small area within an EM copper grid. Textural investigations included biotic and abiotically incubated surfaces from which all organic matter had been removed prior to imaging as well as imaging of a surface underneath a biofilm after cell displacement.

1.1 Natural glass features

Occasional large pits (6–20 μm across, ~100–300 nm deep, not shown) are apparent in all samples but based on their regular, smooth shape and their resemblance to features seen in hornblende glass (Buss et al. 2003) are considered natural and not related to glass alteration processes.

1.2 Biofilm formation and distribution

Biofilm distribution on the fixed "biotic" slide is mostly heterogeneous. Biofilm structures range from patchy (Figure 6.2A) to more laminar layers (Figure 6.2B) of what appears to be a mixture of cells and extracellular polymeric material (EPM). Both biofilm structures were displaced using the AFM tip to check for alteration features (e.g. textural

changes) underneath. Based on the amount of organic material displaced in laminar areas cell/EPM coverage averages 1.2 μm (Figure 6.2B).

1.3 Biotic and abiotic alteration textures

Similar alteration textures were identified on both, biotic and abiotically incubated basalt surfaces. Based on a textural classification of alteration features by (Furnes et al. 2001) they are somewhat similar to the ones classified as “granular bio-alteration” textures in basaltic glass (see Staudigel et al., 2008 for most recent review). While the size and “granular” character the surface textures observed on our glass are similar to the ones described by (Staudigel et al. 2008) none of them can be directly associated with microbial activity since they are apparent on both exposed and unexposed surfaces (Figure 6.3). Even underneath parts of laminar cell coverage (Figure 6.2B) no indication for such microbially mediated alteration textures is apparent (Figure 6.4). While only a small area of the glass surface was analyzed, the irregularly shaped (2-6 μm in diameter and 1-6 nm deep, Figure 6.2) alteration fronts are also not found to be particularly associated with natural defects of the glass (e.g. scratch marks, large pits described under 1.1) as described previously by Staudigel et al. (2008). Instead they appeared to be frequently and unevenly distributed over the entire surface.

1.4 Linear “ridges”

Very noticeable on all sample surfaces are linear elevated features. The appearance of these “ridges” differs between the sample surfaces. While they are considerably (1-3 nm) elevated on the unexposed basalt, their height is significantly

reduced on the samples that had been exposed to both, the medium only and medium and bacterial strain (Figure 6.5). Their overall height reduction therefore can not be specifically related to the microbial activity. This observation however represents the only indication for a minor form of basalt dissolution and leads to the conclusion that overall we did not obtain any evidence for microbially-derived alteration.

2. Elemental release into the medium over time

The chemical nature of water/microbe/glass interactions was examined by looking at the abundance of elements in the incubation solution. A first indication for a release of elements (e.g. silica) from the glass was apparent after about two weeks as authigenic minerals appeared to form in the solution (first floating at the surface of the culture then settling to the bottom of the flasks). Bulk chemical analysis and magnetic characteristics of the mineral phase were used to determine its origin.

2.1 Authigenic mineral phase composition and magnetic characteristics

2.1.1 Chemical composition

EDS analysis resulted in a bulk chemical composition of the mineral phase (Figure 6.6, Table 6.1). The overall texture of the mineral consortium appears to be homogenous enough to allow a rough chemical analysis by EDS. Several measurements were made in different locations giving generally matching results. The presence of elements present in basalt but not the minimal medium allows for interpretation of the material as a dissolution product of the glass.

2.1.2 Magnetic properties

A variety of magnetic measurements gave information on the presence ferromagnetic minerals and grain sizes in the mineral phase. Low temperature magnetism measurements of the show the presence of a smooth bump (Figure 6.7 A) at around 75 K that could be associated with the contribution of Ti-magnetite. Stoichiometric magnetite has a transition at 120 K (Verwey transition). This transition shifts to lower temperatures due to oxidation or iron replacement, e.g. Ti. RTSIRM curve (Figure 6.7 B) show a typical Verwey transition for magnetite. The noise curve was indicative of very low content of this Fe phase. The AC susceptibility curves (Figure 6.7 C) and hysteresis loops (Figure 6.7 D) present the same behavior associated with paramagnetic phases and indicative of magnetic order below 2 K. Mössbauer spectra (Figure 6.8) show a dominance of Fe^{3+}(74 %) over Fe^{2+} (26%, Table 6.2). The presence of Ti-magnetite as indicated by RTSIRM curves could not be confirmed base on these data, which is likely due to its abundance below 1%, the detection limit for Mössbauer analysis.

Overall the magnetic characterization of the mineral phase indicats the presence of Ti-magnetite, a mineral commonly found in basalt, and further confirms the material as an alteration product of the basaltic glass.

2.2 Chemical digestion

Another indication for basalt dissolution based on the release of elements, Fe in particular, into solution becomes apparent during the chemical digestion of samples. A yellow color appears in the centrifuged fraction (biotic set-up only) with increasing

intensity over time (Figure 6.9, taken from earlier experiments). The cause of this color can not be elucidated but is likely to be associated with the precipitation of Fe (hydr)oxides. While the intensity of the color generally increases it appears to decrease at two time points in the time series. This may be indicative of sampling issues later explained in the text. Cell growth in the biotic set-up was consistently monitored and shows increasing growth of the bacterium (comparable to growth curves in thesis Chapter IV).

Once digested in 0.5 ml conc. HCl and incubated at room temperature over night the biotic samples shows a purple-ish color that also appears to intensify over time (Figure 6.10, from an earlier experiment). The origin of this color could not be determined.

Chemical digestion of samples appears to be complete due to no visible residue left over in the polypropylene tubes.

2.3 ICP-OES analysis

Based on the results from EDS and magnetic data obtained from the authigenic mineral phase, four elements (Fe, Al, Ti and Mn) were analyzed in all wet digestion fractions. Due to their absence in both medium and glassware these elements are considered to represent basalt dissolution over time. Si was for the most part removed during the digestion process to prevent the precipitation of the other elements in the form of insoluble fluorides.

The ICP-OES measurement of all three fractions (centrifuged, HCl, HF for each sample) data were combined giving one elemental concentration for each time point in each experimental set-up (Figure 6.11, elemental conc. in mg/L). The concentrations differences (between t_0 and t_{46}) in μM are listed in Table 6.3.

Elements in all blanks (acids and water) can only be detected in traces that lie within the manufacturer's description. A mean average concentration in mg/L for each element was determined from the blanks and the readings for each respective sample were corrected for these values. Overall, in the biotic set-up the concentrations of most elements (Fe, Ti and Al) slowly increase (Figure 6.11 A). Both abiotic set-ups exhibit the same trend for Ti and Mn while the elemental concentrations of Fe and Al decrease over the time (Figure 6.11 B and C).

Elemental increase in all experiments is inconsistent showing mostly fluctuating amounts of elements detectable in the supernatant over time (Figure11, in particular day 10). Overall the chemical analysis of elements indicative for basalt dissolution over time gave inconclusive data indicating only minor dissolution of the glass under biotic conditions and no apparent dissolution under abiotic conditions with and without microbial ligands.

Discussion

Volcanic glass has been shown to alter by different processes depending on pH, temperature, solution composition, fluid/rock ratio and the participation of microbial byproducts such as siderophores and organic acids (Buss et al. 2003; Buss et al. 2007; Crovisier et al. 1983; Gislason and Oelkers 2003; Pierce et al. 2008). The morphology of biotic and abiotic alteration textures (Staudigel et al. 2008) and chemical models of glass alteration have been described (Eick et al. 1996; Staudigel and Hart 1983). More recently Eick et al. specified in detail the processes during chemically dissolution of lunar glass under reduced pH values: the dissolution sets-off with a rapid, parabolic release of elements followed by a slower more linear release rate indicating a rate-determining step involving diffusion. The first step is initiated by hydrogen ions, which are involved in diffusion exchange with cations and surface protonation reactions. These reactions weaken the metal oxygen bonds enhancing the release of Si from the surface. The second, more linear step often seen under the impact of organic acids in the reaction solution is thought to represent an accelerated dissolution through chemisorption of organic ligands in the basalt surface. A charge transfer between ligand and rock surface is considered to weaken the framework of the rock increasing the susceptibility of Si-O bonds to hydrolysis and overall leading to accelerated diffusion of elements into the medium over time. According to Eick et al. the order of major ion release during basalt dissolution is as follows: Fe ≈ Mg > Si > Al > Ca. The rate of elements released from the glass in our experiments correlate with this finding at least with regard to Fe and Al. Release of elements into solution has been shown however to be largely controlled by solution

chemistry (saturation with regard to a particular element) and by the precipitation of secondary minerals such as Fe (hydr)oxides, microcrystalline gibbsite ($Al(OH)_3$), sepiolite ($Mg_4Si_6O_{15}(OH)_2 \cdot 6H_2O$), montmorillonite ($(Na,Ca)_{0.33}(Al,Mg)_2(Si_4O_{10})(OH)_2 \cdot nH_2O$), analcime ($NaAlSi_2O_6 \cdot H_2O$), goethite (FeO(OH)) and most of all palagonite, the first stable product of congruent and incongruent dissolution of volcanic glass (Stroncik and Schmincke 2002).

In our cultures the formation of authigenic mineral phases suggests that basalt dissolution does take place. The amorphous or crystalline texture of the mineral could not be fully determined. SEM data however suggest an amorphous textures of the material justifying the determination of a bulk chemical composition by EDS analysis. Potentially crystalline parts resulting in the analysis of specific mineral phases were not considered. Evidence for basalt dissolution as indicated by the formation of a mineral phase is not overly supported by our morphological and chemical data. While granular glass surface textures appear to resemble the ones previously reported for bio-alteration (Buss et al. 2003; Daughney et al. 2004) we lack evidence for their biotic or abiotic origin. The height of linear “ridges”, apparent on both exposed and unexposed surfaces, did however appear significantly reduced after samples were exposed to both medium only or the microbial strain. This indicates at least to some extend a general reduction of the glass surface indicating glass dissolution. Chemically a minor impact of microbial activity on the dissolution of the glass could be shown while we could not demonstrate an effect of the medium only or metabolic byproducts such as siderophores previously shown for

iron-silicate glass planchets (Buss et al. 2007). Possible reasons for the lack of morphological and chemical data indicative for basalt dissolution are numerous:

1. Issues with the starting material

Morphological studies of the basalt surface and identification of alteration textures strongly depends on the quality and alteration status of the unexposed surfaces. Failure to store the basaltic glass thick sections in a desiccator in the years prior to analysis is likely to have resulted in a slight auto-oxidation of surfaces, which, in return could have lead to the occurrence of the granular alteration textures apparent on all surfaces. Freshly prepared, epi-polished slabs would represent a much more appropriate surface to work with in the future.

2. Solution chemistry and the precipitation of authigenic minerals

Numerous previous studies showed that the dissolution kinetics of glass and aluminosilicate minerals are likely controlled by the chemistry of the interacting solution either by inhibition or by reaching a solid/solution saturation state (Berger et al. 1994; Daux et al. 1997; Techer et al. 2001; Welch and Ullman 1996). Most studies on natural glass dissolution were performed in either high ionic strength seawater solutions or at high temperatures and many were carried out in closed batch systems. These conditions promote the formation of secondary phases, which renders it difficult to unequivocally determine individual dissolution rates of the dissolving glass (Wolffe-Boenisch et al. 2004). Secondary phases and their effect on the dissolution rate are probably related to the glass composition (Ebert 1997). Seawater, used in our experiments is already rich in

many components (Na^+, Mg^{2+}, K^+ and Ca^{2+}) and represents a dilute solution only with respect to Si, Al and Fe (Crovisier et al. 1987). Release of Si was apparent after about two weeks which, over time, lead to the overall precipitation of substantial amounts of authigenic minerals. Previous studies have shown that precipitation of such secondary minerals on basaltic glass can cause blocking of the reactive surface area (Stockmann et al. 2008) and also lead to incorporation of elements into alteration phases or surface adsorption. All these reactions result in overall decreasing concentration of certain elements such as aluminum in the reaction solution (Wronkiewicz and Arbesman 2000). This could to some extent explain the results from the chemical analysis. In addition to the lower than expected increase of elements released from the glass under biotic conditions both abiotic experiments showed an overall decrease of ions in solution represented by negative concentration differences seen in Table 6.3. Abiotic experiments involving siderophores therefore seemingly disagree with previous work showing siderophore-mediated dissolution of minerals including goethite, hematite, ferrihydrite and kaolinite (Hersman et al. 1995; Kraemer et al. 1999; Rosenberg and Maurice 2003; Yoshida et al. 2002) and crystalline and glassy hornblende (Buss et al. 2007; Kalinowski et al. 2000; Liermann et al. 2000). They also appear to disagree with results presented in Chapter III where siderophore-mediated acquisition of Fe from basalt and rhyolite, equatable to alteration of the volcanic rocks, was successfully shown. Siderophore concentrations in the studies referenced above ranged between 1 and 240 μM and therefore by far exceed the ones reported for marine systems (0.3-7 nm, Gledhill and Van den Berg 1994; Gledhill et al. 1998; Powell and Donat 2001; Rue and Bruland 1997; Van den Berg 1995; Witter and Luther 1998). Most of them were conducted at neutral pH

matching the conditions in our experiment (Buss et al. 2007; Liermann et al. 2000; Rosenberg and Maurice 2003; Yoshida et al. 2002).

It is likely that dissolution rates vary depending on the texture of the substratum and correlate with the Fe content of the material as suggested previously (Rosenberg and Maurice 2003). Overall this may partly explain the disagreement of data from previous studies (including Chapter III) and the ones presented here. Hematite, goethite, ferrihydrite, crystalline hornblende and basalt powder all represent materials from which siderophore-mediated Fe acquisition is likely to be elevated compared to materials with a glassy texture (due to higher surface areas and lower stability constants). Studies conducted on hornblende glass (Buss et al. 2007) represent the only system comparable to ours. Texture and Fe content (hornblende: total Fe ~11 wt %, Buss et al. 2007) in both glasses are very similar. But contrary to our findings Buss et al. show that significant amounts of Fe (3.1 ± 0.3 μM) and Al (9.5 ± 0.9 μM) are released from hornblende glass in the presence of 240 μM desferrioxamine-B mesylate (DFAM) after a comparable incubation time. Higher ligand concentrations as well as structural differences between DFAM and amonabactin could potentially lead to the different Fe complexation rates observed.

As tetradentate ligands amonabactins form 2:3 metal:ligand complexes at high pH and excess ligand based on the following reaction (Telford and Raymond 1998):

$$2Fe(H_2O)_6^{3+} + 3Amo^{4-} \leftrightarrow Fe_2(Amo)_3^{6-}$$

In comparison DFAM 1:1 complexes with Fe^{3+}. This results in more Fe^{3+} ions being complexed by DFAM than by amonabactins at the same molarity which could account for the generally lower concentrations of Fe detected in our reaction solution. In addition further investigation of the purified amonabactin P750 used in our experimental set-up revealed that part (~¼) of it was already Fe-loaded (data not shown). While this may account for the generally higher initial concentration of Fe in the experimental set-up containing amonabactin and may also lead to overall lower dissolution rates it does not explain the decreasing concentrations of ions detected over the course of the experiment.

One potential explanation for this phenomenon is the adsorption of siderophores to Fe(III) hydroxide minerals such as goethite or biofilms likely to form due to the static nature of the experimental set-up (as described below). Such adsorption processes have been described in earlier studies (Carrasco et al. 2009; Cervini-Silva 2008; Lavie and Stotzky 1985).

3. Shortcomings of the experimental set-up and insufficient sampling technique

The experimental set-up described above and insufficient sampling techniques (see below) likely lead to negative results in both surface-based and chemical studies.

No preliminary washing steps were performed on the basalt grains used in the chemical set-up. Such steps would have resulted in the partial removal of surface-bound metal ions preventing an initial saturation of these ions in the reaction solution. The

presence of such ions may account for the overall negligible rates of basalt dissolution. Based on the static nature of the experiments, saturation of elements is likely to favor the precipitation of authigenic minerals as well as the formation of mineral- and biofilms on the glass surface potentially resulting in decreaseing concentrations of ions in solution.

All forms of precipitate result in the removal of ions from the solution. Insufficient homogenization of solutions and extended time spend on letting the basalt particles settle to the bottom of the flasks prior to sampling may have lead to a failure to catch the majority of these minerals/biofilm. This could have resulted in no detection of elements trapped inside the precipitate. These problems are related to the batch nature of the experimental design. Because solutions were not replenished, solution chemistry changed with time, presumably also affecting the rate of dissolution. In inorganic kinetic experiments with mineral dissolution, most investigators have abandoned batch experiments, and instead run flow-through chemical reactors (Brantley and Chen 1995). Compared to static incubation conditions, flow-through systems not only mimic natural conditions in a more realistic way but are also more likely to prevent extensive precipitation of secondary minerals. They do however represent a bigger challenge to measuring the release of ions into solution since they operate under higher water/rock ratios and overall lead to diluted concentrations.

We have already argued that the formation minerals/biofilms settling to the bottom of the flasks instead of being sampled, could potentially explain the results from the chemical analysis. The physical protection of such films, leading to a limited

diffusion of the reaction solution and resulting in generally limited reaction rates (Stewart 1988) may also partially account for a lack of bio-alteration textures on the polished basalt surface. Another factor might have been insufficient incubation times.

4. Shortcomings of analytical techniques

Unwisely chosen parameters and techniques used to represent and investigate basalt dissolution could have caused the lack of results from both studies.

4.1 Inappropriate chemical parameters chosen to represent basalt dissolution

Hopf et al. (2008) investigated the influence of microorganisms on biotite dissolution and showed a similar phenomenon of steady or even decreasing element concentrations in solution over time. They used element ratios such as K/Si or Mg/Si that overall did show an accelerated dissolution when incubated under biotic conditions. For two reasons we were unable to obtain these ratios in our study: 1) Si was removed during the digestion process to liberate elements associated/co-precipitated with amorphous silicates; 2) K^{+} and Mg^{++} were not analyzed based on their abundance in the minimal (seawater) medium. These two ratios are also associated with another factor that can be considered a shortcoming of the experimental set-up: the lack of normalization of data to a specific surface area of the glass. Basalt pieces (~ 3 mm in diameter) were chosen over glass powder to minimize unintentional resuspension and subsequent contamination of sampling solutions with the rock powder. Hopf et al. avoided this issue by centrifuging and filtering the sample solutions prior to analysis. We chose not to do that to ensure detection and subsequent digestion of all metal oxides known to form under aerobic

conditions. Overall other methods such as isotopic ratios of radiogenic-elements abundant in both rock and seawater (such as Sr^{86}/Sr^{87}) might present a more powerful tool to determine the rate of mineral/rock dissolution over time as shown previously (Staudigel et al. 1998).

4.2 Issues during the chemical digestion

While a three-set chemical digestion method has likely resulted in the digestion and dissolution of most oxides and minerals it is possible that small amounts of residual minerals are lost during the process. Chemical digestion with concentrated hydrofluoric acid should have dissolved most of the fluorides in solution liberating all elements associated with them. After evaporation to dryness samples were resuspended and taken up in 1 % HNO_3 for further analysis by ICP-OES. This method is commonly used in the chemical digestion of minerals, but additional dissolution and repeated evaporation steps including $HClO_4$ or nitric acid could have been performed to increase the chance for a more complete uptake of any up to this point undigested minerals.

4.3 Insufficient microscopical techniques

While AFM represents a very high-resolution technique with resolution of a fraction of a nanometer, the often uneven distribution of alteration fronts makes it more difficult to use this instrument for the identification of such textures. Only a small fraction of the basalt surfaces (within a TEM grid) could be analyzed and an overall conclusion from this limited area had to be drawn. It is unlikely that observations can be applied to the entire surface of the basalt. A combination of nm- and μm-scale

microscopic techniques aside from AFM could have been beneficial in further identification of various alteration textures. In our case, a combination of AFM and SEM (data not shown) analysis was attempted. However due to the non-conductive nature of the basalt surfaces, visualization of untreated glass surfaces (even in environmental mode) was unsuccessful due to significant surface charging, while application of only a light coat of platinum (grain size 1-3 nm) prior to imaging resulted in the coverage of most (on average 1-3 nm deep) surface/alteration features. More advanced surface-related techniques such as **V**ertical **S**canning **I**nterferometry (VSI) could be used in the future to help identify changes in surface morphology of volcanic glasses more precisely than AFM alone.

Even though the lack of results from both, morphological and chemical studies do not correlate well with investigations of microbially promoted glass dissolution that has been conducted for decades, they do to some extent fit with results from a more recent study. Templeton et al. (2009) investigated a seafloor biome of basalt surfaces formed under natural conditions at Loihi Seamount. Investigations were based on a combination of synchrotron-based X-ray microprobe mapping, X-ray absorption spectroscopy and high-resolution scanning and transmission electron microscopy. Researchers detected little microscopic evidence for hydration features or evidence for microbial dissolution of basaltic glass exposed to ambient seawater conditions at Loihi Seamount after an even longer period of time than 46 days. The topographical and chemical lack of evidence for microbially-derived dissolution in combination with large amounts of mineral precipitates detected on the glass surface resulted in the conclusion that soluble energy

sources (Fe(II), Mn (II), organic carbon) abundant in seawater are likely to support microbial communities inhabiting basalt surfaces to a greater extent than nutrients and energy derived from the dissolution of the volcanic rocks. It has to be considered though that Templeton et al. investigated surfaces exposed to natural seawater conditions where diffusion is significantly higher than in our set-up. This makes it even more surprising that we did not see any significant impact of microbial activity or purified ligands on the basalt dissolution as previously reported for batch experiments (Buss et al. 2003). Reduced flow/diffusion commonly found within biofilms and often associated with the accumulation of nutrients and metabolic byproducts (e.g. acids, siderophores) should instead have lead to both predominant alteration textures and chemically increased dissolution.

Conclusion

Results from the study of basaltic glass alteration by *Pseudomonas stutzeri* VS-10 remain inconclusive. Siderophore production by this bacterium was shown not to play a role in its growth on basalt under nutrient-limited conditions (see Chapter IV). Based on the variety of its metabolic characteristics (Chapter VI) *P. stutzeri* VS-10 represents a suitable model organism to study the bio-alteration of basaltic glass. To improve our understanding of the effects of this strain on basalt dissolution will require careful, controlled experiments in chemical reactors. In addition further refinement of the

experimental techniques will allow better quantification of its effect on weathering rates of submarine basaltic glass.

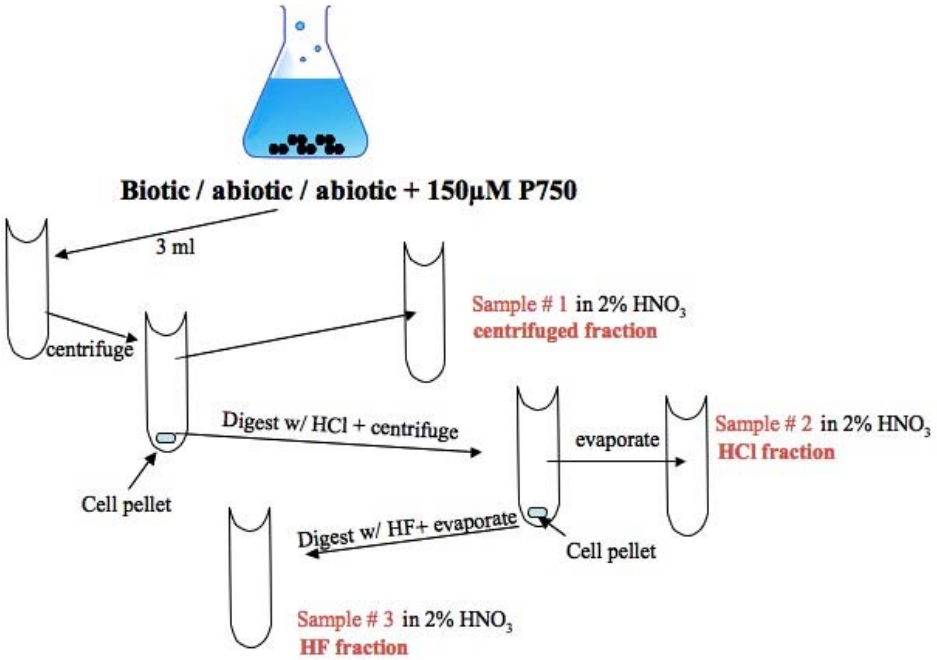

Figure 6.1: Sketch of the wet-digestion process and the resulting sample fractions analyzed by ICP-OES.

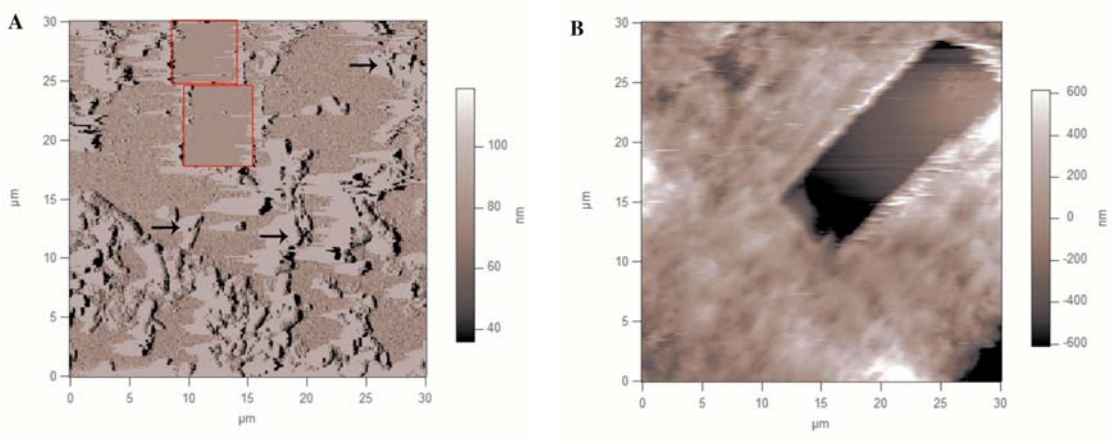

Figure 6.2: AFM images of the basalt glass slide exposed to a culture of *Pseudomonas stutzeri* VS-10 for 35 days. Biofilm formation is inhomogenous and sometimes patchy. Coverage by organic material ranges from patchy (A) to laminar (B). In both areas cell/EPM layers (Figure 6.2, continued) were displaced with the AFM tip. The clean basalt surfaces are indicated by red rectangles in A and a black area in B. Black arrows in A indicate relocated organic material. B: The distance from the top of the organic matter to the black area, representing the underlying basalt surface, was used to determine the thickness of the cell/EPM coverage. Scan Size: 30 µm, Scan rate: 1.00 Hz, Scan points: 256.

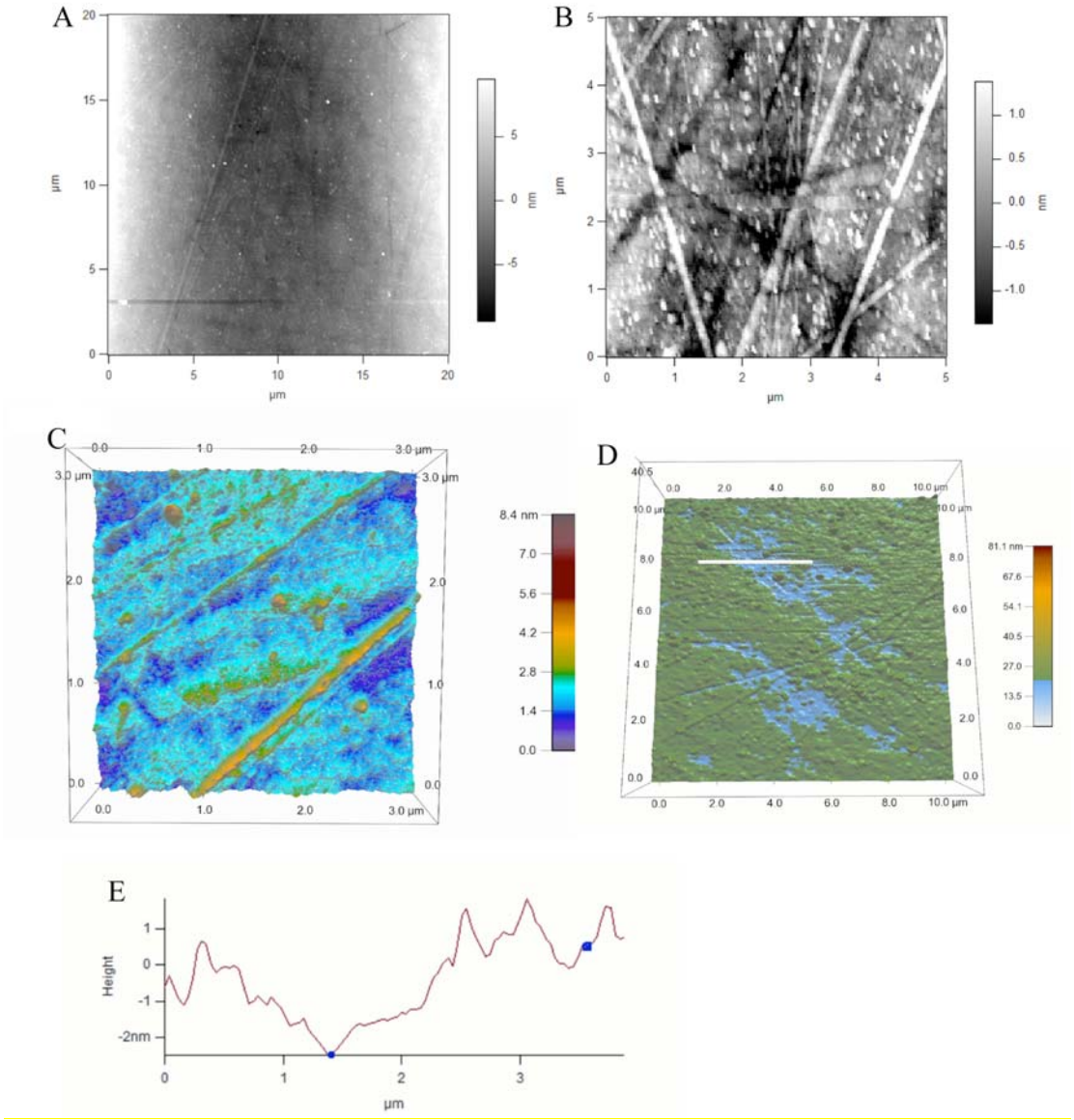

Figure 6.3: Frequent distribution of irregular eroded areas representing "granular alteration" on the basalt surface prior and after being exposed to a *Pseudomonas stutzeri* VS-10 culture for 35 days: A) and B) unexposed surface: irregular black patches visible in B) represent eroded areas. C) and D) images after basalt has been exposed to the culture: C) biotic, biofilm conserved and heterogeneous cells/EPM layer was displaced prior to imaging (alteration features in dark blue), D) biofilm was chemically removed prior to imaging (alteration features in light blue). E) cross-section of eroded area in D) (white bar) showing the depth and width of an eroded area,. A) Scan size: 20 µm, scan rate: 1.00 Hz, scan points: 256, B) Scan size: 5 µm, scan rate: 1.00 Hz, scan points: 256 C) Scan size: 10 µm, scan rate: 1.00 Hz, scan points: 256. D) Scan size: 3 µm, scan rate: 1.00 Hz, scan points: 256. The scale bars on the right indicate the depth of features seen on the images.

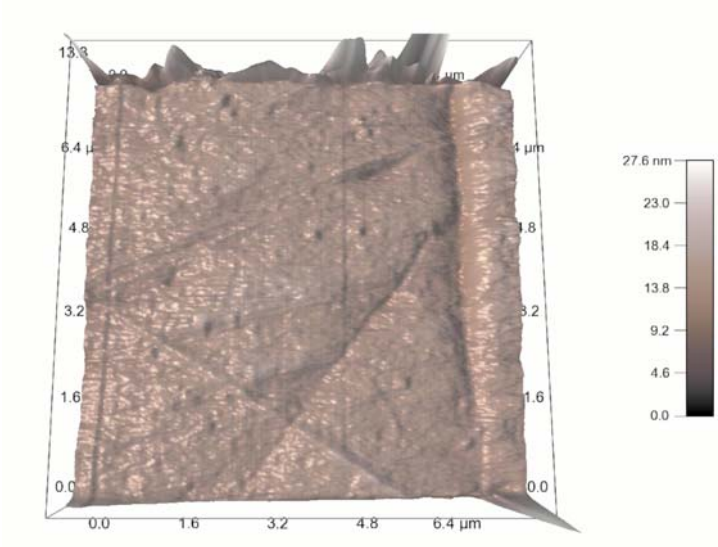

Figure 6.4: 3-dimensional height image of the basalt glass surface underneath areas of laminar biofilm coverage(Figure 6.2 B). While irregularly eroded areas seen in Figure 6.3 B -D were apparent (difficult to see in 3-D), alteration features that could specifically be attributed to the activity of the biofilm were absent. Scan size: 7.26 μm, Scan rate: 3.00 Hz, Scan points: 256.

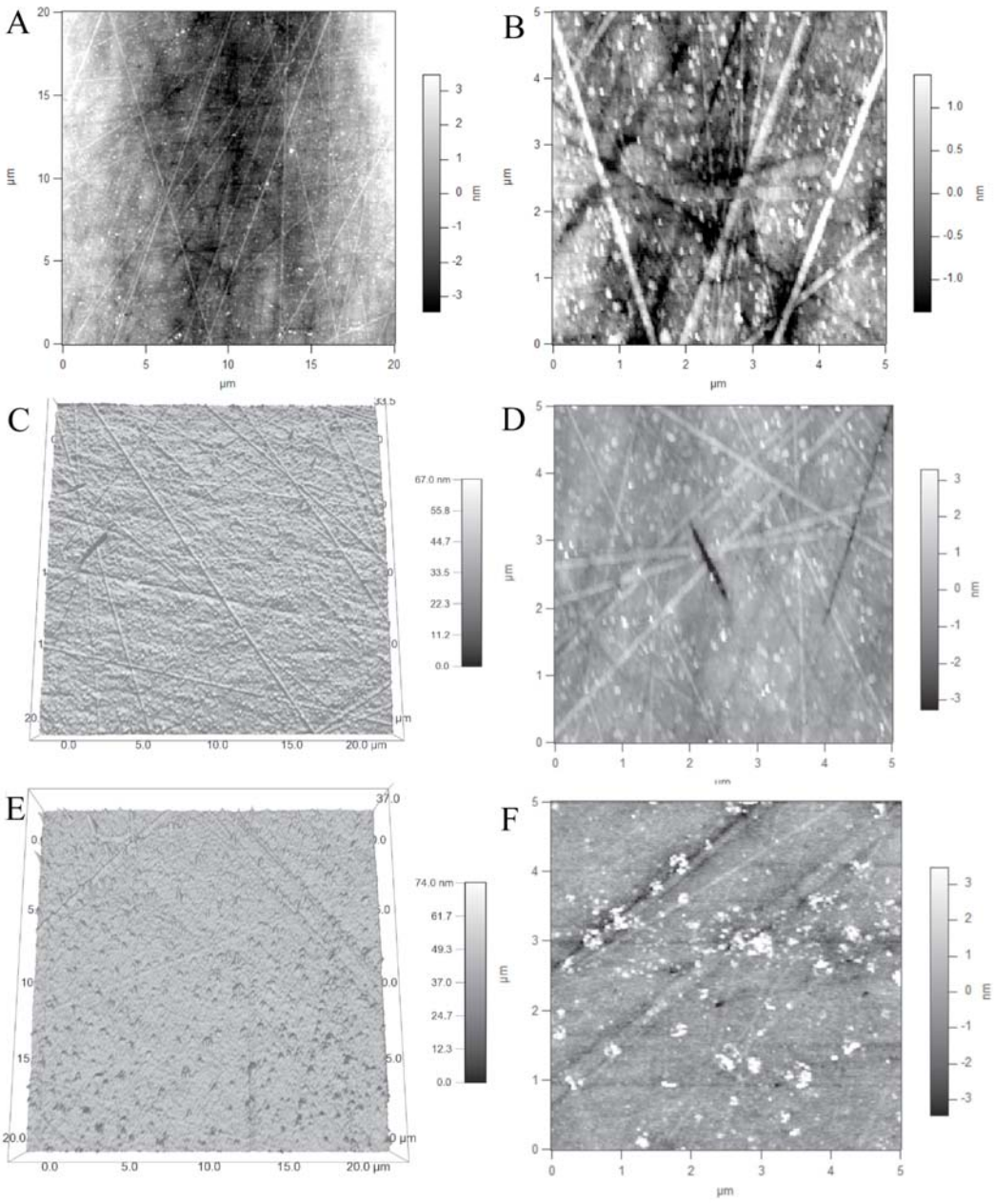

Figure 6.5: AFM images of a "fresh", unexposed basalt (A-D) versus the abiotically (E and F) incubated basalt after 35 days. C and E represent 3-D height images of the surfaces. Based on their height (see scale bars next to images) the linear features ("ridges") are a few nm elevated and are apparent on all samples. After exposure to a minimal medium for 35 days, their appearance seems significantly reduced (E and F) compared to the unexposed basalt (A-D). A: Scan size: 20 μm, Scan rate: 1.00 Hz, Scan points: 256. B: Scan size: 5 μm, Scan rate: 1.00 Hz, Scan points: 256. C and E: Scan size: 20 μm, Scan rate: 1.00 Hz, Scan points: 256. D and F: Scan size: 5 μm, Scan rate: 1.00 Hz, Scan points: 256.

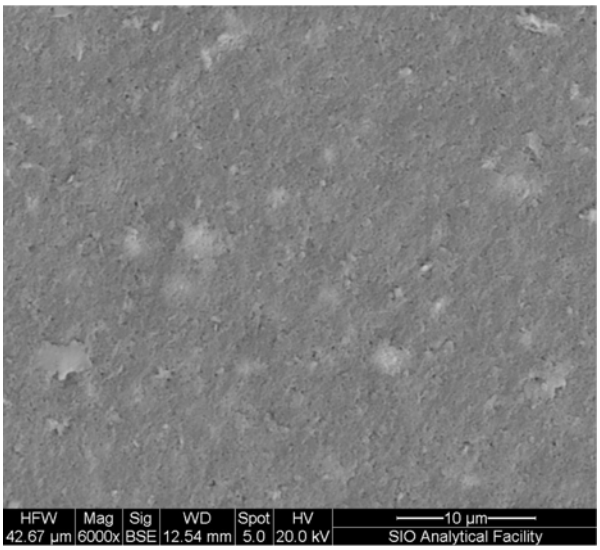

Figure 6.6: Scanning electron micrograph of the authigenic mineral phase formed in an experiment in which basalt grains had been exposed to a culture of *Pseudomonas stutzeri* VS-10 for 2.5 weeks (in 2006).

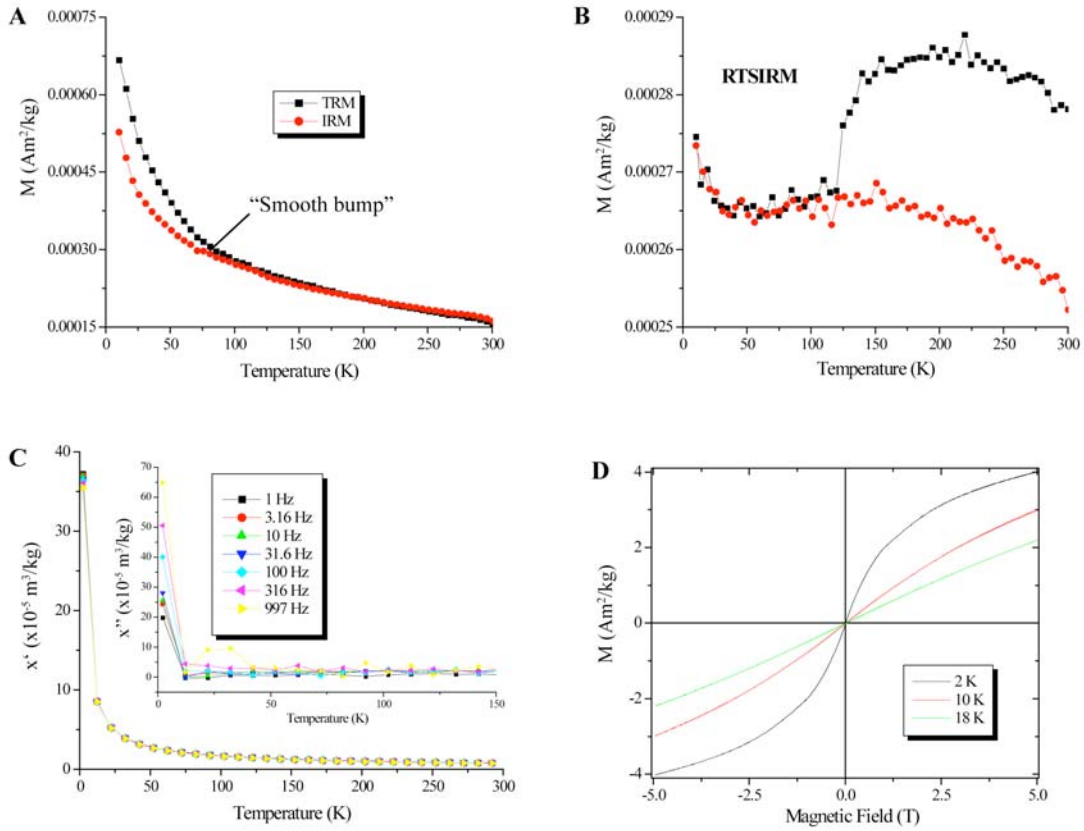

Figure 6.7: Low temperature magnetism results for the amorphous mineral phase. Data include two remanent magnitization curves (A) TRM/IRM, B) RTSIRM), an ac susceptibility curve (C) and the hysteresis loops (D).

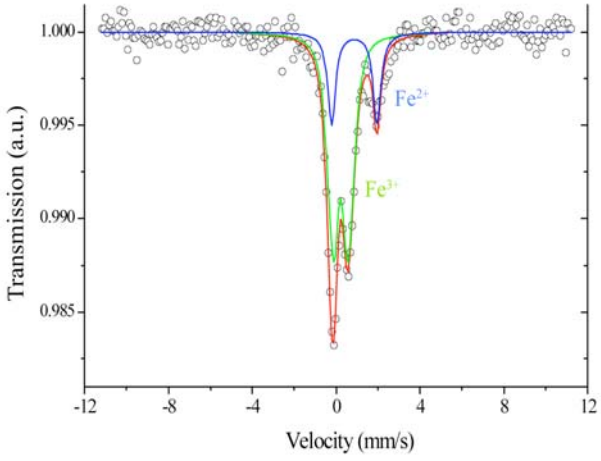

Figure 6.8: Mössbauer spectra taken at room temperature. Circles are experimental data. Lines represent the best fit (green line – Fe^{3+}, blue line – Fe^{2+}).

Figure 6.9: Centrifuged fractions of all samples from day 4-24. Compared to the abiotic and abiotic/amonabactin set-up the biotic samples show a yellow color of the supernatant that intensifies with time.

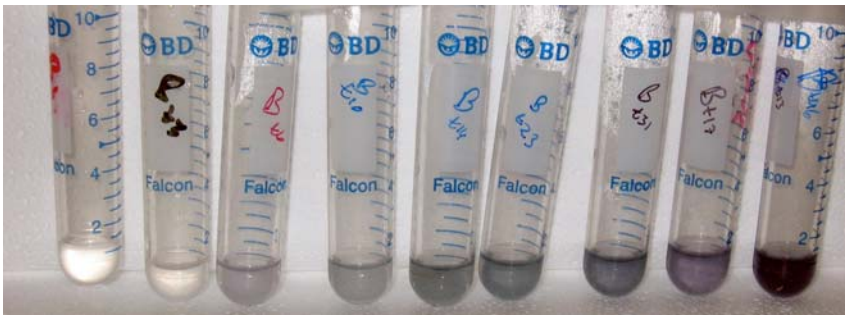

Figure 6.10: Blue/purple color in all the biotic and the abiotic/ amobactin samples after being digested in 0.5 ml conc. HCl over night.

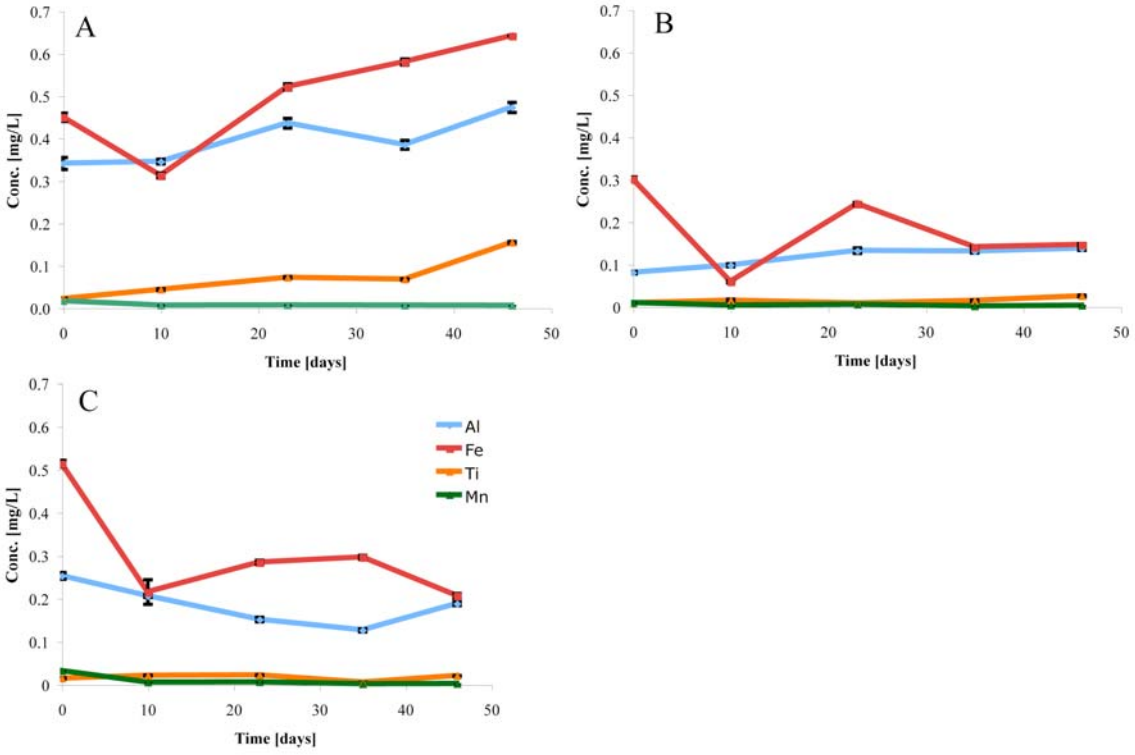

Figure 6.11: Concentration of Al, Fe, Ti and Mn in the solution as a function of time for all set-ups A: biotic, B: abiotic, C: abiotic/ 150 μM amonabactin P750. Data were obtained by ICP-OES measurements. While all values except for Mn in the biotic experiment increase there is no apparent increase and even a drop in Fe concentration visible in both abiotic experiments. The error bars show standard deviations.

Table 6.1: Approximate chemical composition of the mineral phase as obtained by SEM-EDS.

Element	App Conc.	Intensity Corrn.	Weight%	Weight% Sigma	Atomic%
O K	19.35	0.7957	40.91	0.49	57.75
Na K	0.71	0.7685	1.56	0.14	1.53
Mg K	0.79	0.7151	**1.86**	0.12	1.73
Al K	3.29	0.8108	**6.82**	0.16	5.71
Si K	15.34	0.8247	**31.26**	0.33	25.14
Cl K	0.27	0.6930	0.66	0.09	0.42
K K	0.79	0.9897	**1.35**	0.10	0.78
Ca K	1.85	0.9570	3.25	0.12	1.83
Ti K	0.82	0.8212	**1.67**	0.12	0.79
Fe K	5.32	0.8395	**10.65**	0.26	4.31
Totals			100.00		

Table 6.2: Magnetic hyperfine parameters of Mössbauer spectra at room temperature. QS – quadrupole splinting, IS – isomer shift, % relative proportion. Errors are quoted in parenthesis.

Fe^{3+}			**Fe^{2+}**		
QS (mm/s)	**IS (mm/s)**	**%**	**QS (mm/s)**	**IS (mm/s)**	**%**
0.73(2)	0.35(1)	74	2.17(5)	0.99(2)	26

Table 6.3: Concentration differences of elements in all three experimental set-ups as detected on day 46.

Day 46	*Biotic*	*Abiotic*	*Abiotic/amonabactin*
Aluminum (Al)	4.9 μM	2.1 μM	-2.4 μM
Iron (Fe)	3.4 μM	-2.8 μM	-5.5 μM
Titanium (Ti)	2.8 μM	0.4 μM	0.1 μM
Manganese (Mn)	-0.2 μM	-0.1 μM	-0.5 μM

References

Alt J. C. and Mata P. 2000. On the role of microbes in the alteration of submarine basaltic glass: a TEM study. Earth and Planet. Sci. Letters 181:301-313.

Banfield J. F., Barker W. W., Welch S. A. and Taunton A. 1999. Biological impact on mineral dissolution: application of the lichen model to understanding mineral weathering in the rhizosphere. Proc Natl Acad Sci U S A 96:3404-3411.

Barker W. W., Welch S. A., Chu S. and Banfield J. F. 1998. Experimental observations of the effects of bacteria on aluminosilicate weathering. Amer Mineral 83:1551-1563.

Barker W. W., Welch S. A., Chu S. and Banfield J. F. 1998. Experimental observations of the effects of bacteria on aluminosilicate weathering. American Mineralogist 83:1551-1563.

Bennett P. C., Choi W. J. and Rogers J. R. 1998. Microbial destruction of feldspar. Mineral. Mag. 62A:149-150.

Bennett P. C., Hiebert F. K. and Choi W. J. 1996. Microbial colonization and weathering of silicates in a petroleum-contaminated groundwater. Chem Geol 132:45-53.

Bennett P. C., Rogers J. R. and Choi W. J. 2001. Silicates, Silicate Weathering, and Microbial Ecology. Geomicrobiology Journal 18:3-19.

Berger G., Claparois C., Guy C. and Daux V. 1994. Dissolution rate of a basaltic glass in silica rich solutions: implications for long-term alteration. Geochim Cosmochim Acta 58:4875-4886.

Bonatti E. 1965. Palagonite, hyaloclastites and alteration of volcanic glass in the ocean. Bill. Volcanol. 28:251-269.

Brantley S. L. and Chen Y. 1995. Chemical weathering rates of pyroxenes and amphiboles. In: Chemical Weathering Rates of Silicate MineralsRev. Mineral. White A. F. and Brantley S. L., editors. 119-172.

Brehm U., Gorbushna A. and Mottershead D. 2005. The role of microorganisms and biofilms in the breakdown and dissolution of quartz and glass. Palaeogeography Palaeoclimatology Palaeoecology 219:117-129.

Brisou J. F. 1995. J.F. Brisou, Biofilms: Methods for Enzymatic Release of Microorganisms. Boca Raton, Florida: CRC Press.

Buss H. L., Brantley S. L. and Liermann L. J. 2003. Nondestructive Methods for Removal of Bacteria from Silicate Surfaces. Geomicrobiology Journal 20:25-42.

Buss H. L., Luettge A. and Brantley S. L. 2007. Etch pit formation on iron silicate surfaces during siderophore-promoted dissolution. Chem Geol 240:326-342.

Carrasco N., Kretzschmar R., Jide X. and Stephan M. K. 2009. Adsorption of hydroxamate siderophores and EDTA on goethite in the presence of the surfactant sodium dodecyl sulfate. Geochem Trans 10:1-9.

Cengiz Cinku M., Rammlmair D., Hisarli M. Z. and Orbay N. 2009. A combined rock magnetic and geochemical investigation of Upper Cretaceous volcanic rocks in the Pontides, Turkey. Studia Geophysica et Geodaetica 53:475-494.

Cervini-Silva J. 2008. Adsorption of trihydroxamate and catecholate siderophores on alpha- Iron (hydr)oxides and their dissolution at pH 3.0 to 6.0. Soil Sci Soc Am J 72:1557-1562.

Chongdar S., Gunasekaran G. and Kumar P. 2005. Corrosion inhibition of mild steel by aerobic biofilm. Electrochimica Acta 50:4655-4665.

Cockell C. S., Olsson-Francis K., Herrera A. and Meunier A. 2008. Alteration textures in terrestrial volcanic glass and the associated bacterial community. Geobiology 7:50-65.

Costerton W. J. and Wilson M. 2004. Introducing Biofilms. Biofilms 1:1-4.

Crovisier J. L., Honnorez J. and Eberhart J. P. 1987. Dissolution of basaltic glass in seawater: Mechanism and rate. Geochim Cosmochim Acta 51:2977-2990.

Crovisier J. L., Thomassin J. H., Juteau T., Eberhart J. P., Touray J. C. and Baillif P. 1983. Experimental seawater-basaltic glass interaction at 50 C: Study of early developed phases by electron microscopy and X-ray photoelectron spectrometry. Geochim Cosmochim Acta 47:377-387.

Daughney C. J., Rioux J. P., Fortin D. and Pichler T. 2004. Laboratory Investigation of the Role of Bacteria in the Weathering of Basalt Near Deep Sea Hydrothermal Vents. Geomicrobiology Journal 21:21-31.

Daux V., Guy C., Advocat T., Crovisier J. L. and Stille P. 1997. Kinetic aspects of basaltic glass dissolution at 90C: role of aqueous silicon and aluminum. Chem Geol 142:109-126.

Davis K. J. and Luettge A. 2005. Quantifyin the relationship between microbial attachment and mineral surface dynamics using vertical scanning interferometry (VSI). American Journal of Science 305:727-751.

Douglas S. 2005. Mineralogical footprints of microbial life. American Journal of Science 305:503-525.

Ebert W. L. (1997). Effect of alteration pahse formation on the glass dissolution rate. Glass: Scientific Research Toward High Performance Confinement Conference, CEA-Valrho Summer Workshop. Mejannes-le-Clap, France.

Edwards K. J., Rogers D. R., Wirsen C. O. and McCollom T. M. 2003. Isolation and characterization of novel psychrophilic, neutrophilic, Fe-oxidizing, chemolithoautotrophic alpha- and gamma-proteobacteria from the deep sea. Appl Environ Microbiol 69:2906-2913.

Eick M. J., Grossl P. R., Golden D. C., Sparks D. L. and Ming D. W. 1996. Dissolution kinetics of a lunar glass simulant at 25 degrees C: the effect of pH and organic acids. Geochim Cosmochim Acta 60:157-170.

Fisk M. R., Giovannoni S. J. and Thorseth I. H. 1998. Alteration of oceanic volcanic glass textural evidence of microbial activity. Science.

Flemming H.-C., Wingender J., Griegbe and Mayer C. 2000. Physico-chemical propertis of biofilms. In: Biofilms: recent advances in their study and control. Evans L. V., editors. 19-34.

Fletcher M. and Marshall K. C. 1982. Bubble Contact Angle Method for Evaluating Substratum Interfacial Characteristics and Its Relevance to Bacterial Attachment. Appl Environ Microbiol 44:184-192.

Forsythe J. H. and Maurice P. A. 1998. Attachment of a Pseudomonas sp. to Fe(III)-(hydr)oxide Surfaces. . Geomicrobiology Journal 15:293-308.

Furnes H. 1975. Experimental palagonitization of basaltic glasses of varied composition. Contributions to Mineralogy and Petrology 50:105-113.

Furnes H., Banerjee N. R., Staudigel H., Muehlenbachs K., McLoughlin N., de Wit M. and Van Kranendonk M. J. 2007. Comparing petrographic signatures of bioalteration in recent to Mesoarchean pillow lavas: Tracing subsurface life in oceanic igneous rocks. Precambrian Research 158:156-176.

Furnes H., Muehlenbachs K., Tumyr O., Torsvik T. and Thorseth I. H. 1999. Depth of active bio-alteration in the ocean crust Costa Rica Rift (Hole 504B). Terra Nova 11:228-233.

Furnes H. and Staudigel H. 1999. Biological mediation in ocean crust alteration: how deep is the deep biosphere. Earth and Planet. Sci. Letters 166:97-103.

Furnes H., Staudigel H., Thorseth I. H., Torsvik T., Muehlenbachs K. and Tumyr O. 2001. Bioalteration of basaltic glass in the oceanic crust. Geochemistry Geophysics Geosystems 2:1049.

Furnes H., Thorseth I. H. and Tumyr O. 1996. Textural and chemical effects of bacterial activity on basaltic glass: an experimental approach. Chem Geol 119:139-160.

Giovannoni S. J., Fisk M. R., Mullins T. D. and Furnes H. 1996. Genetic evidence for endolithic microbial life colonizing basaltic glass/seawater interfaces. Proc. ODP Sci. Results 148:207-214.

Gislason S. R. and Oelkers E. H. 2003. Mechanism, rates, and consequences of basaltic glass dissolution: II. An experimental study of the dissolution rates of basaltic glass as a function of pH and temperature. Geochim Cosmochim Acta 67:3817-3832.

Gledhill M. and Van den Berg C. M. G. 1994. Determination of complexation of iron(III) with natural organic complexing ligands in seawater using cathodic stripping voltammetry. Mar. Chem. 47:41-54.

Gledhill M., Van den Berg C. M. G., Noldting R. F. and Timmermans K. R. 1998. Variability in the speciation of iron in the nothern North Sea. Mar. Chem. 59:283-300.

Grantham M. C., Dove P. M. and DiChristina T. J. 1997. Microbially catalyzed dissolution of iron and aluminim oxyhydroxide mineral surface coatings. Geochim Cosmochim Acta 60.

Hargraves R. B. and Banerjee S. K. 1973. Theory and nature of magnetism in rocks. Annu. Rev. Earth Planet. Sci. 1:269-296.

Hersman L. E., Lloyed T. and Sposito G. 1995. Siderophore-promoted dissolution of hematite. Geochim Cosmochim Acta 59:3327-3330.

Hopf J., Langhorst F., Pollok K., Merten D. and Kothe E. 2008. Influence of microorganisms on biotite dissolution: An experimental approach. Chemie der Erde-Geochemistry 69:45-56.

Kalinowski B. E., Liermann L. J., Givens S. and Brantley S. L. 2000. Rates of bacteria promoted solubilization of Fe from minerals: A review of problems and approaches. Chem Geol 169:357-370.

Kraemer S. M., Cheah S.-F., Zapf R., Xu J. D., Raymond K. N. and Sposito G. 1999. Effect of hydroxamate siderophores on Fe release and Pb(II) adsorption by goethite. Geochim Cosmochim Acta 63:3003-3008.

Lavie S. and Stotzky G. 1985. Interactions between clay minerals and siderophores affect the respiration of Histoplasma casulatum. Appl Environ Microbiol 51:74-79.

Liermann L. J., Kalinowski B. E., Brantley S. L. and Ferry J. G. 2000. Role of bacterial siderophores in dissolution of hornblende. Geochim Cosmochim Acta 64:587-602.

Madigan M. T., Martinko J. M. and Parker J. 2000. Brock Biology of Microorganisms. Prentice Hall, Upper Saddle River, New Jersey.

Mangold S., Harneit K., Rohwerder T., Claus G. and Sand W. 2008a. Novel combination of atomic force microscopy and epifluorescence microscopy for visualization of leaching bacteria on pyrite. Appl Environ Microbiol 74:410-415.

Mangold S., Laxander M., Harneit K., Rohwerder T., Claus G. and Sand W. 2008. Visualization of Acidithiobacillus ferrooxidans biofilms on pyrite by atomic force and epifluorescence microscopy under various experimental conditions. Hydrometallurgy 94:127-132.

Mason O. U., Stingl U., Wilhelm L. J., Moeseneder M. M., Di Meo-Savoie C. A., Fisk M. R. and Giovannoni S. J. 2007. The phylogeny of endolithic microbes associated with marine basalts. Environ Microbiol 9:2539-2550.

Maurice P. A. and Forsythe J. H. 1997. Aerobic bacterial interactions with hydrous Fe(III) oxides: attachment features observed using atomic-force microscopy. GSA Abstracts with Prgrams 29:295.

Pierce E. M., Rodriguez E. A., Calligan L. J., Shaw W. J. and McGrail B. P. 2008. An experimental study of the dissolution rates of simulated aluminoborosilicate waste glasses as a function of pH and temperature under dilute conditions. Appl Geochem. 23:2559-2573.

Powell R. T. and Donat J. R. 2001. Organic complexation and speciation of iron in the South and Equatorial Atlantic. Deep-Sea Res. II 48:2877-2893.

Rogers J. R., Bennett P. C. and Choi W. J. 1998. Feldspars as a source for nutrients for microorganisms. Amer Mineral 83:1532-1540.

Rosenberg D. R. and Maurice P. A. 2003. Siderophore adsorption to and dissolution of kaolinite at pH 3 and 7 and 22 degrees C. Geochim Cosmochim Acta 67:223-229.

Rue E. L. and Bruland K. W. 1997. The role of organic complexation on ambient iron chemistry in the equatorial Pacific Ocean and the response of a mesoscale iron addition experiment. Limnol Oceanogr. 42:902-920.

Santelli C. M., Orcutt B. N., Banning E., Bach W., Moyer C. L., Sogin M. L., Staudigel H. and Edwards K. J. 2008. Abundance and diversity of microbial life in ocean crust. Nature 453:653-656.

Schneider R. P. 1997. Bacterial adhesion to solid substrata coated with conditioning films derived from chemical fractions of natural waters. J. Adhes. Sci. Technol. 11:979-994.

Staudigel H., Furnes H., McLoughlin N., Banerjee N. R., Connell L. B. and Templeton A. S. 2008. 3.5 billion years of glass bioalteration: Volcanic rocks as a basis for microbial life? Earth-science Reviews (in press).

Staudigel H. and Hart S. R. 1983. Alteration of basaltic glass: Mechanisms and significance from the oceanic crust-seawater budget. Geochim. Cosmochim. Acta 47.

Staudigel H., Yayanos A., Chastain R., Davies G., Verdurmen E. A. T., Schiffman P., Bourcier R. and De Baar H. 1998. Biologically mediated dissolution of volcanic glass in seawater. Earth and Planet. Sci. Letters 164:233-244.

Staudigel H., Yayanos A., Chastain R., Davies G., Verdurmen E. A. T., Schiffman P., Bourcier R. and DeBaar H. 1998. Biologically mediated dissolution of volcanic glass in seawater. Earth and Planet. Sci. Letters 164:233-244.

Stewart P. S. 1988. A review of experimental measurements of effective diffusion permeabilities and effective diffusion coefficients in biofilm. Biotechnol Bioeng 59:261-272.

Stockmann G., Wolff-Boenisch D., Gislason S. R. and Oelkers E. H. 2008. Dissolution of diopside and basaltic glass: the effect of carbonate coating. Mineralogical Magazine 72:135-139.

Straub S. M. and Schmincke H.-U. 1998. Evaluation the tephra input into Pacific Ocean sediments: distribution in space and time. Geol Rundschau 87:462-476.

Stroncik N. A. and Schmincke H.-U. 2002. Palagonite - a review. Int J Earth Sci (Geol Rundsch) 91:680-697.

Sudek L. A., Templeton A. S., Tebo B. and Staudigel H. 2009. Microbial Ecology of Fe (hydr)oxide mats and basaltic rock from Vailulu'u Seamount, American Samoa. Geomicrobiology Journal 26:581-596.

Taunton A., E., Welch S. A. and Banfield J. F. 2000a. Geomicrobiological Controls on Lanthanide Distribution during Granite Weathering and Soil Formation. Journal of Alloys and Compounds 303-304:30-36.

Taunton A. E., Welch S. A. and Banfield J. F. 2000b. Microbial controls on phosphate weathering and lanthanide distribution during granite weathering and soil formation. Chem Geol 169:371-382.

Taunton A. E., Welch S. A., Santelli C. M., Fournelle J. and Banfield J. F. 1998. Apatite Weathering and Cerium Fractionation: Possible Microbial Influences. In: Abstracts with Programs. editors. A304-305.

Techer I., Advocat T., Lancelot J. and Liotard J.-M. 2001. Dissolution kinetics of basaltic glasses: control by solution chemistry and protective effect of the alteration film. Chem Geol 176:235-263.

Telford J. R. and Raymond K. N. 1998. Coordination chemistry of the amonabactins, bis(catecholate) siderophores from Aeromonas hydrophila. Inorg Chem 37:4578-4583.

Templeton A. S., Knowles E. J., Eldridge D. L., Arey B. W., Dohnalkova A. C., Webb S. M., Bailey B. E., Tebo B. M. and Staudigel H. 2009. A seafloor microbial biome hosted within incipient ferromanganese crusts. Nature Geoscience 2:872-876.

Templeton A. S., Staudigel H. and Tebo B. M. 2005. Diverse Mn(II)-oxidizing bacteria isolated from submarine basalts at Loihi Seamount. Geomicrobiology Journal 22:127-139.

Thanyakoop C. (2009). Characterization and biosynthesis of siderophores from marine bacteria. Chemistry. Santa Barbara, University of California, Santa Barbara.

Thorseth I. H., Furnes H. and Heldal M. 1992. The importance of microbiological activity in the alteration of natural basaltic glass. Geochim Cosmochim Acta 56:845-850.

Thorseth I. H., Furnes H. and Tumyr O. 1995. Textural and chemical effects of bacterial activity on basaltic glass: an experimental approach. Chem Geol 119:139-160.

Thorseth I. H., Pedersen R. B. and Christie D. 2003. Microbial alteration of 0-30-Ma seafloor and sub-seafloor basaltic glasses from the Australian Antarctic Discordance. Earth and Planet. Sci. Letters 215:237-247.

Torsvik T., Furnes H., Muehlenbachs K., Thorseth I. H. and Tumyr O. 1998. Evidence for microbial activity at the glass-alteration interface in oceanic basalts. Earth and Planet. Sci. Letters 162:165-176.

Van den Berg C. M. G. 1995. Evidence for organic complexation of iron in seawater. Mar. Chem. 50.

Wacey D. 2009. ~3,200 Ma, Moodies Group, Barberton, South Africa. In: Topics in Geobiology: Early Life on Earth. editors. 229-233.

Welch S. A. and Ullman W. J. 1996. Feldspar dissolution in acidic and organic solutions: compositional and pH dependence of dissolution rate. Geochim Cosmochim Acta 60:2939-2948.

Witter A. E. and Luther G. W. 1998. Variation in Fe-organic complexation with depth in the Northwestern Atlantic Ocean as determined using a kinetic approach. Mar. Chem. 62:241-258.

Wolffe-Boenisch D., Gislason S. R., Oelkers E. H. and Putnis C. V. 2004. The dissolution rates of natural glasses as a function of their composition at pH 4 and 10.6, and temperatures from 25 to 74 C. Geochim Cosmochim Acta 68:4843-4858.

Wronkiewicz D. J. and Arbesman K. A. 2000. The role of alteration phases in influencing the kinetics of glass dissolution. Mat. Res. Soc. Symp. Proc. 608:745-750.

Yoshida T., Hayashi K. and Ohmoto H. 2002. Dissolution of iron hydroxides by marine bacterial siderophore. Chem. Geol. 184:1-9.